Chapter 8

Drillstem Testing

8.1 Introduction

A *drillstem test* (DST) is normally run in a zone of undetermined potential in a well being drilled, although DST's are sometimes run in known productive zones in development wells. A DST provides a temporary completion of the test interval; the drillstring serves as the flowstring. A good DST yields a sample of the type of reservoir fluid present, an indication of flow rates, a measurement of static and flowing bottom-hole pressure, and a short-term pressure transient test. The DST helps determine the possibility of commercial production by virtue of the types of fluids recovered and the flow rates observed. Analysis of the DST transient pressure data can provide an estimate of formation properties and wellbore damage. Those data may be used to estimate the well's flow potential with a regular completion that uses stimulation techniques to remove damage and increase effective wellbore size.

To run a drillstem test, a special DST tool is attached to the drillstring and lowered to the zone to be tested.[1-6] The tool isolates the formation from the mud column in the annulus, allows formation fluid to flow into the drillpipe, and continuously records the pressure during the test. Most DST's include a short production period (the initial flow period), a short shut-in period (the initial buildup), a longer flow period (the second flow period), and a longer shut-in period (the final buildup).[1,2] Fig. 8.1 is a schematic DST pressure chart for a two-cycle test (note that pressure increases downward in most DST charts shown in this chapter). The first cycle in Fig. 8.1 includes the initial flow and buildup periods, while the second cycle includes the second flow and final buildup periods. Early drillstem testing techniques used only one cycle with a longer flow duration. Fig. 8.2 shows tests with more than two cycles are possible.[1,3] (Note that pressure increases upward in that figure.)

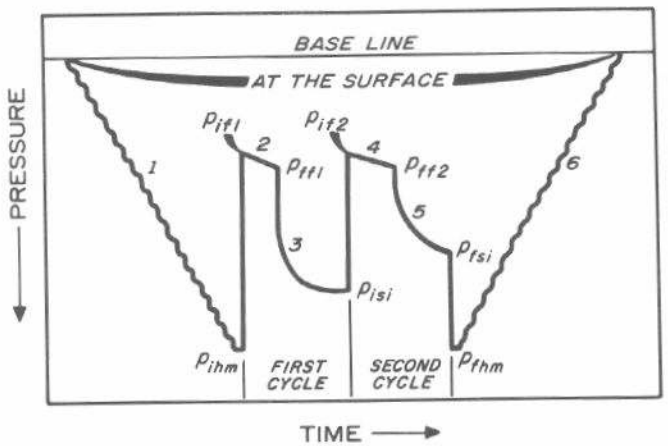

Fig. 8.1 Schematic of a DST chart: (1) going into hole; (2) initial flow period; (3) initial shut-in period; (4) final flow period; (5) final shut-in period; and (6) coming out of hole. p_{ihm} = initial hydrostatic mud pressure; p_{if1} = initial flowing pressure in first flow period; p_{ff1} = final flowing pressure in first flow period; p_{isi} = initial shut-in pressure; p_{if2} = initial flowing pressure in second flow period; p_{ff2} = final flowing pressure in second flow period; p_{fsi} = final shut-in pressure; and p_{fhm} = final hydrostatic mud pressure.

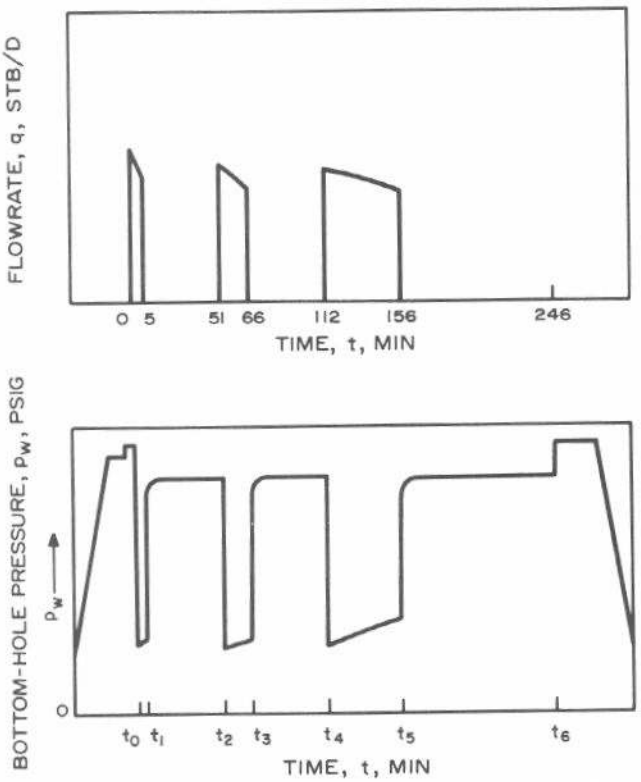

Fig. 8.2 Example of a three-cycle drillstem test. After McAlister, Nutter, and Lebourg.[3]

This chapter discusses the DST testing technique and presents methods for analyzing pressure data from both the flow and shut-in portions of a DST. A series of example DST pressure charts illustrates various DST operational conditions and test malfunctions. A short section on the wireline formation tester is also included.

8.2 Drillstem Testing Tools and Technique

Most drillstem testing tools include two or more clock-driven, Bourdon-tube recording pressure gauges, one or two packers, and a set of flow valves. The tool is attached to the drillstem and is lowered to the test interval where the packer is set, then the valves in the tool are opened and closed by manipulation of the drillpipe. The DST is run while the flow valves are being manipulated.

Fig. 8.3 shows typical drillstem testing tools used by the Halliburton Co. for the three basic types of tests: the single-packer test, the straddle-packer test, and the hook-wall packer test. Fig. 8.4 shows the operating states of a Halliburton DST tool during a test. Johnston Schlumberger, Lynes, Inc., Arrow Testers, and others also offer DST service and tools.

As shown in Fig. 8.3, the upper section of the DST tool is the same for all three test types. The uppermost part of the tool is an impact-reversing sub that allows produced fluids to be reverse-circulated out of the drillpipe (Fig. 8.4e). The closed-in pressure (CIP) valve is the main flow-control valve in the DST tool string. In conjunction with the hydrospring tester valve, it allows the two flow periods, the two closed-in periods, and reverse circulation.

As shown in Fig. 8.4a, the CIP valve is open and the hydrospring tester valve is closed as the DST tool is run into the hole. The bypass ports are open while the tool is being run into and out of the hole to allow fluid to flow through the tool to help minimize pressure surges caused by running the relatively large-diameter packer.

The hydrospring tester valve is a hydraulic time-delay master valve that opens slowly and closes quickly. When the packer is set, weight is applied to cock the hydrospring and activate the hydraulic time delay. A few minutes later, the hydraulic time delay closes the bypass ports and then opens the hydrospring tester valve to start the DST. During the test, the CIP valve is closed and opened to cause the shut-in and flow periods (Figs. 8.4b and 8.4c). The hydrospring tester valve closes immediately when the weight of the pipe is picked up. Then the bypass ports open. With both the hydrospring tester and CIP valves closed, a fluid sample is isolated between those valves when the tool is removed from the hole (Fig. 8.4f).

The optional handling sub and choke assembly aids in making up the tool and also provides a receptacle for a down-hole choke, if such a device is desired. The DST tool contains two Bourdon-tube pressure recording elements. The upper element, in the flowstring, senses the pressure as fluid flows into the drillstring during the test. The lower pressure recorder, near the bottom of the tool (Figs. 8.3a through 8.3d), is "blanked off" from the flow portion of the system. It records the annulus pressure below the packer rather than the pressure of the fluid inside the drillstem. In a good test, the pressures from the two recorders will differ only by the hydrostatic head between them. In poor tests, it is often possible to determine the kind of malfunction by comparing the two pressure charts.

Many DST tools include hydraulic jars and safety joints to aid in removing a stuck tool. If the tool cannot be unstuck by jarring, the drillstring may be backed off at a safety joint, allowing recovery of the pipe and a portion of the tool.

Single-packer tests use either a nonrotating, expanding packer with a tail pipe extending to the bottom of the hole or a hook-wall packer. Both assemblies include a perforated

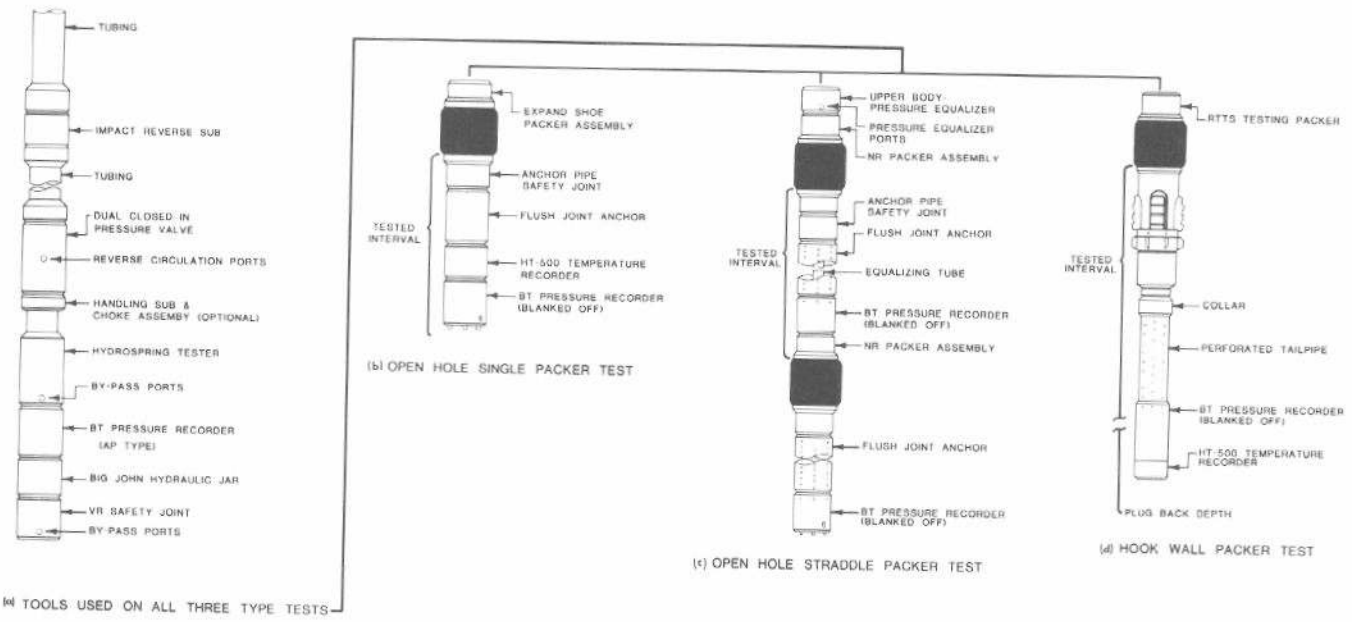

Fig. 8.3 Typical DST tools used for three types of tests. Upper assembly (left) is similar on all three test types. After Edwards and Shryock.[6] Courtesy *Petroleum Engineer*.

anchor pipe and a blanked-off pressure recorder. During the test, fluid flows from the formation through the perforated anchor pipe and into the drillstring. A temperature recorder may or may not be included in the tool string.

The straddle-packer test uses two packers, a perforated anchor pipe, and a blanked-off pressure recorder between the packers. An equalizing tube connects the annulus above the top packer to the hole below the bottom packer. The equalizing tube aids in bypassing wellbore fluid around the packers while running in and out of the hole and balances the load created on the drillstring by the annulus hydrostatic pressure during the test. A third pressure recorder may be included below the bottom packer to indicate whether that packer remains sealed throughout the test.

As indicated in Fig. 8.4a, the CIP valve is open and the hydrospring tester valve is closed while the tool is run into the hole. The bypass ports are open, so mud may flow both around the outside of the tool and through the packer while the tool is in motion. Both pressure recorders are in communication with the mud column and should record hydrostatic pressure as they are lowered into the hole (Fig. 8.1). When the packer is set, the bypass ports close and the hydrospring tester valve opens, resulting in the configuration shown in Fig. 8.4b. Both pressure recorders should show the same pressure response. To shut in the tool for a buildup, the CIP valve is closed (Fig. 8.4c). The CIP valve is opened for the second flow and closed for the second buildup. After the final buildup, the CIP valve remains closed and the hydrospring tester valve is closed, trapping a fluid sample under pressure. Then the bypass ports are opened, and pressure is equalized across the packer (Fig. 8.4d). The packer is unseated, the reverse circulating valve is opened, and mud is pumped down the annulus to displace the produced fluids up the drillstring for measurement at the surface (Fig. 8.4e). As the pipe and tool are removed from the hole (Fig. 8.4f), the mud in the drillstring is allowed to bleed into the annulus through the open reverse-circulating valve.

Hole condition may dictate the total time that the tool can remain in the hole, since a primary consideration is complete removal of the tools at the end of the test. Thus, conditions existing in the well may dictate relatively short testing times. Experience in the area is the best way to determine total allowable testing time. When allowed testing time is short, the division of the test between the various test periods is important. Pages 22 through 24 of Ref. 5 provide guidelines for choosing the length of the flow and shut-in periods in a DST — whether total test time is limited or not. Table 8.1 summarizes that material.

In a standard DST, the initial flow period is usually short, 5 to 10 minutes; the idea is simply to release the high hydrostatic mud pressure. The initial shut-in period should be sufficiently long to allow the measured pressure to approach *stabilized formation pressure*. Experience indicates that 1 hour is usually required for the initial shut-in period.[5,7] The second flow period should be long enough to allow flow

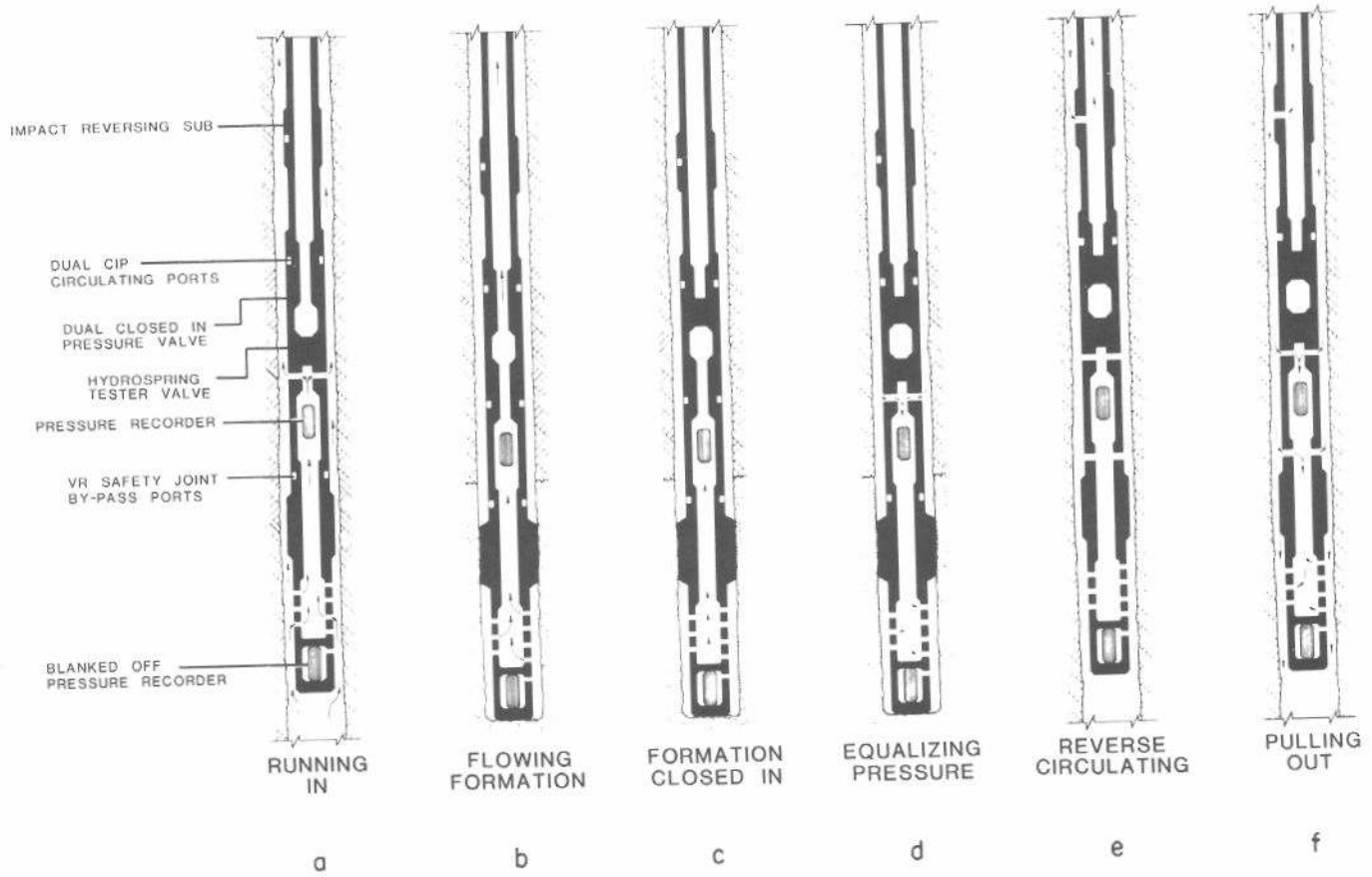

Fig. 8.4 DST-tool operating states for an open-hole formation test. Fluid movement is shown by arrows. After Edwards and Shryock.[6] Courtesy *Petroleum Engineer*.

stabilization; Table 8.1 provides guidelines. The length of the final shut-in period depends on test behavior during the final flow period. Recommendations are given in Table 8.1.

The multiflow evaluator, a tool that allows unlimited sequences of production and shut-in, has been available for drillstem testing since 1965.[3] The tool includes a fluid chamber to recover an uncontaminated formation-fluid sample under pressure at the end of the flow period.

8.3 Analyzing Drillstem-Test Pressure Data

Normal Drillstem-Test Pressure Buildup Analysis

Drillstem-test pressure buildup data are analyzed much like any other pressure buildup data; the techniques of Section 5.2 apply. In a DST, the flow period is about the same duration as the shut-in period, so pressure buildup data *must* be analyzed with the Horner plot, p_{ws} vs $\log[(t_p + \Delta t)/\Delta t]$. The value used for t_p is usually the length of the preceding flow period. However, if the initial flow period is very long, it is more accurate to use the *sum* of the flow-period lengths[3] for t_p for the final buildup.

In liquid-producing wells, the flow rate during a drillstem test decreases with time since the backpressure exerted on the formation face increases as the produced fluid moves up the drillstring. Flow rate may *stabilize if formation fluids flow to the surface*. The increasing flowing pressure is evident in Figs. 8.1 and 8.2. Normally, the decreasing flow rate over the flow period is neglected in analyzing DST pressure buildup data and the average flow rate over the flow period is used. Neglecting the flow-rate decrease is reasonable for a moderate bottom-hole pressure increase compared with total pressure drawdown, but it can lead to significant errors in the buildup analysis for high-productivity wells unless the well flows at the surface for a substantial portion of the flow period.[8]

If the pressure in the flowstring recorder increases linearly with time, liquid flow rate into the drillstring is constant (for a constant-inner-diameter drillstring) until liquid reaches the surface. Such a constant flow rate implies that flow rate is independent of drawdown, since bottom-hole flowing pressure is increasing. Eq. 2.2 indicates that flow rate from a porous medium to a wellbore must decrease with decreasing drawdown (increasing flowing bottom-hole pressure), so something other than the formation must be controlling the flow rate under such circumstances. The controlling factor is critical flow[9] (flow rate independent of pressure drop, see Section 13.6) through the perforations in the anchor pipe. In such an instance, the flowing pressure data from the flowstring recorder are useless, although shut-in data are analyzable. Fortunately, all data from the blanked-off recorder can be analyzed in the normal fashion.

Wellbore storage is not often significant in the buildup portion of a DST since the well is closed in near the formation face. However, if analysis results appear suspicious, the log-log data plot (Section 5.2) should be made to determine what part of the data should be analyzed. If thick sections are being tested in low-permeability or gas reservoirs, wellbore storage can be significant in a DST. Although production during the DST flow period appears to be *wellbore-storage dominated* until flow starts at the surface, the flow rate may be estimated, so normal analysis methods should apply if the varying rate is considered or if the rate variation is less than 5 to 10 percent.

If the shut-in period is long enough, and if wellbore storage is not dominant, a Horner plot of the buildup data should have a straight line section with slope $-m$, as indicated in Section 5.2. The value of m may be used to estimate permeability from Eq. 5.6:

$$k = \frac{162.6\, qB\mu}{mh}. \quad \ldots\ldots\ldots\ldots\ldots\ldots\ldots\ldots (8.1)$$

If μ and h are not known, kh/μ may be estimated by rearranging Eq. 8.1. The flow rate normally used is the average over t_p. The skin factor is estimated from Eq. 5.8:

$$s = 1.1513 \left[\frac{p_{1\text{hr}} - p_{wf}(\Delta t = 0)}{m} + \log\left(\frac{t_p + 1}{t_p}\right) - \log\left(\frac{k}{\phi\mu c_t r_w^2}\right) + 3.2275\right]. \quad \ldots\ldots\ldots\ldots (8.2)$$

The term $\log[(t_p + 1)/t_p]$ is included since it may be important in drillstem testing. The term is normally neglected when $t_p >> 1$ or when the skin factor is high.

DST analyses commonly report *damage ratio*:

$$\frac{J_{\text{ideal}}}{J_{\text{actual}}} = \frac{\bar{p} - p_{wf}}{\bar{p} - p_{wf} - \Delta p_s}, \quad \ldots\ldots\ldots\ldots\ldots (8.3)$$

where the pressure drop across the skin is computed from Eq. 2.9:

TABLE 8.1—RECOMMENDED FLOW AND SHUT-IN TIMES FOR DRILLSTEM TESTING WHEN EXPERIENCE IN THE AREA IS NOT AVAILABLE.
(Information from Pages 22-24 of Ref. 5.)

Test Period	Situation During Test	Recommended Time	Minimum Time (minutes)
Initial flow	All	Short — release hydrostatic mud pressure	3 to 5
Initial shut-in	All	60 minutes unless total test time is too short — 45 minutes then	30
Final flow	Strong, continuing blow	60 minutes	60
	Blow dies	Shut in when blow dies	
	Reservoir fluid produced at surface	60 minutes — longer to gauge flow rates if time is available	60
Final shut-in	Strong continuous blow during flow period	Shut-in time equal to flow time	45
	Blow dies during flow period	Minimum shut-in time of twice flow time*	Two times flow time
	Reservoir fluid produced at surface during flow period	Shut-in time equal to one-half flow time	30

*In this case there will be no buildup, so no buildup analysis. Flow-period data may be analyzed by the type-curve method described following Example 8.1.

$$\Delta p_s = \frac{141.2\,qB\mu}{kh}s \quad \ldots\ldots\ldots\ldots\ldots\ldots (8.4)$$

Initial, or average, reservoir pressure is estimated by extrapolating the Horner straight line to infinite shut-in time, $(t_p + \Delta t)/\Delta t = 1$. Since a DST is a short-duration test, there is generally no need to correct the extrapolated pressure for drainage shape as done in Chapter 6. The extrapolated p_i should be about the same for both the initial and final shut-in periods. If it is significantly different, a *very small reservoir* or a *bad test* is indicated. The definition of a significant difference depends on the reliability of the data and the buildup extrapolation, but a typical value might be 5 percent. When such a difference occurs, the test should be repeated with a longer final flow period, if possible.

If rate varies significantly during the flow period, then the multiple-rate analysis techniques in Chapter 4 should be used. Odeh and Selig[10] propose a simplified analysis technique that is useful for large rate variations when t_p is less than shut-in time. They suggest modifying t_p as given by Eq. 5.29:

$$t_p{}^* = 2\left[t_p - \frac{\sum_{j=1}^{N} q_j(t_j{}^2 - t_{j-1}{}^2)}{2\sum_{j=1}^{N} q_j(t_j - t_{j-1})}\right] \quad \ldots\ldots\ldots\ldots (8.5)$$

Similarly, q is modified as indicated by Eq. 5.30:

$$q^* = \frac{1}{t_p{}^*}\sum_{j=1}^{N} q_j(t_j - t_{j-1}) \quad \ldots\ldots\ldots\ldots\ldots\ldots (8.6)$$

The modified values, $t_p{}^*$ and q^*, are used in the Horner plot and normal analysis given by Eqs. 8.1 through 8.4.

For all practical purposes, the radius of investigation during a DST is equivalent to the radius of drainage given in Eq. 2.41:

$$r_d = 0.029\sqrt{\frac{kt}{\phi\mu c_t}} \quad \ldots\ldots\ldots\ldots\ldots\ldots (8.7)$$

If a barrier to flow exists within the radius of investigation it might affect the semilog plot. In that case, the distance to the barrier may be estimated from material in Chapter 10 or Ref. 11. Generally, DST's are much too short to see the influence of a boundary. If changes in the slope of the semilog plot of DST data are interpreted as reservoir discontinuities, the results should be viewed with a great deal of skepticism.

Drillstem-Test Buildup Analysis With Limited Data

The analysis procedure explained previously cannot be used if the pressure data available are incomplete. That is usually the case immediately after the DST is completed, since the *full* pressure record is read in the service company offices, not at the wellsite. However, a few key data points are read at the wellsite and given to the engineer just after the test. These include the initial hydrostatic mud pressure, p_{ihm}; the initial shut-in pressure, p_{isi}; the pressure at the end of each flow period, p_{ff1} and p_{ff2}; the final shut-in pressure, p_{fsi}; and the final hydrostatic mud pressure, p_{fhm}. The flow and shut-in period durations are usually also reported. Such limited data may be used to estimate reservoir properties. The initial reservoir pressure is taken as

$$p_i \simeq \bar{p} \simeq p_{isi} \quad \ldots\ldots\ldots\ldots\ldots\ldots\ldots\ldots (8.8)$$

The value of m for the semilog straight line is approximated by

$$m \simeq \frac{p_{isi} - p_{fsi}}{\log\left[(t_p + \Delta t)/\Delta t\right]}, \quad \ldots\ldots\ldots\ldots (8.9)$$

where Δt is the total final shut-in time (time when p_{fsi} was read). Permeability may be estimated from Eq. 8.1. (If the initial and final shut-in pressures are the same, m estimated from Eq. 8.9 will be zero and the approximate method will not be usable.) The *damage ratio* is estimated from[4]

$$\frac{J_{\text{ideal}}}{J_{\text{actual}}} \simeq \frac{0.183\,(p_{isi} - p_{ff2})}{m}, \quad \ldots\ldots\ldots\ldots (8.10)$$

or from[5]

$$\frac{J_{\text{ideal}}}{J_{\text{actual}}} \simeq \frac{p_{isi} - p_{ff2}}{m(4.43 + \log t_p)}, \quad \ldots\ldots\ldots\ldots (8.11)$$

where t_p is in hours. Eqs. 8.9 through 8.11 should be used only when more complete data are not available since they can be significantly in error.

Type-curve matching may be used to analyze pressure buildup data from drillstem tests. When wellbore storage is significant, the type curves in Appendix C, Figs. C.8 (Ref. 12) or C.9 (Ref. 13), may be useful. Type-curve methods are more useful for analyzing flow-period data, as discussed following Example 8.1.

Example 8.1 Drillstem Test Analysis by the Horner Method

Figs. 8.5 and 8.6 show DST data given by Ammann[7] for an open-hole test in the Arbuckle formation.

We first check the recorded hydrostatic mud pressure against the value calculated from gauge depth and mud density. From Fig. 8.6, the depth to the gauge is 4,174 ft and mud density is 10.1 lb_m/gal. Therefore, the hydrostatic mud pressure is

$$p_{hm} \simeq (4{,}174\text{ ft})\left(10.1\ \frac{\text{lb}_\text{m}}{\text{gal}}\right)\left(7.4805\ \frac{\text{lb}_\text{m}/\text{cu ft}}{\text{lb}_\text{m}/\text{gal}}\right)\left(\frac{0.43310\text{ psi/ft}}{62.3664\ \text{lb}_\text{m}/\text{cu ft}}\right)$$

$$\simeq (4{,}174\text{ ft})(0.5247\text{ psig/ft})$$

$$\simeq 2{,}190\text{ psig}.$$

From Fig. 8.6,

$p_{ihm} = 2{,}314$ psig, so the deviation is 5.66 percent, and
$p_{fhm} = 2{,}290$ psig, so the deviation is 4.57 percent.

These deviations are primarily a result of errors and variation in the mud density. The difference of 1.04 percent between p_{ihm} and p_{fhm} may be a result of mud loss. Such differences in the range of 0.5 to 1 percent are indicative of the accuracy of p_i estimated from a DST.

Gauge No. 241			Depth 4174			Clock No. 1547			12 hour	Ticket No. 166710				
	First Flow Period		First Closed In Pressure			Second Flow Period		Second Closed In Pressure			Third Flow Period		Third Closed In Pressure		
	Time Defl. .000"	PSIG Temp. Corr.	Time Defl. .000"	Log $\frac{t+\theta}{\theta}$	PSIG Temp. Corr.	Time Defl. .000"	PSIG Temp. Corr.	Time Defl. .000"	Log $\frac{t+\theta}{\theta}$	PSIG Temp. Corr.	Time Defl. .000"	PSIG Temp. Corr.	Time Defl. .000"	Log $\frac{t+\theta}{\theta}$	PSIG Temp. Corr.
0	.000	57	.000		35	.000	32	.000		145					
1	.008	35	.042		1664	.108	37	.0825		1669					
2	.016	32	.084		1701	.216	50	.165		1699					
3	.024	32	.126		1708	.324	65	.2475		1706					
4	.032	32	.168		1711	.432	80	.330		1711					
5	.040	35	.210		1713	.540	97	.4125		1713					
6			.252		1716	.648	112	.495		1713					
7			.294		1716	.756	130	.5775		1713					
8			.336		1716	.864	145	.660		1716					
9			.378		1716			.7425		1716					
10			.420		1718			.825		1718					
11															
12															
13															
14															
15															
Reading Interval	1		6			15		12							Minutes

REMARKS:

FORM 183-RI—PRINTED IN U.S.A.

SPECIAL PRESSURE DATA

LITTLE'S 96679 75C 6/74

Fig. 8.5 Pressure vs time measurements for a DST from the Arbuckle formation; Example 8.1. After Ammann.[7]

Following an initial flow period of 5 minutes, the shut-in period is 60 minutes (Fig. 8.5). Thus, we make a Horner plot of the final flow-period data with t_p = 2 hours, the length of the second flow period. Times in minutes are obtained by using the time-recording interval shown below each set of readings in Fig. 8.5. Fig. 8.7 is the Horner plot for data from

FLUID SAMPLE DATA

Sampler Pressure _____ PSIG at Surface
Recovery: Cu. Ft. Gas _____
cc. Oil _____
cc. Water _____
cc. Mud _____
Tot. Liquid cc _____
Gravity 44 ° API @ °F.
Gas/Oil Ratio _____ cu. ft./bbl.

		RESISTIVITY		CHLORIDE CONTENT
Recovery Water	@ °F.			ppm
Recovery Mud	@ °F.			ppm
Recovery Mud Filtrate	@ °F.			ppm
Mud Pit Sample	@ °F.			ppm
Mud Pit Sample Filtrate	@ °F.			ppm

Mud Weight 10.1 lb/gal vis 48 cp

Cushion: TYPE None; AMOUNT _____ Ft; Depth Back Pres. Valve _____; Surface Choke 5/8"; Bottom Choke 3/8"

Recovered 300 Feet of oil
Recovered 75 Feet of oil and gas cut mud
Recovered _____ Feet of
Recovered _____ Feet of
Recovered _____ Feet of

Remarks: Set packer, opened tool and took a 5 minute first flow pressure. Rotated tool for a closed in pressure of 60 minutes. Tool opened with a good blow. Gas to surface in 4 minutes. Flowed test in 5 minutes on first flow pressure.

5-3/4" OD - 4-3/4" ID x 16' Perforated Anchor

TEMPERATURE	Gauge No. 241, Depth 4174 ft	Gauge No. 3142, Depth 4193 ft	Gauge No. _____, Depth _____ ft	TIME
Est. 110 °F.	12 Hour Clock	- Hour Clock	Hour Clock	Tool Opened A.M.
Actual °F.	Blanked Off -	Blanked Off no	Blanked Off	Opened P.M.
				Bypass A.M. P.M.

		Pressures Field	Pressures Office	Pressures Field	Pressures Office	Pressures Field	Pressures Office	Reported Minutes	Computed Minutes
Initial Hydrostatic		2280	2314						
First Period Flow	Initial	0	32					—	—
	Final							5	
Closed In		1720	1718					60	
Second Period Flow	Initial		35					—	—
	Final	150	145					120	
Closed In		1695	1718					120	
Third Period Flow	Initial							—	—
	Final								
Closed In								—	—
Final Hydrostatic		2205	2290						

Date 2-16-59 Ticket Number 166710
Kind of Job Open Hole Halliburton District Perry
Tester C. E. Sims Witness Mr. Johnson
Drilling Contractor

EQUIPMENT & HOLE DATA

Formation Tested Arbuckle
Elevation 1123 Ft.
Net Productive Interval 4182-4198 Ft.
All Depths Measured From Ground level
Total Depth 4198 Ft.
Main Hole/Casing Size 8-3/4"
Drill Collar Length 240' I.D. 2-1/2"
Drill Pipe Length O.D. 4-1/2 API FH
Packer Depth(s) 4182 Ft.
Depth Tester Valve Ft.

G. K. Walker, North; Sec. 13-22S-4W; 16; 1; North Covington; Arbuckle; Garfield; Sinclair Oil and Gas Company; Oklahoma

FORM 151-RI—PRINTED IN U.S.A.

FORMATION TEST DATA

LITTLE'S 96677 75C 6/74

Fig. 8.6 Drillstem-test data sheet for a DST from the Arbuckle formation; Example 8.1. After Ammann.[7]

both shut-in periods. Each shut-in has a straight line that extrapolates to p_i = 1,722 psig. Although not shown, the log-log data plot indicates no significant wellbore storage effects during the buildup periods.

To analyze the pressure buildup data we must first estimate the average flow rate during each flow period. The drillpipe was initially empty for this test, so the pressure existing before opening the tool for the first flow was atmospheric. At the end of the first flow period, the pressure was 35 psi (Fig. 8.5). Assuming that all fluid flowing during that time was drilling mud, we may estimate the height of the mud column. From the calculation of hydrostatic mud pressure, the mud exerts a pressure of 0.5247 psi/ft of column height, so 35 psi is equivalent to 35/0.5247 = 67 ft of mud. Fig. 8.6 reports that 75 ft of oil- and gas-cut mud were recovered. This agrees well enough with the estimated 67-ft value to use that value for production during the first flow period. Fig. 8.6 reports that 240 ft of 2.5-in.-ID drill collar were used in the tool string. The capacity of the drill collar is 0.00607 bbl/ft, so 67 ft is equivalent to (67)(0.00607) = 0.407 bbl. Assuming that 0.407 bbl of fluid was produced

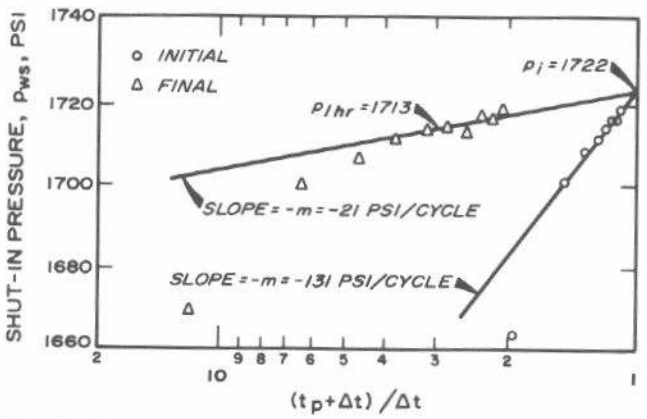

Fig. 8.7 Horner plot for data of Example 8.1. After Ammann.[7]

from the formation in the first 5-minute flow period, we estimate an initial rate of

$$q \simeq (0.407 \text{ bbl}/5 \text{ min})(1{,}440 \text{ min/D}) = 117 \text{ STB/D}.$$

Eq. 8.1 now can be used to estimate kh/μ. Assuming B = 1.0 RB/STB and using m = 131 psi/cycle from Fig. 8.7,

$$\frac{kh}{\mu} \simeq \frac{(162.6)(117)(1)}{131} = 145 \text{ md ft/cp}.$$

If we take h = 16 ft, the tested interval,

$$\frac{k}{\mu} \simeq 145/16 \simeq 9.1 \text{ md/cp}.$$

The pressure increases from 35 psi (at the end of the first flow period) to 145 psi at the end of the second flow period. Measured oil gravity was 44 °API[7] so oil specific gravity is 0.806, corresponding to a gradient of about 0.349 psi/ft. Assuming that all the fluid produced was oil, the pressure increase of 145 − 35 = 110 psi corresponds to 315 ft of oil. Note there are only 240 ft of drill collar (Fig. 8.6); above that there is drillpipe with a capacity of 0.01422 bbl/ft.[7] Assuming that the oil flows through the dense mud, we can estimate the *volume of oil* in the pipe:

$$\begin{aligned} V_o &\simeq (240 \text{ ft drill collar} - 67 \text{ ft mud})(0.00607 \text{ bbl/ft}) \\ &\quad + [315 \text{ ft oil} - (240 - 67) \text{ ft oil in drill collar}] \\ &\quad \times (0.01422 \text{ bbl/ft}) \\ &\simeq 1.05 + 2.02 \\ &\simeq 3.07 \text{ bbl oil recovered}. \end{aligned}$$

Thus,

$$q_o \simeq \frac{3.07 \text{ bbl} \times 1{,}440 \text{ min/D}}{120 \text{ min}} \simeq 36.8 \text{ STB/D}.$$

Using Eq. 8.1 and m = 21 psi/cycle from Fig. 8.7, and assuming B = 1.0 RB/STB,

$$\frac{kh}{\mu} \simeq \frac{(162.6)(36.8)(1)}{21} \simeq 285 \text{ md ft/cp},$$

or

$$\frac{k}{\mu} = 17.8 \text{ md/cp}.$$

This is almost twice the value estimated from the first shut-in period — not unusual in drillstem-test analysis. Part of the discrepancy may be a result of an error in measurement of a flow-period length or in reported pipe sizes. In working this example, Ammann[7] states that there was no drill collar while his data indicate that there was. Most likely, this is where most of the discrepancy arises. Errors are also undoubtedly introduced by the assumption of the type of fluid entering the drillstring (all mud in the first flow period, all oil in the second flow period). Another possible source of some of the discrepancy may be that part of the production during the first flow period is a result of decompression of the wellbore fluid from hydrostatic mud pressure, about 2,300 psig, to the formation pressure of about 1,700 psig. The over-pressure in and near the wellbore can affect both the flow rate and the pressure during the first flow period. Generally, the results from the second flow period and associated buildup are more reliable. In any case, the material above illustrates the approach. Ammann[7] gives a more complete analysis.

To estimate skin factor we assume ϕ = 0.15 and $c_t = 25 \times 10^{-6}$, and use Eq. 8.2 for the second flow period:

$$\begin{aligned} s &\simeq 1.1513 \left\{ \frac{1{,}713 - 145}{21} + \log\left[\frac{2+1}{1}\right] \right. \\ &\quad \left. - \log\left[\frac{17.8}{(0.15)(25 \times 10^{-6})(8.75/24)^2}\right] + 3.2275 \right\} \\ &\simeq 81.5. \end{aligned}$$

The well is severely damaged. We estimate pressure drop across the skin from Eq. 8.4:

$$\begin{aligned} \Delta p_s &\simeq \frac{(141.2)(36.8)(1)}{285}(81.5) \\ &= 1{,}486 \text{ psig}. \end{aligned}$$

From Eq. 8.3, the damage ratio is

$$\frac{1{,}722 - 145}{1{,}722 - 145 - 1{,}486} = 17.3.$$

This indicates the well is producing at only about 6 percent of its ideal capacity. Stimulation would be required for a successful completion.

Although we have sufficient data for a Horner-type analysis, we may apply Eqs. 8.10 and 8.11 to compare methods for estimating the damage ratio. From Eq. 8.10, the damage ratio is

$$\frac{0.183\,(1{,}718 - 145)}{21} = 13.7,$$

and from Eq. 8.11, it is

$$\frac{1{,}718 - 145}{21(4.43 + \log 2)} = 15.8.$$

These values agree reasonably well with the result estimated from the skin factor.

Example 8.1 illustrates some of the problems that can occur in DST pressure analysis. The problem of estimating flow rate is a real one, and must be dealt with by using pressures, densities, volumes of the various fluids produced, and pipe capacities — if flow does not occur at the surface. Inconsistent or inaccurate fluid-volume and pipe-size data, as occur in Example 8.1, make analysis difficult and should be avoided if possible. Normally, one does not analyze pressure data from the first flow and shut-in periods. Results from analyzing those data tend to be less accurate than results from analyzing the second flow and shut-in periods because of longer flow duration and likely absence of mud production during the second flow period.

Analyzing Flow-Period Data

If rate variation can be estimated during the flow period, it is possible to analyze pressure data from the flow period with methods given in Section 4.2. Such multiple-rate

analyses can be particularly useful for wells with substantial flowing bottom-hole pressure increase that either do not flow to the surface or have insufficient surface flow time at a stable rate to provide reliable analysis results from the shut-in pressure data.

Occasionally, the pressure exerted by the produced fluid column can reach the reservoir pressure, causing production to stop during the flow period — the well kills itself. In such cases, data from the shut-in period cannot be analyzed. However, flow-period data can be analyzed by multiple-rate techniques (Section 4.2) or by type-curve matching techniques presented in Refs. 9 and 14 through 17. The type curves in Refs. 14 through 16 do not consider skin factor, so they are not recommended. Ramey, Agarwal, and Martin[9] provide type curves that include skin effect that may be used to analyze DST flow-period data *as long as flow does not reach the surface* and there is no significant change in the wellbore storage coefficient (pipe inner diamater). Figs. 8.8A through 8.8C* are the Ramey-Agarwal-Martin type curves. In those figures, the dimensionless pressure ratio is defined as

$$p_{DR} = \frac{p_D}{p_{Do}} = \frac{p_i - p_{wf}(t)}{p_i - p_o}, \quad \ldots\ldots\ldots\ldots\ldots\ldots (8.12)$$

where p_o is the pressure existing in the drillstring im-

*See footnote on Page 24.

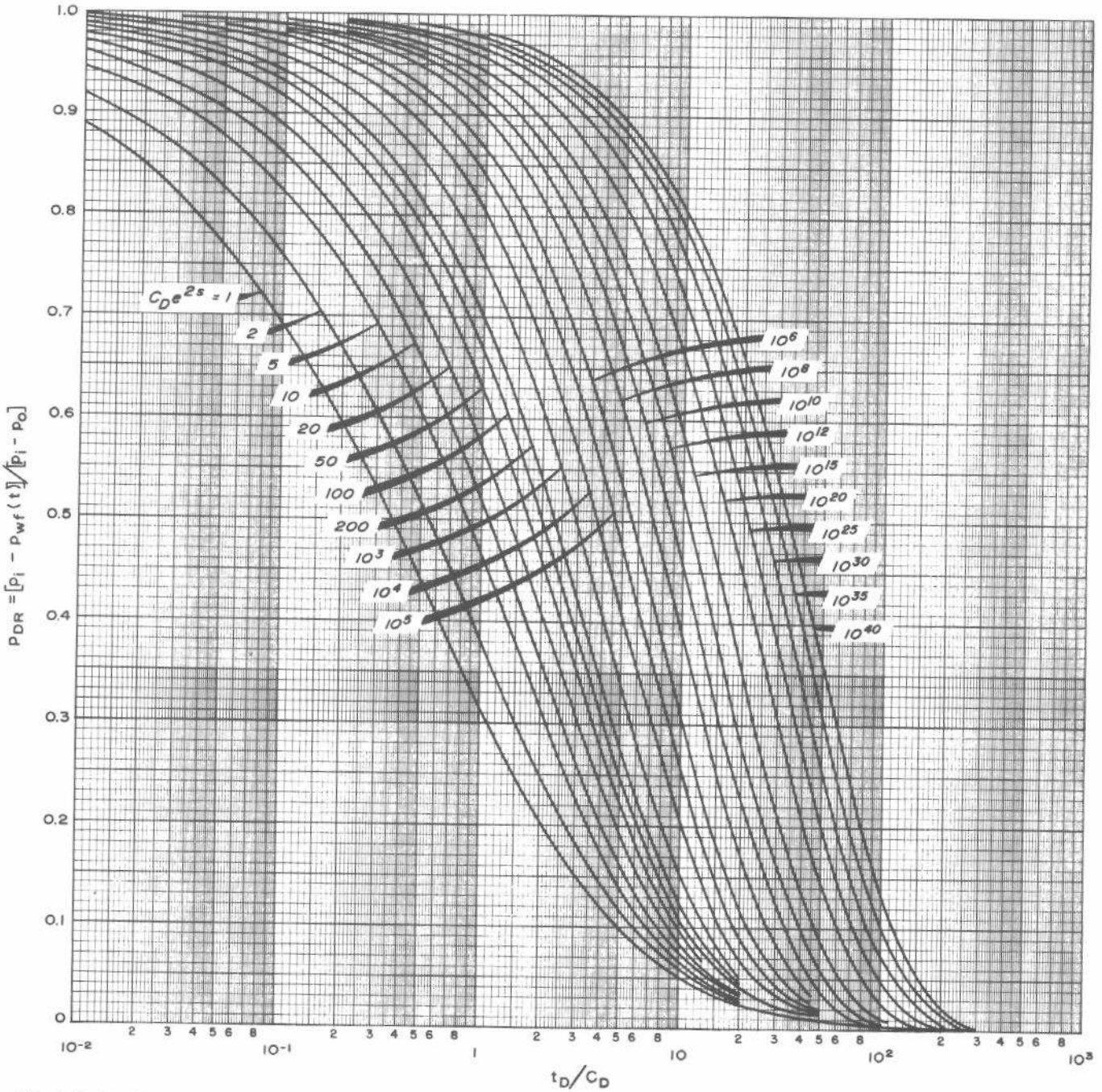

Fig. 8.8A Semilog type curve for DST flow-period data. Best form for early- *and* late-time data. Does not apply to tests that flow at the surface. After Ramey, Agarwal, and Martin.[9] Courtesy CIM.

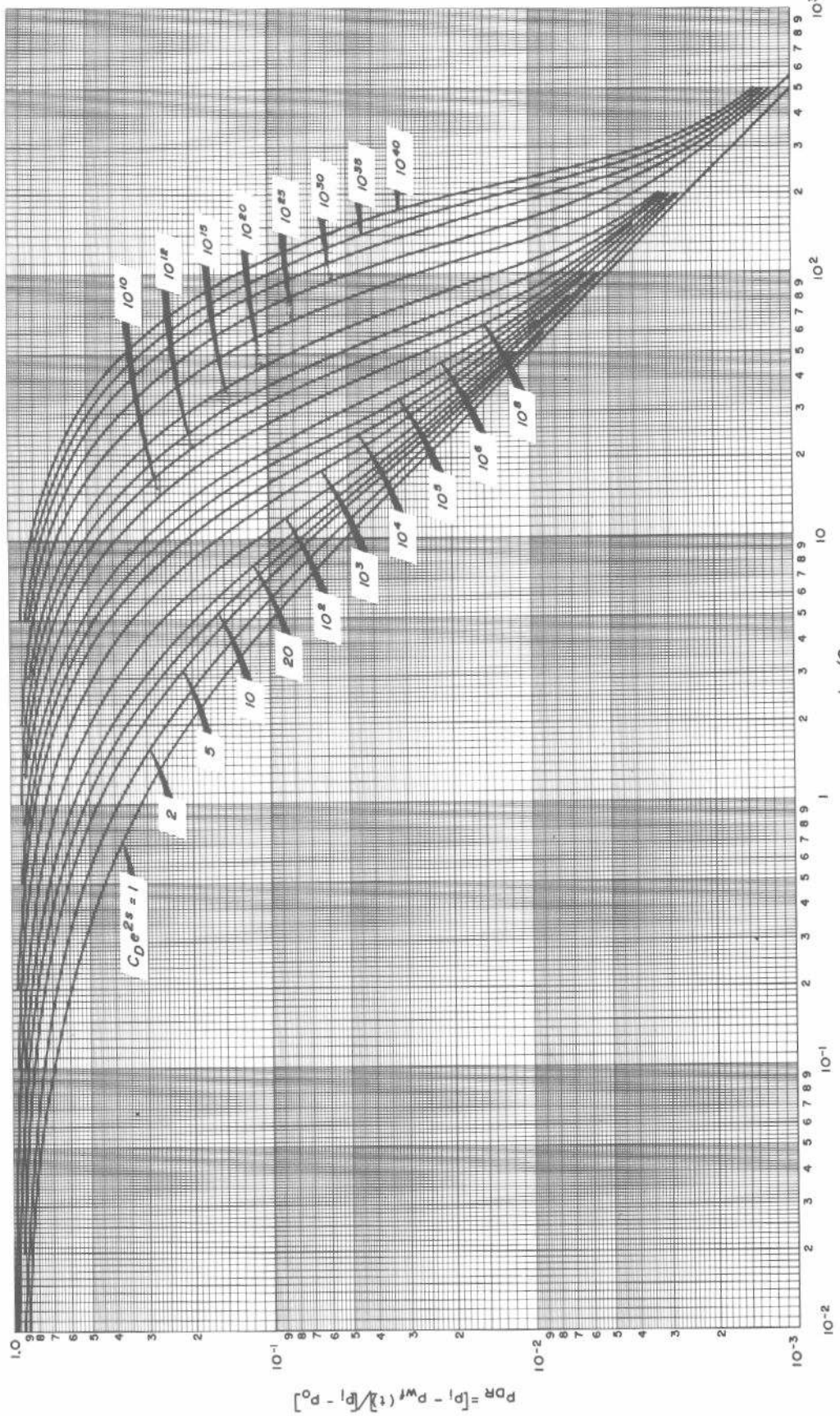

Fig. 8.8B Log-log type curve for DST flow-period data. Best form for late-time data. Does not apply to tests that flow at the surface. After Ramey, Agarwal, and Martin.[9] Courtesy CIM.

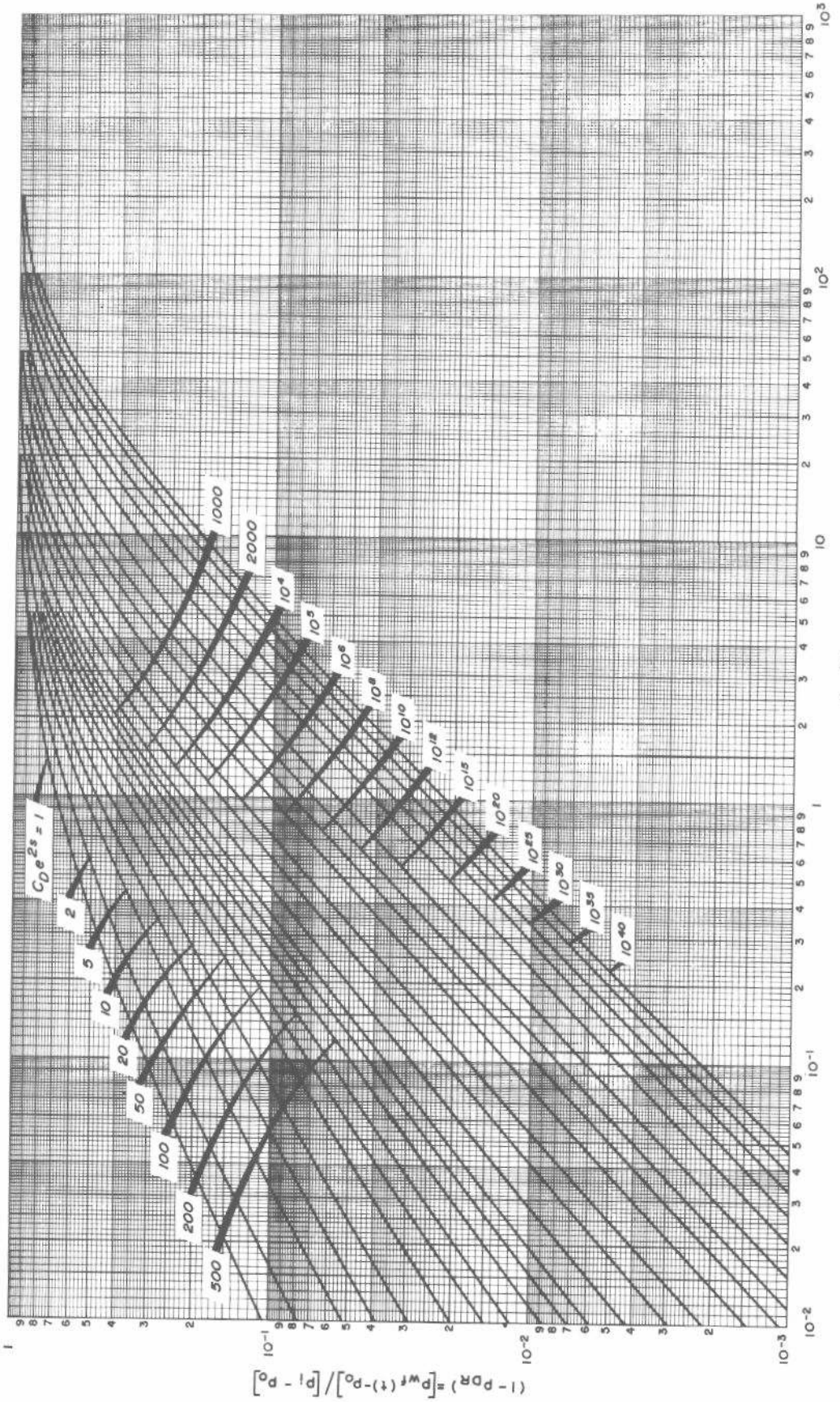

Fig. 8.8C Log-log type curve for DST flow-period data. Best form for early-time data. Does not apply to tests that flow at the surface. After Ramey, Agarwal and Martin.[9] Courtesy CIM.

mediately before the flow period begins. For the initial flow period, p_0 would be atmospheric pressure or the pressure exerted by any fluid cushion in the drillstring; for the final flow period, p_0 would be the pressure at the end of the first flow period. In Fig. 8.8, the dimensionless time is defined by Eq. 2.3a:

$$t_D = \frac{0.0002637\,kt}{\phi\mu c_t r_w^2}, \quad \ldots\ldots\ldots\ldots\ldots\ldots (8.13)$$

and the dimensionless wellbore-storage coefficient is defined by Eq. 2.18:

$$C_D = \frac{5.6146\,C}{2\pi\phi c_t h r_w^2}. \quad \ldots\ldots\ldots\ldots\ldots\ldots (8.14)$$

For a DST flow period, the wellbore storage coefficient usually results from a rising liquid level in the drillpipe. Thus, Eq. 2.16 applies:

$$C = \frac{V_u}{\left(\frac{\rho}{144}\,\frac{g}{g_c}\right)}, \quad \ldots\ldots\ldots\ldots\ldots\ldots (8.15)$$

where V_u is the volume per unit length of the drillpipe in barrels per foot. Note that this monograph uses different units for C than do Ramey, Agarwal, and Martin.[9]

The type-curve matching technique is similar to the method described in Section 3.3, with one important simplification: the pressure ratio in Fig. 8.8 always goes from zero to one and is independent of flow rate and formation properties. Thus, when plotting data on the tracing paper laid over the grid of Fig. 8.8A, 8.8B, or 8.8C, the pressure scale is fixed. When the tracing-paper data plot is slid to match one of the type curves, only horizontal motion is used. That simplifies the matching technique. Once the experimental data have been matched to one of the type curves, data from both the overlay and the underlying type curve are read at a convenient match point. Three data items are required: the parameter on the curve matched, $(C_D e^{2s})_M$; the time-scale match point, t_M, from the data plot; and the corresponding point from the type curve, $(t_D/C_D)_M$. Permeability may be estimated from the time-scale match point by using

$$k = 3{,}389\,\frac{\mu}{h}\,\frac{C}{t_M}\left(\frac{t_D}{C_D}\right)_M. \quad \ldots\ldots\ldots\ldots\ldots\ldots (8.16)$$

It is not necessary to know the flow rate to estimate permeability by this method. It is necessary to estimate the wellbore storage coefficient from Eq. 8.15, so the fluid density must be known. Skin factor is estimated from the parameter on the curve matched:

$$s = \frac{1}{2}\ln\left[\frac{\phi c_t h r_w^2\,(C_D e^{2s})_M}{0.89359\,C}\right]. \quad \ldots\ldots\ldots\ldots\ldots\ldots (8.17)$$

As usual, it is necessary to have values for porosity, total system compressibility, formation thickness, and wellbore radius to estimate the skin factor. Damage ratio then may be estimated from Eq. 8.3.

Ramey, Agarwal, and Martin[9] suggest that all three type curves be used to analyze DST flow-period data. That requires plotting the data three times and making three curve matches. Eqs. 8.16 and 8.17 apply to all three curve matches. The semilog type curve, Fig. 8.8A, usually should be best when both early and relatively late-time data are available. Fig. 8.8B provides poor resolution of early-time data, while Fig. 8.8C is useful for early-time data.

Type curves in Figs. 8.8A through 8.8C can be used to conveniently estimate permeability and skin factor from DST flow-period data. However, they are not applicable when fluid influx to the drillstem is at essentially constant rate; that is, when flow occurs at the surface. They are also not applicable when the wellbore storage coefficient changes (because of pipe size or compressibility changes). Such changes are illustrated by Figs. 8.20 and 8.21.

Example 8.2 Analysis of Drillstem-Test Flow Data by Type-Curve Matching

Ramey, Agarwal, and Martin[9] give the pressure data in Table 8.2 for the second flow period of a DST. Other data are

$p_i = 3{,}475$ psig (initial shut-in pressure)	$\phi = 0.16$
$p_0 = 643$ psig	$c_t = 8.0 \times 10^{-6}$ psi^{-1}
$r_w = 3.94$ in.	$\mu = 1.0$ cp
$V_u = 0.0197$ bbl/ft	$h = 17$ ft
	$\rho = 52.78$ lb$_m$/cu ft.

TABLE 8.2—DST DATA FOR FLOW-PERIOD ANALYSIS OF EXAMPLE 8.2.
(From Ramey, Agarwal, and Miller.[9])

Time (minutes)	p_{wf} (psig)	$\frac{p_i - p_{wf}(t)}{p_i - p_0}$
0	643	1.0000
3	665	0.9922
6	672	0.9898
9	692	0.9827
12	737	0.9668
15	786	0.9495
18	832	0.9333
21	874	0.9184
24	919	0.9025
27	962	0.8874
30	1,005	0.8722
33	1,046	0.8577
36	1,085	0.8439
39	1,128	0.8287
42	1,170	0.8139
45	1,208	0.8005
48	1,248	0.7864
51	1,289	0.7719
54	1,318	0.7617
57	1,361	0.7465
60	1,395	0.7345
63	1,430	0.7221
66	1,467	0.7090
69	1,499	0.6977
72	1,536	0.6847
75	1,570	0.6727
78	1,602	0.6614
81	1,628	0.6522
84	1,655	0.6427
87	1,683	0.6328
90	1,713	0.6222
93	1,737	0.6137
96	1,767	0.6031
99	1,794	0.5936
102	1,819	0.5847
105	1,845	0.5756
108	1,869	0.5671
111	1,894	0.5583
114	1,917	0.5501
117	1,948	0.5392
120	1,969	0.5318

Fig. 8.9 shows the data of Table 8.2 matched to Fig. 8.8A. The matchpoint data are

$$(C_D e^{2s})_M = 10^{10},$$

$$(t_D/C_D)_M = 0.65,$$

and

$$t_M = 10 \text{ minutes} = 0.1667 \text{ hour}.$$

We estimate permeability from Eq. 8.16, but to do this the wellbore storage coefficient must first be estimated from Eq. 8.15:

$$C = \frac{0.0197}{\left(\frac{52.78}{144}\right)\left(\frac{32.17}{32.17}\right)} = 0.0537 \text{ bbl/psi}.$$

Then, using Eq. 8.16,

$$k = \frac{(3{,}389)(1.0)(0.0537)(0.65)}{(17)(0.1667)}$$

$$= 41.7 \text{ md}.$$

Using the parameter on the matched curve and Eq. 8.17,

$$s = \frac{1}{2} \ln \left[\frac{(0.16)(8.0 \times 10^{-6})(17)(3.94/12)^2(10^{10})}{(0.89359)(0.0537)} \right]$$

$$= 6.5.$$

Ramey, Agarwal, and Martin[9] indicate that the flow rate was constant owing to critical flow at early flow time. This curve-matching technique does not apply under constant-rate conditions, so the early data should not be considered in the curve match. Clearly, they do not match the entire $C_D e^{2s} = 10^{10}$ curve of Fig. 8.8A, as shown in Fig. 8.9. In fact, they do not completely match other curves in Fig. 8.8A. Unfortunately, several curves can be matched with the late-time data. The match shown in Fig. 8.9 is the lowest value of $C_D e^{2s}$ for which the most points matched the curve. At lower $C_D e^{2s}$ values fewer points match; at higher values no more points match.

Ramey, Agarwal, and Martin[9] report that (1) core analysis showed an average permeability of 35.4 md for the zone tested; and (2) a Horner-type analysis of the second shut-in period (with average flow rate) indicated $k = 22.2$ md, and a damage ratio of 1.16.

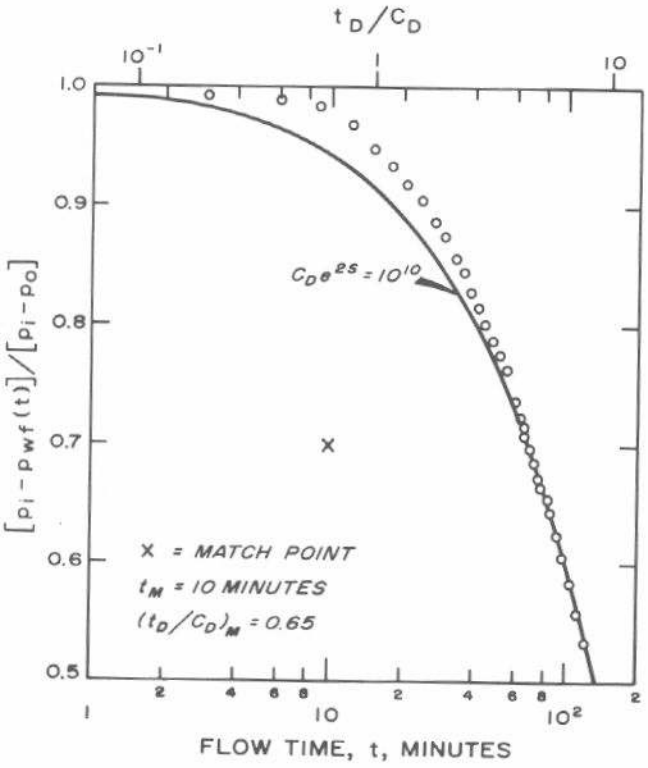

Fig. 8.9 Type-curve match for DST flow data of Example 8.2; type curve of Fig. 8.8A. After Ramey, Agarwal and Martin.[9]

Example 8.2 illustrates the mechanics of using Figs. 8.8A through 8.8C for analysis of DST flow-period data. It also illustrates that the technique should be used with caution. Periods of constant rate flow during a DST (manifested by a linear p vs t trace on the DST chart) are not unusual. When they occur, they can rule out analysis by curve matching with Figs. 8.8A through 8.8C — or at best make the results have doubtful validity.

Computer Matching Drillstem-Test Data

It does appear feasible to use all the data obtained during a DST for test analysis.[18] Such analysis requires a numerical reservoir simulator and uses a history-matching approach to vary formation properties until the DST pressure and rate behavior are matched by the simulator. Since the technique uses all the data, it should be particularly useful when conventional interpretation techniques cannot be applied with confidence.

8.4 Trouble Shooting Drillstem-Test Pressure Charts

Because of the complexity of the DST tool operation, there are many opportunities for test failure. Therefore, it is important to carefully examine the DST charts and decide if the test was mechanically and operationally successful. That should be done at the wellsite so that the option of rerunning the test may be exercised if necessary.

To recognize a poor DST, one must be familiar with DST chart characteristics. Murphy[19] and Timmerman and van Poollen[20] provide such information. A good DST chart has the following characteristics.

1. The pressure base line is straight and clear.
2. Recorded initial and final hydrostatic mud pressures are the same and are consistent with depth and mud weight.
3. Flow and buildup pressures are recorded as smooth curves.

Frequently, bad hole conditions, tool malfunctions, and other difficulties can be identified from the DST charts. Figs. 8.10 through 8.23 illustrate many situations. The captions explain the characteristic indicated by each figure.

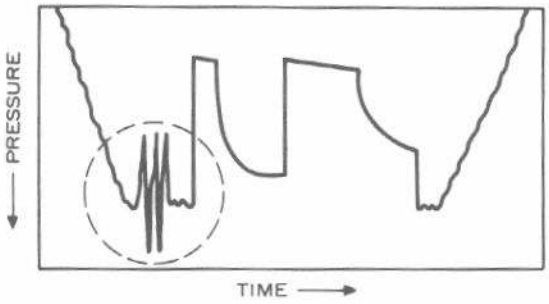

Fig. 8.10 Tight hole condition. This may cause pressure surging or tool sticking.

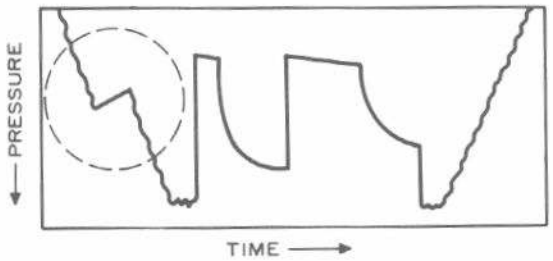

Fig. 8.11 Leaking drillpipe or mud loss to some formation, or both, are indicated by the hydrostatic mud-pressure decrease shown here. A leaking drillpipe may be confirmed if an abnormally large amount of mud is recovered with the produced fluids. In this case test data must be disregarded.

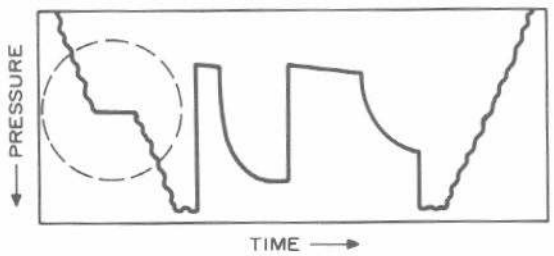

Fig. 8.12 Delay while going into the hole without mud loss.

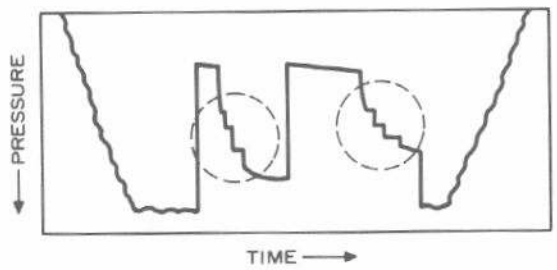

Fig. 8.13 The stair-stepping pattern in the buildup curves indicates a malfunctioning pressure gauge or recorder. Such test data cannot be analyzed.

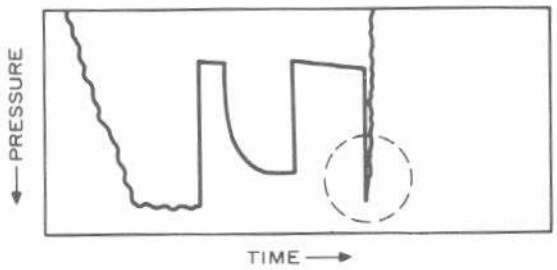

Fig. 8.14 Clock stopped.

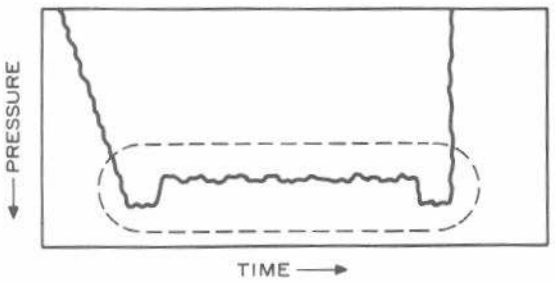

Fig. 8.15 Clock ran away.

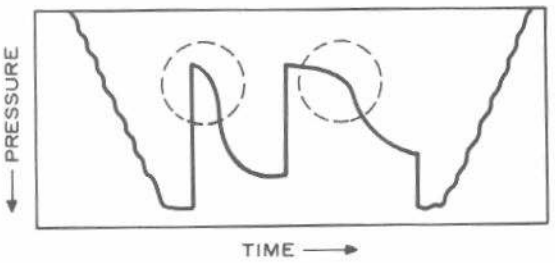

Fig. 8.16 The S shape of the latter part of the flow curve and the early part of the buildup curve indicates fluid communication around the packer. This may be caused by a fracture or a poorly seated packer.

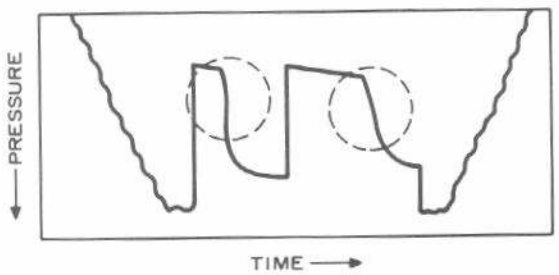

Fig. 8.17 An S shape occurring only in the buildup portion of the curve indicates gas is going into solution in the wellbore. This mechanism is characterized by a *sharp transition* between the flow and buildup curves.

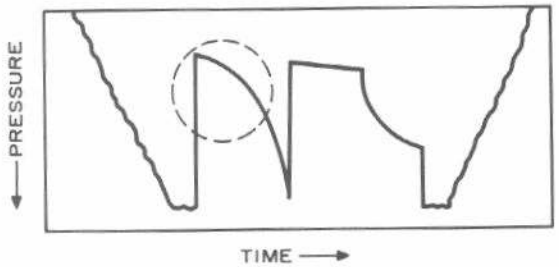

Fig. 8.18 An S-shaped curve occurs only in the first flow period when the volume below the closed-in pressure valve is large compared with the volume of the fluid flowed during the flow period. A wellbore storage effect caused by the relatively large volume between the hydrospring tester and CIP valves.

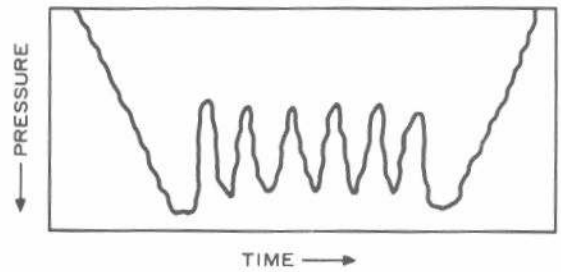

Fig. 8.19 This behavior indicates a plugged bottom-hole choke or perforated anchor. The up-and-down nature of the pressure curve is caused by momentary breakthrough and release of the pressure.

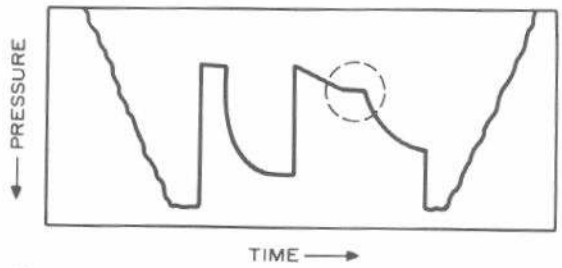

Fig. 8.20 The flat portion in the second flow period indicates the well is flowing at the surface.

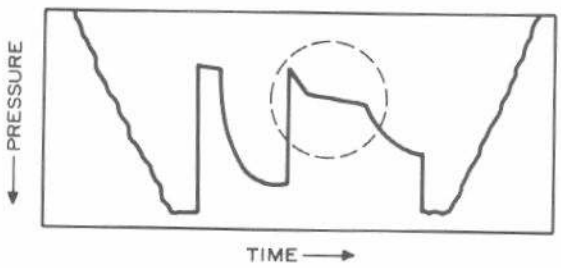

Fig. 8.21 A decrease in slope in either flow period indicates fillup of the drill collar and transition to a drillpipe of a larger internal diameter.

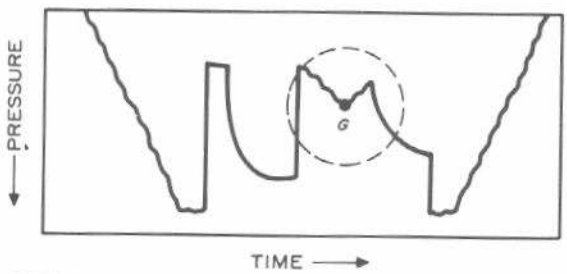

Fig. 8.22 This behavior typically occurs in gas reservoirs when flow occurs at the surface. The pressure decrease at Point G is caused by the water cushion flowing at the surface, which decreases average density of the flowing column.

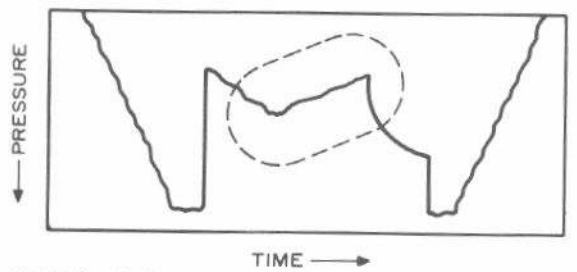

Fig. 8.23 The rippled appearance in the flow curve indicates that gas has broken through the liquid in the drillstring and the well is flowing by heads.

8.5 Wireline Formation Tests

A quick and inexpensive alternative to a drillstem test may be a test run with a wireline formation tester.[21-24] That tool, run on a wireline from a logging truck, includes a pad on an expanding mechanism that presses against the formation face, a means for establishing fluid communication between the formation and the tool, a sample chamber, and a pressure transducer with surface recorder.

The tester is lowered into the well on a logging cable while the mechanism is collapsed. The tool is located opposite the formation to be tested, the mechanism is expanded, and fluid communication is established. Formation fluid flows into the chamber and the pressure response is recorded. A new version of the tool may be set and used at several locations during a single run.[24]

Interpretation of wireline-formation-tester pressure data is semiqualitative, so the information obtained is inferior to that of a normal DST. More recent tools with larger fluid chambers (~12 gal vs 2.75 to 5 gal) tend to give reasonable fluid-recovery and p_i results. Although permeability may be estimated from the wireline formation tester, the degree of uncertainty is high. The skin factor cannot be estimated. A general rule for interpretation based on experience in Canada and in the Rocky Mountain region is presented in Refs. 22 and 23.

References

1. Matthews, C. S. and Russell, D. G.: *Pressure Buildup and Flow Tests in Wells*, Monograph Series, Society of Petroleum Engineers of AIME, Dallas (1967) **1**, Chap. 9.

2. van Poollen, H. K.: "Status of Drill-Stem Testing Techniques and Analysis," *J. Pet. Tech.* (April 1961) 333-339. Also *Reprint Series, No. 9 — Pressure Analysis Methods*, Society of Petroleum Engineers of AIME, Dallas (1967) 104-110.

3. McAlister, J. A., Nutter, B. P., and Lebourg, M.: "A New System of Tools for Better Control and Interpretation of Drill-Stem Tests," *J. Pet. Tech.* (Feb. 1965) 207-214; *Trans.*, AIME, **234.**

4. Edwards, A. G. and Winn, R. H.: "A Summary of Modern Tools and Techniques Used in Drill Stem Testing," Publication T-4069, Halliburton Co., Duncan, Okla. (Sept. 1973).

5. "Review of Basic Formation Evaluation," Form J-328, Johnston Schlumberger, Houston (1974).

6. Edwards, A. G. and Shryock, S. H.: "New Generation Drill Stem Testing Tools/Technology," *Pet. Eng.* (July 1974) 46, 51, 56, 58, 61.

7. Ammann, Charles B.: "Case Histories of Analyses of Characteristics of Reservoir Rock From Drill-Stem Tests," *J. Pet. Tech.* (May 1960) 27-36.

8. Kazemi, Hossein: "Damage Ratio From Drill-Stem Tests With Variable Back Pressure," paper SPE 1458 presented at the SPE-AIME California Regional Meeting, Santa Barbara, Nov. 17-18, 1966.

9. Ramey, Henry J., Jr., Agarwal, Ram G., and Martin, Ian: "Analysis of 'Slug Test' or DST Flow Period Data," *J. Cdn. Pet. Tech.* (July-Sept. 1975) 37-42.

10. Odeh, A. S. and Selig, F.: "Pressure Build-Up Analysis, Variable-Rate Case," *J. Pet. Tech.* (July 1963) 790-794; *Trans.*, AIME, **228.** Also *Reprint Series, No. 9 — Pressure Analysis Methods*, Society of Petroleum Engineers of AIME, Dallas (1967) 131-135.

11. Gibson, J. A. and Campbell, A. T., Jr.: "Calculating the Distance to a Discontinuity From D.S.T. Data," paper SPE 3016 presented at the SPE-AIME 45th Annual Fall Meeting, Houston, Oct. 4-7, 1970.

12. Earlougher, Robert C., Jr., and Kersch, Keith M.: "Analysis of Short-Time Transient Test Data by Type-Curve Matching," *J. Pet. Tech.* (July 1974) 793-800; *Trans.*, AIME, **257.**

13. McKinley, R. M.: "Wellbore Transmissibility From Afterflow-Dominated Pressure Buildup Data," *J. Pet. Tech.* (July 1971) 863-872; *Trans.*, AIME, **251.**

14. Papadopulos, Istavros S. and Cooper, Hilton H., Jr.: "Drawdown in a Well of Large Diameter," *Water Resources Res.* (1967) **3,** No. 1, 241-244.

15. Cooper, Hilton H., Jr., Bredehoeft, John D., and Papadopulos, Istavros S.: "Response of a Finite-Diameter Well to an Instantaneous Charge of Water," *Water Resources Res.* (1967) **3,** No. 1, 263-269.

16. Kohlhaas, Charles A.: "A Method for Analyzing Pressures Measured During Drillstem-Test Flow Periods," *J. Pet. Tech.* (Oct. 1972) 1278-1282; *Trans.*, AIME, **253.**

17. Ramey, Henry J., Jr., and Agarwal, Ram G.: "Annulus Unloading Rates as Influenced by Wellbore Storage and Skin Effect," *Soc. Pet. Eng. J.* (Oct. 1972) 453-462; *Trans.*, AIME, **253.**

18. Brill, J. P., Bourgoyne, A. T., and Dixon, T. N.: "Numerical Simulation of Drillstem Tests as an Interpretation Technique," *J. Pet. Tech.* (Nov. 1969) 1413-1420.

19. Murphy, W. C.: "The Interpretation and Calculation of Formation Characteristics From Formation Test Data," Pamphlet T-101, Halliburton Co., Duncan, Okla. (1970).

20. Timmerman, E. H. and van Poollen, H. K.: "Practical Use of Drill-Stem Tests," *J. Cdn. Pet. Tech.* (April-June 1972) 31-41.

21. Moran, J. H. and Finklea, E. E.: "Theoretical Analysis of Pressure Phenomena Associated With the Wireline Formation Tester," *J. Pet. Tech.* (Aug. 1962) 899-908; *Trans.*, AIME, **225.**

22. Burnett, O. W. and Mixa, E.: "Application of the Formation Interval Tester in the Rocky Mountain Area," *Drill. and Prod. Prac.*, API (1964) 131-140.

23. Banks, K. M.: "Recent Achievements With the Formation Tester in Canada," *J. Cdn. Pet. Tech.* (July-Sept. 1963) 84-94.

24. Schultz, A. L., Bell, W. T., and Urbanosky, H. J.: "Advances in Uncased-Hole, Wireline Formation-Tester Techniques," *J. Pet. Tech.* (Nov. 1975) 1331-1336.

Chapter 9

Multiple-Well Testing

9.1 Introduction

A multiple-well transient test, including both interference (Section 9.2) and pulse (Section 9.3) tests, directly involves more than one well. In an interference test, a long-duration rate modification in one well creates a pressure interference in an observation well that can be analyzed for reservoir properties. A pulse test provides equivalent data by using shorter-rate pulses (with smaller observed pressure changes), but the analysis technique is more complicated. While numerous variations are possible, this chapter presents only basic techniques for analyzing simple interference and pulse tests. For more complex tests, material in Chapter 2 may be used to devise an appropriate analysis technique. Computer assistance may be helpful in analyzing multiple-well tests, but usable answers can be easily computed in many cases using techniques presented in this chapter.

The multiple-well test requires at least one active (producing or injecting) well and at least one pressure-observation well. Fig. 9.1 schematically illustrates two wells being used in an interference or pulse test in a large reservoir. The observation well is shut in for pressure measurement. (Theory does not preclude an active observation well, but practical considerations rule that out.) In multiple-well testing, the flow rate at the active well is varied while bottomhole pressure response is measured at the observation wells.

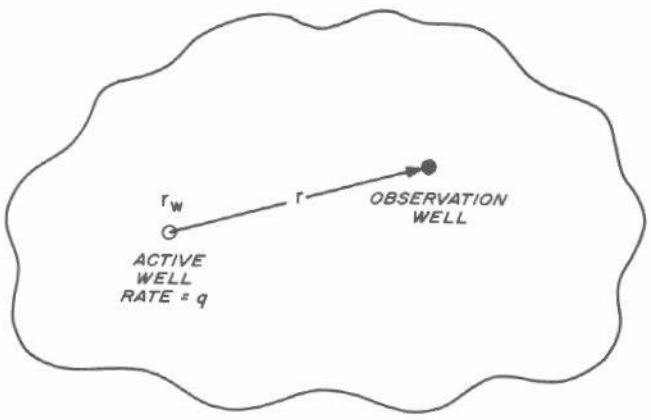

Fig. 9.1 Active and observation wells in an interference or pulse test.

Fig. 9.2 is a schematic illustration of rate history at the active well and pressure response at both the active and observation wells.

Multiple-well testing has the advantage of generally investigating more reservoir than a single-well test.[1-4] Although it is a common belief that interference testing provides information about only the region between the wells, test results are actually influenced by a much larger region. Vela and McKinley[5] show that the influence region for pulse

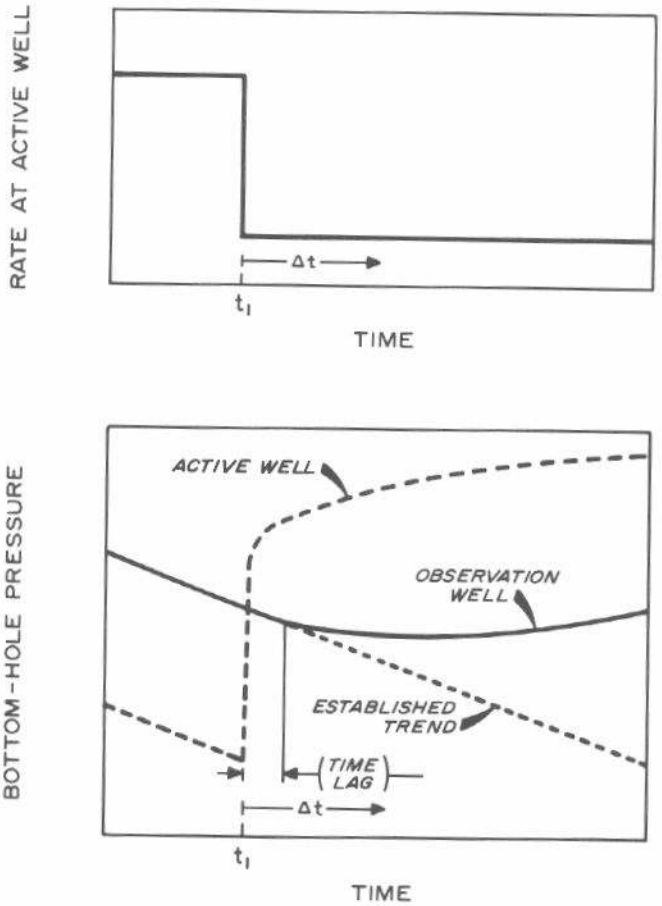

Fig. 9.2 Schematic illustration of rate history and pressure response for an interference test.

testing is approximately as indicated in Fig. 9.3. The radius of influence is given by

$$r_{inf} = 0.029\sqrt{\frac{kt}{\phi\mu c_t}}. \quad \ldots\ldots\ldots\ldots\ldots\ldots (9.1)$$

We can expect a similar influence region in normal interference testing. The major difference is that the testing time, t, is much larger in interference testing than in pulse testing. Thus, r_{inf} and the total influence region are substantially larger in interference testing than in pulse testing. In general, we cannot estimate quantitative areal variations in permeability and porosity-compressibility product without using some type of reservoir simulator.[6] That is partially because of inhomogeneities and anisotropy and partly because of the nonuniqueness of analysis techniques.[6-8] If the reservoir can be assumed to be homogeneous, then it may be possible to estimate anisotropic reservoir properties[9-11] by using multiple observation wells.

The skin effect does not influence a multiple-well test since the skin affects only the active well — as long as the skin is concentrated directly around the well. However, a large negative skin or a fracture can affect observation-well response.[12] Wellbore storage effects are minimized by interference and pulse testing, but are not completely eliminated. More research is required to understand the effect of wellbore storage on multiple-well testing.

Usually, both the mobility-thickness product, kh/μ, and the porosity-compressibility-thickness product, $\phi c_t h$, may be estimated from a multiple-well test. In some cases, reservoir extent (Section 9.2) or anisotropic permeability values and orientation (Section 9.4) may be estimated. In reservoirs with fluid-fluid contacts (gas cap-oil zone, for example) in the influence region, interference and pulse tests may yield unreliable or meaningless results because of the different properties in the different fluid regions.

9.2 Interference-Test Analysis

Type-Curve Matching

Type-curve matching is applied to interference-test analysis in basically the same manner as it is applied to drawdown testing (Section 3.3). Fortunately, type-curve matching is simpler for interference testing than for single-well testing because there is usually only one type curve (Fig. C.2) to consider for infinite-acting systems.

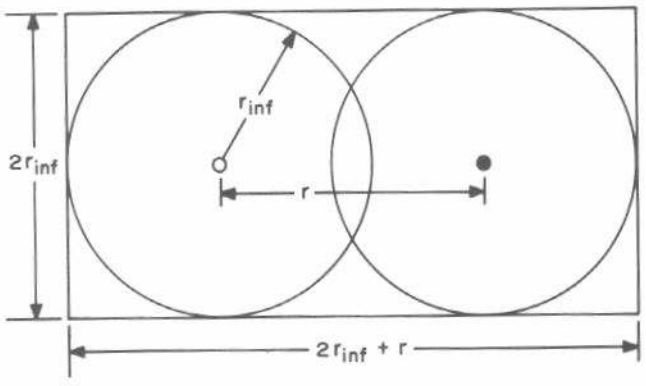

Fig. 9.3 Approximate influence region in interference and pulse testing. After Vela and McKinley.[5]

To analyze an interference test by type-curve matching, one plots the observation-well pressure data as Δp vs t on tracing paper laid over Fig. C.2, using the technique described in Section 3.3 and Fig. 3.5. The major grid lines are traced and the grid of Fig. C.2 is used to locate the data points, without regard for the curve on Fig. C.2. Then the tracing paper is slid horizontally and vertically until the data points match the exponential-integral curve on Fig. C.2, as illustrated in Fig. 9.4. When the data are matched to the curve, a convenient match point such as that shown in Fig. 9.4 is chosen, and match-point values from the tracing paper and the underlying type-curve grid are read. Permeability is estimated from

$$k = \frac{141.2\,qB\mu}{h}\,\frac{(p_D)_M}{\Delta p_M}, \quad \ldots\ldots\ldots\ldots\ldots (9.2)$$

and the porosity-compressibility product is estimated from

$$\phi c_t = \frac{0.0002637}{r^2}\,\frac{k}{\mu}\,\frac{t_M}{(t_D/r_D{}^2)_M}. \quad \ldots\ldots\ldots (9.3)$$

The type-curve analysis method is simple, fast, and accurate when the exponential integral p_D applies; that is, when $r_D = r/r_w > 20$ and $t_D/r_D{}^2 > 0.5$.

If the active well is shut in after time t_1, the resulting change in pressure at the observation well may be further analyzed, thus improving the accuracy of the analysis. (Here we assume that the active well is producing or injecting during the interference test. Of course, it could have been shut in to create the interference test. In that case, the analogy to shutting in a producing or injecting well is resumption of production or injection after the shut-in period.) Fig. 9.5 schematically illustrates how the data are used when the rate condition preceding the test is resumed. The data during the first portion of the test are matched to the type curve of Fig. C.2, as indicated by the data points that fall on the solid line in Fig. 9.5. After the change in rate, the difference between the extrapolated, matched type curve and the actual data points, $\Delta p_{\Delta t}$, is determined from the data plot; Δt is the time from the change in rate at the active well to the time the data are taken. It can be shown by superposition that

$$\Delta p_{\Delta t} = \Delta p_{w\,ext} - \Delta p_{ws}, \quad \ldots\ldots\ldots\ldots\ldots (9.4a)$$

$$= \frac{141.2\,qB\mu}{kh}\,p_D(\Delta t_D, r_D), \quad \ldots\ldots\ldots (9.4b)$$

where p_D is simply the exponential integral (Fig. C.2). Thus, when $\Delta p_{\Delta t}$ is plotted vs Δt on the same data plot, the points should fall on the curve matched by the original data. If they do not, then either (1) the original data were not matched correctly and the match should be repeated until the two portions of the data fall on the same curve; or (2) something else is influencing the response at the interference well that precludes correct type-curve matching. The following example illustrates interference-test analysis by type-curve matching for a 48-hour injection period followed by a long falloff.

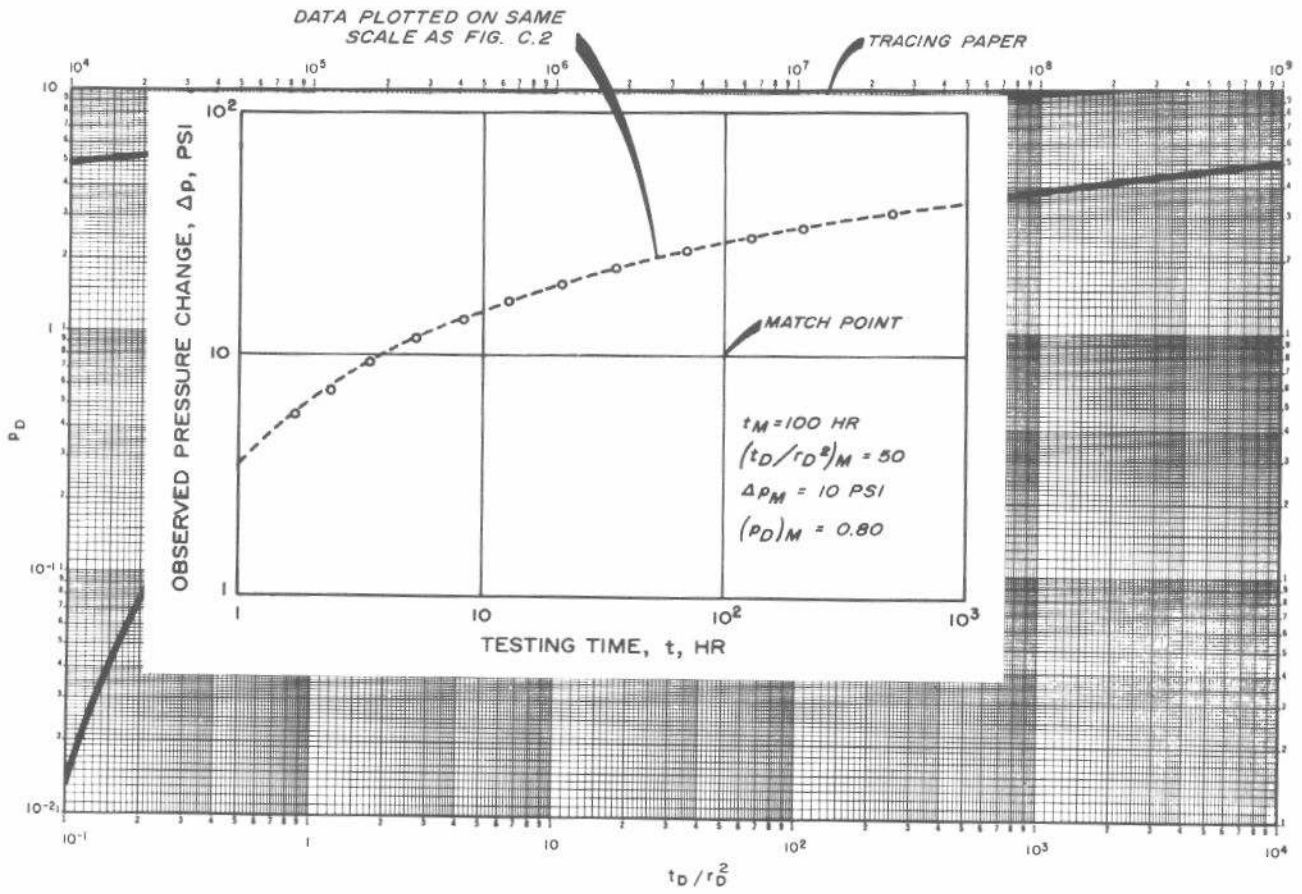

Fig. 9.4 Illustration of type-curve matching for an interference test using the type curve of Fig. C.2.

Example 9.1 Interference-Test Analysis by Type-Curve Matching

During an interference test, water was injected into Well A for 48 hours. The pressure response in Well B, 119 ft away, was observed for 148 hours. Known reservoir properties are

depth = 2,000 ft	$B_w = 1.0$ RB/STB
$q = -170$ B/D	$\mu_w = 1.0$ cp
$h = 45$ ft	$r = 119$ ft
$p_i = 0$ psig	$c_t = 9.0 \times 10^{-6}$ psi^{-1}.
$t_1 = 48$ hours	

Observed pressure data are given in Table 9.1.

The open circles in Fig. 9.6 show the data match to the type curve of Fig. C.2. We have plotted Δp as positive, even though it is actually negative, since it is not possible to take logarithms of negative numbers. We could remember that Δp is negative to prevent confusion in signs in the analysis; however, that is not a major problem because we know that both k and ϕc_t must be positive. The line in Fig. 9.6 was traced from the type curve of Fig. C.2, using the overlay technique for data points before 48 hours. Although we would prefer to have more than four data points, the match is acceptable. At the *match point* marked,

TABLE 9.1—INTERFERENCE DATA FOR EXAMPLES 9.1 AND 9.3, INJECTION FOR 48 HOURS.

t (hours)	p_w (psig)	$\Delta p = p_i - p_w$ (psi)
0.0	0	—
4.3	22	−22
21.6	82	−82
28.2	95	−95
45.0	119	−119
48.0	---------Injection Ends---------	
51.0	109	−109
69.0	55	−55
73.0	47	−47
93.0	32	−32
142.0	16	−16
148.0	15	−15

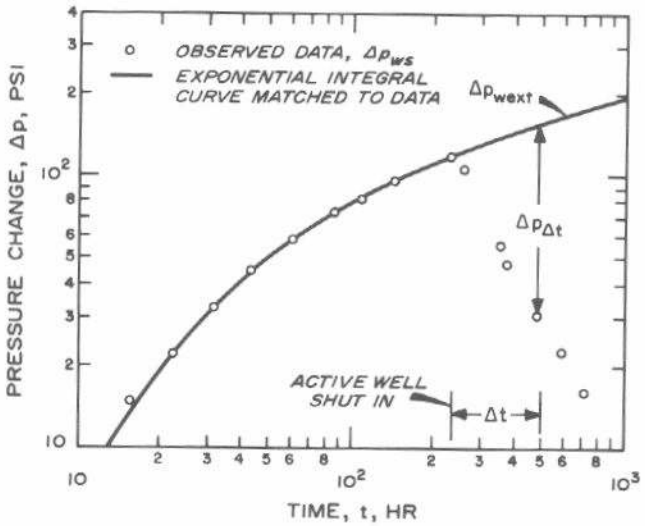

Fig. 9.5 Schematic observation-well pressure response for an interference test with the active well shut in after 240 hours.

$\Delta p_M = -100$ psig at $(p_D)_M = 0.96$,

and

$t_M = 10$ hours at $(t_D/r_D^2)_M = 0.94$.

Using Eq. 9.2,

$$k = \frac{141.2(-170)(1.0)(1.0)}{(45)} \frac{(0.96)}{(-100)}$$

$$= 5.1 \text{ md}.$$

From Eq. 9.3,

$$\phi c_t = \frac{(0.0002637)(5.1)}{(119)^2(1.0)} \frac{10}{0.94}$$

$$= 1.01 \times 10^{-6} \text{ psi}^{-1},$$

and

$$\phi = \frac{1.01 \times 10^{-6}}{9.0 \times 10^{-6}} = 0.11.$$

We can estimate the accuracy of the above analysis by using the data from the declining-pressure part of the test ($t > 48$ hours). We extrapolate the solid line in Fig. 9.6 by tracing the curve from Fig. C.2, and estimate the difference between Δp_{ext} and the observed Δp, $\Delta p_{\Delta t}$. Table 9.2 shows the computations.

The plus symbols in Fig. 9.6 are a plot of $\Delta p_{\Delta t}$ vs Δt. The points fall on just about the same line as the circles, so we can be confident of the analysis results.

Example 12.1 treats the same interference-test data using computer analysis techniques.

Earlougher and Ramey[13] provide dimensionless pressure data that are useful for interference-test analysis in bounded systems. They give p_D at several observation-well locations for a variety of closed rectangular systems with one active well. Fig. 9.7 shows p_D values for a variety of observation-well positions in a 2:1 rectangle. Fig. 9.8 shows the location of the active well in Fig. 9.7 and defines the dimensionless distance coordinates. Note that the dimensionless pressure response at each observation well deviates upward from the exponential-integral solution, as we would expect in a

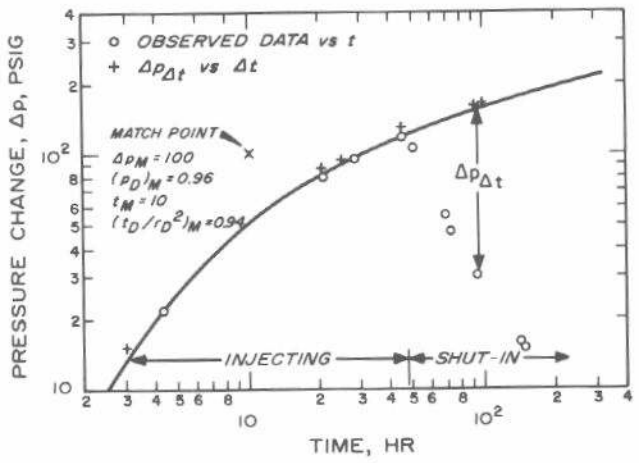

Fig. 9.6 Type-curve match of interference data for Example 9.1.

TABLE 9.2—CALCULATION OF $\Delta p_{\Delta t}$ FOR SHUT-IN PERIOD DATA OF EXAMPLE 9.1.

t (hours)	$\Delta t = t - 48$ (hours)	$\Delta p = p_i - p_{ws}$ (psi)	Δp_{ext}, Fig. 9.6 (psi)	$\Delta p_{\Delta t}$, Eq. 9.4 (psi)
51	3	−109	−124	−15
69	21	−55	−140	−85
73	25	−47	−142	−95
93	45	−32	−155	−123
142	94	−16	−177	−161
148	100	−15	−179	−164

closed system. The parameters on the curves in Fig. 9.7 are the dimensionless locations of the observation wells and the system area divided by the square of the distance between the active and observation wells, A/r^2.

If the system shape and approximate active-well location can be estimated, figures such as Fig. 9.7 may be used for type-curve matching interference data in bounded systems. Such matching may require much patience, since data for more than 150 type curves are given in Ref. 13.

The reciprocity principle[7,13] can be helpful for interference-test analysis in bounded systems when using type

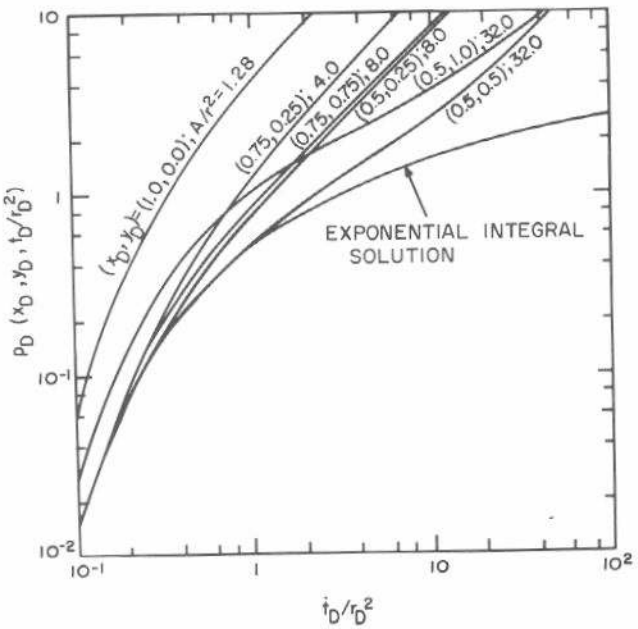

Fig. 9.7 Type-curve plot of p_D vs t_D/r_D^2 for various observation-well locations in a closed 2:1 rectangle with the active well at $x_{Dw} = 0.5$, $y_{Dw} = 0.75$. After Earlougher and Ramey.[13] Courtesy CIM.

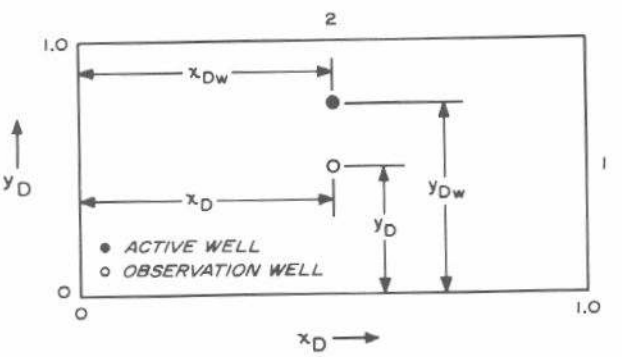

Fig. 9.8 Explanation of dimensions used in Figs. 9.7 and 9.9. Well locations for data match of Example 9.2.

curves such as those in Fig. 9.7. Stated simply, the reciprocity principle says that the pressure response at Observation Well A caused by production at rate q from Well B is equal to the pressure response that would be caused at Observation Well B by production at rate q from Well A. The principle is valid if pressure behavior in the system satisfies the normal diffusivity equation (Eq. 2.1) and if compressibility, permeability, viscosity, and porosity are not pressure-sensitive. The reciprocity principle tells us that it makes no difference which well is the active well and which well is the observation well; the same reservoir properties should be determined for testing either way. McKinley, Vela, and Carlton[7] have demonstrated that principle in the field for pulse testing.

If interference data are matched to a type curve such as one of those in Fig. 9.7, it may be possible to estimate reservoir area from the A/r^2 parameter for the matched curve, as illustrated in the following example.

Example 9.2 Interference-Test Analysis in a Bounded System

Simulated pressure data for an interference test in a closed reservoir[13] are given in Table 9.3. One well produces at 427 STB/D while the second well, 340 ft distant, remains shut in as an observation well. The wells lie in a structure such that a good approximation is a 2:1 closed rectangle with the producing well located at $x_D = 0.5$, $y_D = 0.75$. The size of the reservoir is not known. Other data are

$h = 23$ ft	$r_w = 0.27$ ft
$\mu_o = 0.8$ cp	$\phi = 0.12$
$B_o = 1.12$ RB/STB	$c_t = 8.3 \times 10^{-6}$ psi^{-1}
$q_o = 427$ STB/D	$r = 340$ ft.

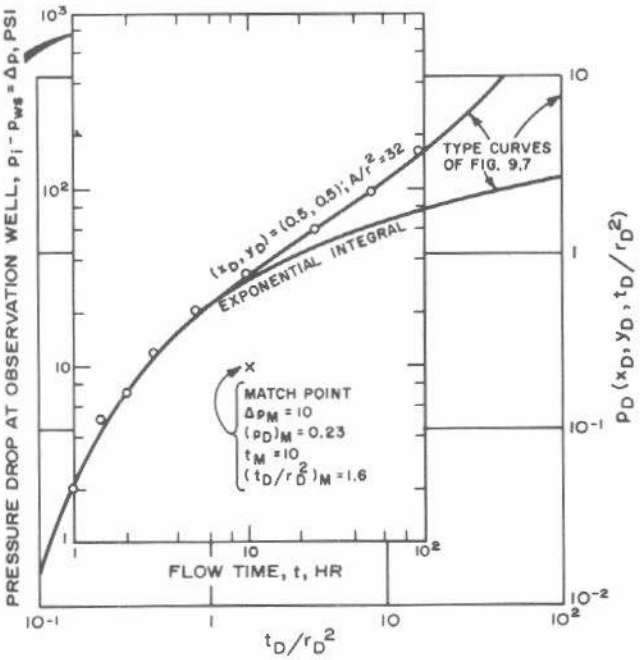

Fig. 9.9 Type-curve match for interference analysis of Example 9.2. After Earlougher and Ramey.[13] Courtesy CIM.

Fig. 9.9 shows the pressure differences of Table 9.3 matched with one of the type curves of Fig. 9.7. The data match the curve for $x_D = 0.5$, $y_D = 0.5$ reasonably well. At the pressure match point indicated in Fig. 9.9,

$$\Delta p_M = 10 \text{ psi at } (p_D)_M = 0.23,$$

and

$$t_M = 10 \text{ hours at } (t_D/r_D^2)_M = 1.6.$$

The permeability is estimated from Eq. 9.2:

$$k = \frac{(141.2)(427)(1.12)(0.8)(0.23)}{(23)(10)}$$

$$= 54.0 \text{ md}.$$

Using Eq. 9.3,

$$\phi c_t = \frac{(0.0002637)(54.0)}{(340)^2(0.8)} \frac{10}{1.6}$$

$$= 9.62 \times 10^{-7} \text{ psi}^{-1},$$

and

$$\phi = 0.116.$$

From the matched curve, $A/r^2 = 32$. Thus, we can estimate the reservoir size:

$$A = 32(340)^2 = 3.70 \times 10^6 \text{ sq ft}$$

$$= 84.9 \text{ acres}.$$

The exponential-integral type curve may not apply for interference-test analysis in some situations. Fig. 9.10 schematically illustrates how the dimensionless pressure deviates from the exponential-integral solution when the active well has a vertical fracture or has a high wellbore storage coefficient. The severity of the fracturing effect[12] depends on both the length of the fracture and the distance between the active well and the observation well. Similar deviations from the exponential-integral solution may be caused by wells with a large negative skin effect ($s << 0$) distributed some distance into the formation. Wellbore storage effects cause the pressure response at the observation well to fall below the exponential-integral solutions at early times because the change in the sand-face rate is less than the change in the surface rate. The degree of deviation from the exponential-integral solution depends on both the wellbore storage coefficient and the distance between the wells. Un-

TABLE 9.3—PRESSURE INTERFERENCE DATA AT OBSERVATION WELL OF EXAMPLE 9.2.
Data of Earlougher and Ramey.[13]

t (hours)	$p_i - p_{ws}$ (psi)
0	0
1	2
1.5	5
2	7
3	12
5	21
10	33
24	62
48	100
96	170

fortunately, very little information is currently available about these phenomena.*

Semilog Analysis Methods

If the two wells in an interference test are much closer together than the distance to the nearest boundary or to another active well (by a factor of about 10) in the system, the pressure response at the observation well eventually will be described by the logarithmic approximation to the exponential integral (Eq. 2.5b). Then the observation-well pressure would be approximated by

$$p_{ws}(t,r) = p_{1hr} + m \log t \quad \ldots\ldots\ldots\ldots\ldots (9.5)$$

Eq. 9.5 is strictly valid for $t_D/r_D^2 > 100$, where

$$\frac{t_D}{r_D^2} = \frac{0.0002637\, kt}{\phi\mu c_t r^2} \quad \ldots\ldots\ldots\ldots\ldots\ldots (9.6)$$

The restriction may be reduced to $t_D/r_D^2 > 10$ with only 1-percent deviation. If t_D/r_D^2 exceeds 2 or 3, Eq. 9.5 is often adequate for data analysis. When Eq. 9.5 can be used for interference-test analysis, observed pressures are plotted as p_{ws} vs log t during the initial phase of an interference test. Such a plot should have a semilog straight-line portion with slope m given by

$$m = \frac{-162.6\, qB\mu}{kh} \quad \ldots\ldots\ldots\ldots\ldots\ldots (9.7)$$

and intercept p_{1hr} given by

$$p_{1hr} = p_i + m\left[\log\left(\frac{k}{\phi\mu c_t r^2}\right) - 3.2275\right] \quad \ldots\ldots (9.8)$$

The skin factor does not appear in Eq. 9.8 since fluid is flowing only at the active well and not into or out of the observation well. The semilog straight-line slope may be used to estimate the system permeability,

$$k = \frac{-162.6\, qB\mu}{mh} \quad \ldots\ldots\ldots\ldots\ldots\ldots (9.9)$$

and the reservoir porosity-compressibility product,

$$\phi c_t = \frac{k}{r^2\mu}\ \text{antilog}\left(\frac{p_i - p_{1hr}}{m} - 3.2275\right). \quad \ldots (9.10)$$

It is usually necessary to extrapolate the pressure response to estimate p_{1hr} (which must be on the semilog straight line), since it usually takes many hours to reach a semilog straight-line response at an observation well.

If the observation well is shut in after time t_1, then normal superposition may be used for analysis of observed pressures. After a long shut-in time, the pressure behavior at the observation well will be given by

$$p_{ws}(t_1 + \Delta t, r) = p_i + m \log\left(\frac{t_1 + \Delta t}{\Delta t}\right). \quad \ldots (9.11)$$

Eq. 9.11 indicates that a plot of observed pressure after the active well is shut in vs $\log[(t_1 + \Delta t)/\Delta t]$ should have a semilog straight-line portion with slope = m. Permeability is estimated from Eq. 9.9 and the porosity-compressibility product is estimated from

$$\phi c_t = \frac{k}{r^2\mu}\ \text{antilog}\left[\frac{p_{1hr} - p_{ws}(\Delta t = 0)}{m} - \log\left(\frac{t_1 + 1}{t_1}\right) - 3.2275\right]. \quad \ldots\ldots\ldots (9.12)$$

As before, the semilog straight line must be extrapolated to p_{1hr}. The term $\log[(t_1 + 1)/t_1]$ is normally small and often can be neglected.

As with single-well testing, the signs of Δp and the rate must be considered when analyzing interference tests, since tests are commonly run with either production or injection at the active well. Eqs. 9.10 and 9.12 will give incorrect results if the signs are not treated properly. No simple rule of thumb can always be applied to prevent errors, but we can state that (1) k must *always* be positive, so the sign of m must be opposite the sign of q; and (2) except when r is small or k is very large, the $(p_i - p_{1hr})/m$ term in Eq. 9.10 (or its equivalent in Eq. 9.12) will be positive. Normally, ϕc_t is of the order of 10^{-7} for liquid-filled systems; it may exceed 10^{-4} for systems with free-gas saturation.

Example 9.3 Interference-Test Analysis Using Long-Time Equations

The interference test of Example 9.1 is analyzed using Eqs. 9.5 through 9.12. The observed pressure data are given

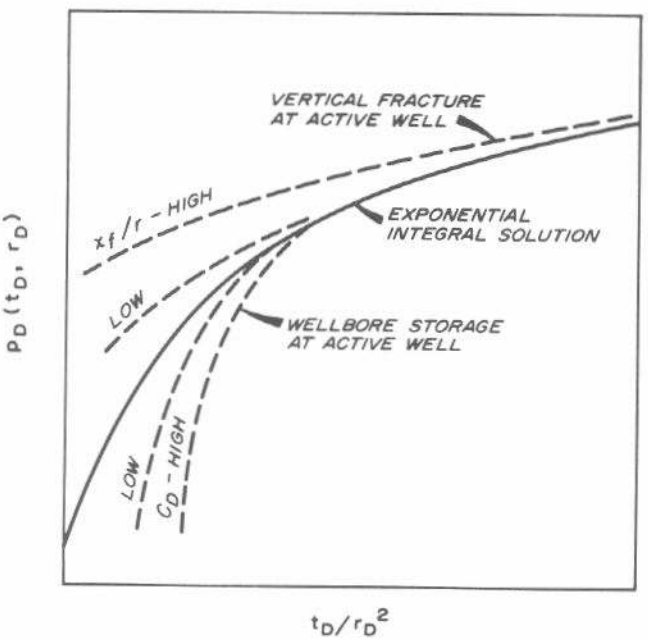

Fig. 9.10 Schematic illustration of the effect of vertical fractures and wellbore storage on observation-well response during an interference test.

*A paper that treats this subject in more detail appeared just before publication of this monograph — Jargon, J. R.: "Effect of Wellbore Storage and Wellbore Damage at the Active Well on Interference Test Analysis," *J. Pet. Tech.* (Aug. 1976) 851-858. Jargon presents several type curves that show the influence of storage and damage at the active well on observation-well response. He indicates that active-well wellbore storage and wellbore damage effects are not important at the observation well when

$$\frac{t_D}{r_D^2} > (230 + 15s)\left(\frac{C_D}{r_D^2}\right)^{0.86}.$$

Before that time, kh/μ estimated from the exponential-integral type curve is low and $\phi c_t h$ estimated is high.

in Table 9.1; other data are given in Example 9.1.

Fig. 9.11 is a semilog plot of the observation-well pressure data. The last three points in the injection part of the test appear to form a straight line, so we attempt analysis. Since there are only three data points on the straight line, and since t_D/r_D^2 (calculated from results below) is only about 5, the analysis is tentative. Type-curve matching is preferred in such a situation. From Fig. 9.11,

$$m = 120 \text{ psig/cycle},$$

and

$$p_{ws}(t = 10 \text{ hours}) = 41 \text{ psig},$$

so extrapolating one cycle,

$$p_{1\text{hr}} = 41 - 120 = -79 \text{ psig}.$$

Using Eq. 9.9,

$$k = \frac{(-162.6)(-170)(1.0)(1.0)}{(120)(45)}$$

$$= 5.1 \text{ md}.$$

We estimate ϕc_t from Eq. 9.10:

$$\phi c_t = \frac{5.1}{(119)^2(1.0)} \text{ antilog}\left[\frac{0 - (-79)}{120} - 3.2275\right]$$

$$= 9.71 \times 10^{-7} \text{ psi}^{-1},$$

and

$$\phi \simeq 0.11.$$

We can also analyze the decreasing-pressure portion of the test. Fig. 9.12 is a plot of the type suggested by Eq. 9.11. The slope taken from the last four points, 111 psi/cycle, may be used in Eq. 9.9 to estimate

$$k = \frac{(-162.6)(-170)(1.0)(1.0)}{(111)(45)} = 5.5 \text{ md}.$$

We estimate $p_{1\text{hr}}$ by extrapolating the line in Fig. 9.12. At 1 hour, $(t_1 + \Delta t)/\Delta t = 49$. We read $p = 72$ psig from Fig. 9.12 at $(t_1 + \Delta t)/\Delta t = 4.9$. Then, extrapolating one cycle,

$$p_{1\text{hr}} = 72 + 111 = 183 \text{ psi}.$$

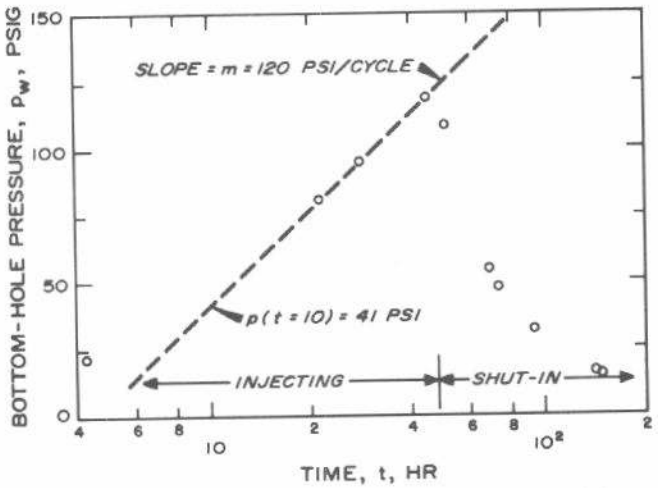

Fig. 9.11 Semilog plot of interference data for Example 9.3.

Fig. 9.11 indicates that $p_{ws}(\Delta t = 0) = 123$ psi. Then, from Eq. 9.12,

$$\phi c_t = \frac{5.5}{(119)^2(1.0)} \text{ antilog}\left[\frac{183 - 123}{111} - \log\left(\frac{48 + 1}{48}\right) - 3.2275\right]$$

$$= 7.82 \times 10^{-7} \text{ psi}^{-1}.$$

Both k and ϕc_t are close to the values computed from the increasing-pressure portion of the analysis. The injection-period semilog analysis agrees well with the type-curve analysis in spite of the fact that (Eq. 9.6)

$$\frac{t_D}{r_D^2} = \frac{(0.0002637)(5.1)(48)}{(9.71 \times 10^{-7})(1.0)(119)^2} = 4.7,$$

for the injection period.

When there is significant rate variation at the active well during an interference test, analysis becomes much more difficult. In this case, complete superposition must be used; but because the logarithmic approximation to the exponential-integral solution generally will not apply, analysis techniques are not so simple. Under these circumstances, results generally must be analyzed by using computer methods such as those discussed by Jahns[6] and Earlougher and Kersch.[10]

9.3 Pulse Testing

Pulse testing is a special form of multiple-well testing first described by Johnson, Greenkorn, and Woods.[14-16] The technique uses a series of short-rate pulses at the active well. Pulses generally are alternating periods of production (or

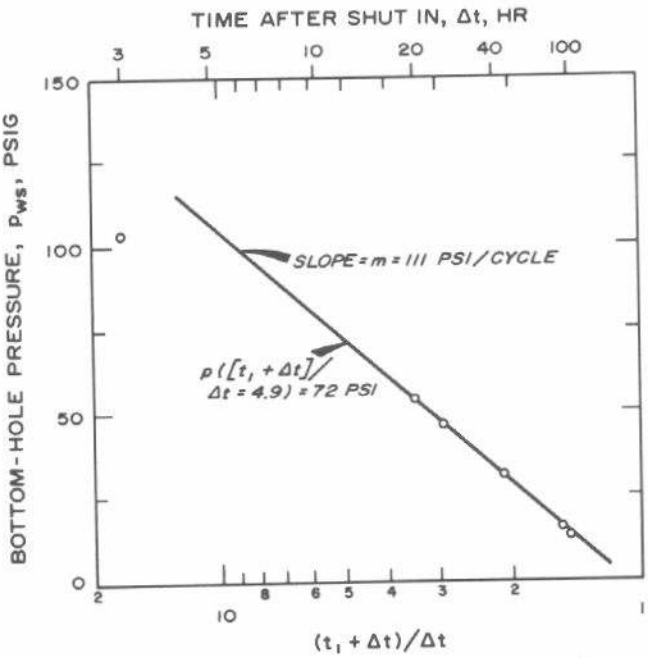

Fig. 9.12 Decreasing pressure portion of observation-well data from the interference test of Example 9.3.

injection) and shut-in, with the same rate during each production (injection) period. The pressure response to the pulses is measured at the observation well. Because the pulses are of short duration, the pressure responses are small, sometimes less than 0.01 psi. Therefore, special pressure-measuring equipment is usually required.[17,18]

The main advantages of pulse testing result from the short pulse length. Infinite-system equations (Eq. 2.5) usually apply at such short times, regardless of the system size. A pulse test may last from a few hours to a few days, so it should disrupt normal operations only slightly compared with interference testing. Reservoir pressure trends and noise are automatically removed by the analysis technique given in this section.

Fig. 9.13 schematically illustrates pulse testing for a two-well system. The figure is for a producing well that is pulsed by shutting in, continuing production, shutting in, continuing production, etc. The upper portion of the figure shows the constant production rate before the test and the rate pulses. The lower portion of the figure illustrates the pressure behavior at the observation well and correlates the pressure pulses with the rate pulses. Although the flow time and shut-in time are equal in Fig. 9.13, pulse testing can be done with unequal flow and shut-in times. However, all flow times must be the same and all shut-in times must be the same.

Two characteristics of the pressure response at the observation well are used for pulse-test analysis. One is the time lag, the time between the *end* of a pulse and the pressure peak caused by the pulse (Fig. 9.14). A time lag is associated with each pulse. (The pulse responses shown in Fig. 9.14 are not necessarily representative of an actual pulse-test response; the relationship of the pulses has been drawn to simplify defining the terms used in pulse-test analysis.) Time lags for the first and fourth pulses are shown in Fig. 9.14; similar definitions apply for the second, third, fifth, sixth, seventh, and eighth pulses in that figure.

The second variable used in pulse-test analysis is the amplitude of the pressure response, Δp_1, Δp_2, etc., shown in Fig. 9.14. We determine pulse-response amplitude by first constructing the tangent between the two peaks (or valleys) on either side of the pulse to be measured. Then we draw a line parallel to that tangent at the peak of the subject response. The pressure amplitude is the *vertical* distance between the two lines. The same approach applies to both peaks and valleys. Strictly speaking, the Δp value for the first peak in Fig. 9.14 is negative, as it is for all other odd peaks; Δp is positive for even responses. In the analysis methods presented in this section, the *sign convention is eliminated*, since it tends to be confusing. Rather, we designate that the sign of Δp is the same as the sign of the rate in the flowing part of the test, so $\Delta p/q > 0$.

Pulse-test analysis techniques have been outlined by Johnson, Greenkorn, and Woods,[14] Culham,[19] Startzman,[20] and Brigham and Kamal.[21,22] The Kamal-Brigham technique[22] has the advantage of being flexible and convenient to use for hand analysis, so it is presented here. Many analysis techniques require use of a digital computer.

The Kamal-Brigham analysis method uses several definitions. The ratio of pulse length to the total cycle length is defined as

$$F' = \frac{\Delta t_P}{\Delta t_C}, \quad \ldots\ldots\ldots\ldots\ldots\ldots\ldots\ldots\ldots\ldots (9.13)$$

where Δt_P and Δt_C are indicated in Fig. 9.14. (This nomenclature deviates from that used by Johnson, Greenkorn, and Woods.[14]) The dimensionless time lag is defined analogously to any dimensionless time,

$$(t_L)_D = \frac{0.0002637\, kt_L}{\phi\mu c_t r_w^2}, \quad \ldots\ldots\ldots\ldots\ldots\ldots\ldots (9.14)$$

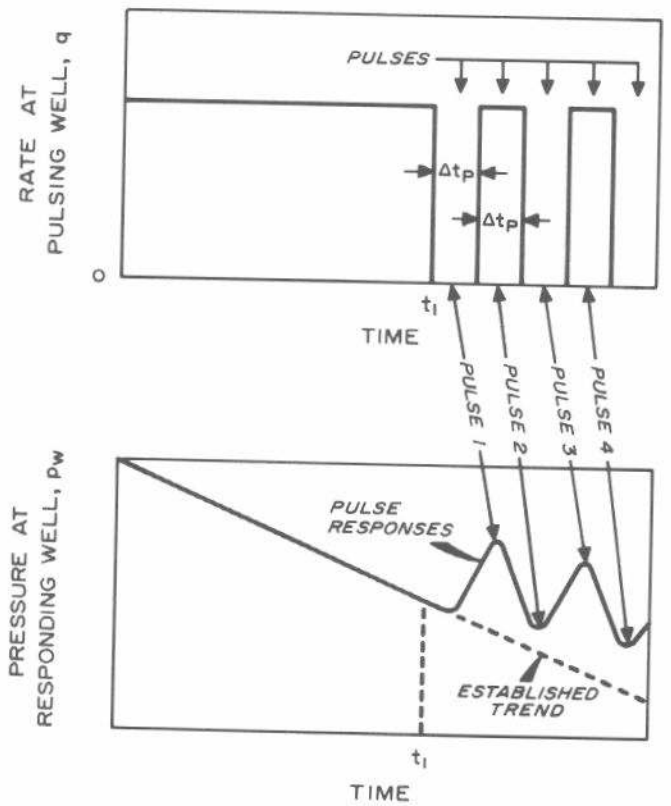

Fig. 9.13 Schematic illustration of rate (pulse) history and pressure response for a pulse test.

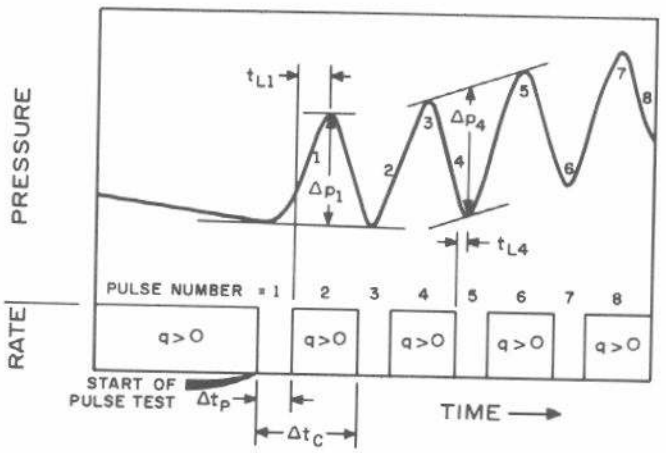

Fig. 9.14 Schematic pulse-test rate and pressure history showing definition of time lag (t_L) and pulse-response amplitude (Δp).

using the wellbore radius of the active well. The dimensionless distance between the active and observation wells is

$$r_D = r/r_w, \quad \ldots\ldots\ldots\ldots\ldots\ldots\ldots\ldots \quad (9.15)$$

where r is indicated in Fig. 9.1. The dimensionless-pressure response amplitude is

$$\Delta p_D = \frac{kh\,\Delta p}{141.2\,qB\mu}, \quad \ldots\ldots\ldots\ldots\ldots\ldots \quad (9.16)$$

where q is the rate at the active well while it is active. We use the sign convention that $\Delta p/q$ is always positive.

The time lag and pressure response amplitude from one or more pulse responses are used to estimate reservoir properties from a pulse test. The permeability is estimated from

$$k = \frac{141.2\,qB\mu\left\{\Delta p_D\left[t_L/\Delta t_C\right]^2\right\}_{\text{Fig.}}}{h\Delta p\left[t_L/\Delta t_C\right]^2}. \quad \ldots\ldots \quad (9.17)$$

In Eq. 9.17, Δp and t_L are from the observation-well response for the pulse being analyzed; Δt_C is the cycle length at the pulsing well; and $\left\{\Delta p_D\left[t_L/\Delta t_C\right]^2\right\}_{\text{Fig.}}$ is from Fig. 9.15, 9.16, 9.17, or 9.18 for the appropriate values of $t_L/\Delta t_C$ and F'. It is necessary to use the figure specifically applying to the pulse being analyzed. Fig. 9.15 is for analysis of the *first odd pulse* (first pulse); Fig. 9.16 is for the *first even pulse* (second pulse); Fig. 9.17 is for all *odd pulses after the first* (3, 5, 7, ...); and Fig. 9.18 is for all *even pulses after the first* (4, 6, 8, ...).

Once the permeability is estimated from Eq. 9.17, we estimate the porosity-compressibility product from

$$\phi c_t = \frac{0.0002637\,k\,t_L}{\mu r^2\left\{(t_L)_D/r_D{}^2\right\}_{\text{Fig.}}}. \quad \ldots\ldots\ldots\ldots \quad (9.18)$$

In Eq. 9.18 the value of $\left\{(t_L)_D/r_D{}^2\right\}_{\text{Fig.}}$ is from Fig. 9.19, 9.20, 9.21, or 9.22. As before, the figure used depends on whether the first odd or even pulse or one of the remaining odd or even pulses is being analyzed.

Once pulse-test data are available and plotted and time lags and pressure responses are measured, pulse-test analysis by the Kamal-Brigham technique is rapid. It is good practice to analyze several pulses to get an idea of the reliability of the results.

Prats and Scott[23] have presented preliminary data showing the effect of wellbore storage at the observation well on pulse-test response. Wellbore storage effects at the observation well increase the time lag (t_L) and reduce the response amplitude (Δp) of the first pulse. Data are not presented for later pulses, but they can be expected to be affected, also. Using the Prats and Scott[23] data, we can approximate that the effect of wellbore storage at the responding well will result in less than a 5-percent increase in time lag and a virtually unaffected response amplitude when the distance between pulsed and responding wells satisfies

$$r_D > 34\,C_D{}^{0.54}. \quad \ldots\ldots\ldots\ldots\ldots\ldots \quad (9.19a)$$

Eq. 9.15 gives r_D using r_w of the *observation* well and C_D is from Eq. 2.18. In terms of physical quantities, Eq. 9.19a becomes

$$r > 32\,r_w\left(\frac{C}{\phi c_t h r_w{}^2}\right)^{0.54}, \quad \ldots\ldots\ldots\ldots \quad (9.19b)$$

or approximately,

$$r > 32\left(\frac{C}{\phi c_t h}\right)^{0.54}. \quad \ldots\ldots\ldots\ldots\ldots \quad (9.19c)$$

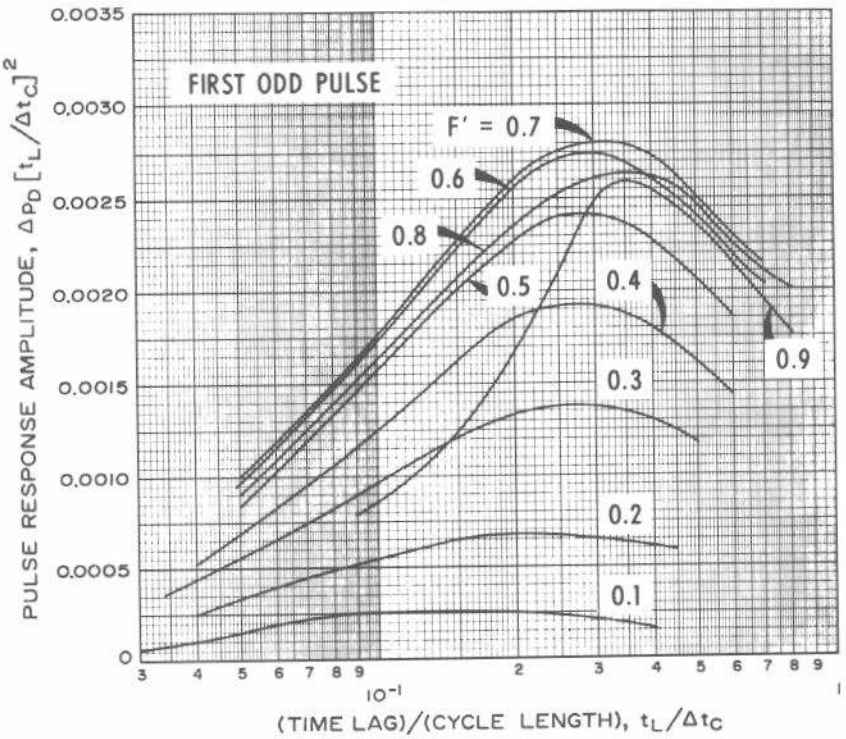

Fig. 9.15 Pulse testing: relation between time lag and response amplitude for first odd pulse. After Kamal and Brigham.[22]

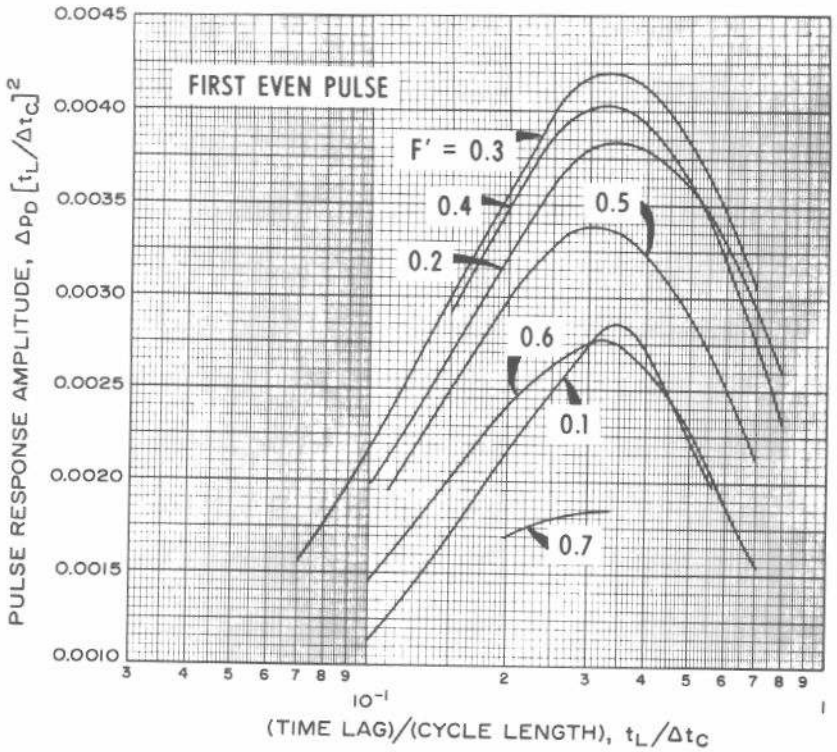

Fig. 9.16 Pulse testing: relation between time lag and response amplitude for first even pulse. After Kamal and Brigham.[22]

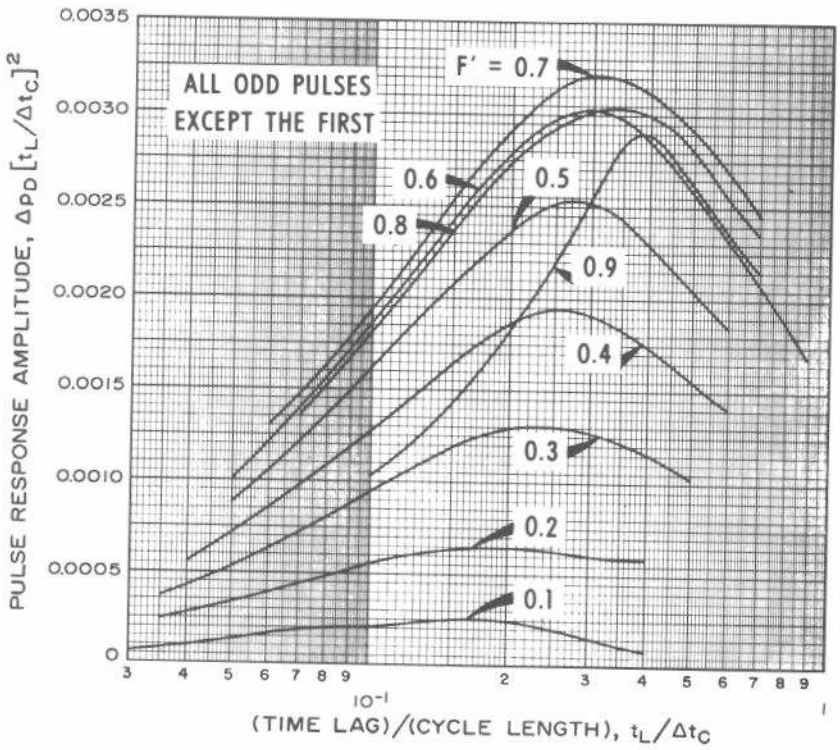

Fig. 9.17 Pulse testing: relation between time lag and response amplitude for all odd pulses after the first. After Kamal and Brigham.[22]

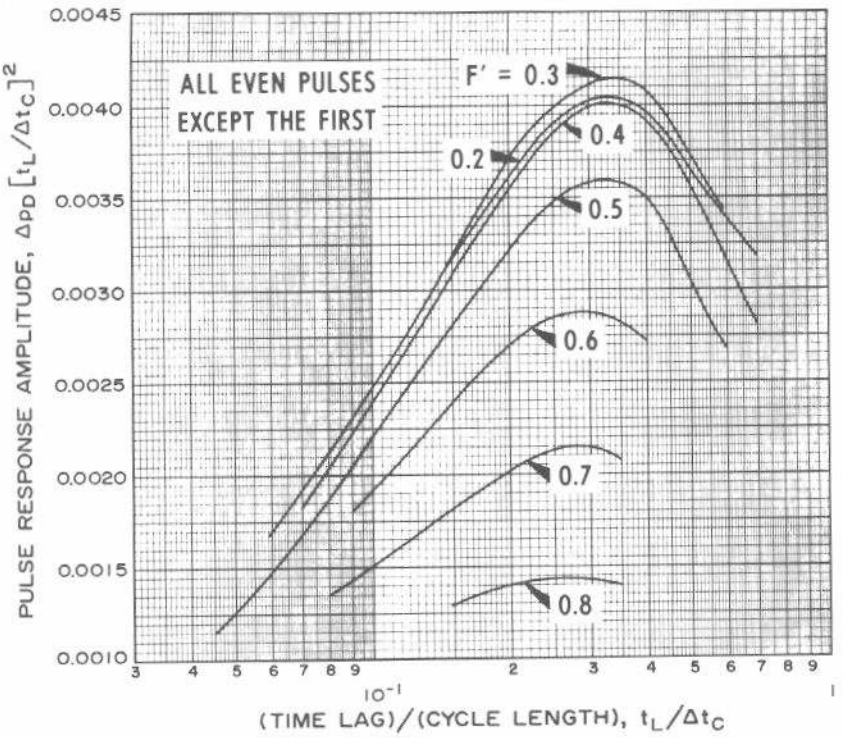

Fig. 9.18 Pulse testing: relation between time lag and response amplitude for all even pulses after the first. After Kamal and Brigham.[22]

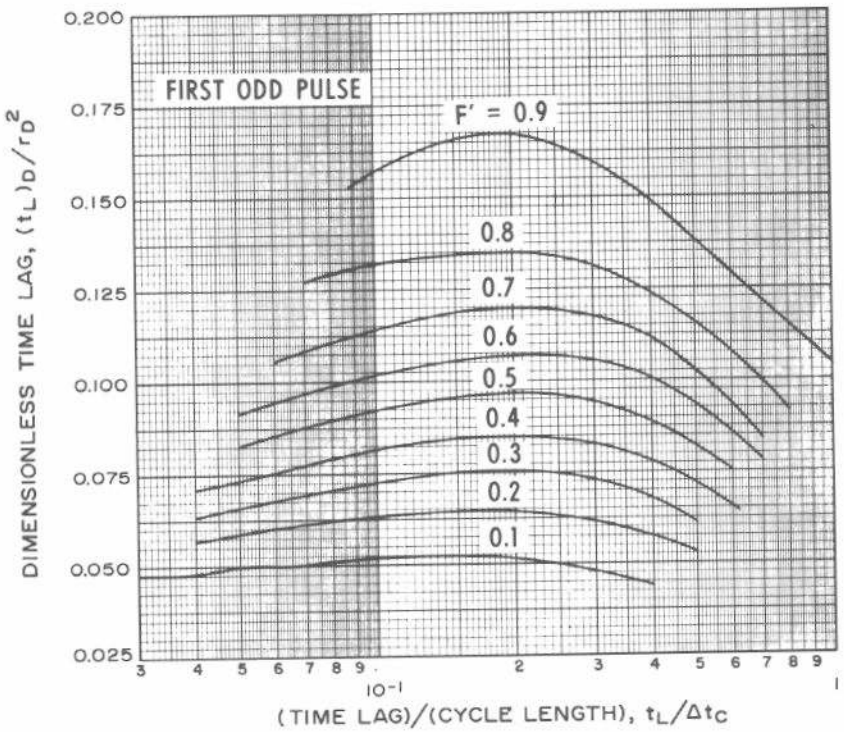

Fig. 9.19 Pulse testing: relation between time lag and cycle length for first odd pulse. After Kamal and Brigham.[22]

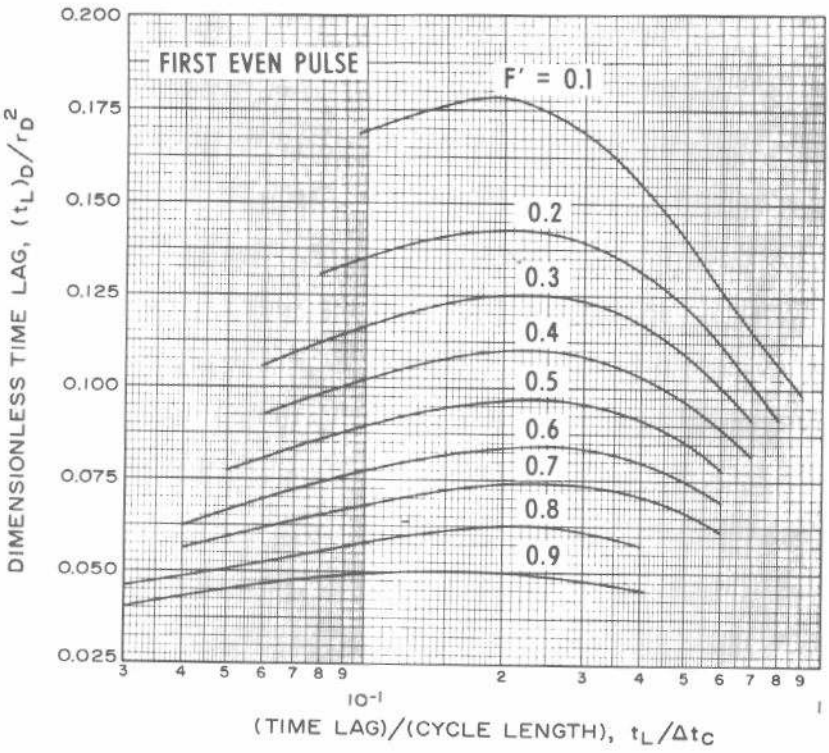

Fig. 9.20 Pulse testing: relation between time lag and cycle length for first even pulse. After Kamal and Brigham.[22]

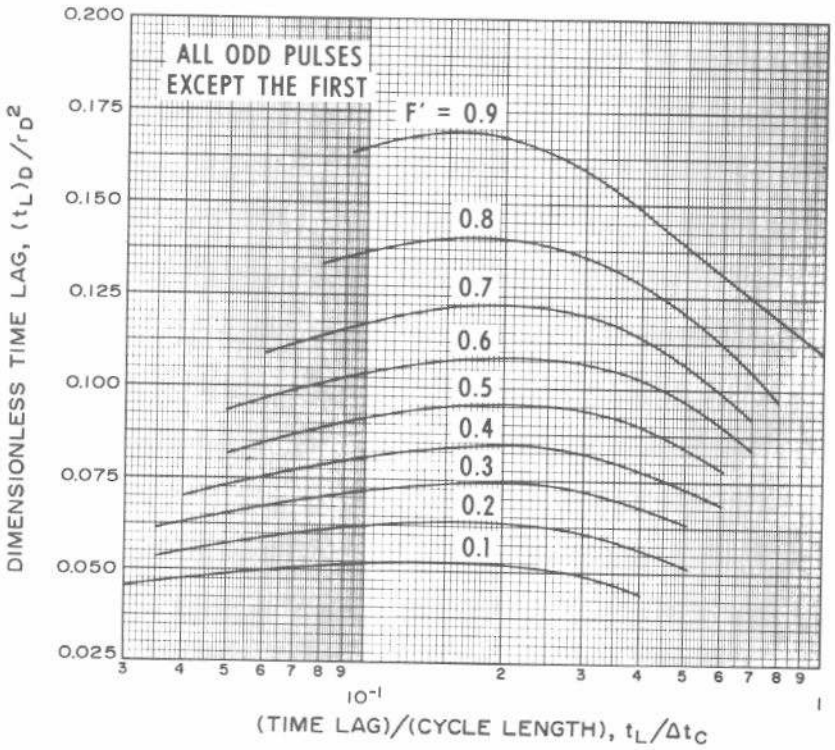

Fig. 9.21 Pulse testing: relation between time lag and cycle length for all odd pulses after the first. After Kamal and Brigham.[22]

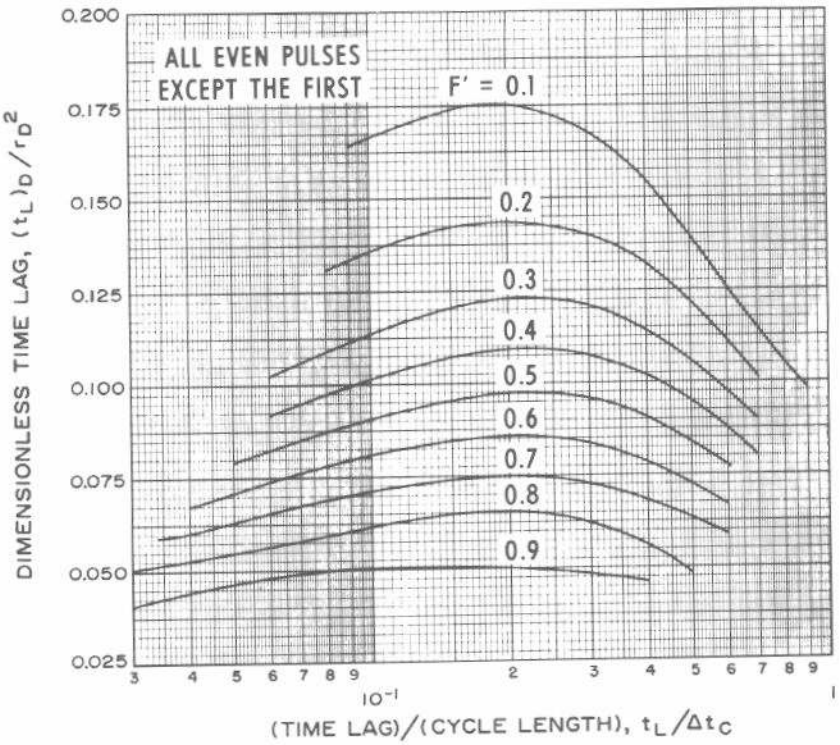

Fig. 9.22 Pulse testing: relation between time lag and cycle length for all even pulses after the first. After Kamal and Brigham.[22]

Wellbore storage at the active well also can be expected to influence pulse-test response; details are not currently available.*

Example 9.4 Pulse-Test Analysis

Fig. 9.23 shows pulse-test data from McKinley, Vela, and Carlton.[7] Producing Wells A8 and A9 were tested by pulsing Well A8 (Δt_P = 1 hour, q = 550 STB/D) and observing the response at Well A9 (plus symbols in Fig. 9.23). At some other time, Well A9 was pulsed (Δt_P = 1 hour, q = 450 STB/D), and the response at Well A8 was observed (open circles in Fig. 9.23). Reservoir data include B = 1.0 RB/STB and r = 1,320 ft (40-acre spacing).

We analyze the second peak (*third pulse response*) of Fig. 9.23 for illustration. From each set of data on the figure,

$$\frac{\Delta p}{q} = 7.6 \times 10^{-4} \text{ psi/(STB/D)},$$

and

$$t_L = 0.15 \text{ hours}.$$

For these tests, Δt_C = 2 hours and Δt_P = 1 hour. Thus,

$$t_L/\Delta t_C = \frac{0.15}{2.00} = 0.075,$$

and

$$F' = 1.0/2.0 = 0.5.$$

There is not enough information to estimate permeability from Eq. 9.17, but the equation can be rearranged to compute kh/μ. Use Fig. 9.17 for all odd pulses after the first with $F' = 0.5$ and $t_L/\Delta t_C = 0.075$ and read $\{\Delta p_D[t_L/\Delta t_C]^2\}_{\text{Fig.}} = 0.00128$. Then,

$$\frac{kh}{\mu} = \frac{(141.2)(1.0)\{0.00128\}}{(7.6 \times 10^{-4})[0.075]^2} = 42{,}300 \text{ md ft/cp}.$$

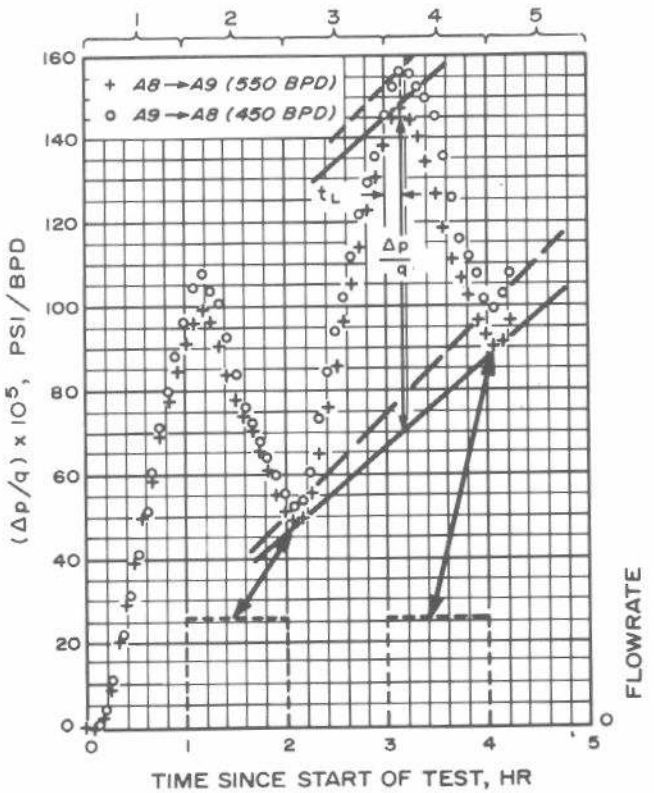

Fig. 9.23 Pulse-test data for a well pair tested in both directions, Example 9.4. After McKinley, Vela, and Carlton.[7]

*A paper that briefly discusses this subject appeared just before publication of the monograph — Jargon, J. R.: "Effect of Wellbore Storage and Wellbore Damage at the Active Well on Interference Test Analysis," *J. Pet. Tech.* (Aug. 1976) 851-858. That paper states that wellbore storage at the pulsing well reduces pulse amplitude and increases the time lag.

To estimate $\phi c_t h$ we use a rearranged form of Eq. 9.18 and $\{(t_L)_D/r_D^2\}_{\text{Fig.}} = 0.0876$ from Fig. 9.21 for all later odd pulses.

$$\phi c_t h = \frac{(0.0002637)(42{,}300)(0.15)}{(1{,}320)^2(0.0876)}$$
$$= 11.0 \times 10^{-6} \text{ ft/psi}.$$

Using their analysis technique, McKinley, Vela, and Carlton[7] estimated $kh/\mu = 40{,}000 \pm 2{,}000$ and $\phi c_t h = 11.0 \times 10^{-6} \pm 1.1 \times 10^{-6}$ for Well A8 pulsing and Well A9 responding. For Well A9 pulsing and Well A8 responding, they estimated $kh/\mu = 46{,}000 \pm 7{,}000$ and $\phi c_t h = 12.7 \times 10^{-6} \pm 1.3 \times 10^{-6}$.

For best results, pulse tests should be run with a good combination of pulse length, pulse amplitude, and pressure-measuring equipment. To accomplish this, we recommend designing pulse tests using estimated reservoir properties. Test design utilizes Figs. 9.15 through 9.22, as illustrated in the following example.

Example 9.5 Pulse-Test Design

We wish to design a pulse test for a reservoir with the following approximate properties:

$q = 100$ B/D	$r = 660$ ft
$k = 200$ md	$c_t = 10 \times 10^{-6}$ psi^{-1}
$\mu = 3$ cp	$\phi = 0.18$
$h = 25$ ft	$B = 1.1$ RB/STB.

The pulsing well is a producer, so to minimize shut-in time we choose a short shut-in pulse, such as $F' = 0.3$. For initial design calculations, we choose the *maximum* $\Delta p_D[t_L/\Delta t_C]^2$ points from Figs. 9.15 and 9.16 for the *first* odd and even pulses. For the first *even* pulse and $F' = 0.3$, $\{\Delta p_D[t_L/\Delta t_C]^2\}_{\text{Fig.}} \simeq 0.0042$ at $t_L/\Delta t_C \simeq 0.33$ from Fig. 9.16. Using Fig. 9.20 for that value of $t_L/\Delta t_C$, $\{(t_L)_D/r_D^2\}_{\text{Fig.}} = 0.122$. Rearranging Eq. 9.18,

$$t_L \simeq \frac{\{(t_L)_D/r_D^2\}_{\text{Fig.}} r^2 \phi\mu c_t}{(0.0002637)\,k}$$
$$\simeq \frac{\{0.122\}(660)^2(0.18)(3)(10 \times 10^{-6})}{(0.0002637)(200)}$$
$$\simeq 5.4 \text{ hours}.$$

Cycle time is given by

$$\Delta t_C = t_L/[t_L/\Delta t_C] = 5.4/0.33 = 16.4 \text{ hours},$$

and the pulse length is

$$\Delta t_P = F'\Delta t_C = 4.9 \text{ hours}.$$

We estimate pressure response by rearranging Eq. 9.17:

$$\Delta p \simeq \frac{(141.2)qB\mu\{\Delta p_D[t_L/\Delta t_C]^2\}_{\text{Fig.}}}{kh[t_L/\Delta t_C]^2}$$
$$\simeq \frac{(141.2)(1.1)(3)\{0.0042\}}{(200)(25)[0.33]^2}\,q$$
$$\simeq 3.6 \times 10^{-3}\,q \text{ psi}.$$

Thus, $\Delta p = 3.6 \times 10^{-3}(100) = 0.36$ psi is the expected response amplitude for *even-pulse* analysis. We would shut in the well for 5 hours, produce for 11 hours, and so forth.

If we wish to analyze the first odd-pulse response, we design in a similar way:

$$\{\Delta p_D[t_L/\Delta t_C]^2\}_{\text{Fig.}} \simeq 0.0014$$
$$\text{at } t_L/\Delta t_C \simeq 0.27 \text{ from Fig. 9.15},$$

and

$$\{(t_L)_D/r_D^2\}_{\text{Fig.}} = 0.074 \text{ from Fig. 9.19}.$$

Estimating as above, $t_L \simeq 3.3$ hours, $\Delta t_C \simeq 12.2$ hours, $\Delta t_P \simeq 3.7$ hours, and $\Delta p \simeq 0.12$ psi at a 100-B/D rate; we would shut in for 4 hours, produce for 8 hours, etc. We would require pressure-measuring instrumentation that will provide reliable pressure-change data when $\Delta p \simeq 0.1$ psi. We should analyze the even pulses, since they will show the greatest pressure response.

Alternatively, we could have chosen a convenient pulse length and calculated $\Delta p/q$. We could then use $\Delta p/q$ to choose pulse height (q) or the pressure-measuring instruments. Of course, for many wells, we may not be able to change the pulse magnitude (rate) significantly.

We could get a larger response amplitude with a longer test. For example, if we choose $\{\Delta p_D[t_L/\Delta t_C]^2\}_{\text{Fig. 9.16}} = 0.00156$ at $[t_L/\Delta t_C] = 0.07$, then $\{(t_L)_D/r_D^2\}_{\text{Fig. 9.20}} = 0.109$ and we get $t_L = 4.86$ hours, $\Delta t_C = 69.4$ hours, and $\Delta p = 2.96 \times 10^{-2} q$. Thus, by increasing cycle (and test) time by a factor of 4.23, we can increase the response amplitude by over eight times. However, a main advantage of pulse testing is the short test time, so it may be better to accept a smaller pressure response to keep test time short.

9.4 Heterogeneous and Anisotropic Reservoirs

Most multiple-well testing techniques are based on the assumptions that the reservoir system is isotropic and homogeneous in the influence region. If those restrictions are not satisfied, the analysis techniques presented in this chapter generally provide results that are some type of an average of the properties within the influence region (Fig. 9.3).[5] Vela and McKinley[5] propose a method for correcting values of kh/μ and $\phi c_t h$ determined from a *series* of pulse tests to reservoir average properties. This method should also apply to normal interference testing when sufficient data are available.

If enough observation wells are used, interference-test data sometimes can be analyzed by computer methods to give a description of the variation of reservoir properties with location. Jahns[6] describes a technique that applies to heterogeneous and anisotropic reservoirs. The technique presented by Earlougher and Kersch[10] applies to anisotropic but otherwise homogeneous, infinite-acting reservoirs. Other techniques also have been suggested.[8,9]

Pierce, Vela, and Koonce[24] describe a method for estimating the orientation and length of hydraulic fractures by pulse testing. Although that method requires computer simulation, it is potentially useful for estimating the existence and direction of permeability anisotropies. The

method is qualitative unless the computer simulation is used, so it is not discussed further here.

Based on work by Papadopulos,[25] Ramey[11] presents a method for estimating anisotropic reservoir properties from interference data. Although more complex than single-well interference analyses, the method does not require computer assistance. Fig. 9.24 defines the necessary nomenclature. The major permeability axis, k_{max}, is rotated from the axis used for measuring well coordinates by the angle θ. The minor permeability axis, k_{min}, is oriented at 90° to the major permeability axis. The active well is located at the origin of the coordinate system and the observation wells are each located at coordinates indicated as (x,y). The anisotropic analysis requires pressure data from at least three observation wells located on different rays extending from the active well. It assumes that the active-well/observation-well system is infinite-acting and homogeneous (with the exception of having anisotropic permeability).

Ramey shows that the pressure at an observation well is

$$p(t,x,y) = p_i - \frac{141.2\,qB\mu}{\sqrt{k_{max}k_{min}}\,h}\,p_D\left(\left[t_D/r_D^2\right]_{dir}\right) \quad \ldots (9.20)$$

Eq. 9.20 has the familiar form of Eq. 2.2, except that the permeability has been replaced by $\sqrt{k_{max}k_{min}}$ and the definition

$$\left(\frac{t_D}{r_D^2}\right)_{dir} = \frac{0.0002637t}{\phi\mu c_t}\left[\frac{k_{max}k_{min}}{(k_x y^2 + k_y x^2 - 2\,k_{xy}xy)}\right], \quad \ldots (9.21)$$

is used. In Eq. 9.21, k_x, k_y, and k_{xy} are components of the symmetrical permeability tensor aligned with the coordinate system.[11] To estimate k_{max}, k_{min}, and θ, it is necessary to first estimate k_x, k_y, and k_{xy} as described below.

Type-curve matching is the first step of the analysis technique. Observed pressure data from at least three wells are plotted and matched to the type curve of Fig. C.2, as described in Section 9.2. Each of the three data sets must be matched so the *pressure match point* $\left[\Delta p_M,(p_D)_M\right]$ is the *same for all three observation-well responses*. The time match point $\left[t_M,(t_D/r_D^2)_M\right]$ will be different for each set of observation-well data. By making the match this way, and by obtaining the best match for all three data sets, the directional permeability characteristics and ϕc_t may be estimated.

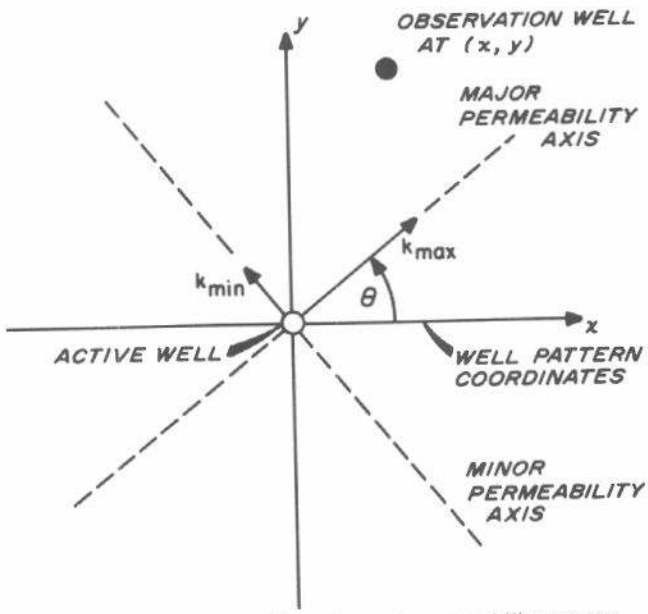

Fig. 9.24 Nomenclature for anisotropic permeability system. After Ramey.[11]

Once observed pressure responses are matched, average system permeability is estimated from

$$\bar{k} = \sqrt{k_{max}k_{min}} = \frac{141.2\,qB\mu(p_D)_M}{h\Delta p_M}, \quad \ldots (9.22)$$

where the pressure match points are the same for all pressure observation responses. Each of the three time match points, $\left[t_M,(t_D/r_D^2)_M\right]$, is used with a rearranged version of Eq. 9.21:

$$y^2k_x + x^2k_y - 2xy\,k_{xy} = \frac{(0.0002637)\,k_{max}k_{min}}{\phi\mu c_t}\,\frac{t_M}{(t_D/r_D^2)_M}. \quad \ldots (9.23)$$

We write Eq. 9.23 three times, once for each observation-well match. That gives three equations in four unknowns, k_x, k_y, k_{xy}, and $\phi\mu c_t$. They may be solved simultaneously to obtain k_x, k_y, and k_{xy}, each in terms of the unknown $\phi\mu c_t$. Then k_x, k_y, and k_{xy} (in terms of $\phi\mu c_t$) are substituted into

$$k_xk_y - k_{xy}^2 = k_{max}k_{min} = \bar{k}^2. \quad \ldots (9.24)$$

Since the right side of Eq. 9.24 is known (from Eq. 9.22), it can be solved to estimate $\phi\mu c_t$. Then we estimate k_x, k_y, and k_{xy} from their relationships to $\phi\mu c_t$. To complete the analysis and estimate the maximum and minimum directional permeabilities and the angle of orientation, we use

$$k_{max} = 0.5\left\{(k_x + k_y) + \left[(k_x - k_y)^2 + 4k_{xy}^2\right]^{1/2}\right\}, \quad \ldots (9.25)$$

$$k_{min} = 0.5\left\{(k_x + k_y) - \left[(k_x - k_y)^2 + 4k_{xy}^2\right]^{1/2}\right\}, \quad \ldots (9.26)$$

and

$$\theta = \arctan\left(\frac{k_{max} - k_x}{k_{xy}}\right) \quad \ldots (9.27)$$

Example 9.6 Interference-Test Analysis in an Anisotropic Reservoir

Ramey[11] gives data for an interference test in a nine-spot pattern at the end of a waterflood. Before testing, all wells were shut in. The test was run by injecting at −115 STB/D and observing the fluid levels in eight of the shut-in production wells, both during injection and during the subsequent falloff period. Ramey[11] tabulates complete pressure data during injection and falloff for all eight observation wells and falloff data for the injection well. Only a portion of the data is used here to illustrate the use of Eqs. 9.22 through 9.27.

Fig. 9.25 shows the well locations. Table 9.4 gives observed pressure changes during the injection period. Other data are

TABLE 9.4—PRESSURE DATA FOR INTERFERENCE TEST OF EXAMPLE 9.6.
After Ramey.[11]

Well 1-D		Well 5-E		Well 1-E	
t (hours)	Δp (psi)	t (hours)	Δp (psi)	t (hours)	Δp (psi)
23.5	−6.7	21	−4	27.5	−3
28.5	−7.2	47	−11	47	−5
51	−15	72	−16.3	72	−11
77	−20	94	−21.2	95	−13
95	−25	115	−22	115	−16
		122	−25		

$q = -115$ STB/D $\quad B = 1.0$ RB/STB
$h = 25$ ft $\quad \phi = 0.20$
$\mu = 1.0$ cp $\quad p_i = 240$ psi.

Fig. 9.26 shows the match of the data in Table 9.4 to the type curve of Fig. C.2. The match was made so the pressure match point $[p_M,(p_D)_M]$ is the same for all three responses, while the time match points vary.

Match-point data are $p_M = -10$ psi and $(p_D)_M = 0.26$.

	Well 1-D	Well 5-E	Well 1-E
t_M, hours	72	92	150
$(t_D/r_D^2)_M$	1.0	1.0	1.0

Average permeability is estimated from Eq. 9.22:

$$\bar{k} = \sqrt{k_{\max}k_{\min}} = \frac{(141.2)(-115)(1)(1)}{25}\ \frac{(0.26)}{(-10)}$$

$$= 16.89 \text{ md.}$$

$$k_{\max}k_{\min} = (16.89)^2 = 285.3.$$

We now write Eq. 9.23 for *each* time match point:

For Well 1-D,

$$(475)^2 k_x + (0)^2 k_y - 2(0)(475)\,k_{xy} = \frac{(0.0002637)(285.3)}{\phi\mu c_t}\ \frac{(72)}{(1.0)}.$$

For Well 5-E,

$$(0)^2 k_x + (475)^2 k_y - 2(475)(0)\,k_{xy} = \frac{(0.0002637)(285.3)}{\phi\mu c_t}\ \frac{(92)}{(1.0)}.$$

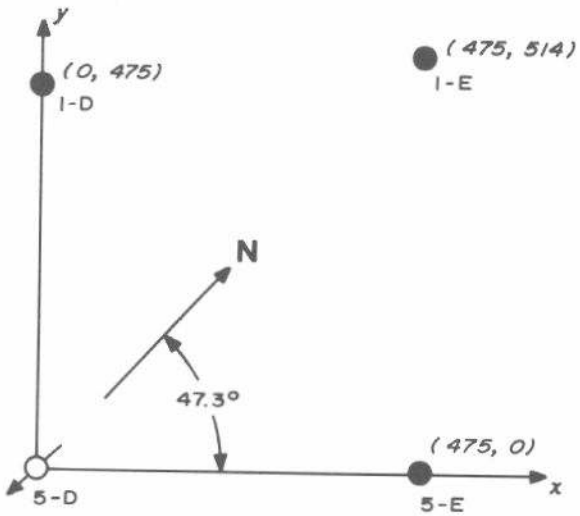

Fig. 9.25 Well locations for Example 9.6.

For Well 1-E,

$$(514)^2 k_x + (475)^2 k_y - 2(475)(514)\,k_{xy} = \frac{(0.0002637)(285.3)}{\phi\mu c_t}\ \frac{(150)}{(1.0)}.$$

Simplifying and normalizing, these equations become

$$k_x = \frac{2.401 \times 10^{-5}}{\phi\mu c_t} \quad \ldots \text{(A)}$$

$$k_y = \frac{3.068 \times 10^{-5}}{\phi\mu c_t} \quad \ldots \text{(B)}$$

$$0.5411k_x + 0.4621\,k_y - k_{xy} = \frac{2.311 \times 10^{-5}}{\phi\mu c_t} \quad \ldots \text{(C)}$$

Combining Eqs. A, B, and C gives

$$k_{xy} = (0.5411)\ \frac{2.401 \times 10^{-5}}{\phi\mu c_t} + (0.4621)\ \frac{3.068 \times 10^{-5}}{\phi\mu c_t} - \frac{2.311 \times 10^{-5}}{\phi\mu c_t}$$

$$= \frac{4.059 \times 10^{-6}}{\phi\mu c_t} \quad \ldots \text{(D)}$$

Using Eqs. A, B, and D in Eq. 9.24 results in

$$\frac{(2.401 \times 10^{-5})(3.068 \times 10^{-5})}{(\phi\mu c_t)(\phi\mu c_t)} - \left(\frac{4.059 \times 10^{-6}}{\phi\mu c_t}\right)^2 = 285.3, \quad \ldots \text{(E)}$$

so

$$\phi\mu c_t = \sqrt{\frac{(2.401 \times 10^{-5})(3.068 \times 10^{-5}) - (4.059 \times 10^{-6})^2}{285.3}}$$

$$= 1.589 \times 10^{-6} \text{ cp/psi.}$$

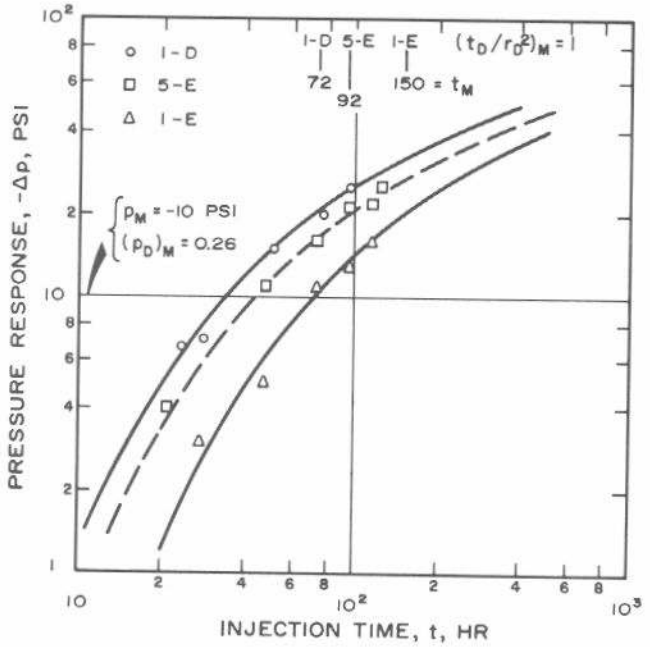

Fig. 9.26 Interference data of Example 9.6 matched to Fig. C.2. Pressure match is the same for all curves.

Thus,

$$c_t = \frac{1.589 \times 10^{-6}}{(0.20)(1)} = 7.95 \times 10^{-6}\ \text{psi}^{-1}.$$

Now, Eqs. A, B, and D are solved using the computed $\phi\mu c_t$:

$$k_x = \frac{2.401 \times 10^{-5}}{1.589 \times 10^{-6}} = 15.11\ \text{md},$$

$$k_y = \frac{3.068 \times 10^{-5}}{1.589 \times 10^{-6}} = 19.31\ \text{md},$$

$$k_{xy} = \frac{4.059 \times 10^{-6}}{1.589 \times 10^{-6}} = 2.55\ \text{md}.$$

We use Eq. 9.25 to estimate the major permeability value,

$$k_{\max} = 0.5\left[(15.11 + 19.31) + \sqrt{(15.11 - 19.31)^2 + 4(2.55)^2}\right]$$
$$= 20.5\ \text{md},$$

and Eq. 9.26 to estimate the minor permeability value,

$$k_{\min} = 0.5\left[(15.11 + 19.31) - \sqrt{(15.11 - 19.31)^2 + 4(2.55)^2}\right]$$
$$= 13.9\ \text{md}.$$

We know $\sqrt{k_{\max}k_{\min}} = 16.89$ from Eq. 9.22, so we can check the computations:

$$\sqrt{k_{\max}k_{\min}} = \sqrt{(20.5)(13.9)}$$
$$= 16.88.$$

Finally, we estimate the direction of $k_{\max}$ from Eq. 9.27:

$$\theta = \arctan\left(\frac{20.5 - 15.11}{2.55}\right)$$
$$= 64.7^\circ \text{ from the } x \text{ axis}.$$

Correcting for the orientation of the axes, the maximum permeability direction is

$$\theta = 64.7 - 47.3 = \text{N}17.4^\circ\text{W}.$$

Example 9.6 indicates that although estimating anisotropic reservoir parameters may be a lengthy procedure, it is not particularly difficult, and does not necessarily require a computer. The most difficult part of the analysis is the simultaneous solution of the equations indicated as Eqs. A, B, and C in Example 9.6. In that example, solution was simple since two of the equations solved themselves. That is often the case, if the coordinate system is chosen judiciously. As indicated in the example, it is not necessarily easiest to choose the coordinate system so it is aligned with north and south.

Swift and Brown[26] propose a computationally different approach to estimating directional properties that is still based on the exponential integral. When applied in a manner similar to that described above, it will give the same results as Ramey's[11] technique, although solution of the simultaneous equations may be more difficult. Swift and Brown[26] suggest that, if enough data are available, a regression approach could be used to estimate $k_{\max}$, $k_{\min}$, and θ. They also state that, if the reservoir is heterogeneous, permeability values estimated by conventional interference-test analysis for homogeneous, anisotropic reservoirs (for example, by Eq. 9.2) may imply directional properties directly contrary to the true situation.

References

1. Matthews, C. S. and Russell, D. G.: *Pressure Buildup and Flow Tests in Wells*, Society of Petroleum Engineers of AIME, Dallas (1967) **1**, Chap. 7.
2. Driscoll, Vance J.: "Use of Well Interference and Build-Up Data for Early Quantitative Determination of Reserves, Permeability and Water Influx," *J. Pet. Tech.* (Oct. 1963) 1127-1136; *Trans.*, AIME, **228.**
3. Matthies, E. Peter: "Practical Application of Interference Tests," *J. Pet. Tech.* (March 1964) 249-252. Also *Reprint Series, No. 9 — Pressure Analysis Methods*, Society of Petroleum Engineers of AIME, Dallas (1967) 145-148.
4. Warren, J. E. and Hartsock, J. H.: "Well Interference," *Trans.*, AIME (1960) **219,** 89-91. Also *Reprint Series, No. 9 — Pressure Analysis Methods*, Society of Petroleum Engineers of AIME, Dallas (1967) 93-95.
5. Vela, Saul and McKinley, R. M.: "How Areal Heterogeneities Affect Pulse-Test Results," *Soc. Pet. Eng. J.* (June 1970) 181-191; *Trans.*, AIME, **249.**
6. Jahns, Hans O.: "A Rapid Method for Obtaining a Two-Dimensional Reservoir Description From Well Pressure Response Data," *Soc. Pet. Eng. J.* (Dec. 1966) 315-327; *Trans.*, AIME, **237.**
7. McKinley, R. M., Vela, Saul, and Carlton, L. A.: "A Field Application of Pulse-Testing for Detailed Reservoir Description," *J. Pet. Tech.* (March 1968) 313-321; *Trans.*, AIME, **243.**
8. Woods, E. G.: "Pulse-Test Response of a Two-Zone Reservoir," *Soc. Pet. Eng. J.* (Sept. 1970) 245-256; *Trans.*, AIME, **249.**
9. Elkins, Lincoln F. and Skov, Arlie M.: "Determination of Fracture Orientation From Pressure Interference," *Trans.*, AIME (1960) **219,** 301-304. Also *Reprint Series, No. 9 — Pressure Analysis Methods*, Society of Petroleum Engineers of AIME, Dallas (1967) 97-100.
10. Earlougher, Robert C., Jr., and Kersch, Keith M.: "Field Examples of Automatic Transient Test Analysis," *J. Pet. Tech.* (Oct. 1972) 1271-1277.
11. Ramey, Henry J., Jr.: "Interference Analysis for Anisotropic Formations — A Case History," *J. Pet. Tech.* (Oct. 1975) 1290-1298; *Trans.*, AIME, **259.**
12. Gringarten, A. C. and Witherspoon, P. A.: "A Method of Analyzing Pump Test Data From Fractured Aquifers," *Proc.*, Symposium on Percolation Through Fissured Rock, International Society for Rock Mechanics, Stuttgart (Sept. 18-19, 1972).
13. Earlougher, R. C., Jr., and Ramey, H. J., Jr.: "Interference Analysis in Bounded Systems," *J. Cdn. Pet. Tech.* (Oct.-Dec. 1973) 33-45.
14. Johnson, C. R., Greenkorn, R. A., and Woods, E. G.: "Pulse-Testing: A New Method for Describing Reservoir Flow Properties Between Wells," *J. Pet. Tech.* (Dec. 1966) 1599-1604; *Trans.*, AIME, **237.**

15. Greenkorn, R. A. and Johnson, C. R.: "Method for Defining Reservoir Heterogeneities," U.S. Patent No. 3,285,064 (Nov. 15, 1966).

16. Johnson, C. R.: "Portable 'Radar' for Testing Reservoirs Developed by Esso Production Research," *Oil and Gas J.* (Nov. 20, 1967) 162-164.

17. Johnson, C. R. and Raynor, R.: "System for Measuring Low Level Pressure Differential," U.S. Patent No. 3,247,712 (April 26, 1966).

18. Miller, G. B., Seeds, R. W. S., and Shira, H. W.: "A New, Surface Recording, Down-Hole Pressure Gauge," paper SPE 4125 presented at the SPE-AIME 47th Annual Fall Meeting, San Antonio, Tex., Oct. 8-11, 1972.

19. Culham, W. E.: "Amplification of Pulse-Testing Theory," *J. Pet. Tech.* (Oct. 1969) 1245-1247.

20. Startzman, R. A.: "A Further Note on Pulse-Test Interpretation," *J. Pet. Tech.* (Sept. 1971) 1143-1144.

21. Brigham, W. E.: "Planning and Analysis of Pulse-Tests," *J. Pet. Tech.* (May 1970) 618-624; *Trans.*, AIME, **249.**

22. Kamal, Medhat and Brigham, William E.: "Pulse-Testing Response for Unequal Pulse and Shut-In Periods," *Soc. Pet. Eng. J.* (Oct. 1975) 399-410; *Trans.*, AIME, **259.**

23. Prats, M. and Scott, J. B.: "Effect of Wellbore Storage on Pulse-Test Pressure Response," *J. Pet. Tech.* (June 1975) 707-709.

24. Pierce, A. E., Vela, Saul, and Koonce, K. T.: "Determination of the Compass Orientation and Length of Hydraulic Fractures by Pulse Testing," *J. Pet. Tech.* (Dec. 1975) 1433-1438.

25. Papadopulos, Istavros S.: "Nonsteady Flow to a Well in an Infinite Anisotropic Aquifer," *Proc.*, 1965 Dubrovnik Symposium on Hydrology of Fractured Rocks, Int'l. Assoc. of Sci. Hydrology (1965) **I,** 21-31.

26. Swift, S. C. and Brown, L. P.: "Interference Testing for Reservoir Definition — The State of the Art," paper SPE 5809 presented at the SPE-AIME Fourth Symposium on Improved Oil Recovery, Tulsa, March 22-24, 1976.

Chapter 10

Effect of Reservoir Heterogeneities on Pressure Behavior

10.1 Introduction

Most material elsewhere in this monograph assumes homogeneous and isotropic reservoirs. This chapter discusses the effects of some common reservoir heterogeneities on pressure transient behavior. Heterogeneities — variations in rock and fluid properties from one location to another — may result from deposition, folding and faulting, post-depositional changes in reservoir lithology, and changes in fluid type or properties.[1] Heterogeneities may be small-scale, as in carbonate reservoirs where the rock has two constituents, matrix and fractures, vugs, or solution cavities. They also may be large-scale, such as physical barriers, faults, fluid-fluid contacts, thickness changes, lithology changes, several layers with different properties in each layer, etc.

A related characteristic is permeability anisotropy. An anisotropic reservoir has permeability that varies with flow direction. Anisotropy can be caused by sedimentary processes (channel fill deposits, for example) or by tectonics (parallel fracture orientations). Anisotropy can occur in both homogeneous and heterogeneous reservoirs. As a result, anisotropy does not necessarily imply heterogeneity in the sense defined in the previous paragraph. Most reservoir rocks have a lower vertical permeability than horizontal permeability, and so are anisotropic in that regard.

All the above heterogeneities usually exist in the virgin state. In addition, man may induce heterogeneities in the reservoir. Man-made heterogeneities include changes near the wellbore from mud invasion during drilling, hydraulic fracturing, acidizing, or fluid injection. Chapter 11 treats man-induced changes such as hydraulic fracturing.

Since heterogeneities exist in varying degrees in many reservoirs, it is important to know how much of the information presented elsewhere in this monograph is usable in heterogeneous systems. Fortunately, many of the single-well transient testing techniques for homogeneous reservoirs may be applied to heterogeneous systems with useful results. Heterogeneities affect multiple-well tests more severely.

Jahns[2] and Vela and McKinley[3] propose techniques for estimating heterogeneous reservoir properties from a series of interference and pulse tests. Such techniques generally require a computer and some type of regression analysis. Even when using the computer and regression techniques, it is difficult (if not impossible) to delineate specific heterogeneities from well tests. The difficulty occurs because *many different conditions can cause the same or similar well-test response*. If we have an idea of the type of heterogeneity, it may be possible to determine some of the properties involved by pressure transient testing. However, it is dangerous — and poor engineering practice — to infer heterogeneous reservoir properties based *solely* on transient testing. Geological, seismic, fluid flow, and performance data should be considered before hypotheses are formed about the type and location of heterogeneities. It may be possible to design a specific transient test to investigate the possibility of a particular type of heterogeneity. For instance, if each layer in a layered reservoir is tested with a straddle packer arrangement, permeability, skin factor, and average pressure of that layer may be estimated from the test data. However, if layers are not isolated in the wellbore during such testing, meaningful individual-layer data cannot be obtained with current technology.

Fig. 10.1 illustrates one of many difficulties that arise in attempting to infer heterogeneities from transient data. The reciprocity principle[4] (Section 9.2) indicates that both situations shown in Fig. 10.1 will have *precisely the same interference response*. Thus, interference testing the two wells cannot indicate which of the two situations in Fig. 10.1 exists. The difficulty might be resolved by interference testing with other wells or by using other data. The importance of Fig. 10.1, however, is the indication that even very simple conditions cannot necessarily be resolved by transient testing.

In this chapter, we discuss permeability anisotropy, classify reservoir heterogeneities, and describe how these heterogeneities affect transient testing. We show that several types of heterogeneities can cause similar transient-test pressure response. We provide some analysis techniques, but again, we caution that results should be supported by other data. The main goal here is to illustrate a variety of situations — a comprehensive treatment would require a monograph itself.

10.2 Linear Discontinuities — Faults and Barriers

Linear discontinuities, particularly single sealing faults, have been a popular topic in the transient-testing literature.[1,5-9] Fig. 10.2 shows a single well, Well A, near a linear sealing fault in an otherwise infinite-acting reservoir. Horner[5] considers pressure buildup and Russell[7] discusses two-rate flow testing in that system. Regardless of test type, the linear flow barrier affects the test in about the same way. To obtain the effect of the linear fault, we use the method of images[1,5] (see Appendix B) and add an image well, Well A′, as shown in Fig. 10.2. Then the pressure drop anywhere on the left side of the fault is the sum of the pressure drops caused by Wells A and A′. The following illustrates the process for drawdown testing.

If Well A, near a linear fault, is put on production at $t = 0$, the pressure change at the well is estimated by using the superposition principle (Section 2.9) and the two wells shown in Fig. 10.2. Thus, the pressure drop at Well A is the Δp at Well A caused by production at Well A plus the Δp at Well A caused by production at Well A′:

$$\Delta p = p_i - p_{wf}$$
$$= \Delta p_{A,A} + \Delta p_{A,A'}.$$

Using Eq. 2.2,

$$\Delta p = \frac{141.2}{kh} qB\mu \left\{\left[p_D(t_D, r_D = 1) + s\right] + p_D(t_D, 2L/r_w)\right\}, \quad \ldots\ldots\ldots\ldots\ldots\ldots\ldots\ldots\ldots\ldots (10.1)$$

since q is the same at both wells. For infinite-acting systems, the dimensionless pressure is given by the exponential-integral solution, Eq. 2.5a. At relatively short times, the log approximation applies *at Well A* and p_D is given by Eq. 2.5b.

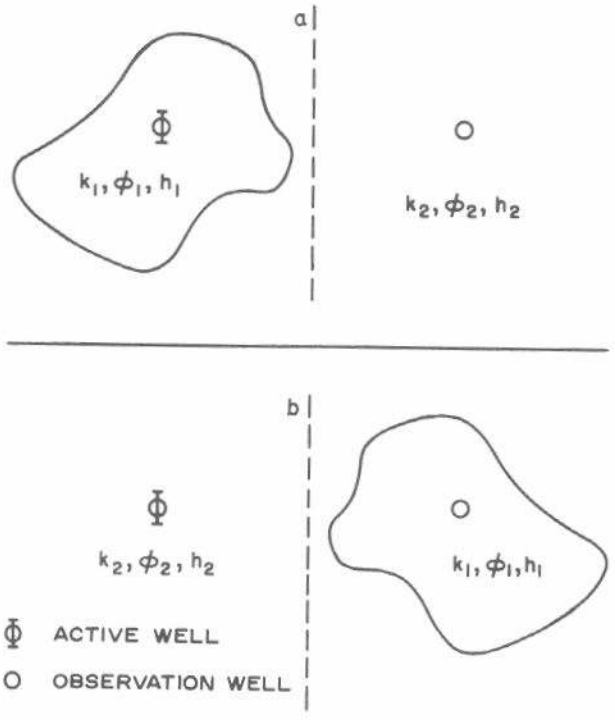

Fig. 10.1 Nonuniqueness because of reciprocity. Mirror-image models give identical multiple-well test responses. After Jahns.[2]

Furthermore, at short times t_D/r_D^2 for the image well is small, so the dimensionless-pressure contribution from the image well is essentially zero (see Fig. C.2). As a result, at short times the flowing bottom-hole pressure at Well A is given by Eq. 3.5, the familiar drawdown relationship:[1,5]

$$p_{wf} = m \log t + p_{1hr}. \quad \ldots\ldots\ldots\ldots\ldots\ldots\ldots\ldots\ldots\ldots (10.2)$$

Eq. 10.2 indicates that a plot of short-time drawdown bottom-hole pressure vs log t should have a straight-line portion with slope m given by Eq. 3.6,

$$m = \frac{-162.6\, qB\mu}{kh}, \quad \ldots\ldots\ldots\ldots\ldots\ldots\ldots\ldots\ldots\ldots (10.3)$$

and intercept p_{1hr} given by Eq. 3.7. Thus, for a well near a linear fault, drawdown (buildup, two-rate, etc.) testing can be used to estimate reservoir permeability and skin factor in the usual fashion, as long as wellbore storage effects do not mask the initial straight-line section. If the well is very close to the fault, the initial straight line may end so quickly that it is masked by wellbore storage.

As the drawdown proceeds, the dimensionless-pressure contribution from Image Well A′ becomes significant, and the pressure at the producing well falls below the initial semilog straight line. After a long-enough production time, p_D for the image well is given by Eq. 2.5b, so[9]

$$p_{wf} = 2(m \log t + p_{1hr}) + \left\{p_i + m\left[0.86859\, s + \log\left(\frac{4L^2}{r_w^2}\right)\right]\right\}. \quad \ldots\ldots\ldots\ldots\ldots\ldots\ldots\ldots\ldots\ldots (10.4)$$

Eq. 10.4 indicates that the p_{wf} vs log t plot will have a second straight-line portion with a slope double that of the initial straight line. The double slope also occurs in two-rate testing, pressure buildup testing, injectivity testing, and pressure falloff testing.[1,5,7] Average drainage-region pressure is estimated in the manner normally used for buildup testing using the *second* straight line.

The simple occurrence of a doubling of slope in a transient test *does not guarantee* the existence of a linear boundary

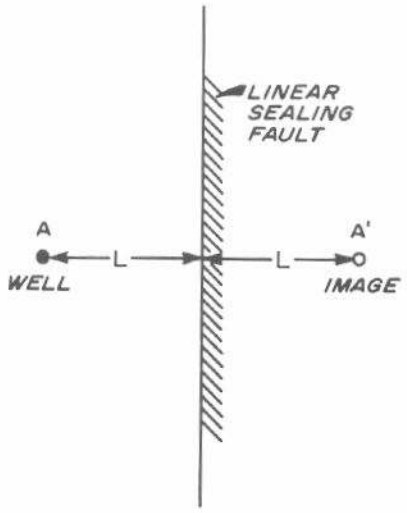

Fig. 10.2 Linear sealing fault near a producing well.

near the well. Pressure data taken during wellbore storage domination can cause two apparent semilog straight lines with a slope increase (for examples, see Figs. 5.2 and 7.4). In such cases, the apparent semilog straight lines are caused completely by wellbore effects and have nothing to do with reservoir characteristics. Thus, it is important to construct the log-log plot of transient test data to determine when wellbore storage effects are no longer important. That is particularly true when a slope increase is *expected* from a transient test.

To estimate distance to a linear discontinuity, we use the intersection time, t_x, of the two straight-line segments of the drawdown curve:[9]

$$L = 0.01217\sqrt{\frac{kt_x}{\phi\mu c_t}} \quad \ldots\ldots\ldots\ldots\ldots\ldots (10.5)$$

Eq. 10.5 applies for drawdown testing. Russell[7] gives an equation for two-rate testing. For pressure buildup testing, the intersection point of the two straight lines is related to the dimensionless pressure at the intersection time by

$$p_D\left[t_D/(2L/r_w)^2\right] = \frac{1}{2}\ln\left(\frac{t_p + \Delta t}{\Delta t}\right)_x \quad \ldots\ldots\ldots\ldots (10.6)$$

Thus, to estimate the distance to a linear fault from a pressure buildup test, we find $[(t_p + \Delta t)/\Delta t]$ when the semilog straight lines intersect and calculate p_D from Eq. 10.6. Then we enter Fig. C.2 with that value of p_D and determine $\left[t_D/(2L/r_w)^2\right]_{\text{Fig. C.2}}$. Finally,

$$L = \sqrt{\frac{0.0002637\,kt_p}{4\phi\mu c_t\left[t_D/(2L/r_w)^2\right]_{\text{Fig. C.2}}}} \quad \ldots\ldots\ldots\ldots (10.7)$$

When $t_p >> \Delta t$, a useful estimate of L may be made from a pressure buildup test by using Eq. 10.5 with Δt_x in place of t_x.

Example 10.1 Distance to a Fault From a Pressure Buildup Test

Pressure buildup data are shown in Figs. 10.3 and 10.4. The log-log plot, Fig. 10.3, indicates that wellbore storage effects are not important, so the increase in slope in Fig. 10.4 is probably caused by reservoir heterogeneity. The ratio of the two slopes is 1.79. Since the absolute value of the slopes is *increasing* with shut-in time, and since the slope ratio is about 2, a linear fault is suspected. Seismic data have verified the existence of a fault near this well.

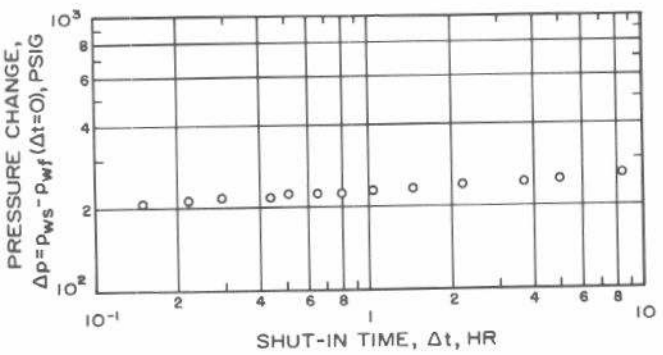

Fig. 10.3 Log-log data plot for Example 10.1.

Test data are

$q = 10{,}250$ STB/D $\quad B = 1.55$ RB/STB
$t_p = 530$ hours $\quad \phi = 0.09$
$p_{wf}(\Delta t = 0) = 3{,}666$ psig $\quad c_t = 22.6 \times 10^{-6}$ psi^{-1}
$h = 524$ ft $\quad r_w = 0.354$ ft.
$\mu = 0.20$ cp

Formation permeability is estimated from the first straight line using Eq. 5.6. Recall that for a Horner plot the slope is $-m$, so $m = 24.3$ psig/cycle.

$$k = \frac{(162.6)(10{,}250)(1.55)(0.20)}{(524)(24.3)}$$

$$= 40.6 \text{ md}.$$

To estimate the distance to the fault, we determine $[(t_p + \Delta t)/\Delta t]_x = 285$ from Fig. 10.4. Then using Eq. 10.6, $p_D\left[t_D/(2L/r_w)^2\right] = (1/2)\ln(285) = 2.83$. Referring to Fig. C.2, we see that $\left[t_D/(2L/r_w)^2\right]_{\text{Fig. C.2}} = 135$ when $p_D = 2.83$. Next, we use Eq. 10.7:

$$L = \sqrt{\frac{(0.0002637)(40.6)(530)}{(4)(0.09)(0.20)(22.6 \times 10^{-6})(135)}}$$

$$= 161 \text{ ft}.$$

Since $t_p >> \Delta t$, we could use Eq. 10.5 with $\Delta t_x = 1.87$ hours to estimate $L = 166$ ft — quite good agreement.

If we wish, we may use Eq. 5.7 and data from the first straight line to estimate $s = 4.4$.

Multiple faults near a well may cause several different transient-test characteristics. For example, two faults intersecting at a right angle near a well may cause the slope to double, then redouble, or may simply cause a fourfold slope increase, depending on well location. It is not safe, however, to assume that additional boundaries continue to double transient-test response slopes. For example, a single well producing from the center of a closed square has an increase

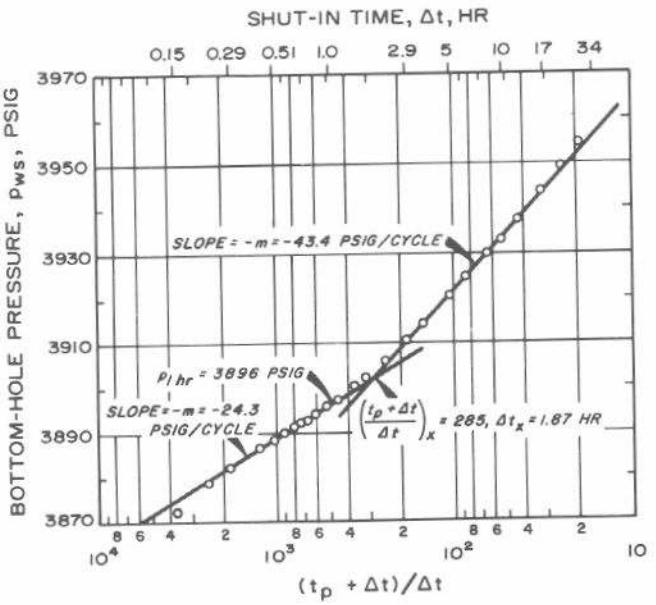

Fig. 10.4 Horner plot for pressure buildup data of Example 10.1.

in slope as the system reaches pseudosteady state; but during a pressure buildup test the slope decreases from the initial semilog straight line as the pressure approaches average reservoir pressure. Ramey and Earlougher[10] illustrate pressure buildup curves for several closed reservoir situations. Figs. 10.5 and 10.6 show such pressure buildup curves for closed-square and rectangular systems. Some of those buildup curves have characteristics commonly attributed to various kinds of heterogeneities. For example, Curve 3 in Fig. 10.5 has a peculiar bend that could be interpreted as the result of natural fracturing, as studied by Warren and Root[11] (Section 10.6). The curve shapes in Fig. 10.6 all show some upward bending that might be misinterpreted as indications of faulting, stratification, or some other reservoir heterogeneity. Yet, in all cases, the curve shapes are caused only by the shape of the closed system. In particular, there is no definite indication of multiple boundaries from any of the curves. Ramey and Earlougher[10] and Earlougher *et al.*[12] show several other pressure buildup curves with shapes that might be interpreted as reservoir heterogeneities. Generally, reservoir simulation must be used to estimate pressure transient response for complex, multiple-fault situations.

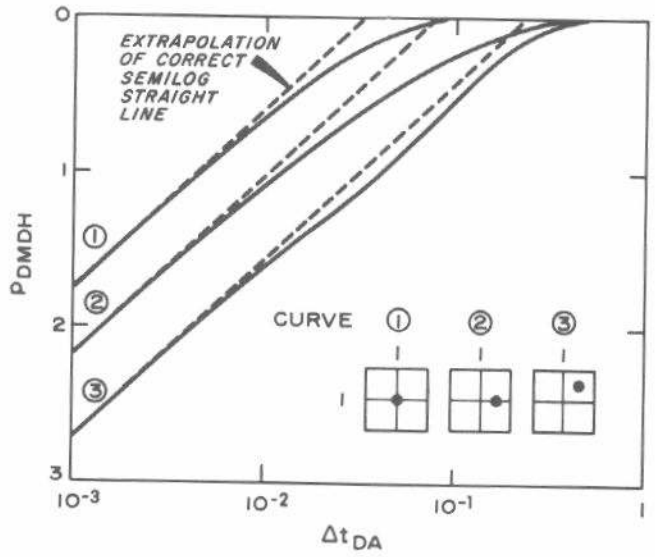

Fig. 10.5 Miller-Dyes-Hutchinson-type pressure buildup curves for square shapes. After Ramey and Earlougher.[10]

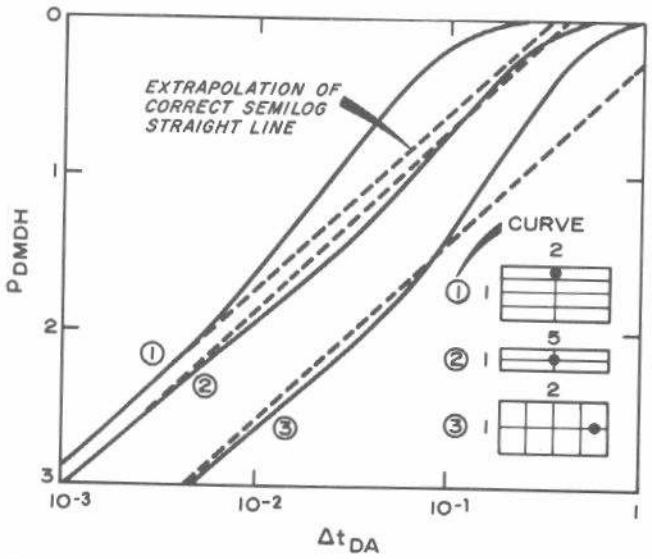

Fig. 10.6 Miller-Dyes-Hutchinson-type pressure buildup curves for rectangular shapes. After Ramey and Earlougher.[10]

Fig. 10.7 illustrates three possible physical models for linear discontinuities in reservoirs. The upper case corresponds to the linear sealing fault already described. The lower two cases correspond to situations with a linear change in reservoir or fluid properties, but with flow still occurring. Bixel, Larkin, and van Poollen[8] discuss the third situation in detail for drawdown and less thoroughly for pressure buildup. They show that in both drawdown and buildup, the semilog straight-line slope may either *increase* or *decrease* depending on the contrast in properties between two reservoir regions. The slope ratio on the semilog plot equals the k/μ ratio *only* if ϕc_t does not vary appreciably across the discontinuity, and if the distance from the well to the reservoir boundary is much greater than the distance between the well and the discontinuity. (A similar situation is discussed in Section 7.5.) Bixel, Larkin, and van Poollen[8] suggest a curve-matching procedure to analyze for reservoir properties on both sides of the discontinuity and to estimate the distance to the discontinuity. Their procedure applies to drawdown testing if sufficient long-time, constant-rate data are available. Although the method could be applied to pressure buildup testing, Ref. 8 does not give the necessary curves.

10.3 Permeability Anisotropy

In some porous materials, permeability varies in different flow directions. In such materials, the permeability may be described mathematically by a symmetric tensor[13,14] or by maximum and minimum permeabilities oriented 90° apart, and by a direction for the maximum permeability. Those quantities are called the principal permeabilities and prin-

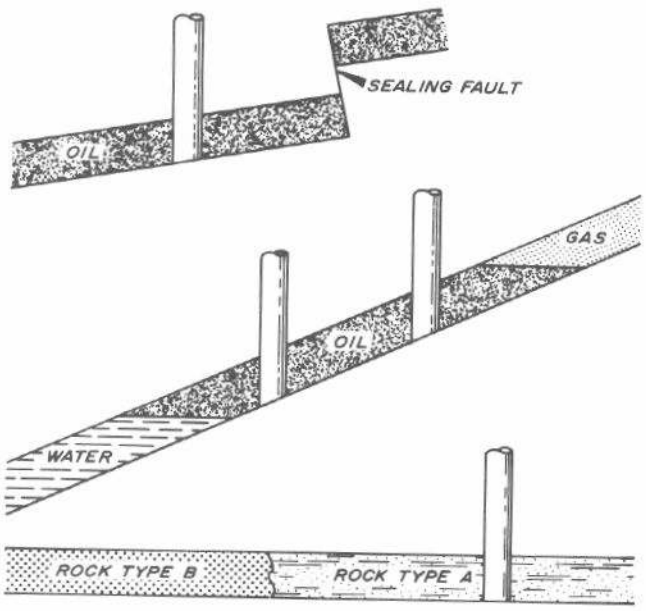

Fig. 10.7 Physical models for linear discontinuities. After Bixel, Larkin, and van Poollen.[8]

cipal direction. Refs. 13 and 14 give a complete treatment of permeability anisotropy. This section briefly describes fluid-flow equations for horizontal homogeneous anisotropic systems and shows the similarity of the equations to those for isotropic systems.

Consider a single well in an infinite, horizontal reservoir containing single-phase fluid of constant and small compressibility. The reservoir is homogeneous but anisotropic with k_{max} and k_{min} oriented in the x and y directions, respectively. (Note that we choose the coordinates for the flow equations to coincide with the principal permeability direction.) We transform the x-y coordinate system by changing the scale along each axis:

$$x' = x\sqrt{\bar{k}/k_{max}}, \quad \ldots\ldots\ldots\ldots\ldots\ldots\ldots\ldots (10.8a)$$

$$y' = y\sqrt{\bar{k}/k_{min}}, \quad \ldots\ldots\ldots\ldots\ldots\ldots\ldots\ldots (10.8b)$$

where

$$\bar{k} = \sqrt{k_{max}k_{min}}. \quad \ldots\ldots\ldots\ldots\ldots\ldots\ldots\ldots (10.9)$$

The diffusivity equation, Eq. 2.1, retains its normal form when expressed in x'-y' coordinates if $\bar{k}$ is used in place of k. Fig. 10.8 illustrates the transformation of Eq. 10.8. In particular, a circular region such as a wellbore is transformed into an elliptical region. The choice of $\bar{k}$ (Eq. 10.9) causes the area of the well to be the same in both the physical and transformed systems. The transformation allows dimensionless-pressure solutions for isotropic systems to be used for anisotropic systems, as long as the shape and well location of the *transformed system* matches that of the p_D chosen. For an infinite-acting anisotropic reservoir, the flowing wellbore pressure is given by

$$p_{wf} = p_i + m\left[\log t + \log\left(\frac{\bar{k}}{\phi\mu c_t r_w^2}\right) - 3.2275 + 0.86859\,(s - s'')\right]. \quad \ldots\ldots\ldots (10.10)$$

The similarity of Eq. 10.10 to Eq. 3.4 for pressure drawdown in an isotropic system is important. In Eq. 10.10, m is the slope of a p_{wf} vs $\log t$ plot and is given by the anisotropic equivalent of Eq. 3.6:

$$m = -\frac{162.6\,qB\mu}{\bar{k}h}. \quad \ldots\ldots\ldots\ldots\ldots\ldots\ldots\ldots (10.11)$$

The effective permeability may be estimated in the usual manner by solving Eq. 10.11 for $\bar{k}$ to obtain the analog of Eq. 3.9. The analogy applies to pressure buildup, injectivity, and falloff testing as well as to drawdown testing. It also carries over to multiple-rate testing, so all single-well testing techniques described elsewhere in this monograph may be used in anisotropic systems. The skin factor, estimated in the usual way, will be $(s - s'')$ in Eq. 10.10, where[11]

$$s'' = 2.303\log\left(\frac{\sqrt{k_{max}} + \sqrt{k_{min}}}{2\sqrt{\bar{k}}}\right). \quad \ldots\ldots\ldots (10.12)$$

The analogy between anisotropic-system and isotropic-system flow equations indicates the following for *single-well* transient testing in anisotropic reservoirs:

1. The permeability estimated by normal methods is $\bar{k}$ defined by Eq. 10.9.
2. The skin factor estimated by normal methods is $s - s''$. Eq. 10.12 shows that $s'' > 0$ always, so the estimated skin factor from a transient test in an anisotropic system will be somewhat low. Nonetheless, Eq. 10.12 does not provide a way to estimate k_{max}/k_{min} because, in general, there is no way to estimate s'' in single-well transient testing.
3. It is impossible to recognize that the system is anisotropic from a single-well test because the appearance of the pressure response curve is the same as for isotropic reservoirs.

Anisotropic reservoirs can be recognized by geological studies, oriented cores, reservoir performance (waterflood behavior, for example), etc. Correctly conducted multiple-well transient tests may be used to recognize and quantify anisotropic reservoir properties.[15-18] Section 9.4 describes a method for estimating anisotropic reservoir characteristics from interference testing. Refs. 2 and 16 describe other methods.

In most petroleum reservoirs, vertical permeability is significantly less than horizontal permeability. Methods for estimating vertical permeability are described in Section 10.8.

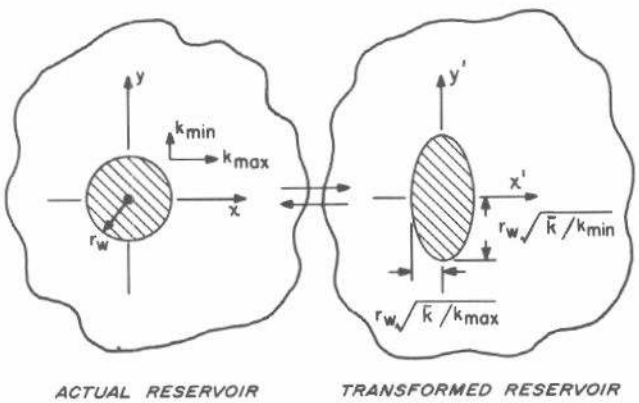

Fig. 10.8 Transformation of a homogeneous, anisotropic, infinite reservoir with a circular well to an equivalent homogeneous, isotropic reservoir.

10.4 Composite Systems

In a composite system, fluid or rock properties vary in a steplike fashion in the radial direction away from a well (Fig. 10.9). (Transient pressure behavior of systems with linear discontinuities is discussed in Section 10.2.) Radial composite systems are generally man-induced. Examples are formation damage or improvement near the wellbore; the bubble formed when natural gas is injected into an aquifer; the burned zone in an in-situ combustion project; the water bank in a waterflood project (see Section 7.5); and the rubble and fracture zones in a nuclear stimulation project.

Both k/μ and ϕc_t may vary from one annular zone to another, as illustrated in Fig. 10.9. Analytical[19-23] and numerical[24-26] solutions have both been used to study transient behavior in composite systems. Refs. 19 through 26 indicate that the k/μ change in the radial direction is re-

flected as a slope change on the semilog plot, as shown in Fig. 7.14. The first straight line may be used to estimate k/μ for the inner region and the skin factor — if wellbore storage effects do not mask that straight line. Equations in Chapters 3 through 7 apply.

Because of the interplay between k/μ and ϕc_t in the two zones, the ratio of the late-time and early-time slopes, m_2/m_1, is not necessarily the same as the ratio of the mobilities $(k/\mu)_1/(k/\mu)_2$. Odeh[23] indicates that the ratios are the same for drawdown (and injection) only if ϕc_t is constant everywhere and if the outer radius or the outer reservoir boundary is more than 10 times the radius of the boundary between the two zones. Merrill, Kazemi, and Gogarty[26] provide similar results for falloff (or buildup). In some cases,[26] there may be no slope change at all.

The second straight-line portion of a falloff or buildup semilog plot may be used to estimate k/μ of the second zone, as indicated in Section 7.5. An alternative approach for pressure drawdown (injectivity) analysis is the curve-matching procedure proposed by Bixel and van Poollen.[24]

When there is an extreme variation in k/μ from Zone 1 to Zone 2, the pressure buildup (falloff) behavior may be similar to that shown by Carter,[22] Fig. 10.10. The figure is for a bounded, two-zone reservoir with the properties given in the caption. The semilog straight line for the first zone ends after about 0.4 day; then the pressure levels off before the slope increases toward that for the second zone. In the case shown in Fig. 10.10, the second straight line never completely develops before the pressure builds to average reservoir pressure. It is significant that the buildup-curve shape in Fig. 10.10 is commonly attributed to pressure buildup behavior in noncommunicating, layered reservoirs (see Section 10.5, Figs. 10.14 through 10.16). This illustrates the difficulty of analyzing transient pressure behavior in heterogeneous systems; many situations can cause pressure transient tests to have similar characteristics, and the characteristics are not always the same for a particular heterogeneity.

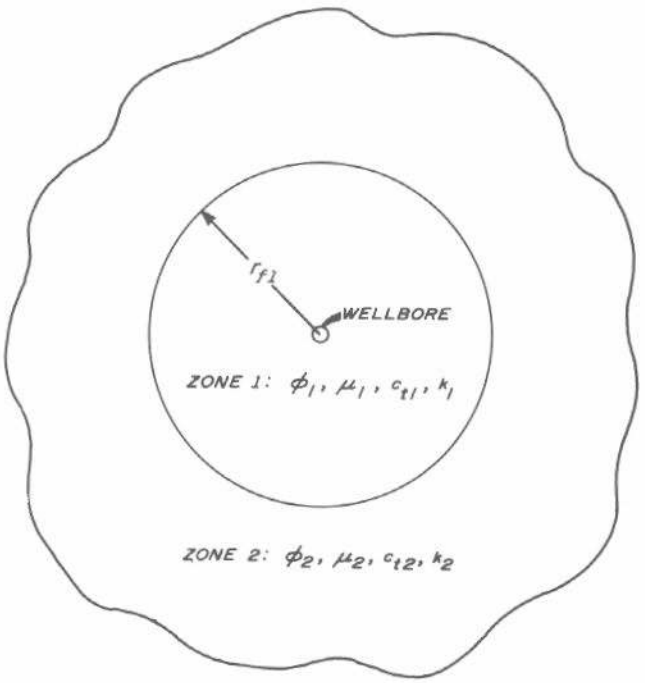

Fig. 10.9 Composite reservoir.

The distance to the boundary between the inner and outer zones, r_{f1}, may be estimated from Eq. 2.41 for a *drawdown* or *injectivity* test,

$$r_{f1} = 0.029\sqrt{\frac{kt^*}{\phi\mu c_t}}, \quad \ldots\ldots\ldots\ldots\ldots\ldots (10.13)$$

where t^* is the time at the *end* of the first semilog straight line. Eq. 10.13 provides an order-of-magnitude estimate only. Section 7.5 gives a method for estimating r_{f1} for buildup and falloff. Eq. 7.16 or Eq. 7.17 and Fig. 7.15 are used. Odeh[23] proposes a trial-and-error method for estimating r_{f1} and $(k/\mu)_2$.

Bixel and van Poollen[24] and Carter[22] state that it may be difficult, or impossible, to estimate average reservoir pressure from pressure buildup (or falloff) tests in composite systems unless very long shut-in times occur. Carter[22] does show that if a drawdown test is continued long enough, the total reservoir volume communicating with the well may be estimated using the analysis techniques of Section 3.5.

10.5 Layered Reservoir Systems

Layered reservoirs can be divided into two groups: *layered reservoirs with crossflow*, in which layers are hydrodynamically communicating at the contact planes (Fig. 10.11), and *layered reservoirs without crossflow*, in which layers communicate only through the wellbore (Fig. 10.12). The latter type of system also has been called a "commingled system".

Layered Reservoirs With Crossflow

Fig. 10.11 schematically shows a three-layer reservoir with crossflow allowed between the layers. Many papers discuss pressure transient testing in such reservoirs; Russell and Prats[27] summarize the practical aspects of those papers. They conclude that pressure transient behavior of a layered reservoir is the same as the behavior of the *equivalent homogeneous system*. Thus, the layered system with crossflow behaves like a homogeneous system with an arithmetic total permeability-thickness product,

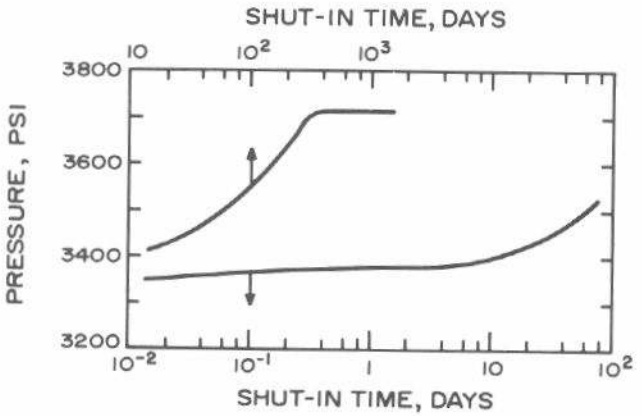

Fig. 10.10 Pressure buildup for a composite gas reservoir with $k_1 = 10$ md, $k_2 = 0.01$ md, $r_{f1} = 500$ ft, $r_e = 1{,}000$ ft, $\phi_1 = \phi_2$, $\mu_1 = \mu_2$, and $c_{t1} = c_{t2}$. After Carter.[22]

$$(kh)_t = \sum_{j=1}^{n} (kh)_j, \quad \ldots\ldots\ldots\ldots\ldots\ldots (10.14)$$

substituted for kh and an arithmetric total porosity-compressibility-thickness product,

$$(\phi c_t h)_t = \sum_{j=1}^{n} (\phi c_t h)_j, \quad \ldots\ldots\ldots\ldots\ldots\ldots (10.15)$$

substituted for $\phi c_t h$. The total number of layers is n. As a result, the appropriate semilog plot for any pressure transient test can be analyzed just like it can for homogeneous systems.

Kazemi and Seth[28] show how a series of drillstem tests on sequential intervals can be used to estimate the average permeability of the tested intervals and, thus, provide a gross picture of layering. A flow profile, such as a spinner survey, may also indicate gross reservoir stratification. If $(kh)_t$ is known from a well test, individual layer permeabilities may be approximated from[29]

$$k_j = (q_j/q)\left[(kh)_t/h_j\right], \quad j = 1, 2, \ldots, n.$$
$$\ldots\ldots\ldots\ldots\ldots\ldots\ldots\ldots (10.16)$$

Layered Reservoirs Without Crossflow

Fig. 10.12 schematically illustrates a two-layer reservoir with the layers separated by a flow barrier. Production is commingled at the well so layers communicate only through the well. Early-time pressure drawdown in such a system yields a straight line on the semilog plot,[30-35] as illustrated in Fig. 10.13. Nothing distinguishes the drawdown curve from that for a single-layer, homogeneous reservoir. The slope of the semilog straight line may be used to estimate $(kh)_t$ and average skin factor with normal drawdown equations. The drawdown curves shown in Fig. 10.13 are for a layered system with no skin damage or with equal skin damage in each layer. If the damage varies from layer to layer, the behavior may differ from that shown. Unfortunately, there is little information available about that situation.

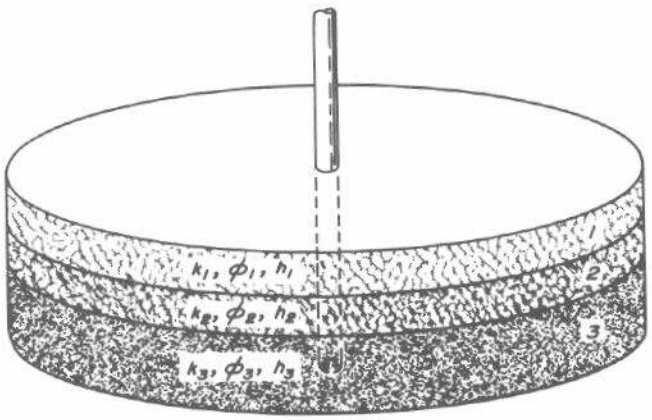

Fig. 10.11 Three-layer reservoir with crossflow.

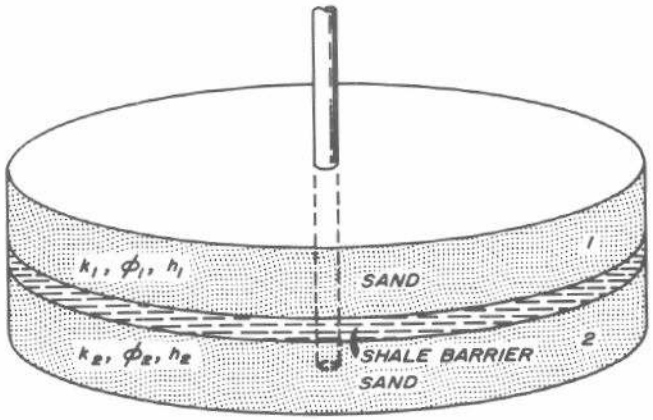

Fig. 10.12 Two-layer reservoir without crossflow.

The upward bending in Fig. 10.13 is caused by boundary effects. After a long enough production time, pseudosteady-state conditions prevail and the pressure behavior will be linear with time. Pseudosteady-state flow generally begins much later in a commingled system than in the equivalent single-layer system because of the complex variation in flow contribution of each layer and the different times required for boundary effects to be felt in each layer. Cobb, Ramey, and Miller[33] indicate that pseudosteady-state flow begins at approximately

$$(t_{DA})_{pss} \simeq 23.5\,(k_1/k_2), \quad k_1 > k_2, \quad \ldots\ldots\ldots (10.17)$$

for a single well in the center of a closed, circular, two-layered reservoir with porosity, compressibility, viscosity, and thickness equal in each layer. (Recall that $(t_{DA})_{pss} \simeq 0.1$ for a single-layer, closed, circular system.) Earlougher, Kersch, and Kunzman[35] indicate that the time to the beginning of pseudosteady state also depends on the relationship between the porosity, thickness, and compressibility in the various layers. We should also expect that time to depend on reservoir shape, number of layers, and well location.

A Horner or Miller-Dyes-Hutchinson plot of pressure buildup data for a single-well, closed, layered, no-crossflow system has an initial straight-line section with slope proportional to $(kh)_t$.[1,30-35] It has been stated that, after the initial semilog straight line, the buildup curve flattens, then steepens, and finally flattens toward static pressure,[1,30,33] as

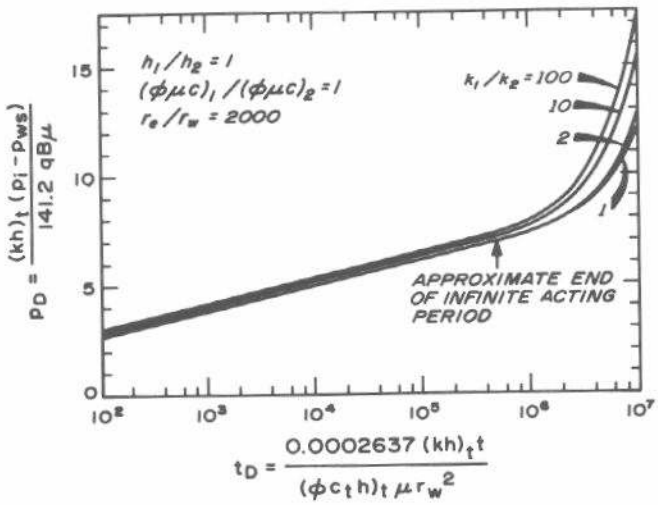

Fig. 10.13 Dimensionless drawdown behavior for a well in the center of a closed, circular, commingled, layered reservoir. After Cobb, Ramey, and Miller.[33]

indicated schematically in Fig. 10.14. *This is not always correct*. Several studies [32-35] show that the first flattening of the buildup curve, F-G in Fig. 10.14, can be insignificant for some systems. That is particularly true for large contrasts in thickness or porosity, for more than two layers, or for nonsymmetrical systems. Figs. 10.15 and 10.16 illustrate flattening and its absence. In Fig. 10.15, the flattening and secondary pressure rise are definitely apparent for the two lower curves. However, in the upper curve, where the *kh* ratio is the result of a large thickness ratio rather than a high permeability ratio, the buildup curve is indistinguishable from that for a single-layer system. Fig. 10.16 shows that the flattening does not occur for a 4:1 rectangle. Rather, the buildup curves take on a shape dominated by the drainage-area shape and the well location. Nevertheless, in all cases, the initial semilog straight-line segment may be used to estimate the total permeability-thickness product.[35] The second (steep) slope is not analyzable by known methods.

An additional danger lies in attributing the shape shown in Fig. 10.14 to layered reservoirs. Fig. 10.10, for a composite reservoir system, has the shape shown in Fig. 10.14. (There is no wellbore storage effect in Figs. 10.10, 10.15, and 10.16.) Changing wellbore storage can also cause the early part of a pressure buildup curve to be similar to the curve shown in Fig. 10.14; for examples, see Fig. 2.12 or Fig. 11.2, and Ref. 36.

Almost all the published material about layered systems is for a single well in the center of a symmetrical bounded system. If there are other wells in the reservoir, and if they continue producing while one well is shut in for a buildup test, none of the pressure response characteristics described in Refs. 30 through 35 and illustrated in Figs. 10.14 through 10.16 necessarily occur. Fig. 10.17 shows pressure behavior when a single well in a developed, two-layer, commingled reservoir is shut in for pressure buildup testing. The initial semilog straight line is observed and may be used to estimate $(kh)_t$. However, neither the flattening nor the secondary pressure rise and eventual leveling to average reservoir pressure occur. Rather, the influence of adjacent producing wells causes the pressure to decline at the shut-in well, completely obscuring evidence of possible layered behavior.

Raghavan *et al.*[34] propose a technique for estimating the *kh* ratio between layers for a single well in the center of a circular, two-layer, commingled system. The method re-

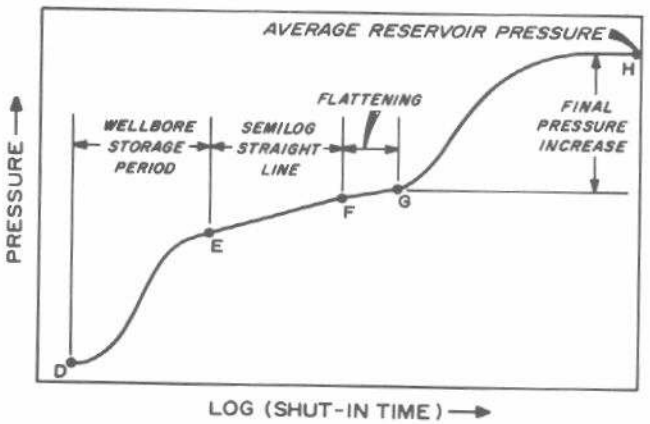

Fig. 10.14 Hypothetical pressure buildup curve for an ideal single-well, multiple-layer, bounded reservoir. After Earlougher, Kersch, and Kunzman.[35]

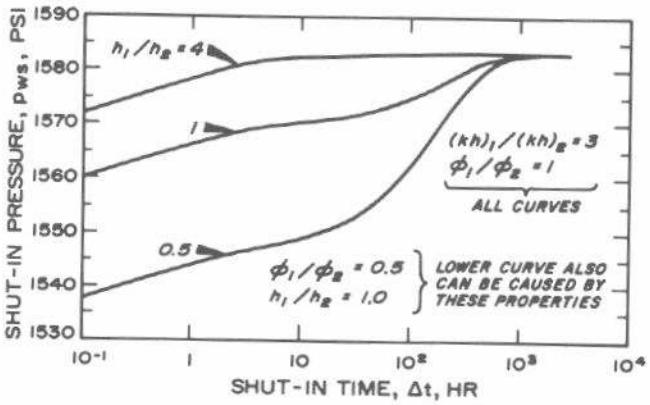

Fig. 10.15 Pressure buildup behavior as a function of thickness ratio for a well in the center of a square, two-layer reservoir; $(kh)_1/(kh)_2 = 3$, $\phi_1/\phi_2 = 1$. After Earlougher, Kersch and Kunzman.[35]

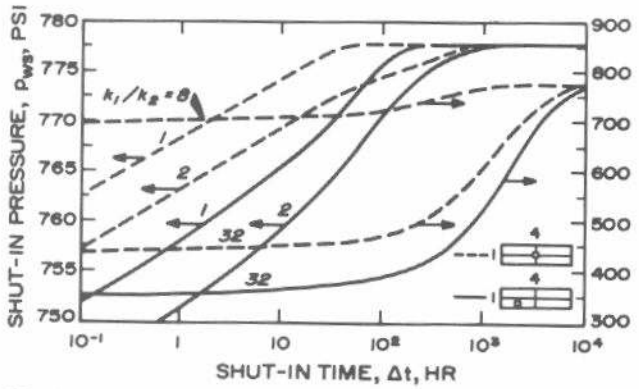

Fig. 10.16 Pressure buildup behavior as a function of permeability ratio for two different well locations in a two-layer, 4:1, rectangular reservoir; $\phi_1/\phi_2 = 1$, $h_1/h_2 = 1$. After Earlougher, Kersch, and Kunzman.[35]

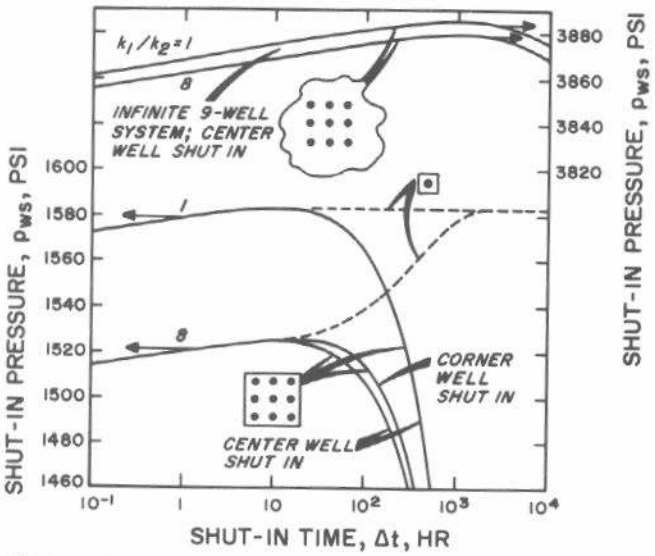

Fig. 10.17 Comparison of pressure buildup behavior in single-well and multiple-well layered systems; $\phi_1/\phi_2 = 1$, $h_1/h_2 = 1$. After Earlougher, Kersch, and Kunzman.[35]

quires a relatively long production time and requires that buildup data be taken *through* the final pressure rise.

Refs. 33 through 35 may be used to estimate average reservoir pressure from buildup tests in commingled systems. The techniques do require some knowledge of the layer properties and utilize correlations for specific systems.

Woods[29] has studied pulse-test behavior in a two-layer reservoir system. His studies include the commingled case, the full-communication case, and intermediate situations. He shows how a combination of single-well tests, pulse tests, and flowmeter surveys may be used to estimate individual-zone properties for two-layer reservoirs with communication only at the wellbores. He points out that the wellbores must be undamaged or uniformly damaged. He extensively studied *pulse-test* behavior in such reservoirs, with the following conclusions:

1. Apparent kh/μ is always equal to or greater than the actual total kh/μ for the reservoir.
2. Apparent $\phi c_t h$ is always equal to or less than total $\phi c_t h$ for the reservoir.
3. The deviation of apparent values from actual total values depends on the pulse duration (see Section 9.3).
4. When wells are undamaged or have uniform damage, the ratio of flow rates into the zones is a good estimator of kh/μ of the zones for noncommunicating systems. The estimate is usually valid within ±15 percent when the zones are partially communicating.

10.6 Naturally Fractured Reservoirs

Naturally fractured reservoirs are among the commonly encountered heterogeneous systems. Two basic behaviors may occur in such reservoirs. If the existing fractures dominantly trend in a single direction, the reservoir may appear to have anisotropic permeability and methods of Sections 9.4 and 10.3 apply. Earlougher and Kersch[16] show interference data from such a reservoir. The second class of naturally fractured reservoirs exhibits two distinct porosity types as shown on the left side of Fig. 10.18. The matrix region contains fine pores and often has low permeability. The remaining region — a set of interconnecting fractures, fissures, and vugs — has a significant porosity and a high permeability compared with the matrix. Ideally, we would like to be able to estimate the permeability and porosity of each region from transient-test data. Much theoretical information is available[11,37-45] about transient testing in fractured reservoirs. Unfortunately, published field data are scarce.

Pollard[37] and Pirson and Pirson[38] suggest analysis techniques for estimating average pressure, wellbore damage, fracture volume, and matrix volume. Warren and Root[11] and Kazemi[44] show that the Pollard-Pirson-Pirson method may be considerably in error for both infinite-acting and finite fractured reservoirs. In addition, unfractured reservoirs may be analyzed by this method and may be reported to be fractured. Thus, we recommend that the Pollard-Pirson-Pirson method not be used.

Warren and Root[11] assume that a fractured reservoir can be represented by the system shown on the right side of Fig. 10.18. The blocks represent the matrix; the space between blocks represents fractures. Warren and Root assume that formation fluid flows from the blocks into the fractures under pseudosteady-state conditions. The fractures carry all fluid to the wellbore. Kazemi[44] uses a similar model but does not require pseudosteady-state flow from the matrix to the fractures. His results verify those presented by Warren and Root.

Warren and Root define two characteristics of the fractured system, the ratio of the porosity-compressibility product of the fractures to the total system porosity-compressibility product,

$$F_{ft} = \frac{(\phi c_t)_f}{(\phi c_t)_f + (\phi c_t)_{ma}}, \quad \ldots\ldots\ldots\ldots (10.18)$$

and the interporosity flow parameter,

$$\epsilon = \frac{\alpha k_{ma} r_w^2}{\bar{k}_f}. \quad \ldots\ldots\ldots\ldots\ldots (10.19)$$

In Eqs. 10.18 and 10.19 the subscript f indicates a fracture property, while ma indicates a matrix property. In Eq. 10.19 α is a matrix-to-fracture geometric factor with dimension of length^{-2}. Warren and Root[11] and Kazemi[44] indicate how this factor may be estimated. The effective fracture permeability is $\bar{k}_f$; Warren and Root consider fractures with different permeabilities in the principal directions.

Fig. 10.19 shows computed drawdown behavior for the Kazemi and Warren and Root analytical models; note the two parallel semilog straight-line portions. The slope of either straight line indicates the total system permeability-

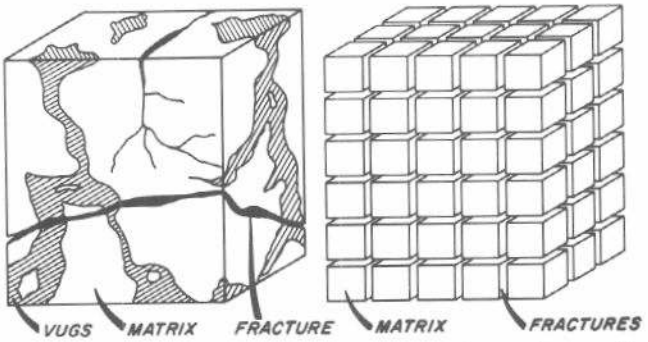

Fig. 10.18 Schematic illustration of a naturally fractured reservoir and its idealization. After Warren and Root.[11]

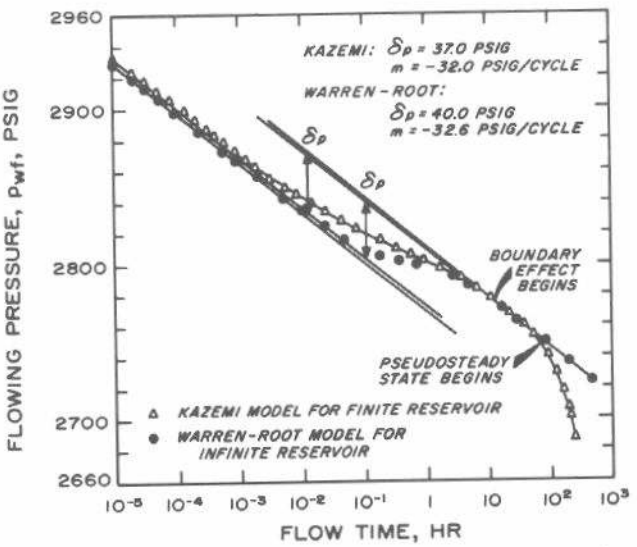

Fig. 10.19 Drawdown in a naturally fractured reservoir; comparing models of Kazemi and Warren and Root. After Kazemi.[44]

thickness product. The first semilog straight line may be obscured by wellbore storage effects, since it occurs at very short shut-in times. Thus, to successfully see both semilog straight lines, it may be necessary to minimize wellbore storage by assuring that the wellbore is full of liquid or by using a bottom-hole shut-in device.

Results from the two models in Fig. 10.19 differ because of the assumptions made in the models. The difference in location between the semilog straight lines results because Warren and Root assume pseudosteady-state flow from the matrix to the fracture, while Kazemi allows transient flow. The late-time deviation is caused by the boundary in the Kazemi model. Kazemi shows that the pseudosteady-state behavior for a naturally fractured system begins at a dimensionless time given by

$$(t_{DA})_{pss} = \frac{0.0002637\,(kh)_t\,t_{pss}}{\left[(\phi c_t)_f + (\phi c_t)_{ma}\right]h\mu A}$$

$$\simeq 0.13. \quad \ldots\ldots\ldots\ldots\ldots\ldots\ldots\ldots \quad (10.20)$$

Eq. 10.20 applies for a single well in the center of a closed, circular drainage region. It also can be expected to apply to square and triangular regions. It is interesting that the time to beginning of pseudosteady state is about the same as for a homogeneous reservoir — when total-system properties are used in computing t_{DA}.

Fig. 10.20 shows actual pressure buildup data for a naturally fractured reservoir.[40] Theory[11,44] predicts such a pressure-buildup curve shape. As for drawdown, wellbore storage effects may obscure the initial semilog straight line. If both semilog straight lines develop, as in the test in Fig. 10.20, analysis for total permeability-thickness product is by normal methods. Skin factor is estimated using normal equations, taking p_{1hr} from the *second* straight line. Average reservoir pressure is estimated by extrapolating the *second* straight line to infinite shut-in time to obtain p^* and then using the methods of Chapter 6. The vertical distance between the two semilog straight lines, identified as δp in Figs. 10.19 and 10.20, may be used to estimate the ratio of the porosity-compressibility product in the fracture to that for the total system for isotropic or anisotropic systems:[11,44]

$$F_{ft} = \text{antilog}\,(-\delta p/m). \quad \ldots\ldots\ldots\ldots \quad (10.21)$$

The pressure buildup curve shown in Fig. 10.20 has a semilog straight line, then flattens and then steepens again. That is precisely the characteristic in Fig. 10.14 that is often attributed to reservoirs with noncommunicating layers. Thus, we again see that several types of heterogeneous systems may have transient response curves with similar shapes. Note also that Curve 3 in Fig. 10.5 has the same general shape as the curves in Figs. 10.19 and 10.20.

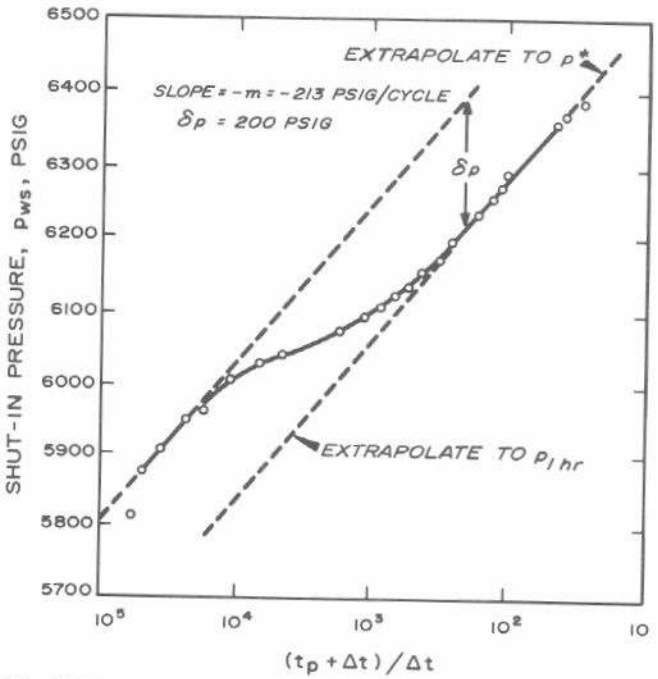

Fig. 10.20 Buildup curve from a fractured reservoir. After Warren and Root.[40]

Example 10.2 Estimating the Ratio of Fracture to Total ϕc_t

Fig. 10.20 is an example pressure buildup test presented by Warren and Root.[40] From that figure, $m = 213$ psig/cycle, and $\delta p = 200$ psig. From Eq. 10.21,

$$F_{ft} = \text{antilog}(-200/213)$$

$$= 0.12.$$

This may be interpreted that the fracture pore volume is 12 percent of the total pore volume, provided $(c_t)_{ma} = (c_t)_f$.

Odeh,[39] Warren and Root,[40] and Kazemi[44] show that when ϵ (Eq. 10.19) is relatively large (approaching 1), the Warren-Root model degenerates to the normal model for a homogeneous reservoir. For practical purposes, this may happen when the block dimensions are small, on the order of 3 ft, and the matrix permeability exceeds 0.01 md. In support of the Warren-Root model, fractured reservoirs in southwestern Iran have matrix permeabilities in the range of 0.00005 to 0.5 md, and have huge fracture blocks.[46]

Kazemi, Seth, and Thomas[44,45] show that observation-well behavior in interference testing in naturally fractured reservoirs can be substantially different from that of homogeneous reservoirs. Fig. 10.21 is a comparison of calculated interference pressures using a fracture model and a homogeneous model with equivalent permeability-thickness and porosity-compressibility characteristics. At short times, the pressures are significantly different in the two systems. However, at longer times, say for $t_D/r_D^2 > 5$ ($t_D > 1.6 \times 10^7$ in Fig. 10.21), based on the Kazemi-Seth-Thomas[45] data, normal analysis techniques should apply. Thus, it should be possible to analyze interference tests in naturally fractured reservoirs by the semilog methods of Section 9.2. *Type-curve methods and pulse testing may not provide correct results.* Kazemi[44] suggests a technique for using both pressure drawdown (or buildup) data and interference data to estimate properties of both fracture and matrix.

10.7 Effect of Pressure-Dependent Rock Properties

In some reservoirs, particularly low-permeability, deep gas reservoirs, rock properties can change significantly as reservoir fluid pressure declines. Although both permeability and porosity tend to decline with declining reservoir pressure, the permeability change is most frequently studied.[47-50] Vairogs *et al.*[47] and Thomas and Ward[48] studied the effect of declining permeability on gas production. Raghavan, Scorer, and Miller[50] provide some information on flow of liquids when permeability and porosity are pressure dependent.

Vairogs and Rhoades[49] studied pressure drawdown and buildup in low-permeability gas reservoirs with pressure-dependent permeability. Fig. 10.22 shows simulated drawdown curves for such a situation. The upper three curves are for real gas at different production rates; the lower curve is for an ideal gas at a relatively high production rate. If drawdown data for such a system could be analyzed using techniques like those given in Chapter 3, all four curves in Fig. 10.22 would be identical. Not only do the curves differ, but they have different slopes. The slopes taken at t_D = 1,000 for the upper three curves decrease as the rate decreases, but are greater than the theoretically expected value, 1.15, that is observed for the ideal-gas, constant-permeability case. Based on analysis of such data, Vairogs and Rhoades conclude that *neither* permeability nor skin factor should be estimated from *drawdown* tests in formations with pressure-dependent permeability. Wattenbarger and Ramey[51,52] reach a similar conclusion for testing gas wells with damage and wellbore storage in *constant-permeability* formations.

Fig. 10.23 shows simulated pressure buildup curves taken from Ref. 49. Table 10.1 shows the results of analyzing 12 such pressure buildup curves for pressure-dependent permeability. In all cases, the permeability at initial pressure was 0.061 md. For correct analysis by methods of Chapter 5, we would expect all curves in Fig. 10.23 to have m = 1.15. That is the case for the short production period, but m exceeds 1.15 for longer production periods. Vairogs and Rhoades conclude that the permeability value estimated from a *buildup* test in such a reservoir is a good estimate of the permeability of that reservoir. For short production times, the initial permeability is calculated. For longer production times, the reservoir pressure has decreased and the actual reservoir permeability decreases as a result. Thus, the increase in slope with increasing production time shown in Fig. 10.23 indicates that the buildup-test analysis could give useful estimates of average reservoir permeability *at the time of the buildup test*.

The calculated skin factors for the first six cases in Table 10.1 are not a result of physical damage, but are caused by low permeability around the wellbore owing to pressure drawdown. Thus, a positive skin factor is estimated from buildup tests in formations with pressure-dependent permeability when no actual wellbore damage is present. The same is true if turbulence exists.[51] Vairogs and Rhoades point out that it may be impossible to determine whether an excessive pressure drop (positive skin factor) is a result of pressure-dependent permeability, skin damage, or turbulent

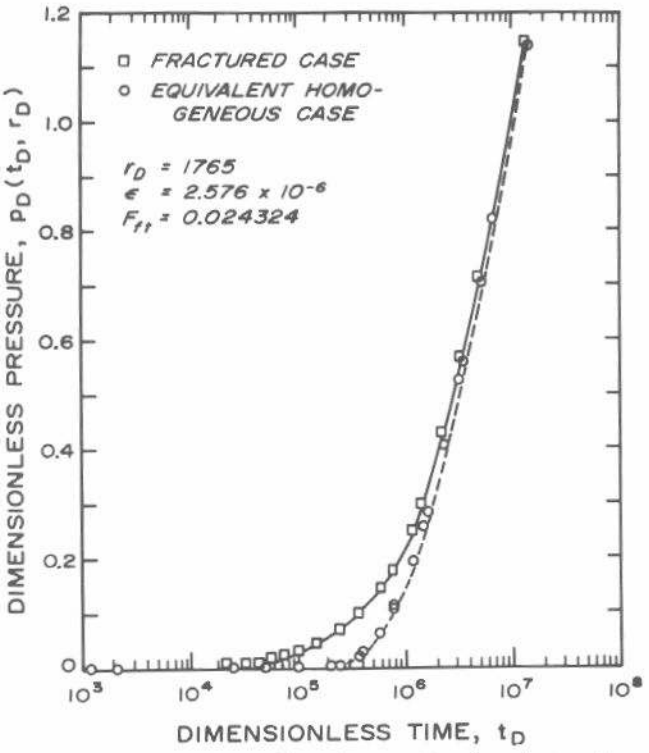

Fig. 10.21 Comparison of interference effect for a fractured reservoir with that for the equivalent homogeneous reservoir. After Kazemi, Seth, and Thomas.[45]

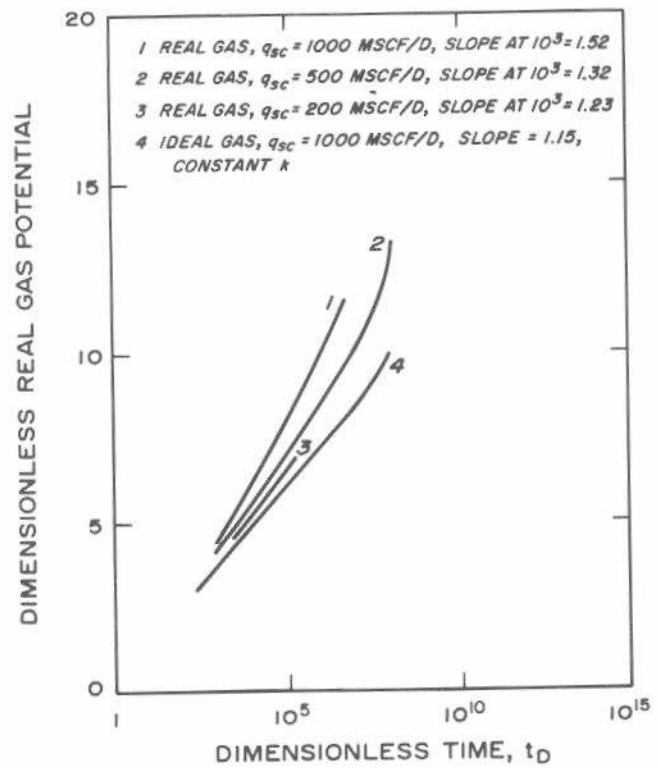

Fig. 10.22 Dimensionless drawdown curves for a gas well in a sand with pressure-dependent permeability. Well in the center of a closed circular reservoir. After Vairogs and Rhoades.[49]

flow at the wellbore. They also point out that when the well is mechanically damaged, the skin factor estimated from buildup-test analysis will be large for short production times and will decrease for significantly longer production times. A stimulated well will show a negative skin factor of about the right magnitude for all production times (Table 10.1).

10.8 Well Tests for Vertical Permeability

The vertical permeability in a formation is normally different from horizontal permeability, even when the system is otherwise homogeneous. Such vertical anisotropic effects are generally a result of depositional environment and post-depositional compaction history. In addition to microscopic characteristics that may cause the vertical permeability to be lower on a pore-to-pore basis, macroscopic features such as shale-sand interbedding can also create that effect. All transient testing and analysis methods described elsewhere in this monograph provide information about only the horizontal (radial or x and y direction) permeability. This section discusses techniques for estimating vertical permeability, k_z.

The transient tests proposed for estimating vertical permeability generally may be classified as vertical interference testing[53,54] or vertical pulse testing.[55-57] In such tests the well must be completed so that part may be used for production or injection (that is, be active) and part may be used for pressure observation (Fig. 10.24). Although Fig. 10.24 shows injection in the upper perforations and observation in the lower perforations, the opposite situation is equally acceptable theoretically. Operational considerations generally favor the situation illustrated in Fig. 10.24. A single-interval test for estimating vertical permeability also has been proposed.[58]

Vertical inferference testing is similar to normal interference testing. Of course, equipment and operational requirements are more demanding, since only one well is used. Burns[53] gives a good discussion of test design, well selection, and test operation. Vertical interference tests use

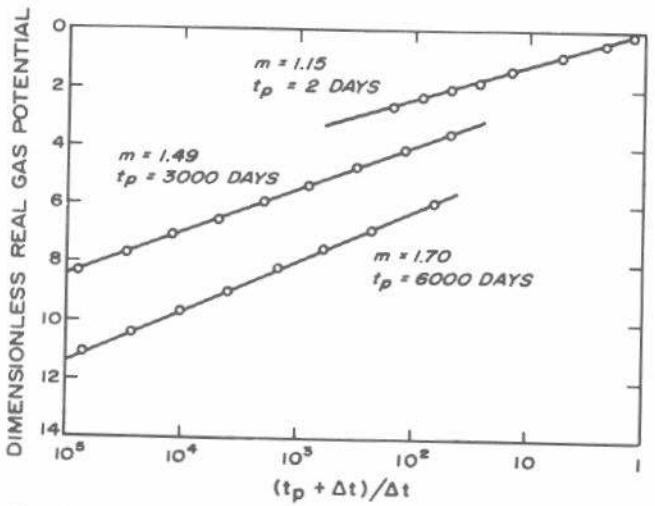

Fig. 10.23 Dimensionless pressure-buildup curves for a gas well in a sand with pressure-dependent permeability. Well in the center of a closed circular system. After Vairogs and Rhoades.[49]

TABLE 10.1—SUMMARY OF SIMULATED BUILDUP TEST ANALYSES FOR RESERVOIRS WITH PRESSURE-DEPENDENT PERMEABILITY.
After Vairogs and Rhoades.[49]

Test Parameters			Buildup-Curve Analysis Results	
q (Mscf/D)	t_p (days)	s	k (md)	Skin Factor
500	2	0	0.061	1.19
1,000	2	0	0.055	2.22
1,250	2	0	0.053	4.86
500	3,000	0	0.054	2.15
500	6,000	0	0.050	2.98
500	9,000	0	0.050	5.13
1,000	2	−3	0.061	−2.60
1,000	2	1	0.061	4.72
500	3,000	−3	0.047	−2.82
500	3,000	1	0.047	1.98
500	6,000	−3	0.041	−2.91
500	6,000	1	0.041	1.85

relatively short-time pressure response data, so wellbore storage may have a significant effect on the observed pressure response. Unfortunately, that problem has not been studied to date, so no quantitative information can be provided here. Based on the behavior of other kinds of well tests, it is recommended that all possible efforts be made to minimize the effects of wellbore storage. If possible, testing in wells with a changing fluid level should be avoided. If that is not possible, consideration should be given to down-hole shut-in devices or to loading the wellbore with a low-density liquid to minimize the wellbore storage coefficient. We also recommend using a tubing packer (see Fig. 10.25) to minimize any fluid entry or exit from the observation perforations.

It should be clear that fluid communication through the wellbore behind the pipe or through vertical fractures in the formation cannot be tolerated. If such conditions are expected, an alternate well should be chosen for the test. Such conditions will cause a rapid pressure response at the observation perforations and will preclude analysis for vertical permeability. The test interval should not contain fluid-fluid contacts, since they will affect pressure response in a currently unknown way. It is recommended that both the active and test perforations be over a short interval. Because of that requirement and the requirement for a relatively long unperforated interval in the center of the well, it is expected that

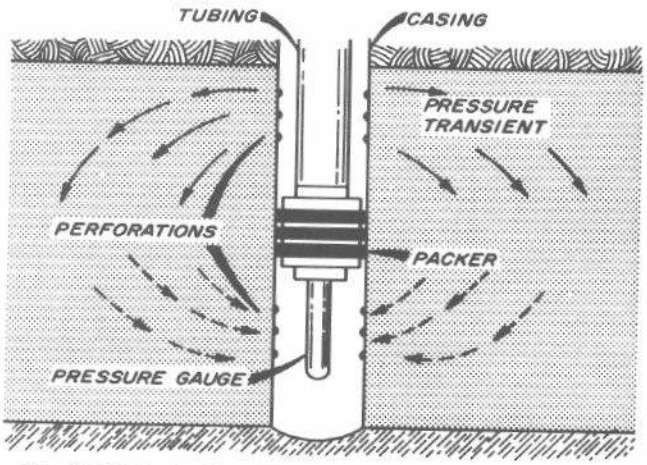

Fig. 10.24 Vertical interference or pulse test. After Burns.[53]

most existing wells would not be suitable for the testing described in this section. The possibility of using long packers or a straddle packer setup exists, but normally a special completion of a new well is necessary for vertical permeability testing.

As in any transient well test, good data collection is important. Rate control is essential for all the analysis techniques described in this section. If the rate varies significantly, computer analysis beyond the scope of this monograph is required.[53]

Vertical Pulse Testing

Hirasaki[55] proposes using vertical pulse testing to estimate k_z. He describes a testing and analysis technique based on arrival time of the first pressure peak. He considers the situation with perforations at the upper and lower reservoir boundaries. Because of that and because the very short pulse periods used can be expected to be influenced significantly by wellbore storage, we prefer the vertical pulse-testing technique described by Falade and Brigham.[56,57]

Fig. 10.25 shows the well configuration and the nomenclature used for vertical pulse testing and for vertical interference testing. Although flow perforations are shown at the top and observation perforations are shown at the bottom of the well, the arrangement may be reversed without affecting the analysis techniques presented here.

The techniques of this section apply only for wells far from a boundary that limits the reservoir laterally, such as a pinchout. Fortunately, vertical well tests are of short duration, so boundaries should not have much effect unless they are closer than given by Eq. 2.41 for the longest test time.

Fig. 10.26 is a schematic representation of rate history and pressure response for a vertical pulse test. The method presented here requires equal pulse times. Cycle time (Δt_C), pulse time (Δt_P), time lag (t_L), and pressure response amplitude (Δp) are identified. The pressure response amplitude for vertical pulse testing is determined just as it is for normal pulse testing. A tangent is drawn between the two peaks (or valleys) of the pressure response and a line parallel to that is drawn tangent to the valley (or peak) being analyzed. Pressure response amplitude is the vertical distance between those two lines.

Falade and Brigham[56,57] base dimensionless pulse time on the vertical permeability, k_z, and the vertical distance between the flow and observation perforations, ΔZ_R:

$$\Delta t_{PDV} = \frac{0.0002637\, k_z\, \Delta t_P}{\phi \mu c_t \Delta Z_R^2} \quad \ldots\ldots\ldots\ldots (10.22)$$

Since this dimensionless time differs significantly from dimensionless times used elsewhere in this monograph, we have used subscript V to identify it as applying to vertical testing. Falade and Brigham[56,57] also define a dimensionless pulse response amplitude:

$$\Delta p_{DV} = \frac{k_r\, \Delta Z_R\, \Delta p}{141.2\, qB\mu} \quad \ldots\ldots\ldots\ldots\ldots\ldots (10.23)$$

The vertical dimensionless pressure is based on the horizontal permeability, k_r, and the distance between the two sets of perforations, ΔZ_R. Again, because of the difference from the dimensionless pressures used elsewhere in this monograph, subscript V is added.

Once the test well is chosen, it is important to design the pulse length and magnitude to be compatible with formation characteristics and the pressure instrument resolution. The pulse duration must be long enough so the pressure instrument detects the pulses, but short enough so the pulses are easily identified. Analysis techniques are simpler for short pulses because the upper and lower boundary effects are less important for short pulses. Fig. 10.27 is a design curve for vertical pulse testing. The middle of the operational range, near the maximum of the upper curve in Fig. 10.27, should be chosen. That corresponds to a dimensionless pulse length of about 0.05 and a value of $(\Delta p_{DV})_\infty \left[(t_L)_\infty / \Delta t_P\right] = 0.0175$. Although those precise values need not be used, the values chosen should be close to those. Once the values of the parameters in Fig. 10.27 have been chosen, the pulse length is designed using a rearranged form of Eq. 10.22:

$$\Delta t_P = \frac{\phi \mu c_t \Delta Z_R^2\, (\Delta t_{PDV})_{\text{Fig. 10.27}}}{0.0002637\, k_z} \quad \ldots\ldots\ldots\ldots (10.24)$$

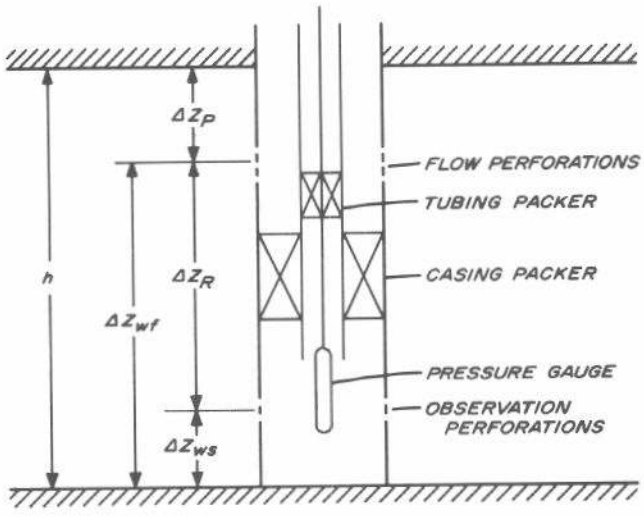

Fig. 10.25 Vertical interference and pulse test nomenclature.

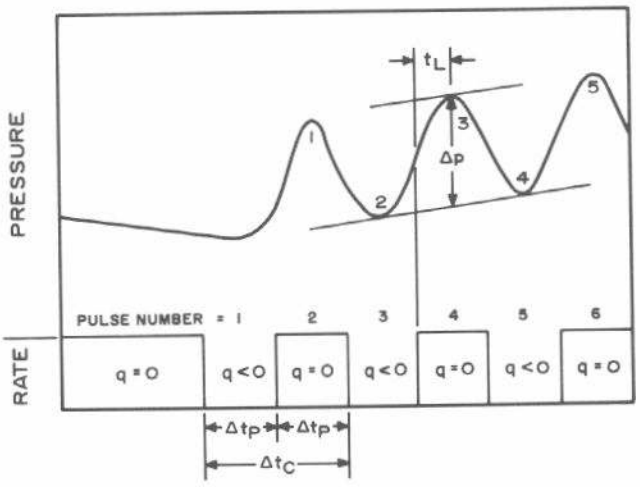

Fig. 10.26 Vertical pulse-testing rate and pressure history and nomenclature. Analysis procedure requires equal pulse lengths.

The expected response amplitude is estimated from a form of Eq. 10.23:

$$\Delta p = \frac{141.2\, qB\mu \left\{(\Delta p_{DV})_\infty \left[(t_L)_\infty/\Delta t_P\right]\right\}_{\text{Fig. 10.27}}}{k_r \Delta Z_R \left[(t_L)_\infty/\Delta t_P\right]_{\text{Fig. 10.27}}}, \quad \ldots\ldots\ldots\ldots\ldots\ldots\ldots\ldots (10.25)$$

and the expected time lag is estimated from

$$t_L = \left[(t_L)_\infty/\Delta t_P\right]_{\text{Fig. 10.27}} \Delta t_P \ldots\ldots\ldots\ldots\ldots (10.26)$$

The expected response amplitude may be used to choose the combination of rate and pressure instrument for good resolution.

Example 10.3 Vertical Pulse Testing: Test Design

Falade and Brigham[57] give the following estimated parameters for a formation to be vertically pulse tested:

$k_z \simeq 1.0$ md
$k_r \simeq 20.0$ md
$\phi = 0.20$
$\mu = 2.0$ cp
$c_t = 1.0 \times 10^{-5}$ psi^{-1}
$\Delta Z_R = 50$ ft
$B = 1.0$ RB/STB.

We wish to design a pulse test. From Fig. 10.27 we choose

$$(\Delta t_{PDV})_{\text{Fig. 10.27}} = 0.05,$$

$$\left\{(\Delta p_{DV})_\infty \left[(t_L)_\infty/\Delta t_P\right]\right\}_{\text{Fig. 10.27}} = 0.0175,$$

and

$$\left[(t_L)_\infty/\Delta t_P\right]_{\text{Fig. 10.27}} = 0.37.$$

We estimate pulse length from Eq. 10.24:

$$\Delta t_P = \frac{(0.20)(2.0)(1.0 \times 10^{-5})(50)^2(0.05)}{(0.0002637)(1.0)}$$

$$\simeq 1.9 \text{ hours}.$$

The time lag is estimated from Eq. 10.26:

$$t_L \simeq (0.37)(1.9) \simeq 0.7 \text{ hour}.$$

Finally, we estimate the response amplitude from Eq. 10.25:

$$\Delta p \simeq \frac{(141.2)(1.0)(2.0)(0.0175)}{(20.0)(50)(0.37)} q$$

$$\simeq 0.0134\, q \text{ psi}.$$

Thus, for an injection (or production) rate of 500 STB/D we would expect a pressure change of about

$$\Delta p = (0.0134)(500) = 6.7 \text{ psi}.$$

The pressure gauge should be chosen appropriately.

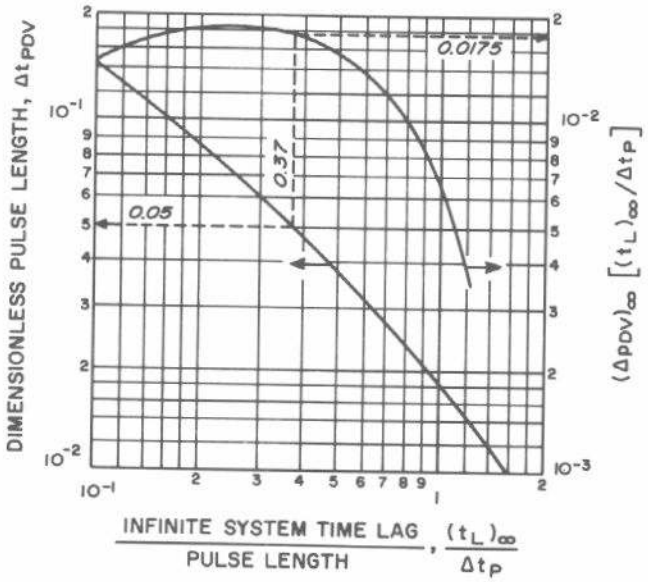

Fig. 10.27 Vertical pulse testing: design curve. After Falade and Brigham.[57]

Vertical pulse-test data analysis is more complex than horizontal test analysis. That is because of the influence of the upper and lower formation boundaries on the test. For thick formations or short pulses, the system is infinite-acting and the upper and lower boundaries do not influence the observed pressures. For longer pulses, thinner formations, or when the perforations tested are close to one of the boundaries, either one or both of the boundaries influence the test response. In the latter cases, an iterative analysis procedure is required.

Regardless of the analysis procedure used (infinite-acting, single boundary, or double boundary), the first step in vertical pulse-test analysis is to calculate the geometric fraction (factor) needed for the correlation curves. The *primal geometric factor* is

$$G_P = \frac{\Delta Z_P}{\Delta Z_R}, \quad \ldots\ldots\ldots\ldots\ldots\ldots\ldots (10.27a)$$

and the *reciprocal geometric factor* is

$$G_R = \frac{h}{\Delta Z_R} - G_P - 1. \quad \ldots\ldots\ldots\ldots\ldots (10.27b)$$

By a clever application of the reciprocity principle, Falade and Brigham[56] show that all pulse-test responses can be correlated with only the two geometric factors. Once the two factors are calculated, if $G_P > G_R$, the two values are interchanged. Thus, the analysis techniques in this section and in Ref. 57 *require* that $G_P < G_R$. The values of G_P and G_R determine the type of analysis used.

Infinite-Acting System Analysis ($G_P > 2$, $G_R > 2$)

When G_P and G_R are each greater than 2, the system is infinite-acting and analysis is noniterative. The measured ratio of time lag to pulse length, $(t_L)_\infty/\Delta t_P$, is used with Fig. 10.28 to determine the dimensionless pulse length, Δt_{PDV}. Fig. 10.28 has curves for the first and second pulses. All later pulses fall between the curves shown. The vertical permeability is estimated from

$$k_z = \frac{\phi \mu c_t \Delta Z_R^2}{0.0002637\, \Delta t_P} (\Delta t_{PDV})_{\text{Fig. 10.28}}. \quad \ldots\ldots\ldots (10.28)$$

To estimate horizontal permeability, the dimensionless pulse time from Fig. 10.28 is used with Fig. 10.29 to obtain a dimensionless pulse response amplitude for the infinite system, $(\Delta p_{DV})_\infty$. Horizontal permeability is estimated from

$$k_r = \frac{141.2\, qB\mu}{\Delta Z_R\, \Delta p} \left[(\Delta p_{DV})_\infty\right]_{\text{Fig. 10.29}}, \quad \ldots\ldots\ldots (10.29)$$

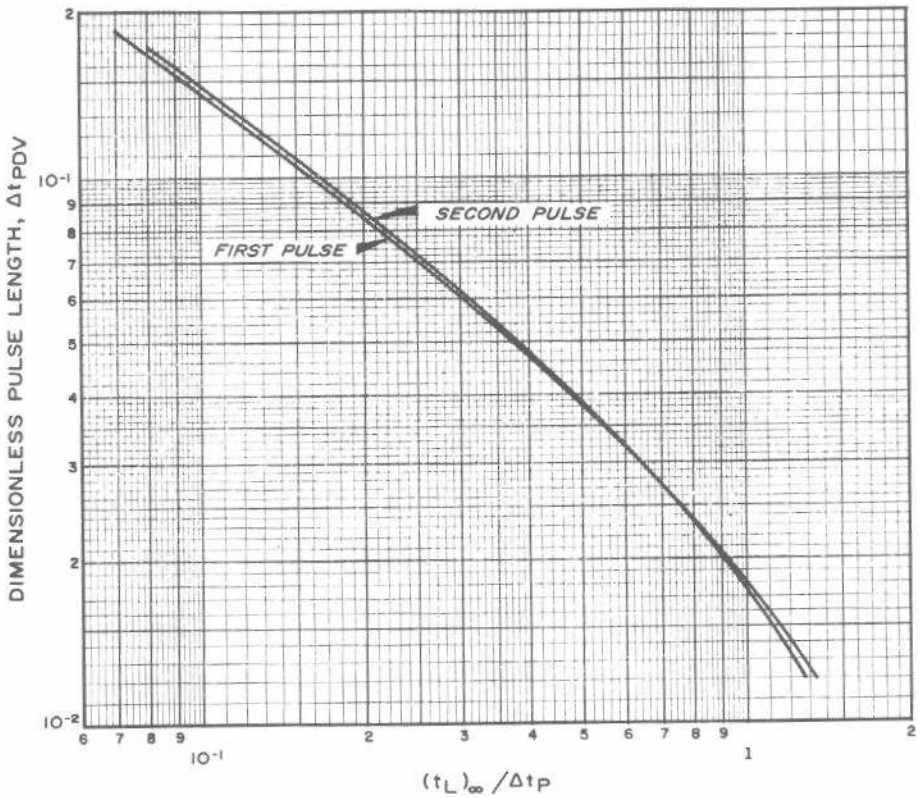

Fig. 10.28 Vertical pulse testing: infinite-acting system relation between dimensionless pulse length and time lag. After Falade and Brigham.[57]

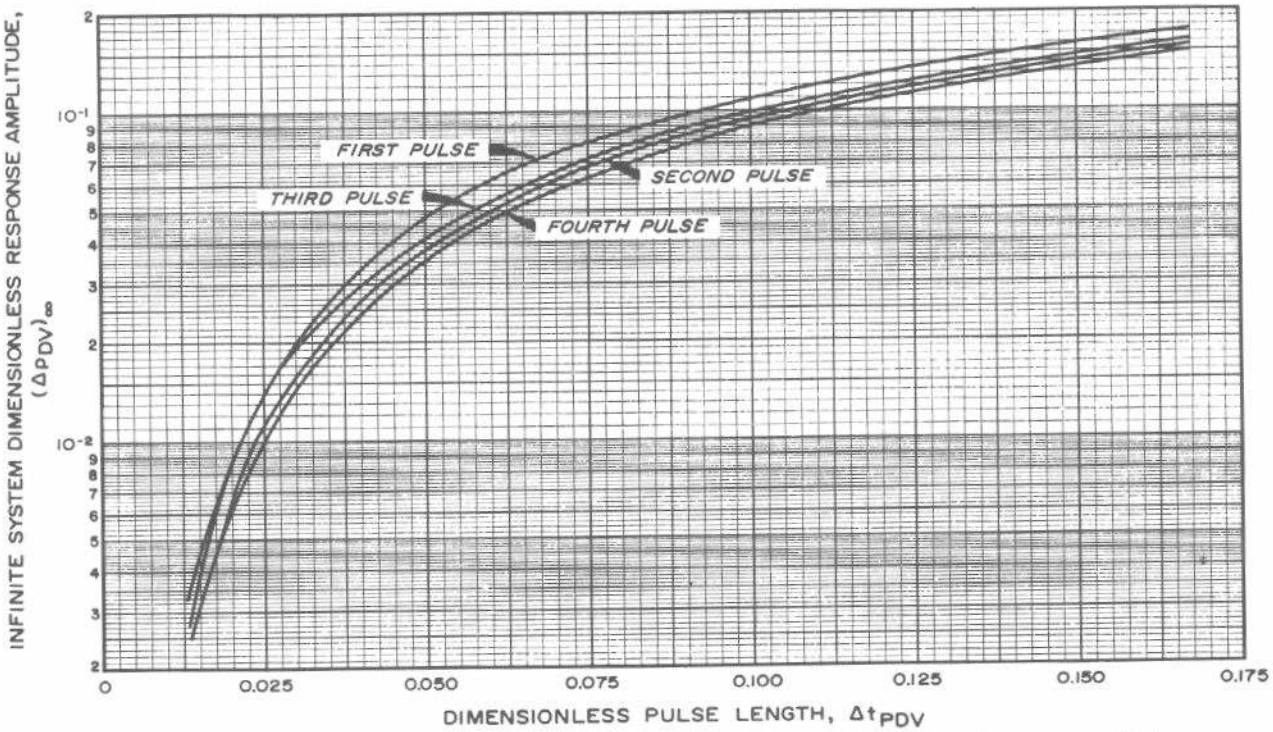

Fig. 10.29 Vertical pulse testing: infinite-acting system relationship between pulse length and response amplitude. After Falade and Brigham.[57]

where Δp is the observed pulse response amplitude. No iteration is required.

Example 10.4 Vertical Pulse Testing in an Infinite-Acting System

Falade and Brigham[57] provide the following data for the *first* pulse of a vertical pulse test:

$\phi = 0.20$ $\quad$ $\Delta t_P = 1.9$ hours
$\mu = 2.0$ cp $\quad$ $t_L = 0.837$ hour
$c_t = 1.0 \times 10^{-5}$ psi^{-1} $\quad$ $\Delta p = -1.0$ psi
$\Delta Z_R = 50$ ft $\quad$ $B = 1.0$ RB/STB.
$q = -100$ B/D

(Note that $\Delta p/q$ is always positive.) We wish to estimate the horizontal and vertical permeabilities.

We assume that the system is infinite-acting (Examples 10.5 and 10.6 show the analysis when one and two boundaries influence the test) and use Fig. 10.28. Because the system is infinite-acting, we take

$$(t_L)_\infty = t_L = 0.837 \text{ hour},$$

so

$$(t_L)_\infty/\Delta t_P = 0.837/1.9 = 0.441.$$

From the first-pulse curve of Fig. 10.28, $(\Delta t_{PDV})_{\text{Fig. 10.28}} = 0.0425$, and from Fig. 10.29, $[(\Delta p_{DV})_\infty]_{\text{Fig. 10.29}} = 0.037$.

We estimate the vertical permeability from Eq. 10.28,

$$k_z = \frac{(0.20)(2.0)(1.0 \times 10^{-5})(50)^2(0.0425)}{(0.0002637)(1.9)}$$

$$= 0.85 \text{ md},$$

and the horizontal permeability from Eq. 10.29,

$$k_r = \frac{(141.2)(-100)(1.0)(2.0)(0.037)}{(50)(-1.0)}$$

$$= 20.9 \text{ md}.$$

Analysis When One Boundary Affects Pulse Response ($G_P < 2$, $G_R > 2$)

If $G_P < 2$ and $G_R > 2$ (recall that we require that $G_P < G_R$ — if not, the values are interchanged), then one of the two horizontal boundaries is affecting the pulse-test response and an iterative analysis is required. Fig. 10.30, Fig. 10.31, or Fig. 10.32 is entered with G_P (after it has been interchanged with G_R, if necessary) and $(\Delta t_{PDV})_{\text{Fig. 10.28}}$. From the figure for the pulse being analyzed, $[t_L/(t_L)_\infty]_{\text{Fig.}}$ is obtained. Since Δt_{PDV} is a parameter in Figs. 10.30 through 10.32, a cross-plot (Fig. 10.33) for the appropriate geometric factor is usually helpful. Once $[t_L/(t_L)_\infty]_{\text{Fig.}}$ is estimated from Fig. 10.30, Fig. 10.31, or Fig. 10.32, we calculate

$$[(t_L)_\infty/\Delta t_P]_{\text{new}} = \frac{(t_L/\Delta t_P)}{[t_L/(t_L)_\infty]_{\text{Fig.}}} \quad \ldots\ldots\ldots (10.30)$$

The new value of $(t_L)_\infty/\Delta t_P$ is used in Fig. 10.28 to estimate a new value of $(\Delta t_{PDV})_{\text{Fig. 10.28}}$. If that value does not agree with the previous value, Fig. 10.30, Fig. 10.31, or Fig. 10.32 is used again and Eq. 10.30 is applied again. This process continues until two successive values of $(\Delta t_{PDV})_{\text{Fig. 10.28}}$ are the same. Then the vertical permeability is estimated from Eq. 10.28 using the final $(\Delta t_{PDV})_{\text{Fig. 10.28}}$ value.

Horizontal permeability is estimated from

$$k_r = \frac{141.2\, qB\mu}{\Delta Z_R\, \Delta p} \left[\frac{\Delta p_{DV}}{(\Delta p_{DV})_\infty}\right]_{\text{Fig.}} [(\Delta p_{DV})_\infty]_{\text{Fig. 10.29}}, \quad \ldots\ldots\ldots\ldots\ldots\ldots\ldots\ldots (10.31)$$

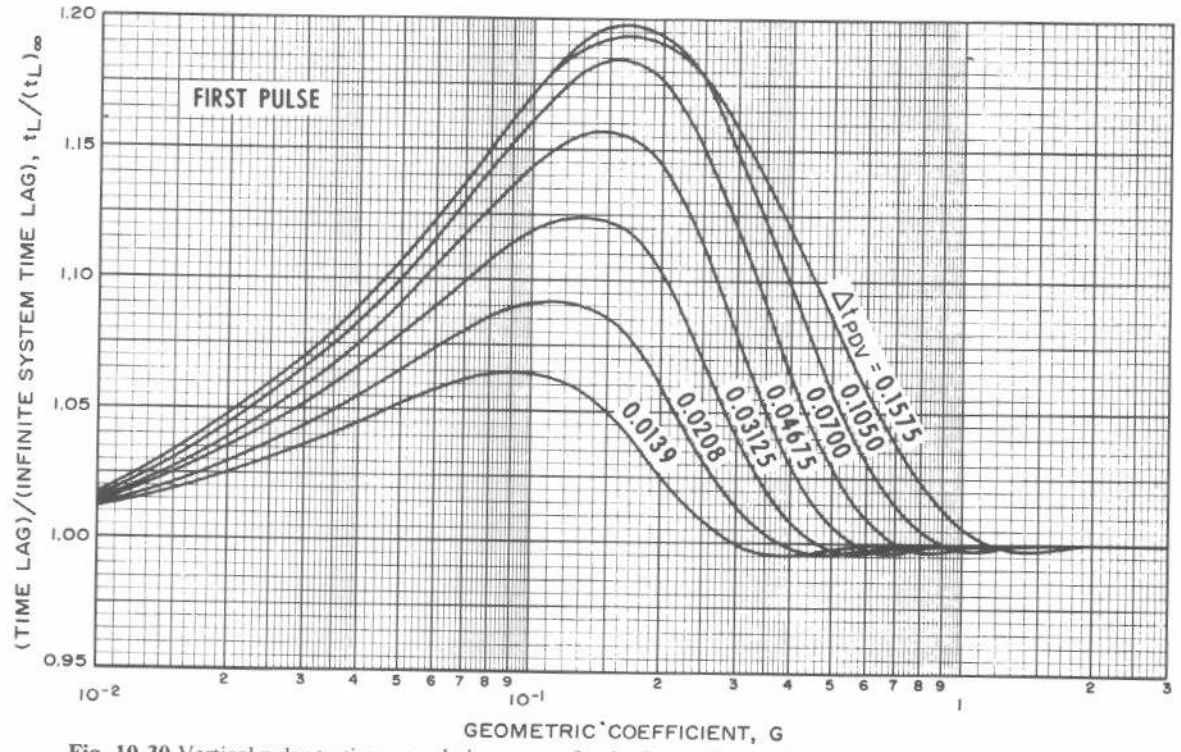

Fig. 10.30 Vertical pulse testing: correlation curves for the first-pulse time lag. After Falade and Brigham.[57]

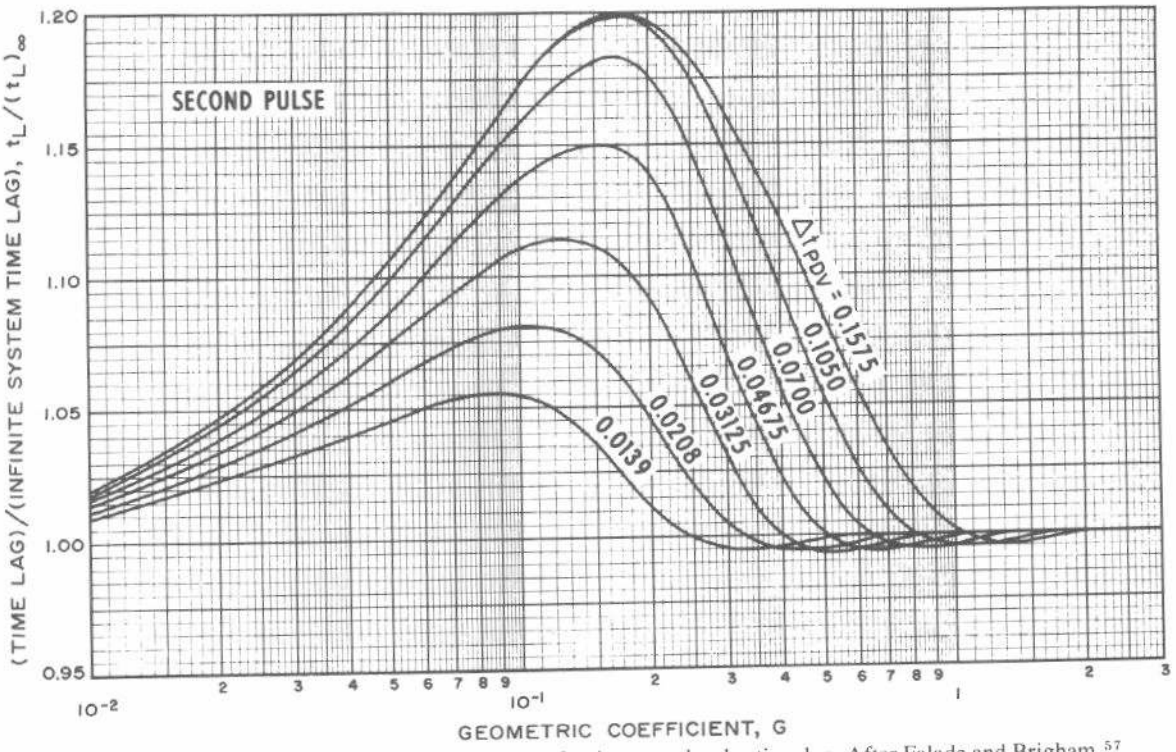

Fig. 10.31 Vertical pulse testing: correlation curves for the second-pulse time lag. After Falade and Brigham.[57]

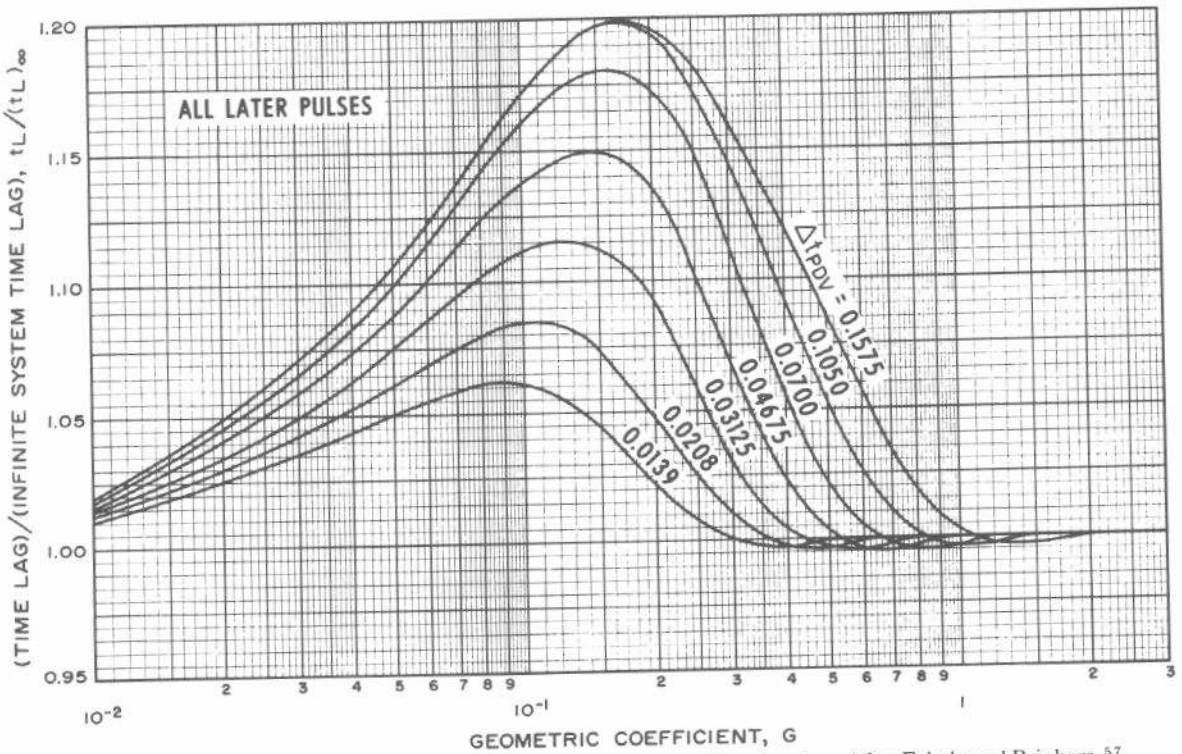

Fig. 10.32 Vertical pulse testing: correlation curves for all-later-pulses time lag. After Falade and Brigham.[57]

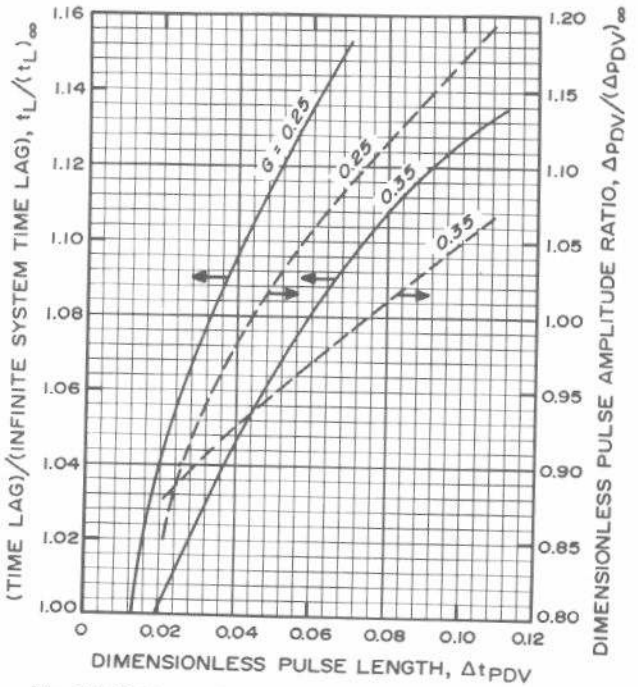

Fig. 10.33 Cross-plot of data in Figs. 10.30 and 10.34 for Examples 10.5 and 10.6.

where Fig. 10.34, Fig. 10.35, Fig. 10.36, or Fig. 10.37 is used to estimate $\left[\Delta p_{DV}/(\Delta p_{DV})_\infty\right]_{\text{Fig.}}$. $\left[(\Delta p_{DV})_\infty\right]_{\text{Fig. 10.29}}$ is estimated from Fig. 10.29 using the final $(\Delta t_{PDV})_{\text{Fig. 10.28}}$ value. No iteration is required to estimate the horizontal permeability once $(\Delta t_{PDV})_{\text{Fig. 10.28}}$ is estimated by the iterative technique described above. A cross-plot of material from Fig. 10.34, Fig. 10.35, Fig. 10.36, or Fig. 10.37 is usually helpful in this analysis (see Fig. 10.33).

Example 10.5 Vertical Pulse Testing in a System With One Nearby Boundary

We continue with the example of Falade and Brigham[57] using the data of Example 10.4 plus $\Delta Z_P = 12.5$ ft and $h = 250$ ft.

We use Eq. 10.27 to calculate the geometric factors

$$G_P = \frac{12.5}{50} = 0.25,$$

and

$$G_R = \left(\frac{250}{50} - 0.25 - 1\right) = 3.75.$$

We must use the smallest of G_P and G_R as G_P, in this case 0.25. Since $G_R = 3.75 > 2$, we analyze for a system with a single influencing boundary. The analysis starts as if the system were infinite-acting, so it is like that in Example 10.4. For the first iteration, $(t_L)_\infty/\Delta t_P = 0.837/1.9 = 0.441$ and

$$(\Delta t_{PDV})_{\text{Fig. 10.28}} = 0.0425.$$

Fig. 10.30 provides the first-iteration estimate of $t_L/(t_L)_\infty$; since Δt_{PVD} is a parameter in that figure, we use the cross-plot shown in Fig. 10.33 to determine $\left[t_L/(t_L)_\infty\right]_{\text{Fig.}} = 1.102$ for $G_P = 0.25$. Using Eq. 10.30,

$$\left[(t_L)_\infty/\Delta t_P\right]_{\text{new}} = \frac{(0.837/1.9)}{1.102} = 0.400.$$

Using Fig. 10.28 again,

$$(\Delta t_{PDV})_{\text{Fig. 10.28}} = 0.0465.$$

This completes the first step. Since the new value of $(\Delta t_{PDV})_{\text{Fig. 10.28}}$ does not agree with the previous value, we must iterate. All iterations are summarized in Table 10.2.

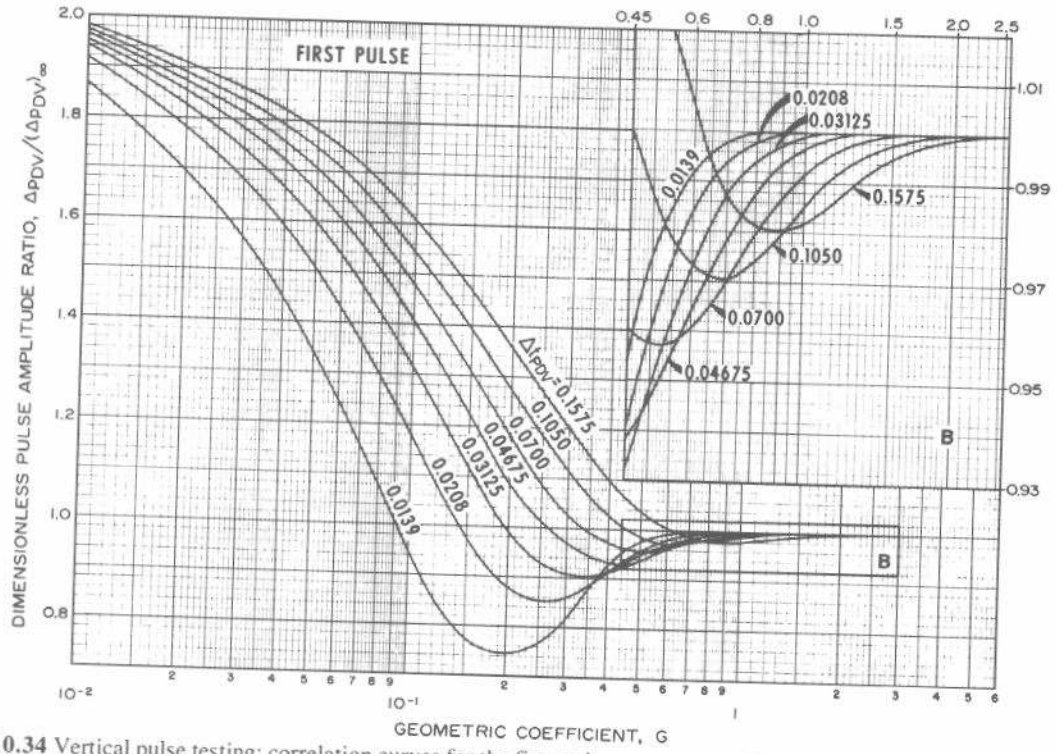

Fig. 10.34 Vertical pulse testing: correlation curves for the first-pulse response amplitude. After Falade and Brigham.[57]

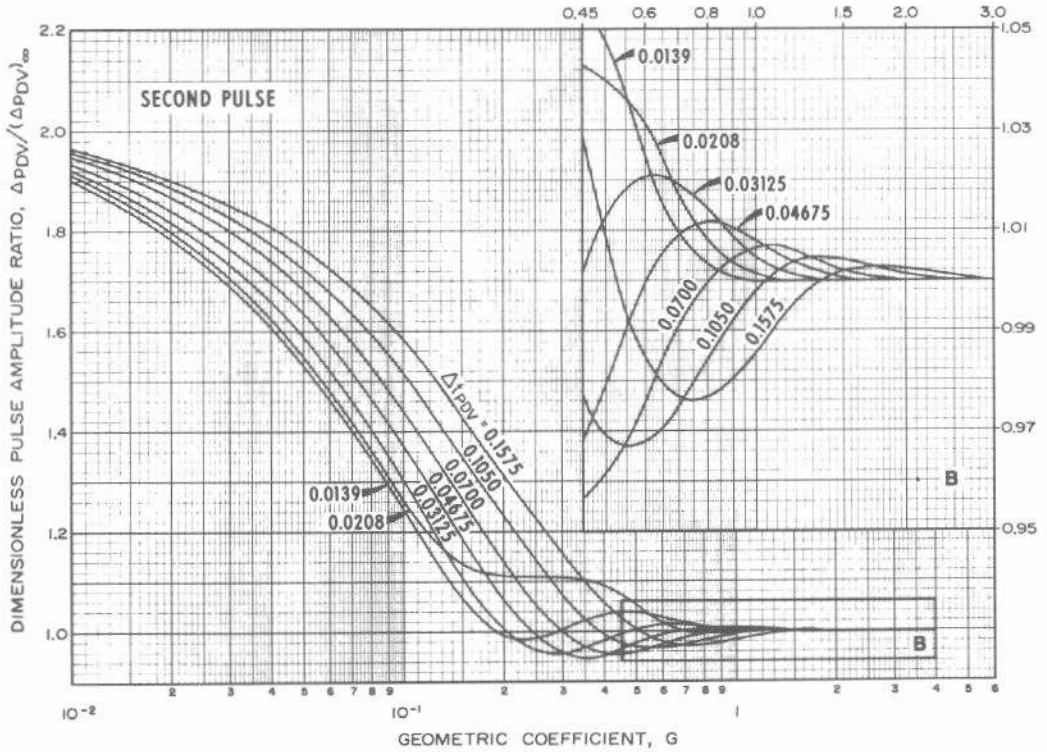

Fig. 10.35 Vertical pulse testing: correlation curves for the second-pulse response amplitude. After Falade and Brigham.[57]

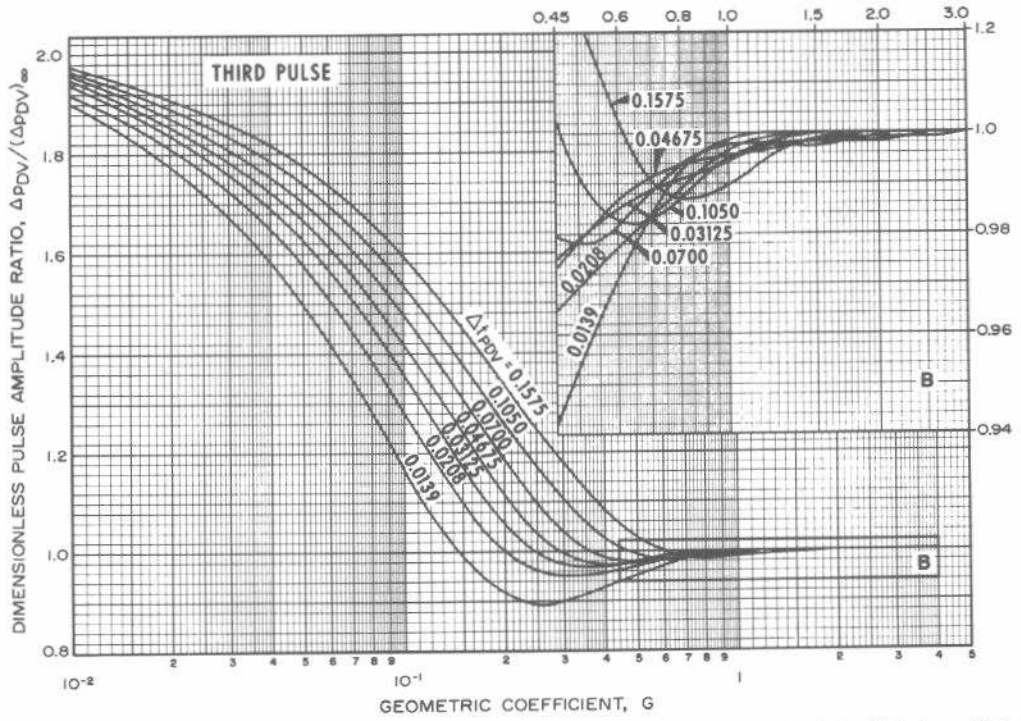

Fig. 10.36 Vertical pulse testing: correlation curves for the third-pulse response amplitude. After Falade and Brigham.[57]

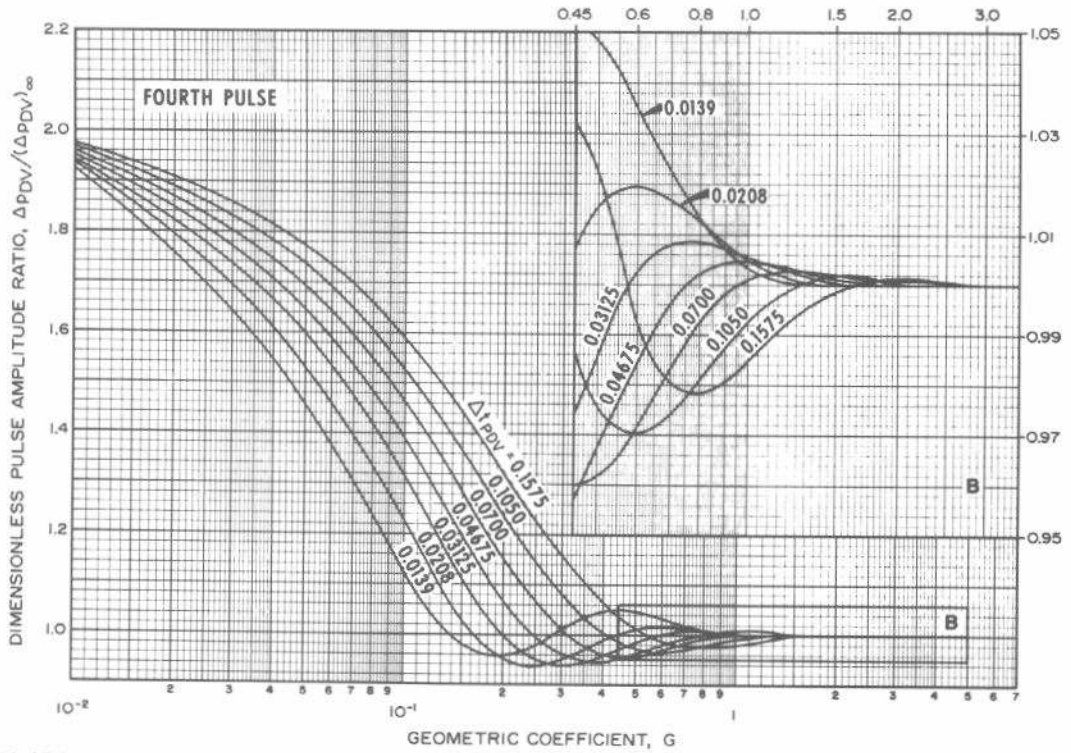

Fig. 10.37 Vertical pulse testing: correlation curves for the fourth-pulse response amplitude. After Falade and Brigham.[57]

The final result is

$$(\Delta t_{PDV})_{\text{Fig. 10.28}} = 0.0468,$$

and

$$\left[t_L/(t_L)_\infty\right]_{\text{Fig.}} = 1.110.$$

The vertical permeability is estimated using Eq. 10.28:

$$k_z = \frac{(0.20)(2.0)(1.0 \times 10^{-5})(50)^2(0.0468)}{(0.0002637)(1.9)}$$

$$= 0.93 \text{ md}.$$

To estimate k_r we use Figs. 10.29 and 10.34 for the first pulse to determine

$$\left[(\Delta p_{DV})_\infty\right]_{\text{Fig. 10.29}} = 0.0430,$$

and

$$\left[\frac{\Delta p_{DV}}{(\Delta p_{DV})_\infty}\right]_{\text{Fig.}} = 1.02.$$

Then, from Eq. 10.31,

$$k_r = \frac{(141.2)(-100)(1.0)(2.0)\left[1.02\right]\left[0.0430\right]}{(50)(-1.0)}$$

$$= 24.8 \text{ md}.$$

TABLE 10.2—ITERATIVE CALCULATION FOR VERTICAL PULSE TEST ANALYSIS IN A SYSTEM INFLUENCED BY ONE HORIZONTAL BOUNDARY; EXAMPLE 10.5.
After Falade and Brigham.[57]

Parameter	Iteration 1	2	3	Use
Δt_{PDV}	0.0425	0.0465	0.0468	Fig. 10.28
$t_L/(t_L)_\infty$	1.102	1.110	1.110	Fig. 10.30
$(t_L)_\infty/\Delta t_P$	0.400	0.397	0.397	Eq. 10.30
$(\Delta t_{PDV})_{new}$	0.0465	0.0468	0.0468	Fig. 10.28

Analysis When Both Boundaries Affect Pulse Response ($G_P < 2$, $G_R < 2$)

When G_P and G_R are each less than 2, both the upper and lower formation boundaries affect pulse-test response and an iterative analysis is required. We start by estimating Δt_{PDV} from Fig. 10.28, then use Fig. 10.30, Fig. 10.31, or Fig. 10.32 to estimate values of $t_L/(t_L)_\infty$ for both G_P and G_R. Next, a corrected value of $t_L/(t_L)_\infty$ is estimated from

$$\left[\frac{t_L}{(t_L)_\infty}\right]_{\text{Fig.}} = \left[\frac{t_L}{(t_L)_\infty}\right]_{\text{Fig., } G_P} \left[\frac{t_L}{(t_L)_\infty}\right]_{\text{Fig., } G_R} \quad \ldots\ldots\ldots\ldots\ldots\ldots\ldots\ldots\ldots (10.32)$$

Eq. 10.30 is used to estimate a new value of $(t_L)_\infty/\Delta t_P$. That $\left[(t_L)_\infty/\Delta t_P\right]_{\text{new}}$ is used with Fig. 10.28 to estimate the next value of Δt_{PDV}. If that value does not agree with the previous value, the computation is repeated until two successive values of Δt_{PDV} are the same. Finally, Eq. 10.28 is used to estimate k_z.

To estimate horizontal permeability, Fig. 10.34, Fig. 10.35, Fig. 10.36, or Fig. 10.37 is used for both G_P and G_R. Then we apply

$$\left[\frac{\Delta p_{DV}}{(\Delta p_{DV})_\infty}\right]_{\text{Fig.}} = \left[\frac{\Delta p_{DV}}{(\Delta p_{DV})_\infty}\right]_{\text{Fig., } G_P} \times \left[\frac{\Delta p_{DV}}{(\Delta p_{DV})_\infty}\right]_{\text{Fig., } G_R} \quad \ldots\ldots\ldots (10.33)$$

Finally, the horizontal permeability is estimated from Eq. 10.31 without iteration.

Example 10.6 Vertical Pulse Testing in a System With Two Nearby Boundaries

The Falade-Brigham[57] example can be carried one step further by assuming that the test geometric configuration is $\Delta Z_P = 12.5$ ft and $h = 80$ ft. Other data are the same.

From Eq. 10.27,

$$G_P = \frac{12.5}{50} = 0.25,$$

and

$$G_R = \frac{80}{50} - 0.25 - 1 = 0.35.$$

Since $G_P < G_R$ we need not exchange the values. Both values are less than 2, so a finite-system analysis is required. As in Example 10.5, we start by using an infinite-acting system analysis, then iterating. To start the first iteration we enter Fig. 10.28 with $(t_L)_\infty/\Delta t_P = 0.837/1.9 = 0.441$ to get

$$(\Delta t_{PDV})_{\text{Fig. 10.28}} = 0.0425.$$

From Fig. 10.33, the cross-plot of data in Fig. 10.30, we get the *two* required values of $\{t_L/(t_L)_\infty\}$ for the first pulse:

$$[t_L/(t_L)_\infty]_{\text{Fig., } G_P = 0.25} = 1.102,$$

and

$$[t_L/(t_L)_\infty]_{\text{Fig., } G_R = 0.35} = 1.051.$$

Applying Eq. 10.32,

$$[t_L/(t_L)_\infty]_{\text{Fig.}} = (1.102)(1.051) = 1.158.$$

Then, Eq. 10.30 is used to get

$$[(t_L)_\infty/\Delta t_P]_{\text{new}} = \frac{(0.837)/(1.9)}{1.158}$$

$$= 0.3804.$$

Using Fig. 10.28 again,

$$[\Delta t_{PDV}]_{\text{Fig. 10.28}} = 0.0488.$$

The first iteration is complete. Since the new $\{\Delta t_{PDV}\}_{\text{Fig. 10.28}}$ does not agree with the initial value, we must continue. All iterations are summarized in Table 10.3. The final iteration gives

$$[\Delta t_{PDV}]_{\text{Fig. 10.28}} = 0.0492,$$

TABLE 10.3—ITERATIVE CALCULATION FOR VERTICAL PULSE TEST ANALYSIS IN A SYSTEM INFLUENCED BY TWO HORIZONTAL BOUNDARIES; EXAMPLE 10.6.
After Falade and Brigham.[57]

Parameter	Iteration 1	Iteration 2	Iteration 3	Use
Δt_{PDV}	0.0425	0.0488	0.0492	Fig. 10.28
$t_L/(t_L)_\infty$	1.102	1.113	1.114	Fig. 10.30; G_P=0.25
$t_L/(t_L)_\infty$	1.051	1.063	1.063	Fig. 10.30; G_R=0.35
$t_L/(t_L)_\infty$	1.158	1.183	1.184	Eq. 10.32
$(t_L)_\infty/\Delta t_P$	0.3804	0.3724	0.3721	Eq. 10.30
$(\Delta t_{PDV})_{\text{new}}$	0.0488	0.0492	0.0492	Fig. 10.28

TABLE 10.4—COMPARISON OF RESULTS FOR THREE VERTICAL PULSE TEST ANALYSIS METHODS.

Analysis Method	k_z	k_r
Infinite-acting	0.85	20.9
One boundary	0.93	24.8
Two boundaries	0.98	26.3

and

$$[t_L/(t_L)_\infty]_{\text{Fig.}} = 1.184.$$

We estimate vertical permeability from Eq. 10.28:

$$k_z = \frac{(0.20)(2.0)(1.0 \times 10^{-5})(50)^2(0.0492)}{(0.0002637)(1.9)}$$

$$= 0.98 \text{ md}.$$

To estimate k_r we use Figs. 10.29 and 10.33 (the cross-plot of Fig. 10.34) for both geometric factors:

$$[(\Delta p_{DV})_\infty]_{\text{Fig. 10.29}} = 0.0470,$$

$$[\Delta p_{DV}/(\Delta p_{DV})_\infty]_{\text{Fig., } G_P = 0.25} = 1.030,$$

$$[\Delta p_{DV}/(\Delta p_{DV})_\infty]_{\text{Fig., } G_R = 0.35} = 0.961.$$

From Eq. 10.33,

$$[\Delta p_{DV}/(\Delta p_{DV})_\infty]_{\text{Fig.}} = (1.030)(0.961)$$

$$= 0.990$$

Then k_r is from Eq. 10.31:

$$k_r = \frac{(141.2)(-100)(1.0)(2.0)(0.990)(0.0470)}{(50)(-1)}$$

$$= 26.3 \text{ md}.$$

Table 10.4 compares the results from Examples 10.4 through 10.6. For the situations used in those examples, the estimated vertical permeability changes by about 13 percent, while the horizontal permeability changes by about 21 percent. Thus, for the conditions used in the examples, the results do not vary as widely as might have been anticipated. Nevertheless, we recommend using the full iterative analysis if it is indicated by the values of G_P and G_R.

Vertical Interference Testing

Burns[53] proposes a method for vertical interference testing that has considerable utility. Unfortunately, it requires the use of a computer for test analysis. Although Burns' technique can be used with type-curve matching, a computer program is still required to generate the type curves. Thus, the Burns approach is not discussed further here. Prats[54] suggests a vertical interference testing method that does not require computer solutions. He shows that if observed pressure, p_{ws}, is plotted vs the logarithm of time from the beginning of injection or production, a straight line should result with slope m and intercept at $t = 1$ hour of $p_{1\text{hr}}$. The horizontal permeability is estimated from the slope using

$$k_r = \frac{-162.6\,qB\mu}{mh} \quad \ldots\ldots\ldots\ldots\ldots\ldots (10.34)$$

The vertical permeability is estimated from the slope and intercept using

$$k_z = \frac{\phi\mu c_t h^2}{0.0002637} \text{ antilog}\left(\frac{p_{1\text{hr}} - p_i}{m} - \frac{G^* + h/|\Delta Z_{wf} - \Delta Z_{ws}|}{2.3025}\right) \quad \ldots\ldots\ldots (10.35)$$

G^* in Eq. 10.35 is a geometric factor (fraction) provided by Prats and shown in Fig. 10.38. The vertical distances used in Eq. 10.35 and Fig. 10.38 are defined in Fig. 10.25. As in all transient test analysis, p_{1hr} must be taken from the semilog straight line, which is extrapolated if necessary.

Example 10.7 Vertical Interference Test Analysis

Prats[54] presents example data from a vertical interference test. Fig. 10.39 is the plot of observed pressure vs log of injection time. Other data are

$h = 50$ ft
$\Delta Z_{wf} = 45$ ft
$\Delta Z_{ws} = 10$ ft
$q = -50$ STB/D
$B = 1.0$ RB/STB
$\mu = 1.0$ cp
$c_t = 2.0 \times 10^{-5}$ psi^{-1}
$\phi = 0.10$
$p_i = 3{,}015$ psi.

From Fig. 10.39, $m = 22.5$ psi/cycle and $p_{1hr} = 3{,}022$ psi. Eq. 10.34 is used to estimate horizontal permeability:

$$k_r = \frac{(-162.6)(-50)(1.0)(1.0)}{(22.5)(50)}$$

$$= 7.2 \text{ md.}$$

To estimate the vertical permeability, we use Eq. 10.35 and Fig. 10.38. We enter that figure with

$$\Delta Z_{wf}/h = 45/50 = 0.9$$

and

$$\Delta Z_{ws}/h = 10/50 = 0.2$$

to read $G^* = 0.76$. Then, from Eq. 10.35,

$$k_z = \frac{(0.10)(1.0)(2.0 \times 10^{-5})(50)^2}{0.0002637}$$

$$\text{antilog}\left(\frac{3{,}022 - 3{,}015}{22.5} - \frac{0.76 + 50/|45 - 10|}{2.3025}\right)$$

$$= 4.3 \text{ md.}$$

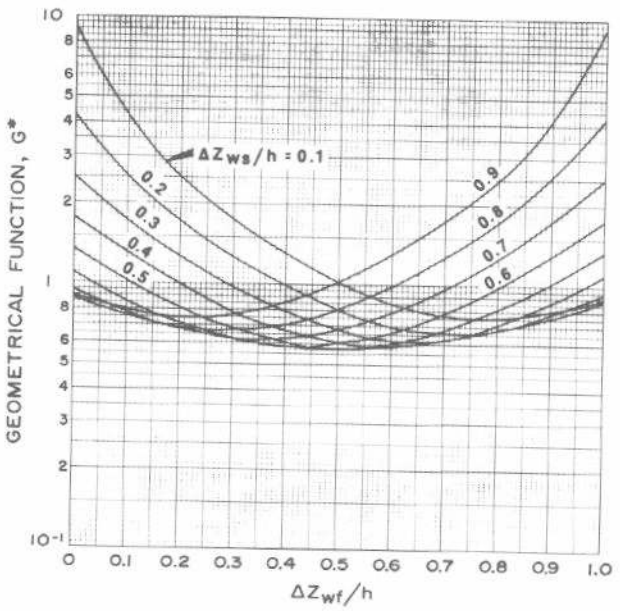

Fig. 10.38 Geometric factor for vertical interference testing. After Prats.[54]

The Prats analysis technique requires the well to be thoroughly stabilized before testing. The initial pressure in the region of the well at the time of the test is p_i. Although Prats does not show it, if the observation pressure at the well is changing according to a trend, that trend may be extrapolated for the test duration, and the pressure difference between the trend and observed pressures can be used in the plot of pressure vs log of time and in the analysis. (That approach is analogous to that given in Section 3.4.) The Prats testing and analysis technique is limited to perforated intervals that are short compared with the distance between the flow and observation perforations.

Because of the repetitive nature of pulse testing, we recommend that vertical pulse testing be used in preference to vertical interference testing. An added advantage of pulse testing is the larger range of allowed perforation locations with respect to the formation boundaries than for the interference method proposed by Prats.[54]

Single-Interval Testing

Raghavan and Clark[58] propose a method for estimating vertical permeability when only a single set of perforations is used. They use a spherical flow equation, so the perforated interval must be small compared with the formation thickness and it should be near the center of the formation interval. The analysis requires that a very restrictive portion of the data response be analyzed. It appears that wellbore storage could mask the data portion being analyzed and, thus, could render the technique ineffective. For this reason, we prefer interference or pulse testing techniques. However, the technique can be applied for many drillstem tests where only a small interval is tested and wellbore storage is suppressed.

10.9 Summary

The surface has just been scratched in the study of the effects of reservoir heterogeneities on well testing and well test analysis. As indicated in this chapter, many different physical situations can cause similar well-test pressure responses. Thus, it can be dangerous to infer a particular reservoir condition or heterogeneity from a single well-test response. Generally, much additional data from other types of tests, geology, cores, logs, etc., are required to verify the existence of reservoir heterogeneities. The nonexpert should

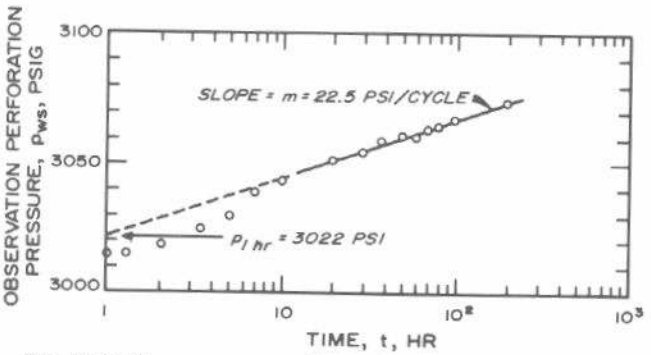

Fig. 10.39 Pressure response for vertical interference test with injection; Example 10.7. After Prats.[54]

be reluctant to make positive interpretations in heterogeneous systems. Perhaps the best thing to do is recognize that a test is unusual because of some peculiarity either in the test or in the reservoir and then call on the services of an expert. In many cases, it will not be possible to determine what the actual situation is to any degree of certainty. Often, even sophisticated computer analyses of single- or multiple-well test results cannot provide a definitive indication of the actual situation.

Vertical well testing is one area that is well enough developed for general application — when the test is performed with sufficient care. The analysis methods presented apply to specific restricted testing conditions but are sufficient for estimating vertical and horizontal permeabilities if other needed reservoir data can be estimated from other sources. Many other methods for vertical well testing are also available and should provide adequate results.

References

1. Matthews, C. S. and Russell, D. G.: *Pressure Buildup and Flow Tests in Wells*, Monograph Series, Society of Petroleum Engineers of AIME, Dallas (1967) **1,** Chap. 10.
2. Jahns, Hans O.: "A Rapid Method for Obtaining a Two-Dimensional Reservoir Description From Well Pressure Response Data," *Soc. Pet. Eng. J.* (Dec. 1966) 315-327; *Trans.*, AIME, **237.**
3. Vela, Saul and McKinley, R. M.: "How Areal Heterogeneities Affect Pulse-Test Results," *Soc. Pet. Eng. J.* (June 1970) 181-191; *Trans.*, AIME, **249.**
4. McKinley, R. M., Vela, Saul, and Carlton, L. A.: "Field Application of Pulse-Testing for Detailed Reservoir Description," *J. Pet. Tech.* (March 1968) 313-321; *Trans.*, AIME, **243.**
5. Horner, D. R.: "Pressure Build-Up in Wells," *Proc.*, Third World Pet. Cong., The Hague (1951) Sec. II, 503-523. Also *Reprint Series, No. 9 — Pressure Analysis Methods*, Society of Petroleum Engineers of AIME, Dallas (1967) 25-43.
6. Dolan, John P., Einarsen, Charles A., and Hill, Gilman A.: "Special Application of Drill-Stem Test Pressure Data," *Trans.*, AIME (1957) **210,** 318-324. Also *Reprint Series, No. 9 — Pressure Analysis Methods*, Society of Petroleum Engineers of AIME, Dallas (1967) 68-74.
7. Russell, D. G.: "Determination of Formation Characteristics From Two-Rate Flow Tests," *J. Pet. Tech.* (Dec. 1963) 1347-1355; *Trans.*, AIME, **228.** Also *Reprint Series, No. 9 — Pressure Analysis Methods*, Society of Petroleum Engineers of AIME, Dallas (1967) 136-144.
8. Bixel, H. C., Larkin, B. K., and van Poollen, H. K.: "Effect of Linear Discontinuities on Pressure Build-Up and Drawdown Behavior," *J. Pet. Tech.* (Aug. 1963) 885-895; *Trans.*, AIME, **228.**
9. Gray, K. E.: "Approximating Well-to-Fault Distance From Pressure Build-Up Tests," *J. Pet. Tech.* (July 1965) 761-767.
10. Ramey, H. J., Jr., and Earlougher, R. C., Jr.: "A Note on Pressure Build-Up Curves," *J. Pet. Tech.* (Feb. 1968) 119-120.
11. Warren, J. E. and Root, P. J.: "The Behavior of Naturally Fractured Reservoirs," *Soc. Pet. Eng. J.* (Sept. 1963) 245-255; *Trans.*, AIME, **228.**
12. Earlougher, Robert C., Jr., Ramey, H. J., Jr., Miller, F. G., and Mueller, T. D.: "Pressure Distributions in Rectangular Reservoirs," *J. Pet. Tech.* (Feb. 1968) 199-208; *Trans.*, AIME, **243.**
13. Collins, Royal Eugene: *Flow of Fluids Through Porous Materials*, Reinhold Publishing Corp., New York (1961) 115.
14. Polubarinova-Kochina, P. Ya.: *Theory of Ground Water Movement*, Princeton U. Press, Princeton, N.J. (1962) 343-369.
15. Elkins, Lincoln F. and Skov, Arlie M.: "Determination of Fracture Orientation From Pressure Interference," *Trans.*, AIME (1960) **219,** 301-304. Also *Reprint Series, No. 9 — Pressure Analysis Methods*, Society of Petroleum Engineers of AIME, Dallas (1967) 97-100.
16. Earlougher, Robert C., Jr., and Kersch, Keith M.: "Field Examples of Automatic Transient Test Analysis," *J. Pet. Tech.* (Oct. 1972) 1271-1277.
17. Ramey, Henry J., Jr.: "Interference Analysis for Anisotropic Formations — A Case History," *J. Pet. Tech.* (Oct. 1975) 1290-1298; *Trans.*, AIME, **259.**
18. Papadopulos, Istavros S.: "Nonsteady Flow to a Well in an Infinite Anisotropic Aquifer," *Proc.*, 1965 Dubrovnik Symposium on Hydrology of Fractured Rocks, Int'l. Assoc. of Sci. Hydrology (1965) **I,** 21-31.
19. Hurst, William: "Interference Between Oil Fields," *Trans.*, AIME (1960) **219,** 175-192.
20. Larkin, Bert K.: "Solutions to the Diffusion Equation for a Region Bounded by a Circular Discontinuity," *Soc. Pet. Eng. J.* (June 1963) 113-115; *Trans.*, AIME, **228.**
21. Loucks, T. L. and Guerrero, E. T.: "Pressure Drop in a Composite Reservoir," *Soc. Pet. Eng. J.* (Sept. 1961) 170-176; *Trans.*, AIME, **222.**
22. Carter, R. D.: "Pressure Behavior of a Limited Circular Composite Reservoir," *Soc. Pet. Eng. J.* (Dec. 1966) 328-334; *Trans.*, AIME, **237.**
23. Odeh, A. S.: "Flow Test Analysis for a Well With Radial Discontinuity," *J. Pet. Tech.* (Feb. 1969) 207-210; *Trans.*, AIME, **246.**
24. Bixel, H. C. and van Poollen, H. K.: "Pressure Drawdown and Buildup in the Presence of Radial Discontinuities," *Soc. Pet. Eng. J.* (Sept. 1967) 301-309; *Trans.*, AIME, **240.** Also *Reprint Series No. 9 — Pressure Analysis Methods*, Society of Petroleum Engineers of AIME, Dallas (1967) 188-196.
25. Kazemi, Hossein, Merrill, L. S., and Jargon, J. R.: "Problems in Interpretation of Pressure Fall-Off Tests in Reservoirs With and Without Fluid Banks," *J. Pet. Tech.* (Sept. 1972) 1147-1156.
26. Merrill, L. S., Jr., Kazemi, Hossein, and Gogarty, W. Barney: "Pressure Falloff Analysis in Reservoirs With Fluid Banks," *J. Pet. Tech.* (July 1974) 809-818; *Trans.*, AIME, **257.**
27. Russell, D. G. and Prats, M.: "The Practical Aspects of Interlayer Crossflow," *J. Pet. Tech.* (June 1962) 589-594. Also *Reprint Series, No. 9 — Pressure Analysis Methods*, Society of Petroleum Engineers of AIME, Dallas (1967) 120-125.
28. Kazemi, Hossein and Seth, Mohan S.: "Effect of Anisotropy and Stratification on Pressure Transient Analysis of Wells With Restricted Flow Entry," *J. Pet. Tech.* (May 1969) 639-647; *Trans.*, AIME, **246.**
29. Woods, E. G.: "Pulse-Test Response of a Two-Zone Reservoir," *Soc. Pet. Eng. J.* (Sept. 1970) 245-256; *Trans.*, AIME, **249.**

30. Lefkovits, H. C., Hazebroek, P., Allen, E. E., and Matthews, C. S.: "A Study of the Behavior of Bounded Reservoirs Composed of Stratified Layers," *Soc. Pet. Eng. J.* (March 1961) 43-58; *Trans.*, AIME, **222.**

31. Duvaut, G.: "Drainage des Systèmes Hétérogènes," *Revue IFP* (Oct. 1961) 1164-1181.

32. Kazemi, Hossein: "Pressure Buildup in Reservoir Limit Testing of Stratified Systems," *J. Pet. Tech.* (April 1970) 503-511; *Trans.*, AIME, **249.**

33. Cobb, William M., Ramey, H. J., Jr., and Miller, Frank G.: "Well-Test Analysis for Wells Producing Commingled Zones," *J. Pet. Tech.* (Jan. 1972) 27-37; *Trans.*, AIME, **253.**

34. Raghavan, R., Topaloglu, H. N., Cobb, W. M., and Ramey, H. J., Jr.: "Well-Test Analysis for Wells Producing From Two Commingled Zones of Unequal Thickness," *J. Pet. Tech.* (Sept. 1974) 1035-1043; *Trans.*, AIME, **257.**

35. Earlougher, Robert C., Jr., Kersch, K. M., and Kunzman, W. J.: "Some Characteristics of Pressure Buildup Behavior in Bounded Multiple-Layer Reservoirs Without Crossflow," *J. Pet. Tech.* (Oct. 1974) 1178-1186; *Trans.*, AIME, **257.**

36. Earlougher, Robert C., Jr., Kersch, K. M., and Ramey, H. J., Jr.: "Wellbore Effects in Injection Well Testing," *J. Pet. Tech.* (Nov. 1973) 1244-1250.

37. Pollard, P.: "Evaluation of Acid Treatments From Pressure Build-Up Analysis," *Trans.*, AIME (1959) **216,** 38-43.

38. Pirson, Richard S. and Pirson, Sylvain J.: "An Extension of the Pollard Analysis Method of Well Pressure Build-Up and Drawdown Tests," paper SPE 101 presented at the SPE-AIME 36th Annual Fall Meeting, Dallas, Oct. 8-11, 1961.

39. Odeh, A. S.: "Unsteady-State Behavior of Naturally Fractured Reservoirs," *Soc. Pet. Eng. J.* (March 1965) 60-64; *Trans.*, AIME, **234.**

40. Warren, J. E. and Root, P. J.: "Discussion of Unsteady-State Behavior of Naturally Fractured Reservoirs," *Soc. Pet. Eng. J.* (March 1965) 64-65; *Trans.*, AIME, **234.**

41. Morris, Earl E. and Tracy, G. W.: "Determination of Pore Volume in a Naturally Fractured Reservoir," paper SPE 1185 presented at the SPE-AIME 40th Annual Fall Meeting, Denver, Oct. 3-6, 1965.

42. Huskey, William L. and Crawford, Paul B.: "Performance of Petroleum Reservoirs Containing Vertical Fractures in the Matrix," *Soc. Pet. Eng. J.* (June 1967) 221-228; *Trans.*, AIME, **240.**

43. Adams, A. R., Ramey, H. J., Jr., and Burgess, R. J.: "Gas Well Testing in a Fractured Carbonate Reservoir," *J. Pet. Tech.* (Oct. 1968) 1187-1194; *Trans.*, AIME, **243.**

44. Kazemi, H.: "Pressure Transient Analysis of Naturally Fractured Reservoirs With Uniform Fracture Distribution," *Soc. Pet. Eng. J.* (Dec. 1969) 451-462; *Trans.*, AIME, **246.**

45. Kazemi, H., Seth, M. S., and Thomas, G. W.: "The Interpretation of Interference Tests in Naturally Fractured Reservoirs With Uniform Fracture Distribution," *Soc. Pet. Eng. J.* (Dec. 1969) 463-472; *Trans.*, AIME, **246.**

46. Levorsen, A. I.: *Geology of Petroleum,* 2nd ed., W. H. Freedman and Co., San Francisco (1967) 125.

47. Vairogs, Juris, Hearn, C. L., Dareing, Donald W., and Rhoades, V. W.: "Effect of Rock Stress on Gas Production From Low-Permeability Reservoirs," *J. Pet. Tech.* (Sept. 1971) 1161-1167; *Trans.*, AIME, **251.**

48. Thomas, Rex D. and Ward, Don C.: "Effect of Overburden Pressure and Water Saturation on the Gas Permeability of Tight Sandstone Cores," *J. Pet. Tech.* (Feb. 1972) 120-124.

49. Vairogs, Juris and Rhoades, Vaughan W.: "Pressure Transient Tests in Formations Having Stress-Sensitive Permeability," *J. Pet. Tech.* (Aug. 1973) 965-970; *Trans.*, AIME, **255.**

50. Raghavan, R., Scorer, J. D. T., and Miller, F. G.: "An Investigation by Numerical Methods of the Effect of Pressure-Dependent Rock and Fluid Properties on Well Flow Tests," *Soc. Pet. Eng. J.* (June 1972) 267-275; *Trans.*, AIME, **253.**

51. Ramey, H. J., Jr.: "Non-Darcy Flow and Wellbore Storage Effects in Pressure Build-Up and Drawdown of Gas Wells," *J. Pet. Tech.* (Feb. 1965) 223-233; *Trans.*, AIME, **234.** Also *Reprint Series, No. 9 — Pressure Analysis Methods,* Society of Petroleum Engineers of AIME, Dallas (1967) 233-243.

52. Wattenbarger, Robert A. and Ramey, H. J., Jr.: "Gas Well Testing With Turbulence, Damage, and Wellbore Storage," *J. Pet. Tech.* (Aug. 1968) 877-887; *Trans.*, AIME, **243.**

53. Burns, William A., Jr.: "New Single-Well Test for Determining Vertical Permeability," *J. Pet. Tech.* (June 1969) 743-752; *Trans.*, AIME, **246.**

54. Prats, Michael: "A Method for Determining the Net Vertical Permeability Near a Well From In-Situ Measurements," *J. Pet. Tech.* (May 1970) 637-643; *Trans.*, AIME, **249.**

55. Hirasaki, George J.: "Pulse Tests and Other Early Transient Pressure Analyses for In-Situ Estimation of Vertical Permeability," *Soc. Pet. Eng. J.* (Feb. 1974) 75-90; *Trans.*, AIME, **257.**

56. Falade, Gabriel K. and Brigham, William E.: "The Dynamics of Vertical Pulse Testing in a Slab Reservoir," paper SPE 5055A presented at the SPE-AIME 49th Annual Fall Meeting, Houston, Oct. 6-9, 1974.

57. Falade, Gabriel K. and Brigham, William E.: "The Analysis of Single-Well Pulse Tests in a Finite-Acting Slab Reservoir," paper SPE 5055B presented at the SPE-AIME 49th Annual Fall Meeting, Houston, Oct. 6-9, 1974.

58. Raghavan, R. and Clark, K. K.: "Vertical Permeability From Limited Entry Flow Tests in Thick Formations," *Soc. Pet. Eng. J.* (Feb. 1975) 65-73; *Trans.*, AIME, **259.**

Chapter 11

Effect of Wellbore Conditions on Pressure Behavior

11.1 Introduction

Chapter 2 introduced the concepts of wellbore storage (Section 2.6) and partial well completions (Section 2.5) and indicated how those phenomena affect transient test behavior. This chapter further discusses the effects of more complex wellbore storage conditions and partial completions, as well as the effects of hydraulic fracturing and slanted holes on transient pressure behavior. Such features usually must be considered when analyzing well test data — if they are not, incorrect formation permeabilities and skin factors may be estimated. Therefore, it is important to recognize test data that are influenced by special wellbore conditions.

11.2 Changing Wellbore Storage

Wellbore storage[1-4] influences pressure transient data as discussed in Section 2.6. The wellbore storage coefficient is defined as the change in total volume of wellbore fluids per unit change in bottom-hole pressure,

$$C = \frac{\Delta V}{\Delta p}, \quad \ldots\ldots\ldots\ldots\ldots\ldots\ldots\ldots\ldots\ldots (11.1)$$

where

C = wellbore storage constant (coefficient, factor), bbl/psi

ΔV = change in volume of fluid in the wellbore at wellbore conditions, bbl

Δp = change in bottom-hole pressure, psi.

Sometimes ΔV is defined to include the volume of fractures as well as of the wellbore.

When the relationship between ΔV and Δp does not change during a well test, the wellbore storage coefficient is constant and usually may be estimated from the well completion. Then,

$$C = \frac{V_u}{\left(\frac{\rho}{144}\frac{g}{g_c}\right)}, \quad \ldots\ldots\ldots\ldots\ldots\ldots\ldots\ldots\ldots\ldots (11.2)$$

for a changing liquid level and

$$C = c\,V_w, \quad \ldots\ldots\ldots\ldots\ldots\ldots\ldots\ldots\ldots\ldots (11.3)$$

for a completely liquid- or gas-filled wellbore. The dimensionless wellbore storage coefficient is

$$C_D = \frac{5.6146\,C}{2\pi\phi c_t h r_w^{\,2}}. \quad \ldots\ldots\ldots\ldots\ldots\ldots\ldots\ldots\ldots\ldots (11.4)$$

For a constant wellbore storage coefficient, we may estimate the time when wellbore storage stops influencing a transient well test. That time corresponds to the beginning of the semilog straight line on the normal semilog transient data plot (see Chapters 3 through 5 and Chapter 7). As indicated in Section 2.6, wellbore storage effects are essentially negligible for drawdown and injection when[4]

$$t_D > (60 + 3.5s)\,C_D, \quad \ldots\ldots\ldots\ldots\ldots\ldots\ldots\ldots\ldots\ldots (11.5a)$$

or

$$t > \frac{(200{,}000 + 12{,}000s)\,C}{(kh/\mu)}. \quad \ldots\ldots\ldots\ldots\ldots\ldots\ldots\ldots\ldots\ldots (11.5b)$$

For pressure buildup and falloff tests, the corresponding times are[5]

$$t_D > 50\,C_D e^{0.14s}, \quad \ldots\ldots\ldots\ldots\ldots\ldots\ldots\ldots\ldots\ldots (11.6a)$$

or

$$t > \frac{170{,}000\,C\,e^{0.14s}}{(kh/\mu)}. \quad \ldots\ldots\ldots\ldots\ldots\ldots\ldots\ldots\ldots\ldots (11.6b)$$

The wellbore storage coefficient often is not constant throughout a well test.[6,7] Abrupt changes in the wellbore storage coefficient are easy to visualize and occur relatively frequently. Fig. 11.1 depicts a wellbore condition that can cause an *increasing* wellbore storage coefficient. When an injection well with a positive wellhead pressure is shut in for a falloff test, the wellhead pressure remains high immediately after shut-in. However, a few minutes (or hours) later, the bottom-hole pressure falls below the pressure required to maintain the liquid column to the surface and the liquid level begins to fall (the well "goes on vacuum"). When that happens, the wellbore storage coefficient increases from one for a compressible system (Eq. 11.3) to one for a falling liquid-level system (Eq. 11.2); the change can be by a factor of 100 or more. Fig. 11.2 shows both log-log and semilog falloff curves for such a step increase in wellbore storage coefficient; the light curves are for constant

wellbore storage coefficients, and the heavy curves show what happens when the wellbore storage coefficient increases at shut-in time Δt_1. The log-log data plot initially shows a unit-slope straight-line pressure response; then the response flattens and finally steepens as the pressure approaches the response for the larger wellbore storage coefficient. The semilog data plot shows a flattening period, a steepening, and a final flattening. The correct semilog straight line is reached at Δt_2. The abrupt change in slope of the data plot (flattening period) normally corresponds to the wellhead pressure reaching atmospheric (going on vacuum). Fig. 11.3 shows data from a falloff test with increasing wellbore storage.[7] Example 11.1 discusses that test in more detail. If there is a pressurized gas cushion in the well, the wellbore storage coefficient still decreases, but not as abruptly as illustrated in Fig. 11.2. The flattening occurs, but it is muted considerably. That is actually the case for the test shown in Fig. 11.3.

For the wellbore storage coefficient to increase, the liquid level must begin to fall *during* (rather than at the start of) the well test. A common situation for that occurrence is a pressure falloff test in an injection well. However, similar behavior may occur during drawdown testing of pumping wells. The fluid level starts falling when pumping reduces bottom-hole pressure below that required to maintain a fluid column to the surface or to a packer, thus giving a larger storage coefficient.

It is important to recognize that the shape of the falloff curve shown in Figs. 11.2 and 11.3 is quite similar to the falloff-curve shape that might be expected from a layered reservoir without communication between the layers. Comparing Figs. 11.2 and 11.3 with Fig. 10.14 shows that many physical situations can result in a single characteristic well-test-curve shape.

Decreasing wellbore storage can occur during buildup testing in a production well or during injectivity testing. Fig. 11.4 illustrates a typical production-well completion that can cause a decreasing wellbore storage coefficient. While the well is pumping, the liquid level stands below the packer. The liquid level is low just after shut-in, but rises as pressure increases. Gas in the wellbore is either compressed or redissolved. When the liquid level reaches the packer (there may be a small gas cushion), the wellbore storage coefficient drops from the relatively large value for a rising liquid level with annular volume between the casing and tubing to the relatively small value for a compression-controlled situation. (Normally, in this situation, the tubing is held full of liquid by the standing valve in the pump and that volume does not play a part in test response.) If there is gas above the liquid, its compressibility must be considered when estimating the wellbore storage coefficient. In that case, it is generally best to use Eq. 11.1 and a careful analysis of the situation; Example 11.1 illustrates such a

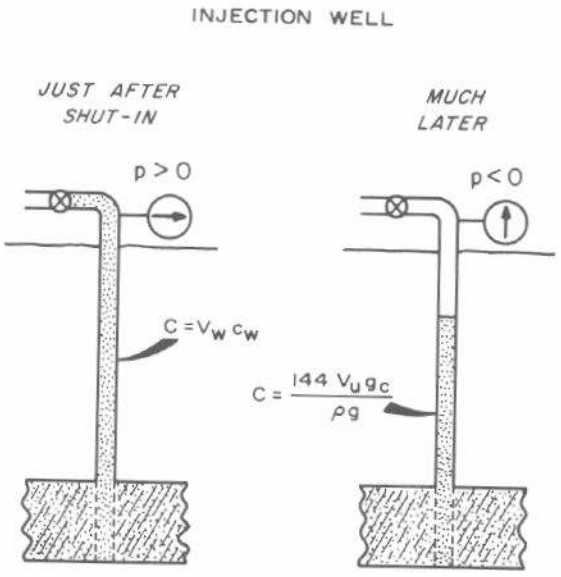

Fig. 11.1 Increasing wellbore storage — shut-in injection well going on vacuum.

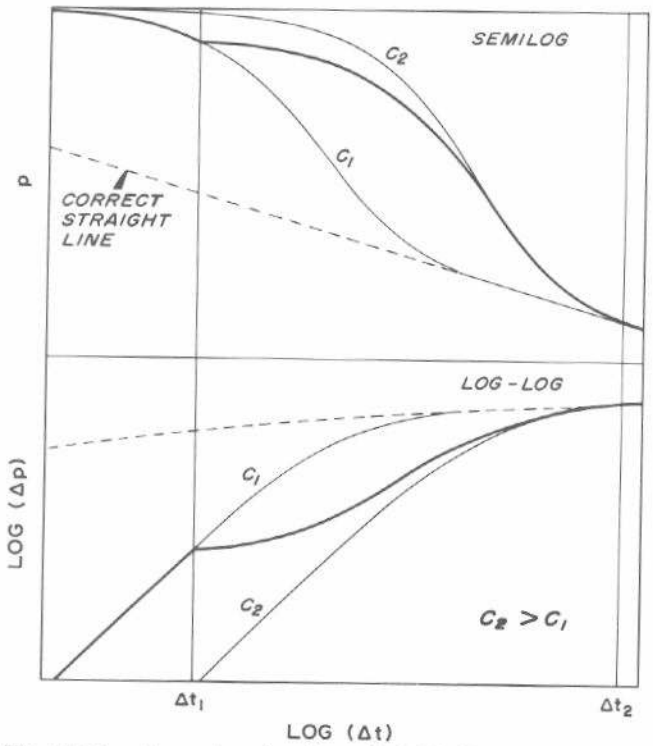

Fig. 11.2 Log-log and semilog theoretical falloff curves for a step increase in wellbore storage coefficient. After Earlougher, Kersch, and Ramey.[7]

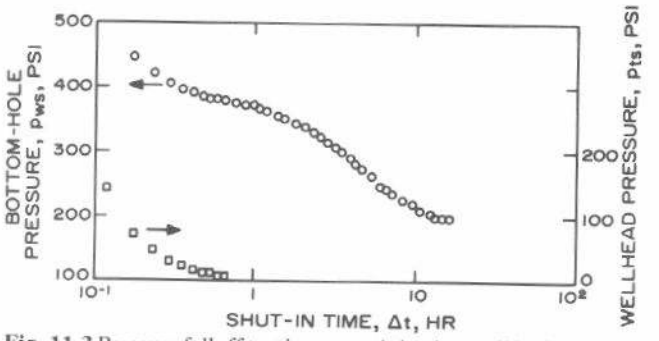

Fig. 11.3 Pressure falloff test in a water injection well in the Illinois basin; increasing wellbore storage. After Earlougher, Kersch, and Ramey.[7]

computation. Wellbore storage also may decrease during an injectivity test. To visualize that case, reverse the sequence shown in Fig. 11.1 and picture injection into a well with a liquid level standing below the surface. As the bottom-hole pressure increases, the liquid level rises until it reaches the surface. The result is a compression-controlled wellbore storage coefficient.

Fig. 11.5 shows theoretical data plots for decreasing wellbore storage.[7] In the log-log plot, the data initially fall on the line for the higher wellbore storage coefficient. When the coefficient decreases at time t_1, the pressure increases rapidly until it reaches the line for the lower wellbore storage coefficient. The semilog plot also shows a rapid increase in slope. Data reach the correct semilog straight line at t_2. Fig. 11.6 shows actual data for an injectivity test with a decreasing wellbore storage coefficient.[7] Note that the test data start with a relatively low slope that rapidly increases and finally flattens to the semilog straight line indicated.

When the wellbore storage coefficient changes during a transient well test, the *second* storage coefficient determines when the correct semilog straight line will begin. Thus, for the case in Fig. 11.2, wellbore storage coefficient C_2 would be used in Eq. 11.5 or Eq. 11.6 to estimate the starting time for the semilog straight line. For the situation in Fig. 11.5, wellbore storage coefficient C_1 would be used. An exception would be certain cases of increasing wellbore storage coefficient where the increase in wellbore storage did not occur until a test time exceeding the "die-out" time (Eq. 11.5 or Eq. 11.6) based on the smaller initial storage coefficient. In any event, afterflow should be negligible at the die-out time based on the larger final wellbore storage coefficient.

Changing wellbore storage is usually easy to detect in a transient well test — if the engineer is cognizant of its characteristics. Since storage usually changes at a bottom-hole pressure corresponding to the hydrostatic pressure of the fluid column in the well, verification is straightforward. In some cases, it is easier to recognize changing wellbore storage effects on the semilog plot than on the log-log plot, although both are recommended for diagnostic purposes. Ref. 7 illustrates when it may be difficult to recognize changing wellbore storage from the log-log plot.

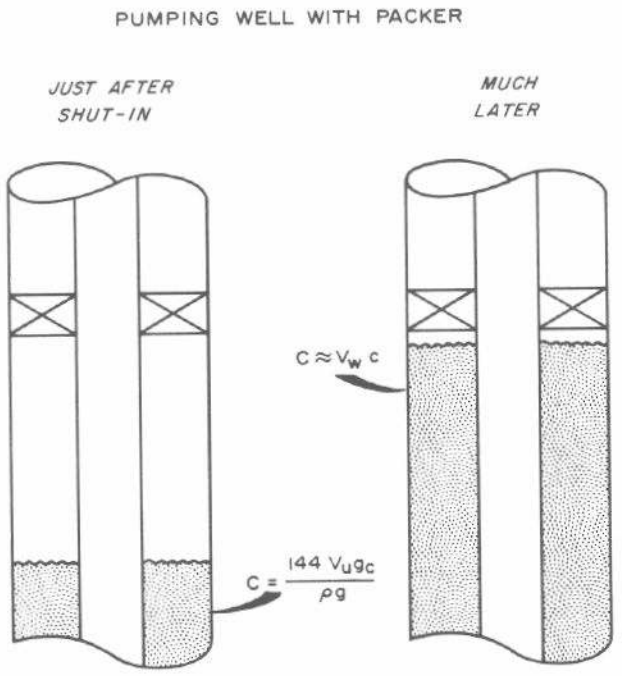

Fig. 11.4 Decreasing wellbore storage — fluid level in shut-in pumping well reaches packer. V_{ac} = total annular volume below the packer.

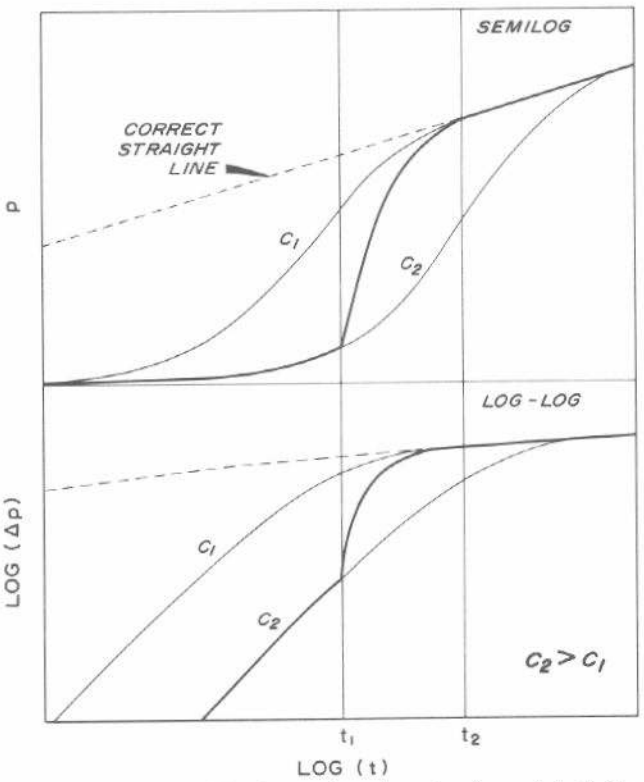

Fig. 11.5 Theoretical log-log and semilog plots for an injectivity test with a step decrease in wellbore storage. After Earlougher, Kersch, and Ramey.[7]

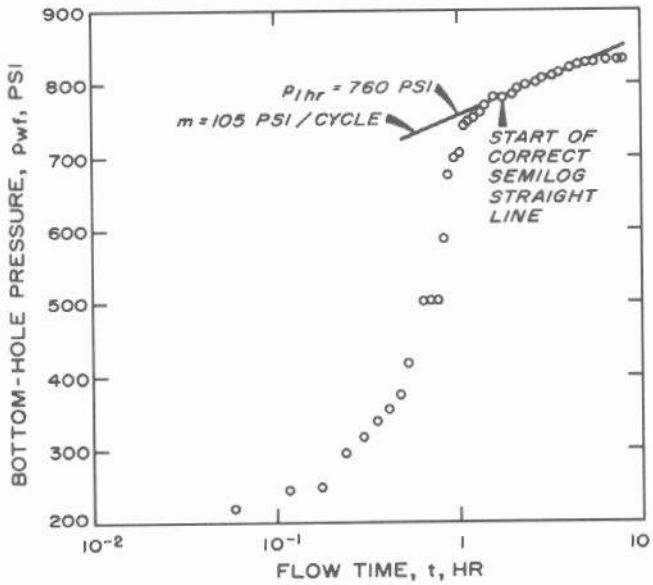

Fig. 11.6 Injectivity test for the well of Fig. 11.3; decreasing wellbore storage. After Earlougher, Kersch, and Ramey.[7]

Example 11.1 Effect of Changing Wellbore Storage on Falloff and Injectivity Tests

Earlougher, Kersch, and Ramey[7] present the falloff and injectivity test data shown in Figs. 11.3 and 11.6. Fig. 11.7 is the log-log data plot for the two tests. Known data are

$q_w = -100$ STB/D
$B_w = 1.0$ RB/STB
$\mu_w = 1.0$ cp
$h = 16$ ft
$\phi = 0.22$
$c_t = 7 \times 10^{-6}$ psi^{-1}
$r_w = 0.29$ ft
depth = 994 ft, and

2-in. EUE tubing with packer set at 979 ft. Also,

$$p_{wf}(\Delta t = 0) = 837 \text{ psi}$$

and

$$p_{tf}(\Delta t = 0) = 457 \text{ psi}$$

for the falloff, and

$$p_{ws}(t = 0) = 194 \text{ psi}$$

and

$$p_{ts}(t = 0) = 0 \text{ psi}$$

for the injectivity test.

The falloff data in Figs. 11.3 and 11.7 have the characteristic shape of an increasing wellbore storage coefficient. The increase starts at about 0.3 hour. That is not when the wellhead pressure reaches atmospheric, as we would expect if the wellbore were *full* of water at the start of the test. The data show that the difference between surface and bottomhole pressure is only 837 − 457 = 380 psi. Using 0.433 psi/ft as the static gradient for water, 380 psi corresponds to 878 ft of water column. Thus, there must have been about 994 − 878 = 116 ft of gas above the water column, assuming no significant static pressure gradient in the gas.

Assuming that the gas column does exist and that it is 116 ft long, the wellbore storage coefficient at the start of the test can be estimated by applying Eq. 11.1. We assume $\Delta V =$ 0.1 bbl and estimate the resulting Δp. For 2-in. tubing, $V_u \simeq$ 0.004 bbl/ft, so 0.1 bbl corresponds to 25 ft of fluid-level change. Applying the static water gradient, and assuming the perfect gas law may be used for the gas column,

$$\Delta p = 25(0.433) + 457\left(\frac{116}{116 - 25} - \frac{116}{116}\right)$$

$$= 136 \text{ psi}.$$

Then,

$$C = 0.1/136 = 7.35 \times 10^{-4} \text{ bbl/psi}.$$

In a similar manner we find that $C = 2.3 \times 10^{-3}$ bbl/psi when the liquid level has fallen 100 ft, indicating a continual increase in C. The maximum value of C must occur when wellhead pressure reaches atmospheric; then Eq. 11.2 applies and

$$C_{\max} = \frac{0.004}{(62.4/144)(32.17/32.17)}$$

$$= 9.23 \times 10^{-3} \text{ bbl/psi}.$$

Since the beginning of the semilog straight line is determined by the final wellbore storage coefficient, Eq. 11.6b can be used with assumed values of $kh/\mu = 155$ md ft/cp and $s = 0.9$ to estimate

$$t_{bsl} > \frac{(170{,}000)(9.23 \times 10^{-3})\, e^{(0.14)(0.9)}}{155}$$

$$> 11.5 \text{ hours}.$$

Only the last four data points in Fig. 11.3 occur after 11.5 hours, and they are not adequate for analysis. Thus, we must conclude that we cannot analyze this increasing-wellbore-storage falloff test.

During the injectivity test the wellbore storage coefficient decreases, as indicated by Figs. 11.6 and 11.7. The correct semilog straight line, with $m = 105$ psi/cycle and $p_{1\text{hr}} = 760$ psi, is shown in Fig. 11.6. Using Eq. 7.4,

$$k = \frac{(-162.6)(-100)(1.0)(1.0)}{(105)(16)} = 9.7 \text{ md},$$

and

$$kh/\mu = (9.7)(16)/(1.0) = 155 \text{ md ft/cp}.$$

From Eq. 7.5,

$$s = 1.1513\left\{\frac{760 - 194}{105} - \log\left[\frac{9.7}{(0.22)(1)(7 \times 10^{-6})(0.29)^2}\right] + 3.2275\right\}$$

$$= 0.9.$$

From the unit-slope straight line in Fig. 11.7 for the injectivity test, $\Delta p = 41.5$ psi at $\Delta t = 0.1$ hour. Then, from Eq. 2.20,

$$C = \frac{(100)(1)(0.1)}{(24)(41.5)} = 0.0100 \text{ bbl/psi}.$$

C_D at the beginning of both the falloff and the injectivity tests can be estimated from the wellbore storage coefficients at the beginning of the tests and Eq. 11.4. For the falloff test,

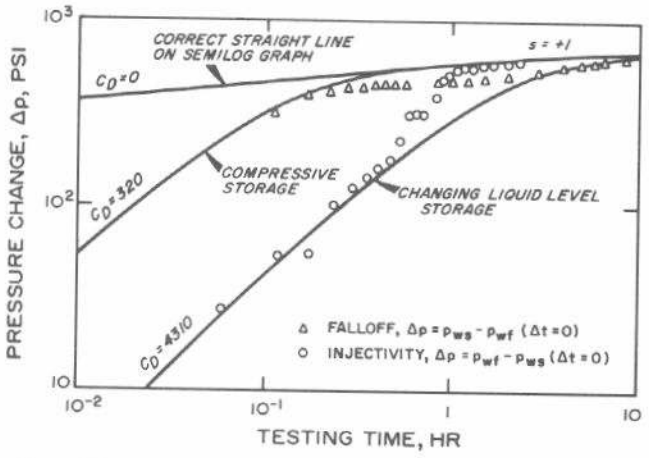

Fig. 11.7 Log-log plot of falloff and injectivity data of Figs. 11.3 and 11.6, Example 11.1. After Earlougher, Kersch, and Ramey.[7]

$$C_{Di} = \frac{(5.6146)(7.35 \times 10^{-4})}{2\pi(0.22)(7 \times 10^{-6})(16)(0.29)^2} \simeq 320,$$

and for the injectivity test,

$$C_{Di} = \frac{(5.6146)(0.0100)}{2\pi(0.22)(7 \times 10^{-6})(16)(0.29)^2} = 4{,}310.$$

The p_D vs t_D curves for those two values of C_D and for $s = 1$ have been matched to the observed data in Fig. 11.7. The curves verify the changing wellbore storage condition.

If a well test encounters a changing wellbore storage condition, it may be possible to analyze test data by being careful, or it may be necessary to devise a test that minimizes or eliminates the wellbore storage change. Frequently, tests with increasing wellbore storage are not interpretable. That is because of the unlikely appearance of the correct semilog straight line during the compressive wellbore storage period and the long duration of the falling-liquid-level wellbore storage period. The second factor often results in an inadequate semilog straight-line definition because of insufficient shut-in time or boundary or interference effects. In fortunate circumstances, the compressive storage may last long enough for the semilog straight line to develop and the test may be analyzed using data before the liquid level starts to fall. Tests with a decreasing storage coefficient (injectivity or buildup) have more potential for analysis than tests with increasing wellbore storage (falloff or drawdown). Figs. 11.2 and 11.5 indicate that the semilog straight line is reached sooner when the wellbore storage decreases than when it increases. In some instances, it may be worthwhile to use a two-rate test (Section 4.3), or some other multiple-rate test (Chapter 4), to attempt preventing a changing storage situation.

11.3 Artificially Fractured Wells

Since the beginning of intentional hydraulic fracturing of wells,[8] thousands of production and injection wells have been fractured hydraulically. Hydraulic fracturing has a definite effect on pressure transient response, so we should be aware of that effect when analyzing well test data. Although both horizontal and vertical fractures may be induced by the hydraulic fracturing process, it is believed that essentially all induced fractures at depths greater than 3,000 ft are vertical.[8] Thus, most studies of pressure transient behavior in fractured wells have been devoted to vertically fractured wells,[9-15] while horizontally fractured wells have been studied less thoroughly.[13,16-18] Gringarten, Ramey, and Raghavan[19] discuss several techniques for analyzing transient test data for fractured wells.

Vertically Fractured Wells

Both infinite and closed systems containing a vertically fractured well have been studied thoroughly. Additional information is still needed about vertically fractured wells in drainage areas with constant-pressure boundaries. Such information would be more applicable to wells in waterfloods after fillup and in strong water-drive reservoirs. Also, more data are needed for geometries other than currently discussed in the literature.

Fig. 11.8 defines nomenclature for a closed-square system with a vertically fractured well at its center. The half-fracture length, x_f, and the half-length of the side of the square, x_e, are commonly used to characterize the system. In all systems discussed in this chapter, we assume that the fracture fully penetrates the vertical extent of the formation and is the same length on both sides of the well; in closed systems the fracture is parallel to a boundary. Only one fracture is considered.

Figs. C.3, C.4, C.17, C.18, and C.19 show dimensionless pressure data for vertically fractured, infinite, and closed systems. The difference between an infinite-conductivity and a uniform-flux fracture is explained in Section C.2. Except for highly propped and conductive fractures, it is thought that the uniform-flux fracture better represents reality than the infinite-conductivity fracture..

In either infinite systems or in closed systems with relatively short vertical fractures ($x_e/x_f > 1.5$), the *early-time* flow behavior is linear* from the formation into the fracture. (If the wellbore storage coefficient is large, the linear flow portion may be obscured.) Eq. C.8 gives the dimensionless pressure as a function of dimensionless time for the linear flow period. By using Eqs. 2.2 and C.8, the pressure at the well during the linear flow period may be written as[10]

$$p_{ws} = p_i + m_{vf}\sqrt{t}. \quad \ldots\ldots\ldots\ldots\ldots\ldots (11.7)$$

Eq. 11.7, which applies for drawdown or injection, indicates that a plot of bottom-hole pressure vs the square root of time should have an early-time straight-line portion with intercept p_i. The slope is

$$m_{vf} = \frac{-4.064\,qB}{h}\sqrt{\frac{\mu}{k\phi c_t x_f^2}}. \quad \ldots\ldots\ldots\ldots (11.8)$$

The slope of the $\sqrt{t}$ plot may be used to estimate

$$kx_f^2 = \left(\frac{-4.064\,qB}{m_{vf}h}\right)^2 \frac{\mu}{\phi c_t}. \quad \ldots\ldots\ldots\ldots (11.9)$$

*But a recent paper indicates that systems with finite conductivity vertical fractures may not exhibit linear flow behavior. See Cinco, Heber, Samaniego-V., F., and Dominguez-A., N.: "Transient Pressure Behavior for a Well With a Finite-Conductivity Vertical Fracture," paper SPE 6014 presented at the SPE-AIME 51st Annual Fall Technical Conference and Exhibition, New Orleans, Oct. 3-6, 1976.

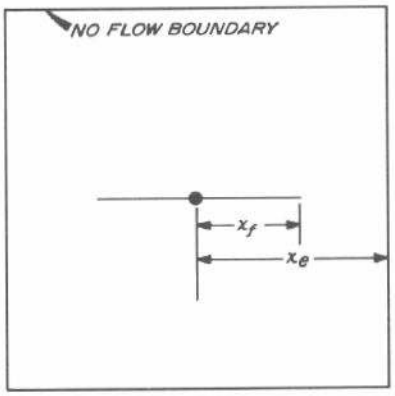

Fig. 11.8 Vertically fractured system.

For values of $x_e/x_f > 1$, the linear flow period ends at about $t_{Dxf} \simeq 0.016$ for an infinite-conductivity vertical fracture and at $t_{Dxf} \simeq 0.16$ for a uniform-flux vertical fracture.

After the initial linear flow period, there is a transition to an infinite-acting, pseudoradial flow period in which the normal semilog analysis (Chapters 3 through 7) applies. The pseudoradial period begins at $t_{Dxf} \simeq 3$ for the infinite-conductivity case and at $t_{Dxf} \simeq 2$ for the uniform-flux case. Eqs. C.7 and C.10 give the dimensionless pressure for that flow period, providing boundary effects are not encountered. In a *closed system*, the infinite-acting, pseudoradial behavior only develops completely if $x_e/x_f > 5$. When pseudoradial flow occurs, permeability may be estimated from the semilog straight-line slope with the familiar equation

$$k = \frac{\pm 162.6\, qB\mu}{mh}, \quad \ldots\ldots\ldots\ldots\ldots\ldots (11.10)$$

where the appropriate sign is chosen depending on the test type, as indicated in Chapters 3 through 7 and Appendix E.

Wattenbarger and Ramey[12] have observed that there is an approximate relationship between the pressure change at the end of the linear flow period, Δp_{el}, and at the beginning of the semilog straight line, Δp_{bsl}. Since the linear flow period is a straight line on a p vs $\sqrt{t}$ plot (or a line of one-half slope on a log Δp vs log Δt plot), it is generally not too difficult to estimate Δp_{el}, the pressure change at the end of the linear flow period. If the semilog straight line develops, it is also possible to estimate Δp_{bsl}, the pressure change at the beginning of the semilog straight line. If the relationship

$$\Delta p_{bsl} \geq 2\,\Delta p_{el}, \quad \ldots\ldots\ldots\ldots\ldots\ldots\ldots\ldots (11.11)$$

is not satisfied, it is likely that either an incorrect linear flow period or an incorrect radial flow period has been chosen. Fig. 11.9 shows dimensionless pressure for an infinite-acting, vertically fractured system during both linear and radial flow periods. Note that the data curve on the $\sqrt{t}$ scale appears to be straight at times after the end of the linear flow period. Both Fig. 11.9 and experience indicate it is not difficult to find an *apparent* $\sqrt{t}$ straight line in the transition period from linear to radial flow. The slope of that apparent straight line is not related to formation permeability and fracture length, as indicated by Eq. 11.9. Fig. 11.9 illustrates the importance of making the check indicated by Eq. 11.11.

Pressure buildup (falloff) testing in vertically fractured wells is similar to that in unfractured wells. However, when performing the superposition to get the effect of the shut-in period (Section 5.2), it must be understood that the linear flow period does not last long. Thus, if the flow period is long enough to deviate from linear flow, Eq. C.8 (or Eq. 11.7), which indicates pressure is a function of $\sqrt{t}$, cannot be used in the flow portion of the superposition. Instead, Eq. C.7 or Eq. C.10, which are longer-time solutions for the

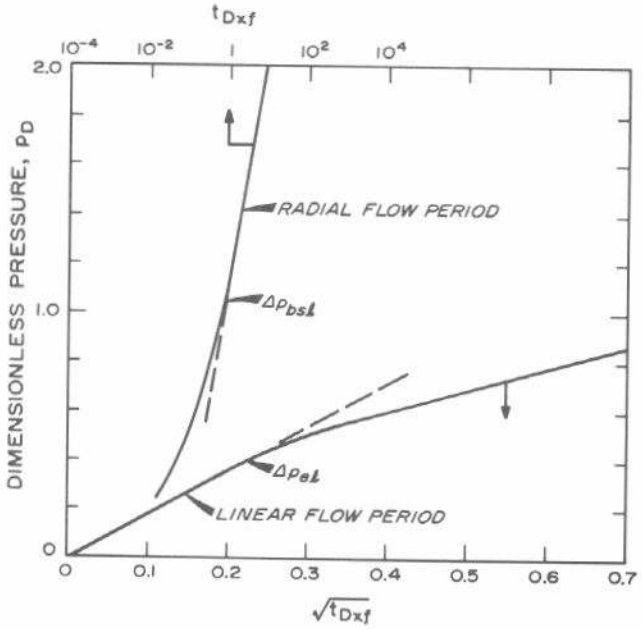

Fig. 11.9 Linear and radial flow periods for a fractured well. After Wattenbarger and Ramey;[12] data of Russell and Truitt.[9]

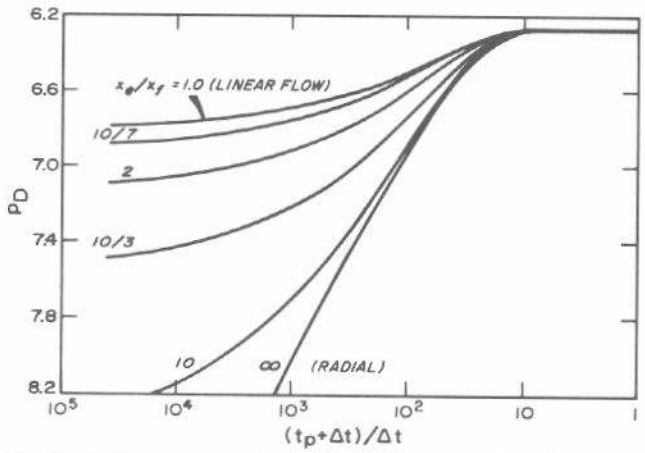

Fig. 11.10 Horner graph for a vertically fractured well in the center of a closed-square reservoir, $t_{pDA} = 1.0$. After Russell and Truitt.[9]

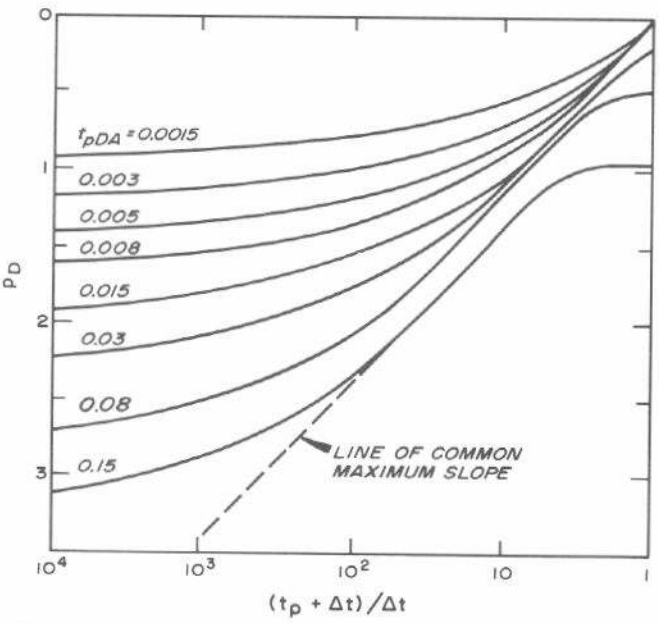

Fig. 11.11 Horner graph for a vertically fractured well in the center of a closed-square reservoir, $x_e/x_f = 10$. After Raghavan, Cady, and Ramey.[11]

pseudoradial flow period (that still assume no boundary effects) may have to be substituted. Care is required in devising an analysis technique under such circumstances.

Pressure data from the pseudoradial flow portion of a buildup (falloff) test is analyzed using the normal Horner plot, p_{ws} vs $\log[(t_p + \Delta t)/\Delta t]$. Figs. 11.10 and 11.11 show theoretical Horner plots for pressure buildup in vertically fractured systems. The two figures indicate the effect of fracture length and producing time on the Horner-plot slope. The maximum Horner-plot slope depends on fracture length (Fig. 11.10), but is independent of producing time for a fixed fracture length (Fig. 11.11) providing the buildup or falloff test is of sufficient duration to show the maximum slope. This indicates that permeabilities estimated from the measured Horner-plot slope must be modified as indicated below.

To correct permeability estimated from a Horner or Miller-Dyes-Hutchinson (MDH) plot, we use (when shut-in lasts long enough to observe the maximum slope)

$$k = k_C \left[\frac{(kh)_{tr}}{(kh)_a}\right]_{\text{Fig. 11.12}} = k_C F_{\text{cor}}, \quad \ldots\ldots\ldots\ldots\ldots\ldots\ldots\ldots (11.12)$$

where k_C is the k value calculated with Eq. 11.10; the ratio of true to apparent kh, F_{cor}, is taken from Fig. 11.12.* In Fig. 11.12 the upper solid line applies to the Horner data plot for any producing time. If the MDH data plot is used, the correction factor is a function of production time up to $t_{pDA} = 0.12$. Because of its independence of t_p and its lower sensitivity (correction factor nearer 1.0), the Horner graph is recommended for analyzing data from vertically fractured wells. To use Eq. 11.12, it is necessary to know x_f/x_e (note in Fig. 11.12 F_{cor} is plotted vs x_f/x_e rather than x_e/x_f used in most figures in this monograph). If both the linear ($\sqrt{t}$) and radial ($\log t$) flow periods develop, it is possible to estimate kx_f^2 from Eq. 11.9 and k from Eq. 11.12 using a reasonable value of x_f/x_e in Fig. 11.12. Then the estimated k may be used with results from Eq. 11.9 to estimate x_f. That x_f is used to compute a new x_f/x_e to be used in Fig. 11.12 and to improve the estimation of k. This process continues until two successive values are the same. If both flow periods do not develop, it is necessary to make an independent estimate of fracture length (from fracture-job parameters) or of permeability (from an unfractured nearby well). (Fig. 9.10 and Ref. 20 indicate that interference testing in a system with a vertically fractured well may provide incorrect results. A more sophisticated analysis is required in that instance.)

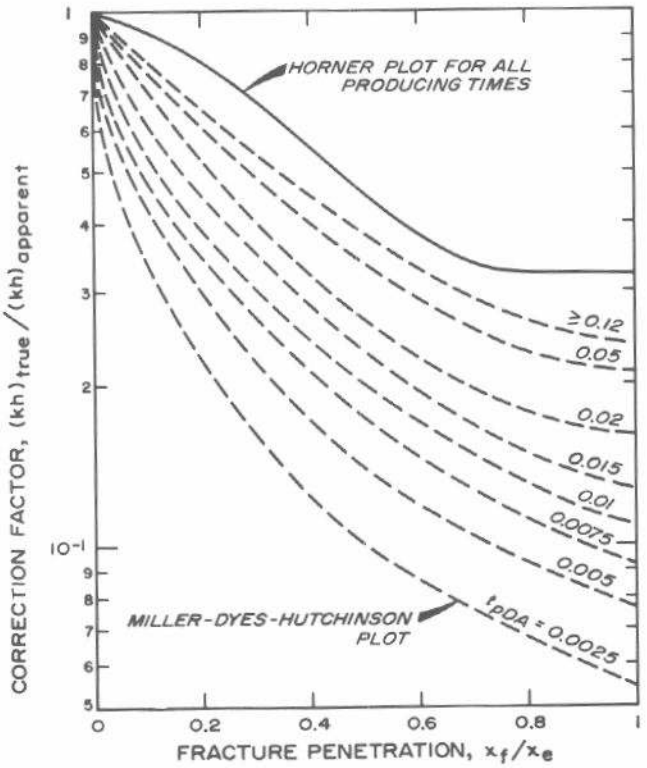

Fig. 11.12 Correction factor for kh estimated from pressure buildup tests in vertically fractured wells, assuming sufficient shut-in time to reach maximum slope. After Raghavan, Cady, and Ramey.[11]

Eqs. 11.9, 11.10, and 11.12 also may be combined to give another useful form for estimating fracture length similar to that proposed by Clark:[10]

$$x_f = \frac{0.3187}{m_{Vf}}\sqrt{\frac{mqB}{\phi c_t h F_{\text{cor}}}}, \quad \ldots\ldots\ldots\ldots\ldots (11.13)$$

where m is the apparent semilog straight-line slope and F_{cor} is the factor that corrects m to the true semilog slope, as in Eq. 11.12. F_{cor}, given in Fig. 11.12, has a minimum value of about 0.32 for a Horner plot and 0.23 for an MDH plot for a closed-square drainage area when production time is sufficient to reach pseudosteady state ($t_{pDA} > 0.12$). When flow times are less than required to reach pseudosteady state, much lower values of F_{cor} (larger corrections) can be applicable. The proper F_{cor} can be estimated by an iterative technique similar to the one described above.

An alternate approach to analyzing fractured-well transient test data is type-curve matching. Gringarten, Ramey, and Raghavan[19] provide a good illustration. Curve matching normally would be performed with Fig. C.3, Fig. C.18, or Fig. C.19 using the technique described in Section 3.3 and illustrated in Fig. 3.5. Once a match point is chosen, the dimensionless parameters on the axis of the type curve are used to estimate formation permeability and fracture length. For Figs. C.3, C.18, and C.19, permeability would be estimated from the pressure match using[19]

$$k = \frac{141.2\,qB\mu}{h}\,\frac{(p_D)_M}{(\Delta p)_M}, \quad \ldots\ldots\ldots\ldots (11.14)$$

where the data-plot match point, $(\Delta p)_M$, falls on top of the type-curve match point, $(p_D)_M$. The fracture length is estimated from the time-axis match point:[19]

$$x_f = \sqrt{\frac{0.0002637\,k\,(\Delta t)_M}{\phi\mu c_t\,(t_{Dxf})_M}}. \quad \ldots\ldots\ldots\ldots (11.15)$$

*Fig. 11.12 applies for a vertical fracture in a closed-square region. A recent paper (Raghavan, R.: "Analysis of Pressure Data for Fractured Wells: The Constant-Pressure Outer Boundary," paper SPE 6015 presented at the SPE-AIME 51st Annual Fall Technical Conference and Exhibition, New Orleans, Oct. 3-6, 1976) gives similar information for a vertically fractured well in a constant-pressure-boundary square. In that case, the Horner graph for pressure buildup analysis is also best, but the correction factors also depend on production time, t_p.

If all test data fall on the half-slope line on the log Δp vs log Δt plot (the straight line in the $\sqrt{t}$ plot), then permeability cannot be estimated by either type-curve matching or semilog plotting. This situation often occurs in tight gas wells, where the linear flow period may last for several hundred hours. However, the last data point on the half-slope line (on the $\sqrt{t}$ straight line) may be used to estimate an upper limit of the permeability:[19]

$$k \leq \frac{(0.215)(141.2)\,qB\mu}{h\,\Delta p}, \quad \ldots\ldots\ldots\ldots (11.16)$$

where Δp is the observed pressure change at the last point on the half-slope ($\sqrt{t}$) straight line. That permeability and the corresponding time value for the last point on the $\sqrt{t}$ straight line, t, may be used to estimate a minimum fracture length:[19]

$$x_f \geq \sqrt{\frac{0.0002637\,kt}{(0.016)\,\phi\mu c_t}}. \quad \ldots\ldots\ldots\ldots (11.17)$$

Eqs. 11.16 and 11.17 apply only for $x_e/x_f >> 1$ and for infinite-conductivity fractures. If the fracture is expected to be more like a uniform-flux fracture, 0.215 in Eq. 11.16 becomes 0.76 and 0.016 in Eq. 11.17 becomes 0.16.

Often in type-curve matching applications, it is also possible to estimate reservoir size. In Figs. C.18 and C.19 the dimensionless pressure deviates upward from the infinite-system solution as boundary effects become important. When observed data fall on one of the upward-deviating curves, the x_e/x_f parameter on that curve may be used to estimate x_e and, thus, drainage area, assuming that the square system shape applies (if it does not, it is unlikely that a good match will be obtained[19]). If the last data point is still on the infinite-acting solution curve, then a limiting estimate can be made concerning the drainage volume. In that case one observes the x_e/x_f parameter for the last upward-deviating curve that the matched data pass and uses that as an indication of the smallest drainage volume for the system.

As additional type curves become available for other fractured systems, capabilities for analyzing fractured-well transient pressure data by curve-matching techniques should expand significantly.

Pierce, Vela, and Koonce[15] propose a method for using pulse testing to estimate the orientation and length of a vertical fracture. Their method requires computer analysis of test data; however, a qualitative idea of fracture orientation may be obtained from pulse testing without computer assistance. See Ref. 15 for details.

Russell and Truitt[9] show that the vertical-fracture half-length can be related to an apparent wellbore radius for a single vertical fracture in a closed square by

$$r_{wa} \simeq 0.48\,x_f, \quad \ldots\ldots\ldots\ldots (11.18a)$$

when $x_e/x_f > 2$.

By using the skin factor equation and Eqs. C.7 and C.10, it is possible to write similar expressions for *infinite-acting systems*. For a uniform-flux fracture,

$$r_{wa} \simeq 0.37x_f, \quad \ldots\ldots\ldots\ldots (11.18b)$$

and for an infinite-conductivity fracture,

$$r_{wa} \simeq 0.50x_f. \quad \ldots\ldots\ldots\ldots (11.18c)$$

Eqs. 11.18a through 11.18c provide only a rough estimate, but may be helpful in estimating fracture length when only an apparent wellbore radius can be estimated from the skin factor using Eq. 2.11. That approach is not recommended.

Square, vertically fractured systems approach pseudosteady state after long enough production time[9] ($t_{pDA} > 0.12$). Then, the dimensionless pressure is

$$p_D = 2\pi t_{DA} + \ln\left(\frac{x_e}{x_f}\right) + \frac{1}{2}\ln\left(\frac{2.2458}{C_A}\right), \quad \ldots. (11.19)$$

where the shape factor, C_A, is given in Table C.1. Note the similarity of Eq. 11.19 to the pseudosteady-state equation for an unfractured well, Eq. 2.23. Russell and Truitt[9] show that reservoir-limit testing techniques (Section 3.5) apply to vertically fractured wells.

Example 11.2 Buildup Test Analysis for a Vertically Fractured Well

Gringarten, Ramey, and Raghavan[13] provide the pressure buildup data in Table 11.1. Other pertinent data are

$q_o = 2{,}750$ STB/D
$\mu_o = 0.23$ cp
$\phi = 0.30$
$c_t = 30 \times 10^{-6}$ psi^{-1}
$h = 230$ ft
$B_o = 1.76$ RB/STB
depth = 9,500 ft.

The usual log-log plot (not shown) has no unit slope, but has a slope of ½ from 5 to 75 minutes. Thus, we suspect a fractured well. For a formation at a depth of 9,500 ft, the fracture should be vertical.[8]

Fig. 11.13 is a plot of Δp vs $\sqrt{t}$, as suggested by Eq. 11.7. The graph has a straight line with $m_{vf} = 97.3$ psi hr$^{-½}$ up to at least $\Delta p = 160$ psi. Eq. 11.9 can be used to estimate

$$kx_f^2 = \left[\frac{-4.064(2{,}750)(1.76)}{(97.3)(230)}\right]^2 \frac{0.23}{(0.30)(30 \times 10^{-6})}$$

$$= 19{,}700 \text{ md sq ft}.$$

According to Eq. 11.11, Δp at the beginning of the semilog straight line should be at least $2 \times 160 = 320$ psi. Since the test ended before that Δp, the semilog plot will not

TABLE 11.1—PRESSURE BUILDUP DATA FROM A WELL WITH A VERTICAL FRACTURE, EXAMPLE 11.2.
After Gringarten, Ramey, and Raghavan.[13]

Δt (min)	$p_{ws} - p_{wf}(\Delta t = 0)$ (psi)
0	0
5	31
10	43
15	54
20	66
25	66
30	72
35	78
40	83
45	89
50	100
55	100
60	100
75	114
120	136
150	159
240	181
285	206
480	218

be helpful. Thus, we must use type-curve matching for further analysis of the test. (This is not meant to imply that type-curve matching would not be useful if we could use the semilog plot; it could be useful, particularly to give limits on x_e/x_f.) Fig. 11.14 shows the data of Table 11.1 matched to Fig. C.19. Note that the data do not show any effects of a boundary. The match-point data are

$$(\Delta p)_M = 100 \text{ psi at } (p_D)_M = 0.77,$$

and

$$(\Delta t)_M = 100 \text{ minutes at } (t_{Dxf})_M = 0.36.$$

Using Eq. 11.14,

$$k = \frac{(141.2)(2{,}750)(1.76)(0.23)(0.77)}{(230)(100)}$$

$$= 5.26 \text{ md}.$$

From Eq. 11.15,

$$x_f = \sqrt{\frac{(0.0002637)(5.26)(100/60)}{(0.30)(0.23)(30 \times 10^{-6})(0.36)}}$$

$$= 55.7 \text{ ft}.$$

These results can be compared with the result of using Fig. 11.13 and Eq. 11.9. The value

$$kx_f^2 = (5.26)(55.7)^2 = 16{,}300 \text{ md sq ft},$$

compares with 19,700 md sq ft computed from Eq. 11.9 — about a 17-percent difference. If k is assumed to be correct, then

$$56 < x_f < 61 \text{ ft};$$

or if x_f is assumed to be correct,

$$5.3 < k < 6.3 \text{ md}.$$

The discrepancy provides an estimate of the accuracy of the type-curve matching method. When the well is retested, it would be advisable to get a longer buildup period in an attempt to define the semilog straight line.

Note from Fig. 11.14 that observed pressure data are still on the infinite-acting curve — at least to $x_e/x_f = 2$. Thus, we can say that x_e/x_f must be greater than 2 for the tested well. Using the value $x_f = 55.7$ ft, we estimate that $x_e > 111$ ft. Thus, we expect the drainage area for the test well to be larger than a 222-ft square, with an equivalent area of 1.13 acres. As we see, this test did not investigate a very large amount of reservoir.

Horizontal Fractures

Dimensionless pressure data for a single horizontal fracture located at the center of the productive interval in an infinite-acting system are given in Fig. C.5. No allowance for wellbore or fracture storage is included in that figure. At *very* short production times, the log-log plot of p_D vs t_D may have a unit slope resulting from storage effects within the fracture.[13,18] In most cases wellbore storage would obscure such fracture storage.

Fig. 11.15 also shows p_D vs t_D for a horizontally fractured well.[18] When plotted as shown in Fig. 11.15 (as contrasted to the log-log plot of p_D/h_D shown in Fig. C.5), the pressure-

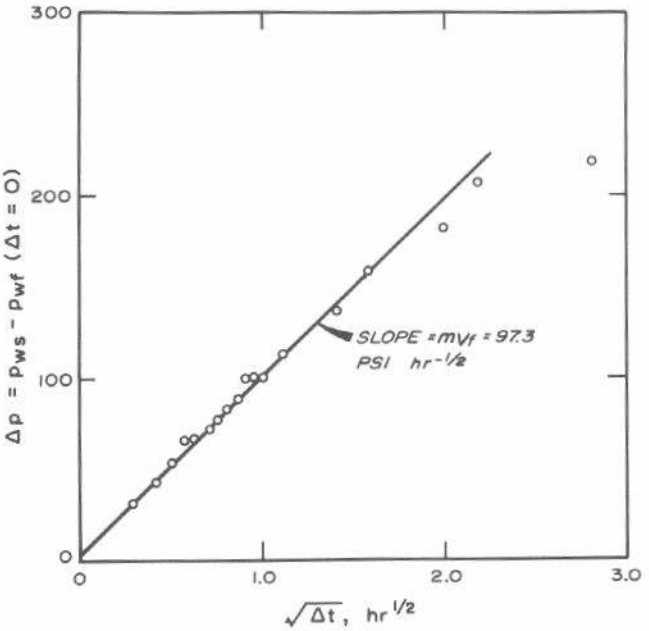

Fig. 11.13 Square-root data plot for buildup test of Example 11.2.

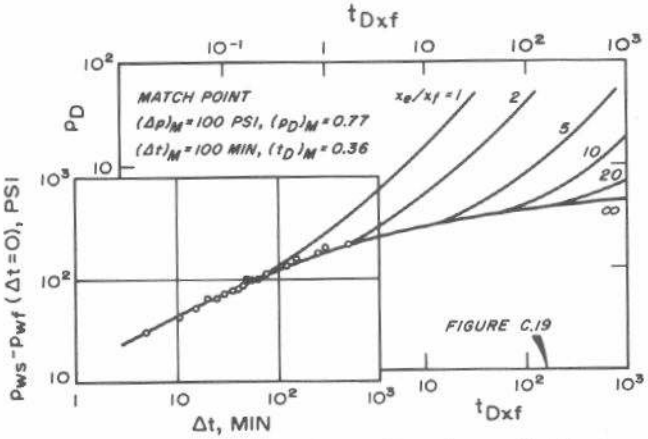

Fig. 11.14 Type-curve match for a uniform-flux vertical fracture, Example 11.2. After Gringarten, Ramey, and Raghavan.[13]

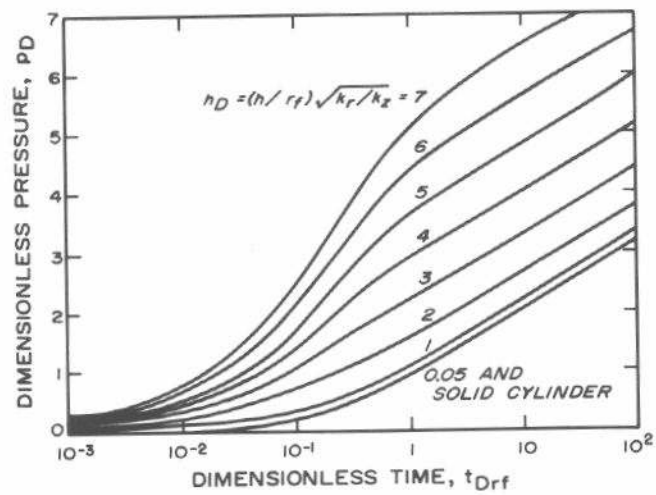

Fig. 11.15 Dimensionless well pressure for a single-plane, uniform-flux, horizontal fracture at center of formation. After Gringarten and Ramey.[18]

time curve has a peculiar S shape when $h_D > 3$ that distinguishes it from the behavior of a vertically fractured well. The log-log plot (Fig. C.5) has an S shape[13,18] for $h_D < 1$. Thus, for low and high h_D values, it may be possible to distinguish between vertical and horizontal fractures based on pressure behavior. However, the semilog curves of Fig. 11.15 for the larger h_D values have a shape typical of pressure data from wells with significant wellbore storage effects (compare Fig. 11.15 with Figs. 5.2 and 7.6).

At short flow times, there is a period of linear vertical flow from the formation to the horizontal fracture. During those times, dimensionless pressure is given by[19]

$$p_D = 2h_D \sqrt{\frac{t_{Drf}}{\pi}}, \quad \ldots\ldots\ldots\ldots\ldots\ldots (11.20)$$

where h_D is given by Eq. C.12 and t_{Drf} is given by Eq. C.11. The p_D in Eq. 11.20 may be used in Eq. 2.2 to obtain an expression for the flowing bottom-hole pressure during drawdown or injection — during the linear flow period;

$$p_{wf} = p_i + m_{Hf}\sqrt{t}. \quad \ldots\ldots\ldots\ldots\ldots\ldots (11.21)$$

Eq. 11.21 indicates that a plot of flowing bottom-hole pressure vs $\sqrt{t}$ should have an early-time straight-line portion with intercept p_i and slope

$$m_{Hf} = \frac{-2.587\,qB}{r_f^2}\sqrt{\frac{\mu}{k_z\,\phi c_t}}. \quad \ldots\ldots\ldots\ldots\ldots (11.22)$$

Note in Eq. 11.22 that the slope is controlled by the formation *vertical* permeability and the fracture radius.

Gringarten, Ramey, and Raghavan[13,19] show that the long-time pressure behavior for an infinite-acting, horizontally fractured well is the same as that for an unfractured well with an additional (negative) skin effect; that is, there is a pseudoradial flow period. Thus, if the fracture is not too long for the test duration, drawdown or injectivity test analysis by normal semilog methods can be used to estimate k_r, the radial direction permeability. Fig. C.5 can be used for curve matching for shorter tests. To date, there are no thorough studies of pressure buildup (falloff) behavior in horizontally fractured wells, so there are no published data for slope or k_r corrections similar to those in Fig. 11.12 for vertically fractured wells. Thus, we would preferably estimate k_r from a drawdown or injectivity test. When we estimate it from a buildup test, we can only assume that the long-time semilog slope gives a reasonable estimate of the true radial permeability when boundary and interference effects are not important.

Type-curve matching with Fig. C.5 may be used to estimate k_r/r_f^2. By using k_r/r_f^2 from type-curve matching and k_r estimated from the semilog straight line (Eq. 11.10), it is possible to estimate r_f. That r_f may be used in a rearranged form of Eq. 11.22 to estimate k_z. Thus, it may be possible to estimate k_r, k_z, and r_f from a single-well test for a well with a horizontal fracture. Of course, the fracture must be at the center of the formation to use Fig. C.5 and Eq. 11.22; the system must be infinite-acting; and the pseudoradial flow period must be fully developed. In addition, wellbore storage effects must not mask the initial $\sqrt{t}$ straight line. It should also be remembered that no data are presented for correcting pressure buildup (falloff) analyses in a horizontally fractured well, so the accuracy of k_r may be in doubt. Eq. 11.20 may be used with superposition to devise a technique for pressure buildup plotting for the linear flow period. Normally, that would be done by having a long production period before the shut-in and using a long-term equation for that period such as one based on a p_D given by[19]

$$p_D = \frac{1}{2}\left(\ln t_{Drf} + 1.80907 + \frac{h_D^2}{6}\right), \quad \ldots\ldots (11.23)$$

where t_{Drf} is given by Eq. C.11. Then the linear-flow portion of the shut-in period would be represented by Eq. 11.20. If Eq. 11.20 is used for the drawdown period as well as the shut-in period, the linear flow period must last *throughout* the *drawdown* portion of the test or the derived equation will be incorrect, as will be the subsequent analysis.

Gringarten, Ramey, and Raghavan[19] also indicate how type-curve matching may be used to estimate k_r, k_z, and r_f for a horizontally fractured well. In that situation pressure drawdown or injection data would be matched to the type curve of Fig. C.5. Sufficient data must be available so one of the h_D curves is clearly matched. The pressure match is used to estimate

$$\sqrt{k_r k_z}\, r_f = \frac{141.2\,qB\mu\,(p_D/h_D)_M}{(\Delta p)_M}. \quad \ldots\ldots (11.24)$$

The time-scale match is used to compute

$$\frac{k_r}{r_f^2} = \frac{\phi\mu\, c_t\,(t_D)_M}{0.0002637\,(t)_M}. \quad \ldots\ldots\ldots\ldots (11.25)$$

Then the value computed in Eq. 11.25 is used with the matched h_D curve to estimate vertical permeability:

$$k_z = \frac{k_r}{r_f^2}\left[\frac{h}{(h_D)_M}\right]^2. \quad \ldots\ldots\ldots\ldots\ldots (11.26)$$

The three results from Eqs. 11.24 through 11.26 are then used simultaneously to obtain k_r and r_f. Gringarten, Ramey, and Raghavan[19] show an example calculation using the procedure.

11.4 Partial Penetration and Partial Completion

Most material presented in this monograph assumes that a single, vertical well completely penetrates a horizontal formation. When a well penetrates (or is completed in) only a portion of the formation, normal transient analysis may still be used to estimate formation kh/μ and $\bar{p}$, but the skin factor estimated with the normal equations will reflect the partial well completion. Fig. 11.16, based on information presented by Kazemi and Seth,[21] indicates that the pressure transient behavior of a partially completed well may show two semilog straight-line portions. The first straight line represents kh/μ of the perforated interval, while the second represents kh/μ of the full formation interval. The initial straight line may not appear because of wellbore storage or other effects; but under ideal conditions, it does exist. Even when it does occur, we do not recommend trying to estimate the total pay thickness based on the interval open in the well and the two values of kh/μ from a semilog plot unless extraordinary steps have been taken to suppress wellbore

storage.[22] Straight lines often seem to appear in data that is dominated completely by wellbore storage effects. As stated elsewhere, the log Δp-log Δt data plot will often clearly identify wellbore-storage-dominated data. Culham[23] shows that the transition between the two semilog straight lines is often characteristic of spherical flow. As such, those data may provide an estimate of k.

The apparent skin factor estimated from normal transient-test analysis methods for a well with restricted flow entry or for a well that is not vertical in the formation is[24]

$$s_a = s_{tr} + s_p + s_{swp} + \ldots, \quad \ldots\ldots\ldots (11.27)$$

where s_{tr} is the true skin factor caused by damage to the completed portion of the well; s_p is the pseudoskin factor resulting from restricted flow entry; and s_{swp} is a pseudoskin factor resulting from a slanted well. Brons and Marting[25] presented pseudoskin factors resulting from partial penetration — wells not drilled completely through the section (Fig. 2.7). Odeh[24] gives information for estimating the pseudoskin factor for wells that are either partially penetrating or are only partially completed (entire productive interval not perforated). His method may be used to estimate the pseudoskin factor for a large variety of completion conditions.

Jones and Watts[26] propose an equation for estimating the actual skin factor resulting from a combination of a partial completion and a change in permeability in an annular zone around the well over the perforated interval, such as might result from a sand consolidation treatment. The skin so estimated is caused only by the effect of the short damaged interval. The pseudoskin resulting from the partial completion must be added to it. The skin factor resulting from the permeability change near the wellbore is

$$s_{cp} = \frac{h}{\Delta Z_P}\left[1 - 0.2\left(\frac{r_s - r_w}{\Delta Z_P}\right)\right]\left(\frac{k - k_s}{k_s}\right)\ln\left(\frac{r_s}{r_w}\right). \quad \ldots\ldots\ldots (11.28)$$

The equation applies when the perforated interval, ΔZ_P, is much smaller than the formation thickness, h, but that is not thought to be a serious restriction.[26]

Fig. 11.17 schematically shows a well penetrating a formation at an angle α from the line perpendicular to the formation top and bottom. Cinco, Miller, and Ramey[27] show that the pseudoskin factor resulting from a slanted, completely perforated well can be approximated by

$$s_{swp} = -(\alpha/41)^{2.06} - (\alpha/56)^{1.865}\log\left(\frac{h}{100\,r_w}\right), \quad \ldots\ldots\ldots (11.29)$$

when $0° \leq \alpha \leq 75°$, $h/r_w > 40$, and $t_D > 100$. Fig. 11.18 shows the pseudoskin factor for a slanted well. The effect of the slanted well is to provide more wellbore area and, thus, a negative pseudoskin factor.

Skin factors estimated from transient testing include all features that affect the efficiency of fluid flow into the wellbore. The material presented in this section may be useful for either predicting the pressure rate behavior of a well, or for attempting to estimate the skin actually caused by damage. Clearly, a large skin factor resulting from a sand consolidation treatment or from partial completion probably cannot be reduced significantly by most stimulation treatments. Thus, it is important that the analyst recognize such situations.

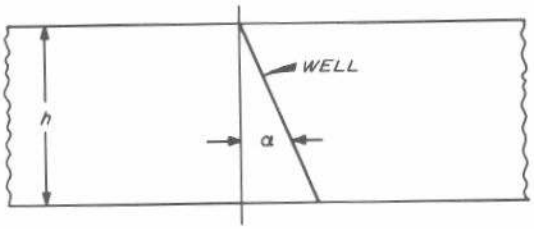

Fig. 11.17 Definition of terms for slanted wells.

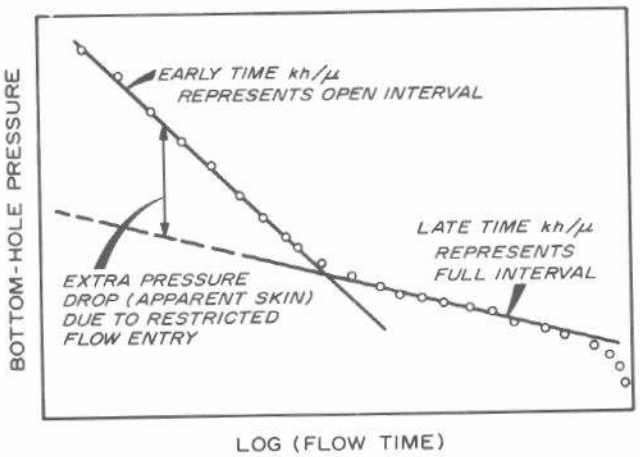

Fig. 11.16 Schematic drawdown behavior for a well with restricted flow entry.

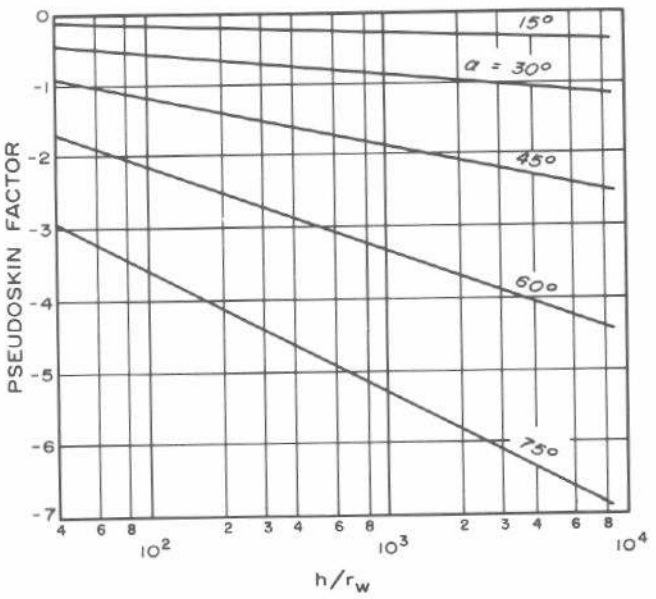

Fig. 11.18 Pseudoskin factor for slanted wells. After Cinco, Miller, and Ramey.[27]

References

1. Matthews, C. S. and Russell, D. G.: *Pressure Buildup and Flow Tests in Wells,* Monograph Series, Society of Petroleum Engineers of AIME, Dallas (1967) **1.**
2. Ramey, H. J., Jr.: "Non-Darcy Flow and Wellbore Storage Effects in Pressure Build-Up and Drawdown of Gas Wells," *J. Pet. Tech.* (Feb. 1965) 223-233; *Trans.*, AIME, **234.** Also *Reprint Series, No. 9 — Pressure Analysis Methods,* Society of Petroleum Engineers of AIME, Dallas (1967) 233-243.
3. Ramey, H. J., Jr.: "Short-Time Well Test Data Interpretation in the Presence of Skin Effect and Wellbore Storage," *J. Pet. Tech.* (Jan. 1970) 97-104; *Trans.*, AIME, **249.**
4. Agarwal, Ram G., Al-Hussainy, Rafi, and Ramey, H. J., Jr.: "An Investigation of Wellbore Storage and Skin Effect in Unsteady Liquid Flow: I. Analytical Treatment," *Soc. Pet. Eng. J.* (Sept. 1970) 279-290; *Trans.*, AIME, **249.**
5. Chen, Hsiu-Kuo and Brigham, W. E.: "Pressure Buildup for a Well With Storage and Skin in a Closed Square," paper SPE 4890 presented at the SPE-AIME 44th Annual California Regional Meeting, San Francisco, April 4-5, 1974.
6. Ramey, Henry J., Jr., and Agarwal, Ram G.: "Annulus Unloading Rates as Influenced by Wellbore Storage and Skin Effect," *Soc. Pet. Eng. J.* (Oct. 1972) 453-462; *Trans.*, AIME, **253.**
7. Earlougher, Robert C., Jr., Kersch, K. M., and Ramey, H. J., Jr.: "Wellbore Effects in Injection Well Testing," *J. Pet. Tech.* (Nov. 1973) 1244-1250.
8. Howard, G. C. and Fast, C. R.: *Hydraulic Fracturing,* Monograph Series, Society of Petroleum Engineers of AIME, Dallas (1970) **2.**
9. Russell, D. G. and Truitt, N. E.: "Transient Pressure Behavior in Vertically Fractured Reservoirs," *J. Pet. Tech.* (Oct. 1964) 1159-1170; *Trans.*, AIME, **231.** Also *Reprint Series, No. 9 — Pressure Analysis Methods,* Society of Petroleum Engineers of AIME, Dallas (1967) 149-160.
10. Clark, K. K.: "Transient Pressure Testing of Fractured Water Injection Wells," *J. Pet. Tech.* (June 1968) 639-643; *Trans.*, AIME, **243.**
11. Raghavan, R., Cady, Gilbert V., and Ramey, Henry J., Jr.: "Well-Test Analysis for Vertically Fractured Wells," *J. Pet. Tech.* (Aug. 1972) 1014-1020; *Trans.*, AIME, **253.**
12. Wattenbarger, Robert A. and Ramey, Henry J., Jr.: "Well Test Interpretation of Vertically Fractured Gas Wells," *J. Pet. Tech.* (May 1969) 625-632; *Trans.*, AIME, **246.**
13. Gringarten, Alain C., Ramey, Henry J., Jr., and Raghavan, R.: "Pressure Analysis for Fractured Wells," paper SPE 4051 presented at the SPE-AIME 47th Annual Fall Meeting, San Antonio, Tex., Oct. 8-11, 1972.
14. Gringarten, Alain C., Ramey, Henry J., Jr., and Raghavan, R.: "Unsteady-State Pressure Distributions Created by a Well With a Single Infinite-Conductivity Vertical Fracture," *Soc. Pet. Eng. J.* (Aug. 1974) 347-360.
15. Pierce, A. E., Vela, Saul, and Koonce, K. T.: "Determination of the Compass Orientation and Length of Hydraulic Fractures by Pulse Testing," *J. Pet. Tech.* (Dec. 1975) 1433-1438.
16. Hartsock, J. H. and Warren, J. E.: "The Effect of Horizontal Hydraulic Fracturing on Well Performance," *J. Pet. Tech.* (Oct. 1961) 1050-1056; *Trans.*, AIME, **222.**
17. Gringarten, Alain C.: "Unsteady-State Pressure Distributions Created by a Well With a Single Horizontal Fracture, Partial Penetration, or Restricted Flow Entry," PhD dissertation, Stanford U., Stanford, Calif. (1971) 106. (Order No. 71-23,512, University Microfilms, P.O. Box 1764, Ann Arbor, Mich. 48106.)
18. Gringarten, Alain C. and Ramey, Henry J., Jr.: "Unsteady-State Pressure Distributions Created by a Well With a Single Horizontal Fracture, Partial Penetration, or Restricted Entry," *Soc. Pet. Eng. J.* (Aug. 1974) 413-426; *Trans.*, AIME, **257.**
19. Gringarten, A. C., Ramey, H. J., Jr., and Raghavan, R.: "Applied Pressure Analysis for Fractured Wells," *J. Pet. Tech.* (July 1975) 887-892; *Trans.*, AIME, **259.**
20. Gringarten, A. C. and Witherspoon, P. A.: "A Method of Analyzing Pump Test Data from Fractured Aquifers," *Proc.*, Symposium on Percolation Through Fissured Rock, Int'l. Society for Rock Mechanics, Stuttgart (Sept. 18-19, 1972).
21. Kazemi, Hossein and Seth, Mohan S.: "Effect of Anisotropy and Stratification on Pressure Transient Analysis of Wells With Restricted Flow Entry," *J. Pet. Tech.* (May 1969) 639-647; *Trans.*, AIME, **246.**
22. Lescarboura, Jaime A.: "New Downhole Shut-in Tool Boosts BPH Test Accuracy," *World Oil* (Nov. 1974) 71-73.
23. Culham, W. E.: "Pressure Buildup Equations for Spherical Flow Regime Problems," *Soc. Pet. Eng. J.* (Dec. 1974) 545-555.
24. Odeh, A. S.: "Steady-State Flow Capacity of Wells With Limited Entry to Flow," *Soc. Pet. Eng. J.* (March 1968) 43-51; *Trans.*, AIME, **243.**
25. Brons, F. and Marting, V. E.: "The Effect of Restricted Fluid Entry on Well Productivity," *J. Pet. Tech.* (Feb. 1961) 172-174; *Trans.*, AIME, **222.** Also *Reprint Series, No. 9 — Pressure Analysis Methods,* Society of Petroleum Engineers of AIME, Dallas (1967) 101-103.
26. Jones, L. G. and Watts, J. W.: "Estimating Skin Effect in a Partially Completed Damaged Well," *J. Pet. Tech.* (Feb. 1971) 249-252; *Trans.*, AIME, **251.**
27. Cinco, H., Miller, F. G., and Ramey, H. J., Jr.: "Unsteady-State Pressure Distribution Created by a Directionally Drilled Well," *J. Pet. Tech.* (Nov. 1975) 1392-1400; *Trans.*, AIME, **259.**

Chapter 12

Application of Computers to Well Testing

12.1 Introduction

Most material in this monograph deals with analysis techniques that do not require the aid of a computer. We have avoided the necessity of using the computer by considering simple transient testing procedures and using simplified dimensionless pressures for analysis. Most transient well tests we have considered use no more than two flow rates plus, perhaps, a shut-in period. All the test analysis techniques have been based on some simple form of a combination of Eqs. 2.30 and 2.31:

$$\Delta p = \frac{141.2\,\mu}{kh} \sum_{j} \sum_{i=1}^{N} \left[(q_i B_i - q_{i-1} B_{i-1}) \right.$$

$$\left. \{ p_D([t - t_{i-1}]_D, r_D) + s \} \right], \quad \ldots\ldots\ldots\ldots (12.1)$$

where the j sum is taken over all wells and r_D refers to the distance between the point of interest and the active well. In most cases we have assumed infinite-acting behavior and have used a logarithmic approximation to the exponential-integral dimensionless pressure expression, Eq. 2.5b.

Sometimes testing situations use so many wells and rate changes that Eq. 12.1 is difficult to use by hand, even though hand calculations are possible with any form of that equation. Earlougher *et al.*[1] provide a means for simplying calculations in bounded systems; but even that technique is burdensome if the system is complex. The approach presented by Jargon and van Poollen[2] is feasible for hand calculations — for a single well with multiple rate changes. Regardless of the number of wells or rate changes involved, it is almost essential to use a digital computer when a system is so complex that tabulated dimensionless pressures do not exist. Examples of such systems are fractured reservoirs;[3,4] stratified reservoirs;[5-9] reservoirs with various kinds of discontinuities;[10-12] reservoirs containing non-Newtonian fluids;[13] and reservoirs with peculiar conditions around the wellbore.[14,15] In such cases, a computer and some sort of mathematical model of the reservoir are required just to simulate* the behavior of the system. Analyzing transient tests in such complex systems generally also requires computer assistance.[16-23] Sometimes simulations lead to empirical hand-analysis techniques; for examples, see Sections 7.5, 9.3, 10.8, and 11.3.

*As used in this monograph, a reservoir simulator is a computer program that solves fluid-flow equations to compute (simulate) reservoir behavior.

A major advantage of using the computer is that we are able to study systems for which dimensionless pressure data are not available. A second advantage is that computer simulation and analysis is fast and *computationally* error-free. That, unfortunately, does not guarantee correct results, since the mathematical model or the computer program may not be *conceptually* error-free or since the data may be incorrect or supplied to the program incorrectly. The major disadvantages in applying the computer to transient testing are that both a computer and a computer program must be available. Surmounting the first problem does not necessarily overcome the second. The engineer may have to write a new program, modify an existing one, or find someone to do that for him. Thus, using computers in well testing can create a major time bottleneck if the required computer programs are not readily available. Fortunately, most large oil companies and many consulting organizations have both computers and libraries of programs that the engineer can use.

This chapter briefly discusses computer-aided transient test analysis, computer-aided transient test design, and reservoir simulation. The material is limited to results without detailed descriptions of the calculation procedures used, since the intent is to demonstrate possibilities rather than provide computational methods. The cited references give computational details.

12.2 Computer-Aided Well Test Analysis

When using the computer for analyzing transient tests, it is important to remember that it is just a tool. The computer does not perform the analysis, even though it may print answers. The engineer is responsible for the analysis — he must ascertain that the data were correctly supplied and that the computed results are consistent with the physical situation. If the results are unreasonable, the engineer must determine the problems and decide how to correct them, whether that involves rerunning the test, reanalyzing the data, or rewriting the computer program.

In the simplest type of computer-aided transient test analysis, the computer does the bulk of the time-consuming computations, but the engineer makes all the decisions related to test analysis. For example, suppose we wish to analyze data from a multiple-rate transient test using the technique of Section 4.2. We might use a computer program to do the computationally tedious superposition calculation. Then we could plot the pressure data vs the time-superposition function, draw the appropriate straight line, and estimate formation characteristics. Jargon and van Poollen[2] describe a technique of that nature. Such a general approach may be applied to almost any testing situation.

A more sophisticated approach to computer-aided test analysis has the computer both calculate and make decisions regarding the analysis. In the automated-analysis approach, the computer prints the answer and gives some indication of how reliable the results are. The engineer must then evaluate the results and accept or reject them.

Any computer program that automatically analyzes transient test data consists of two basic parts: (1) a part to compute pressure behavior for a given set of reservoir properties (for example, superposition in time and space using an appropriate p_D), and (2) a part that judges how well the computed behavior matches observed behavior and then changes the reservoir parameters used in Part 1 until the match of computed and observed data is acceptable.

The first part of the process may be accomplished using techniques of Chapter 2, some variation of those techniques, or a reservoir simulator.[13,19,24] To accomplish the second part of the process, the program may use a regression analysis technique[19,20] or some other technique to minimize the error.[22,23] The following examples indicate the kinds of results that can be obtained from computer-aided transient test analysis.

Example 12.1 Interference Test Analysis by Computer Methods

Examples 9.1 and 9.3 present interference test data and show two analysis techniques. Example 9.1 analysis results are

$$k = 5.1 \text{ md}$$

and

$$\phi c_t = 1.01 \times 10^{-6} \text{ psi}^{-1}.$$

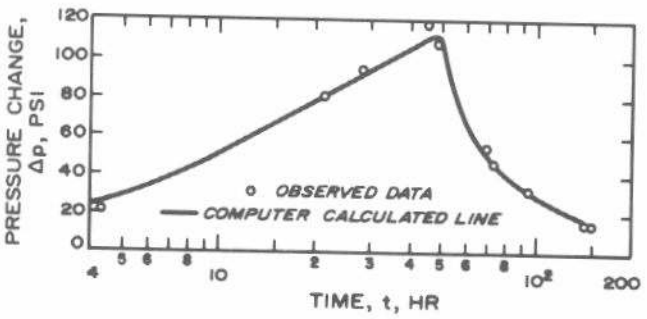

Fig. 12.1 Example 12.1, trial-and-error computer analysis of the interference test of Example 9.1.

We also have analyzed the data by three different computer-aided techniques. The first method, a trial-and-error approach, compares observed pressure response with pressure calculated by a computer program that uses Eq. 12.1 with given reservoir parameters. After several computer runs (sometimes the technique requires 12 to 15 trials), the match shown in Fig. 12.1 was obtained. The parameters used to calculate the line in that figure are

$$k = 6.0 \text{ md}$$

and

$$\phi c_t = 0.8 \times 10^{-6} \text{ psi}^{-1}.$$

The second computer-analysis method uses the regression technique described by Earlougher and Kersch.[20] Fig. 12.2 is a plot of the match obtained by that method. In that case, the computed results are

$$k = 5.7 \text{ md}$$

and

$$\phi c_t = 0.99 \times 10^{-6} \text{ psi}^{-1}.$$

A third computer-analysis technique, similar to that described by Coats, Dempsey, and Henderson,[22] was also used. Although not shown here, it gave essentially the same results as the regression technique.

All these analysis techniques give essentially the same results. If we had to choose one set of results, it would probably be best to use 5.7 md and 0.99×10^{-6} psi^{-1}. We do this because the regression technique provides less chance for an error in subjective judgment during analysis than do the other techniques. This example is a simple one that is analyzed by hand with relative ease. Many transient tests do not provide an option; they can be analyzed within reasonable time only by using computer methods.

Example 12.2 Interference Test Analysis — Heterogeneous Reservoir Case

Jahns[19] describes an interference test in a five-spot pattern with the center well being produced for several hours while the pressure decline in the four surrounding wells was ob-

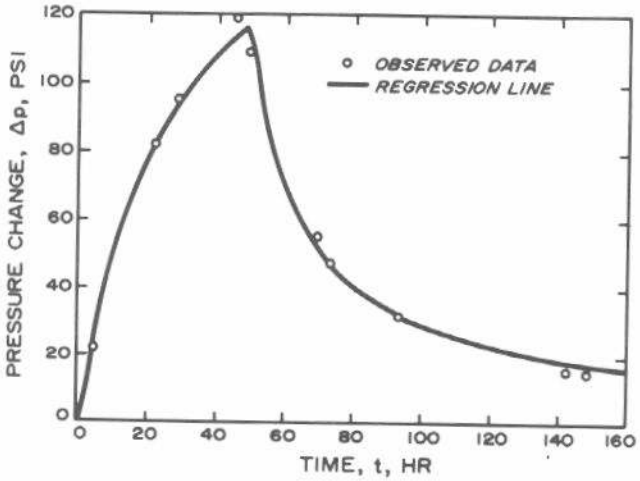

Fig. 12.2 Example 12.1, regression-type computer analysis of the interference test of Example 9.1.

TABLE 12.1—EXAMPLE 12.3: COMPUTER ANALYSIS RESULTS FOR INTERFERENCE TEST OF EXAMPLE 9.6.

Analysis Method and Data Used	Analysis Results k_{max} (md)	k_{min} (md)	$\bar{k}$ (md)	θ (degrees)	ϕc_t (psi^{-1})	Standard Deviation (psi)
Type-Curve Matching						
Three wells, injection only	20.5	13.9	16.9	64.7	1.59×10^{-6}	———
Regression						
Three wells, injection only	17.6	12.1	14.6	60.3	1.61×10^{-6}	1.11
Three wells, injection and falloff	17.2	12.7	14.8	59.3	1.61×10^{-6}	1.86
Seven wells,* injection and falloff	15.8	10.1	12.6	53.7	1.67×10^{-6}	2.07
Eight wells, injection and falloff	14.5	11.1	12.7	63.6	1.60×10^{-6}	2.69

*Omit data from well with poorest match in eight-well analysis.

served. Using a grid-type mathematical simulator and a regression-type analysis technique, Jahns analyzed the data for pattern properties. Fig. 12.3 shows how he segmented the reservoir for analysis of test data. He estimated kh and $\phi c_t h$ in each block from the pressure data at the four observation wells. Jahns gives considerable information about this test, including plots of observed and calculated response data at each observation well. Fig. 12.4 shows results at Observation Well 2. The computed response matches the observed response closely.

Example 12.3 Interference Test Analysis — Anisotropic Reservoir Case

In Example 9.6 we analyzed injection-period pressure response data from three observation wells in an anisotropic reservoir. Ramey[25] gives both injection and shut-in period data for eight observation wells for that test. We have applied the regression analysis described by Earlougher and Kersch[20] to those data in several ways. Table 12.1 summarizes the results. Fig. 12.5 shows the range of data-match results for the analysis corresponding to the next-to-last line in Table 12.1. Clearly, the results depend on the amount of data used, and may be changed by excluding portions of the available data. If a different reservoir model had been chosen (such as one composed of many heterogeneous blocks, each with its own properties, as illustrated in Example 12.2), the estimated reservoir properties might have been quite different.

As seen from Table 12.1, the degree of anisotropy in this example is small ($k_{max}/k_{min} < 2$). Thus, it is possible that reservoir properties estimated from some other type of res-

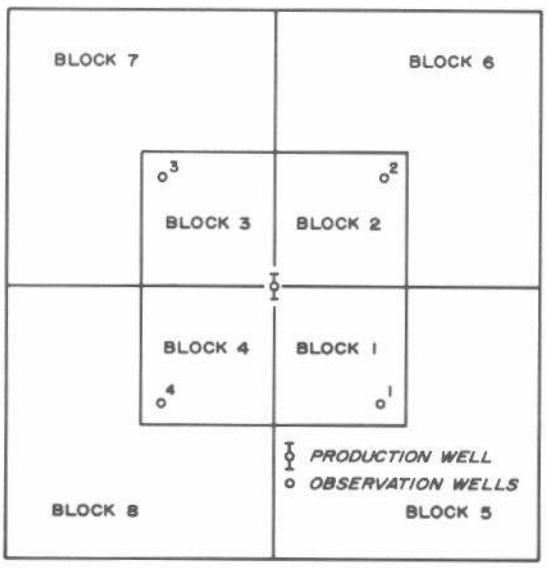

Fig. 12.3 Example 12.2, eight-region model used for a computer-aided analysis of an interference test in a heterogeneous reservoir. After Jahns.[19]

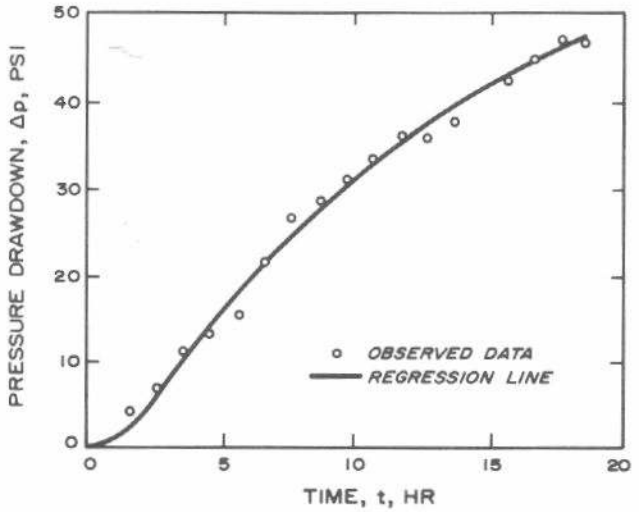

Fig. 12.4 Example 12.2, results of a computer-aided analysis of an interference test in a heterogeneous reservoir. Results for Well 2 of Fig. 12.3. After Jahns.[19]

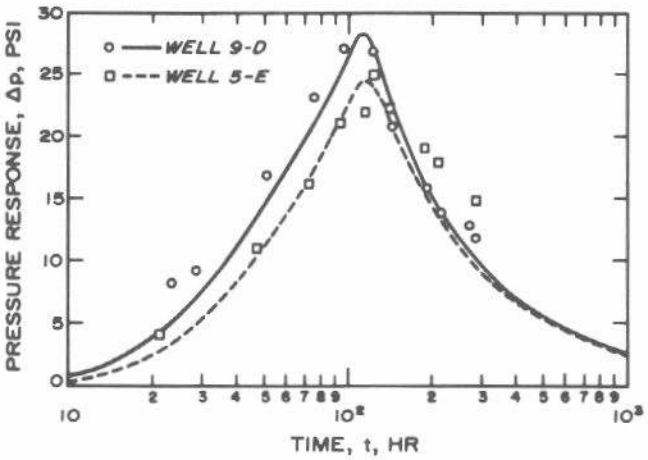

Fig. 12.5 Regression-analysis data fit for seven-well interference-test data analysis of Example 12.3 and Table 12.1.

ervoir model also might be applicable. Nevertheless, there are situations where other data available to the engineer would strongly suggest that extreme anisotropy must exist owing to natural fracturing, depositional trends, etc. Thus, it is important that data other than that of the test be considered during test analysis. In fact, for the data of this example, the sandstone is a channel deposit and directional permeability can be expected as a result of the depositional environment.

Example 12.4 Computer Analysis of Falloff Data With Significant Wellbore Storage

Earlougher and Kersch[20] present an analysis of the falloff test shown in Fig. 12.6. The S shape of the falloff curve is indicative of wellbore storage. The log-log data plot in Fig. 12.7 verifies that wellbore storage is dominant for about 5 hours.

The final straight-line part of the data in Fig. 12.6 can be analyzed using the techniques in Section 7.3 to obtain

$$k = 12.7 \text{ md}$$

and

$$s = 1.7.$$

Earlougher and Kersch used completion data to estimate an afterflow schedule. When they included that schedule in the automated regression-type analysis, the solid curve in Fig. 12.6 resulted. The best match occurred when

$$k = 13.7 \text{ md}$$

and

$$s = 1.7.$$

The data were also analyzed using the regression program, but assuming no wellbore storage. The best-match calculated response for that case is the dashed curve in Fig. 12.6. Clearly, it is not a good representation of observed data. Actually, the analysis shown by the dashed curve was the first one made. In that case, engineering judgment indicated the analysis should be repeated using more realistic conditions. Since the data (especially the log-log data plot) indicated significant wellbore storage, wellbore storage was included in the next analysis, resulting in the solid line in Fig. 12.6.

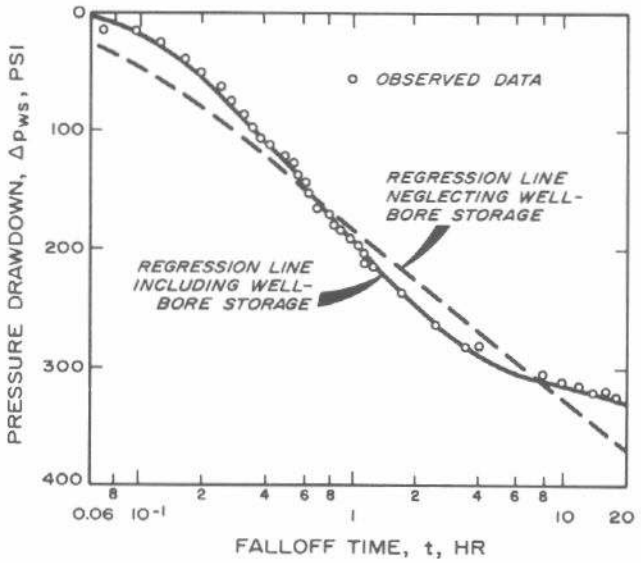

Fig. 12.6 Example 12.4, computer-aided falloff test analysis when test shows significant wellbore storage. After Earlougher and Kersch.[20]

12.3 Computer-Aided Test Design

Chapter 13 provides guidelines for designing transient well tests. One approach includes computing the expected pressure response for the well test. By making such a computation, one can evaluate the consequences of wellbore storage, the type of pressure-measuring equipment necessary, the magnitude of flow rate required, the required test time, or any combination of those factors. If the reservoir system or the flow history is complex, such calculations tend to be time-consuming or must be based on over-idealized, simplified models. Thus, it is sensible to use the computer for test design, both to save labor and to extend the scope of situations the engineer can handle. Such design calculations estimate the expected pressure responses based on assumed reservoir properties, or estimate a range of responses based on a range of possible reservoir properties. Such computations can help insure that one gathers adequate test data.

12.4 Reservoir Simulation

As indicated in Section 12.2, one of the basic chores of any computer program for analyzing transient tests is calculating pressure response caused by a specific flow-rate history. Such computations are referred to by the general term "reservoir simulation." All dimensionless pressure functions in Appendix C, when coupled with the superposition techniques of Section 2.9, result in simple reservoir simulators. However, such simple simulators do not apply to many complex situations. For example, we might be interested in extremely heterogeneous systems, layered systems, systems with two or three phases flowing, systems with fluid-fluid contacts, systems with water or gas coning,

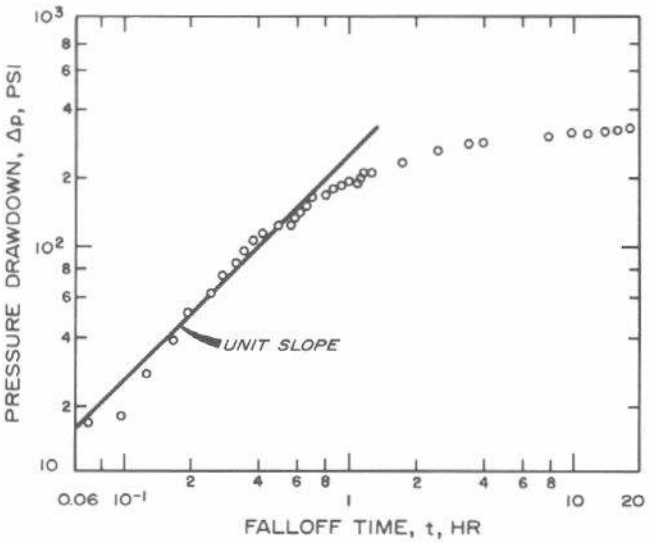

Fig. 12.7 Log-log data plot for falloff test of Example 12.4. After Earlougher and Kersch.[20]

or systems with significant gravity drainage. During the past several years, many papers appearing in the petroleum literature have discussed various kinds of reservoir simulators.[26] Three of the classic references are Aronofsky and Jenkins,[27] Bruce, Peaceman, Rachford, and Rice,[28] and West, Garvin, and Sheldon.[29] Many of the facets of reservoir simulation were summarized by van Poollen, Bixel , and Jargon[30-42] in a series of articles.

Most reservoir simulators are not written for direct application to well testing; rather, they sacrifice description of near-wellbore effects so they can predict over-all reservoir behavior using an economical amount of computer time. Reservoir simulation is used mainly for reservoir analysis — not well analysis — in the petroleum industry. However, special reservoir simulators are being used more frequently for well-testing applications; such simulators commonly include radial flow geometry and wellbore storage effects as well as other special effects.[4-23] The inherent flexibility of the well simulators enables the engineer to tackle difficult, real situations without either a high degree of mathematical skill or programming expertise. It is this flexibility that makes reservoir simulators and computer methods valuable tools in well testing.

References

1. Earlougher, Robert C., Jr., Ramey, H. J., Jr., Miller, F. G., and Mueller, T. D.: "Pressure Distributions in Rectangular Reservoirs," *J. Pet. Tech.* (Feb. 1968) 199-208; *Trans.*, AIME, **243.**
2. Jargon, J. R. and van Poollen, H. K.: "Unit Response Function From Varying-Rate Data," *J. Pet. Tech.* (Aug. 1965) 965-969; *Trans.*, AIME, **234.**
3. Russell, D. G. and Truitt, N. E.: "Transient Pressure Behavior in Vertically Fractured Reservoirs," *J. Pet. Tech.* (Oct. 1964) 1159-1170; *Trans.*, AIME, **231.** Also *Reprint Series, No. 9 — Pressure Analysis Methods,* Society of Petroleum Engineers of AIME, Dallas (1967) 149-160.
4. Kazemi, H.: "Pressure Transient Analysis of Naturally Fractured Reservoirs With Uniform Fracture Distribution," *Soc. Pet. Eng. J.* (Dec. 1969) 451-462.
5. Kazemi, Hossein and Seth, Mohan S.: "Effect of Anisotropy and Stratification on Pressure Transient Analysis of Wells With Restricted Flow Entry," *J. Pet. Tech.* (May 1969) 639-647; *Trans.*, AIME, **246.**
6. Cobb, William M., Ramey, H. J., Jr., and Miller, Frank G.: "Well-Test Analysis for Wells Producing Commingled Zones," *J. Pet. Tech.* (Jan. 1972) 27-37; *Trans.*, AIME, **253.**
7. Kazemi, Hossein: "Pressure Buildup in Reservoir Limit Testing of Stratified Systems," *J. Pet. Tech.* (April 1970) 503-511; *Trans.*, AIME, **249.**
8. Raghavan, R., Topaloglu, H. N., Cobb, W. M., and Ramey, H. J., Jr.: "Well-Test Analysis for Wells Producing From Two Commingled Zones of Unequal Thickness," *J. Pet. Tech.* (Sept. 1974) 1035-1043; *Trans.*, AIME, **257.**
9. Earlougher, Robert C., Jr., Kersch, K. M., and Kunzman, W. J.: "Some Characteristics of Pressure Buildup Behavior in Bounded Multiple-Layer Reservoirs Without Crossflow," *J. Pet. Tech.* (Oct. 1974) 1178-1186; *Trans.*, AIME, **257.**
10. Bixel, H. C., Larkin, B. K., and van Poollen, H. K.: "Effect of Linear Discontinuities on Pressure Build-Up and Drawdown Behavior," *J. Pet. Tech.* (Aug. 1963) 885-895; *Trans.*, AIME, **228.**
11. Kazemi, Hossein: "Locating a Burning Front by Pressure Transient Measurements," *J. Pet. Tech.* (Feb. 1966) 227-232; *Trans.*, AIME, **237.**
12. Bixel, H. C. and van Poollen, H. K.: "Pressure Drawdown and Buildup in the Presence of Radial Discontinuities," *Soc. Pet. Eng. J.* (Sept. 1967) 301-309; *Trans.*, AIME, **240.**
13. van Poollen, H. K. and Jargon, J. R.: "Steady-State and Unsteady-State Flow of Non-Newtonian Fluids Through Porous Media," *Soc. Pet. Eng. J.* (March 1969) 80-88; *Trans.*, AIME, **246.**
14. Kazemi, H.: "A Reservoir Simulator for Studying Productivity Variation and Transient Behavior of a Well in a Reservoir Undergoing Gas Evolution," *J. Pet. Tech.* (Nov. 1975) 1401-1412; *Trans.*, AIME, **259.**
15. Jones, L. G. and Watts, J. W.: "Estimating Skin Effect in a Partially Completed Damaged Well," *J. Pet. Tech.* (Feb. 1971) 249-252; *Trans.*, AIME, **251.**
16. Kazemi, H., Seth, M. S., and Thomas, G. W.: "The Interpretation of Interference Tests in Naturally Fractured Reservoirs With Uniform Fracture Distribution," *Soc. Pet. Eng. J.* (Dec. 1969) 463-472; *Trans.*, AIME, **246.**
17. Brill, J. P., Bourgoyne, A. T., and Dixon, T. N.: "Numerical Simulation of Drillstem Tests as an Interpretation Technique," *J. Pet. Tech.* (Nov. 1969) 1413-1420.
18. Dixon, Thomas N., Seinfeld, John H., Startzman, Richard A., and Chen, W. H.: "Reliability of Reservoir Parameters From History-Matched Drillstem Tests," paper SPE 4282 presented at the SPE-AIME Third Symposium on Numerical Simulation of Reservoir Performance, Houston, Jan. 10-12, 1973.
19. Jahns, Hans O.: "A Rapid Method for Obtaining a Two-Dimensional Reservoir Description From Well Pressure-Response Data," *Soc. Pet. Eng. J.* (Dec. 1966) 315-327; *Trans.*, AIME, **237.**
20. Earlougher, Robert C., Jr., and Kersch, Keith M.: "Field Examples of Automatic Transient Test Analysis," *J. Pet. Tech.* (Oct. 1972) 1271-1277.
21. Pierce, A. E., Vela, Saul, and Koonce, K. T.: "Determination of the Compass Orientation and Length of Hydraulic Fractures by Pulse Testing," *J. Pet. Tech.* (Dec. 1975) 1433-1438.
22. Coats, K. H., Dempsey, J. R., and Henderson, J. H.: "A New Technique for Determining Reservoir Description From Field Performance Data," *Soc. Pet. Eng. J.* (March 1970) 66-74; *Trans.*, AIME, **249.**
23. Hernandez, Victor M. and Swift, George W.: "A Method for Determining Reservoir Parameters From Early Drawdown Data," paper SPE 3982 presented at the SPE-AIME 47th Annual Fall Meeting, San Antonio, Tex., Oct. 8-11, 1972.
24. Breitenbach, E. A., Thurnau, D. H., and van Poollen, H. K.: "Solution of the Immiscible Fluid Flow Simulation Equations," *Soc. Pet. Eng. J.* (June 1969) 155-169. Also *Reprint Series, No. 11 — Numerical Simulation,* Society of Petroleum Engineers of AIME, Dallas (1973) 16-30.
25. Ramey, Henry J., Jr.: "Interference Analysis for Anisotropic Formations — A Case History," *J. Pet. Tech.* (Oct. 1975) 1290-1298; *Trans.*, AIME, **259.**
26. *Reprint Series, No. 11 — Numerical Simulation,* Society of Petroleum Engineers of AIME, Dallas (1973).

27. Aronofsky, J. A. and Jenkins, R.: "A Simplified Analysis of Unsteady Radial Gas Flow," *Trans.*, AIME (1954) **201,** 149-154. Also *Reprint Series, No. 9 — Pressure Analysis Methods*, Society of Petroleum Engineers of AIME, Dallas (1967) 197-202.

28. Bruce, G. H., Peaceman, D. W., Rachford, H. H., Jr., and Rice, J. D.: "Calculations of Unsteady-State Gas Flow Through Porous Media," *Trans.*, AIME (1953) **198,** 79-92.

29. West, W. J., Garvin, W. W., and Sheldon, J. W.: "Solution of the Equations of Unsteady-State Two-Phase Flow in Oil Reservoirs," *Trans.*, AIME (1954) **201,** 217-229.

30. van Poollen, H. K., Bixel, H. C., and Jargon, J. R.: "Reservoir Modeling — 1: What It Is, What It Does," *Oil and Gas J.* (July 28, 1969) 158-160.

31. van Poollen, H. K., Bixel, H. C., and Jargon, J. R.: "Reservoir Modeling — 2: Single-Phase Fluid-Flow Equations," *Oil and Gas J.* (Aug. 18, 1969) 94-96.

32. van Poollen, H. K., Bixel, H. C., and Jargon, J. R.: "Reservoir Modeling — 3: Finite Differences," *Oil and Gas J.* (Sept. 15, 1969) 120-121.

33. van Poollen, H. K., Bixel, H. C., and Jargon, J. R.: "Reservoir Modeling — 4: Explicit Finite-Difference Technique," *Oil and Gas J.* (Nov. 3, 1969) 81-87.

34. van Poollen, H. K., Bixel, H. C., and Jargon, J. R.: "Reservoir Modeling — 5: Implicit Finite-Difference Approximation," *Oil and Gas J.* (Jan. 5, 1970) 88-92.

35. van Poollen, H. K., Bixel, H. C., and Jargon, J. R.: "Reservoir Modeling — 6: General Form of Finite-Difference Approximations," *Oil and Gas J.* (Jan. 19, 1970) 84-86.

36. van Poollen, H. K., Bixel, H. C., and Jargon, J. R.: "Reservoir Modeling — 7: Single-Phase Reservoir Models," *Oil and Gas J.* (March 2, 1970) 77-80.

37. van Poollen, H. K., Bixel, H. C., and Jargon, J. R.: "Reservoir Modeling — 8: Single-Phase Gas Flow," *Oil and Gas J.* (March 30, 1970) 106-107.

38. van Poollen, H. K., Bixel, H. C., and Jargon, J. R.: "Reservoir Modeling — 9: Here are Fundamental Equations for Multiphase Fluid Flow," *Oil and Gas J.* (May 11, 1970) 72-78.

39. van Poollen, H. K., Bixel, H. C., and Jargon, J. R.: "Reservoir Modeling — 10: Applications of Multiphase Immiscible Fluid-Flow Simulator," *Oil and Gas J.* (June 29, 1970) 58-63.

40. van Poollen, H. K., Bixel, H. C., and Jargon, J. R.: "Reservoir Modeling — 11: Comparison of Multiphase Models," *Oil and Gas J.* (July 27, 1970) 124-130.

41. van Poollen, H. K., Bixel, H. C., and Jargon, J. R.: "Reservoir Modeling — 12: Individual Well Pressures in Reservoir Modeling," *Oil and Gas J.* (Oct. 26, 1970) 78-80.

42. van Poollen, H. K., Bixel, H. C., and Jargon, J. R.: "Reservoir Modeling — 13: (Conclusion) A Review — and A Look Ahead," *Oil and Gas J.* (March 1, 1971) 78-79.

Chapter 13

Test Design and Instrumentation

13.1 Introduction

Each transient-test analysis technique described in this monograph requires specific test data. Complete and adequate data are essential for satisfactory transient-test results. Thus, an important part of preparation for a transient well test is deciding which data are needed and how they will be obtained. This chapter discusses the design of transient tests, from the choice of test type to determining data required, and describes characteristics of suitable equipment.

The first step in designing a transient test is to choose the appropriate test for the existing situation: buildup, drawdown, multiple rate, interference, etc. When we desire specific information about a reservoir (for example, an indication of a mobility change or a boundary), test design is critical since many things can mask the response we seek, or can cause a response that is misleading because it merely resembles the behavior expected. (Sections 7.5, 10.1 through 10.7, and 11.2 through 11.4 illustrate a variety of situations that have similar test responses.) Once the test is chosen, the test duration and expected pressure response should be estimated so appropriate pressure-measuring equipment may be used. We also must decide what other data are required, determine how those data will be obtained, and consider how the testing plan will fit into the work schedules of the individuals who will perform the test. Occasionally, this part of test design indicates that a different kind of test than originally chosen should be used. If that happens, the entire design process is repeated.

Test design should minimize problems such as those caused by excessive wellbore storage, unintentional variation in rates, rate changes in nearby wells, etc. This chapter presents a broad approach to test design, emphasizing general design concepts rather than details. The design material in this chapter is limited to conventional transient testing. Pulse test design is discussed in Sections 9.3 and 10.8.

A discussion of pressure- and rate-measuring instruments indicates the kinds of instruments available, and what factors should be considered in instrument choice. We make no attempt to consider all available instruments nor to evaluate the relative merits of the instruments considered.

13.2 Choice of Test Type

When deciding what kind of transient well test to use, the foremost considerations are the type and status of the well: injection or production, active or shut-in. We may choose a single-well or a multiple-well test, depending on what we wish to learn about the reservoir.

When planning a production-well transient test, the engineer can choose between drawdown, buildup, and multiple-rate testing. He also must determine how he will make pressure measurements in artificially lifted wells. It is particularly difficult to measure down-hole pressure in rod-pumped wells unless the well is equipped with a permanent bottom-hole pressure gauge. Although it is possible to run some pressure gauges in the tubing-casing annulus, that can be risky and, generally, is not recommended. Pulling the pump and then running the pressure gauge seldom solves the problem; when the pump is pulled, the fluid in the tubing is dumped in the hole, creating an injection transient. It is possible to pull the pump, run the gauge in tubing below the pump, rerun the pump, continue production for several days, and then test. That approach requires a gauge with a long time span; it also involves considerable expense for the necessary well-service work. One common way to obtain pressure buildup data in a rod-pumped well completed without a packer is to measure the fluid level in the tubing-casing annulus with an acoustic sounder. Pressure measurement in flowing wells, in gas-lift wells, and in some wells with hydraulic or submersible electric pumps is not so difficult. But even in those situations, mechanical problems such as gas-lift valves that open suddenly during pressure-buildup surveys must be considered and avoided in test design.

The composition and rate of the fluid produced is important, since multiple-phase effects may be significant. The system may have to be treated as an oil well or as a gas well, depending on the gas-liquid ratio. As indicated in Section 2.6, phase segregation in the tubing string may create anomalies that make analysis difficult or impossible. Such anomalies should be anticipated and avoided, if possible.

Test duration may be a problem in producing wells; generally, one does not like to shut in a producing well for a long time since delayed production can be a major cost in a test. Deferred income often may be reduced by using a two-rate test.

The choice of test type is less complicated for injection

wells than for production wells — because the difficulties associated with artificial lift are not present. Normally, an injectivity test or falloff test will provide usable results. The pressure falloff is preferred, since it is easier to perform than an injectivity test and since minor rate variations have less influence on falloff-test response. It is good practice to run an injectivity test after the falloff test, since the cost is low and additional information may be obtained. Injection wells that take fluid on vacuum are difficult to test because of high wellbore storage coefficients associated with the free liquid level in the injection string. Usually, it is advisable to test such wells by increasing the injection rate enough to obtain wellhead pressure and then performing either an injectivity test at high rate or a two-rate injection test with positive wellhead pressure maintained during both rates. Changing wellbore storage (Section 11.2) tends to be more of a problem in injection wells than in production wells.

Ideally, pressures should be recorded continuously during a transient test. Best results are obtained when the bottom-hole pressure is measured, although surface pressure often can be converted to bottom-hole values if adequate information is available about the wellbore system. If possible, one should avoid changing pressure gauges during the test because of offsets that usually occur when a gauge is changed — even when the same gauge is removed and rerun with a new chart. Remember, we are often concerned with relatively subtle pressure trends in transient pressure analyses. It is often possible to avoid changing charts in a gauge and still get good short-time and long-time data by running two gauges in tandem with different-speed clocks.

It is usually beneficial to record bottom-hole, tubing-head, and casing-head pressures during a well test. That combination of data can provide information about wellbore effects — such as fluid redistribution, wellbore storage, and leaking packers or tubing — and may allow analysis of a test that could not be analyzed adequately based on bottom-hole pressure data alone. Such surface pressure data may be valuable in verifying correct operation of the down-hole pressure gauge.

Some well tests may require bottom-hole shut-in; some may even require extra packers or drillstem test equipment. Such requirements must be considered in the test design so that all important data are obtained.

13.3 Design Calculations

There are three general approaches to designing a transient well test:

1. Estimate the complete expected pressure response using assumed formation properties.
2. Estimate key factors in test response, such as the end of wellbore storage effects, the end of the semilog straight line, the semilog straight-line slope, and the general magnitude of the pressure response.
3. Just run the test without design calculations.

Option 3 is generally a poor one except in wells or reservoirs that have been tested frequently enough so their behavior is well known. Estimating the entire pressure response for a test can be a time-consuming task and may require computer assistance. (In complex situations, the subsequent analysis also may require the use of a computer.) Nevertheless, in some cases that is the only reliable way to design a test. To estimate pressure response for relatively simple systems, we use superposition and Eq. 2.2:

$$p_{wf} = p_i - 141.2\,\frac{qB\mu}{kh}\left[p_D(t_D, r_D, \ldots) + s\right], \quad \ldots\ldots\ldots\ldots\ldots\ldots\ldots (13.1)$$

For complex systems, or to reduce the labor required for test design, we normally use a computer to estimate expected pressure response. Once the pressure response has been estimated, the data may be analyzed by normal methods to determine potential analysis problems. Example 13.2 illustrates that approach.

In most transient well tests, we need not know the complete pressure response for design purposes. It is normally sufficient to estimate the beginning time of the correct semilog straight line by using Eq. 2.21,

$$t > \frac{(200{,}000 + 12{,}000\,s)\,C}{(kh/\mu)}, \quad \ldots\ldots\ldots\ldots (13.2a)$$

for pressure drawdown or injectivity, or Eq. 2.22,

$$\Delta t > \frac{170{,}000\,C\,e^{0.14s}}{(kh/\mu)}, \quad \ldots\ldots\ldots\ldots\ldots\ldots (13.2b)$$

for falloff or buildup. The wellbore storage coefficient, C, is estimated from completion details using the techniques of Section 2.6. Formation kh/μ and skin factor must be assumed to use Eq. 13.2. If $s < 0$, we recommend using $s = 0$ in Eqs. 13.2a and 13.2b to get conservative results.

The next step is to estimate the end time of the semilog straight line. For drawdown and injectivity tests, we estimate the time when the system no longer acts infinite by using Eq. 2.8:

$$t \simeq \frac{\phi\mu c_t A (t_{DA})_{eia}}{0.0002637\,k}. \quad \ldots\ldots\ldots\ldots\ldots\ldots (13.3a)$$

t_{DA} at the end of the infinite-acting period is taken from the "Use Infinite System Solution With Less Than 1% Error for t_{DA} <" column of Table C.1. The end of the semilog straight line for buildup and falloff tests may be estimated from Eq. 5.16:

$$\Delta t = \frac{\phi\mu c_t A}{0.0002637\,k}(\Delta t_{DA})_{esl}. \quad \ldots\ldots\ldots\ldots\ldots (13.3b)$$

$(\Delta t_{DA})_{esl}$ is from Fig. 5.6 or Fig. 5.7.

Finally, the slope of the semilog straight line is estimated from

$$m = \frac{\pm 162.6\,qB\mu}{kh}, \quad \ldots\ldots\ldots\ldots\ldots\ldots\ldots (13.4)$$

where the sign used depends on the test type. It may be necessary to consider the general pressure-level decline in developed reservoirs when computing m. See Sections 3.4, 4.5, and 5.3 to determine how that would be done.

Once the slope is estimated, the pressure change expected between two times on the semilog straight line, t_1 and t_2, can be estimated from

$$\Delta p = \pm m \log(t_2/t_1). \quad \ldots\ldots\ldots\ldots\ldots\ldots\ldots (13.5)$$

Again, the sign chosen depends on test type. The pressure instrument chosen must be sensitive enough to detect the expected pressure change during the test period. The normal skin equation for the test used may be used to estimate p_{1hr} (after assuming an s value and a value for bottom-hole pressure at the start of the test); thus, we may estimate the pressure at any time on the semilog straight line by appropriate application of Eq. 13.5. The range of the pressure instrument used must be chosen so that the pressure can be measured with acceptable accuracy but without exceeding the instrument upper pressure limit.

Test design also may be important in reservoir limit testing — if it is possible to estimate reservoir parameters well enough to make the design calculations. When that can be done, the time to the start of the straight line on a plot of pressure vs time (arithmetic or linear coordinates) is estimated from

$$t_{pss} \simeq \frac{\phi\mu c_t A}{0.0002637\,k}\,(t_{DA})_{pss}\,, \quad \ldots\ldots\ldots\ldots\ldots\ldots\ldots (13.6)$$

where $(t_{DA})_{pss}$ is taken from the "Exact for $t_{DA}>$" column of Table C.1. By using Eq. 13.6, even when estimates of reservoir parameters are incorrect by a factor of 2 to 3, it is possible to get a reasonable idea of the time to the beginning of analyzable data for a reservoir limit test. In many cases, that time may be impractically long, indicating the inadvisability of attempting to run the test. The slope of the straight-line portion of the Cartesian pressure-time plot is estimated from Eq. 3.33:

$$m^* = -\frac{0.23395\,qB}{\phi c_t h A}\,. \quad \ldots\ldots\ldots\ldots\ldots\ldots\ldots\ldots (13.7)$$

The slope estimate may be used to indicate the sensitivity required of the pressure gauge and to get an idea of how long the test need be run after the straight-line portion starts. Pressure levels generally will be below the initial pressure, so it usually suffices to choose a gauge with a maximum range equivalent to initial reservoir pressure. If there has been a substantial pressure decline, then a lower-range gauge would be sufficient; but reservoir limit testing is not necessarily applicable to wells that have experienced much pressure decline, unless they have been shut in long enough to stabilize at average reservoir pressure.

When designing an interference test, it is best to estimate the pressure response at the observation well as a function of time. That may be done by using Eq. 13.1 with p_D taken from Fig. C.2 (Eq. 2.5a) or Fig. C.12. Such design is particularly important because observation-well response may be small and may occur only after a long time. For a reservoir with several noncommunicating layers, the most rapid response generally will be associated with the most permeable layer. This time of response can be much shorter than the time corresponding to the average permeability. In such cases, we recommend that interference-test design and analysis be backed up with a reservoir simulator, since little has been published about pressure behavior away from the active well in such layered systems.

Pulse-test design is discussed in Sections 9.3 and 10.8.

Example 13.1 Pressure-Buildup Test Design

We wish to run a pressure buildup test in a well in an undersaturated reservoir developed on 40-acre spacing. The field is suspected to be operating at pseudosteady-state conditions; that suspicion is confirmed later in the example. The well is currently producing 132 BOPD and 23 BWPD at a bottom-hole pressure of about 2,450 psi. Known data from production operations, laboratory tests, and log analyses are

$q_o = 132$ BOPD
$q_w = 23$ BWPD
$\mu_o = 2.30$ cp
$\mu_w = 0.940$ cp
$c_o = 14.6 \times 10^{-6}$ psi^{-1}
$c_w = 3.20 \times 10^{-6}$ psi^{-1}
$c_f = 3.40 \times 10^{-6}$ psi^{-1}
$B_o = 1.21$ RB/STB
$B_w = 1.00$ RB/STB
$A = 40$ acres $= 1{,}742{,}400$ sq ft
$h = 63$ ft
$\phi = 16.3$ percent
$r_w = 0.26$ ft
depth $= 3{,}600$ ft
tubing $= 2\frac{3}{8}$ in. OD
$V_u = 0.00387$ bbl/ft.

Estimated data are

$p_{wf} = 2{,}450$ psi
$k = 135$ md
$s = 2$.

Based on observed flow rates, known fluid properties, and relative permeability data, we estimate

$S_w = 0.29$
$S_o = 0.71$
$k_{rw} = 0.02$
$k_{ro} = 0.2$.

Thus, composite properties may be estimated. Using Eq. 2.38,

$$\begin{aligned} c_t &= (0.71)(14.6 \times 10^{-6}) \\ &\quad + (0.29)(3.20 \times 10^{-6}) + 3.40 \times 10^{-6} \\ &= 14.7 \times 10^{-6}\ \text{psi}^{-1} \end{aligned}$$

for the reservoir.

To estimate c_t for the wellbore, we weight the compressibilities by the relative volume of wellbore fluids,

$$\begin{aligned} q_t B_t &= (132)(1.21) + (23)(1.00) \\ &= 182.7, \end{aligned}$$

so

$$\begin{aligned} c_{twb} &= c_o \frac{q_o B_o}{q_t B_t} + c_w \frac{q_w B_w}{q_t B_t} \\ &= \frac{(14.6 \times 10^{-6})(132)(1.21) + (3.2 \times 10^{-6})(23)(1.00)}{182.7} \\ &= 13.2 \times 10^{-6}\ \text{psi}^{-1} \end{aligned}$$

for the wellbore.

We also must estimate total mobility of the fluids flowing

in the formation using Eq. 2.37:

$$\left(\frac{k}{\mu}\right)_t = k\left(\frac{0.2}{2.3} + \frac{0.02}{0.94}\right)$$
$$= 0.11\,k.$$

The semilog straight line will be bounded on the low-time end by wellbore storage effects and on the upper end as indicated by Eq. 13.3b. To estimate the start of the semilog straight line, we determine the wellbore storage coefficient for the liquid-filled wellbore. We use the compressibility estimated above for the wellbore and the total mobility based on an estimated permeability of 135 md. Then we use Eq. 13.2b for pressure buildup with an estimated $s = 2.0$. First we compute the wellbore storage coefficient from Eq. 2.17:

$$C = (0.00387)(3{,}600)(13.2 \times 10^{-6})$$
$$= 1.84 \times 10^{-4}\ \text{bbl/psi}.$$

Then we apply Eq. 13.2b:

$$\Delta t > \frac{(170{,}000)(1.84 \times 10^{-4})\, e^{(0.14)(2)}}{(0.11)(135)(63)}$$
$$> 0.044\ \text{hour} = 2.6\ \text{minutes}.$$

This indicates that wellbore storage should not be a problem.

We may now check the assertion that the well was producing at pseudosteady state. For a square system with a well in the center, $(t_{DA})_{pss} = 0.1$. Using Eq. 2.24,

$$t_{pss} = \frac{(0.163)(14.7 \times 10^{-6})(1{,}742{,}400)(0.1)}{(0.0002637)(0.11)(135)}$$
$$= 107\ \text{hours}$$
$$\simeq 4.5\ \text{days}.$$

Since the well has been operating for many weeks, it can be treated like it is operating at pseudosteady state.

To estimate the end of the semilog straight line, we use Eq. 13.3b and the appropriate figure from Chapter 5. Since the reservoir is producing at pseudosteady state, we assume that the pattern is a closed square with the well in the center. We use $t_{pDA} \simeq 0.1$ (see Sections 5.2, 6.3, and Table C.1) and Curve 1 of Figs. 5.6 and 5.7. From Fig. 5.6 $(\Delta t_{DA})_{esl} \simeq 0.013$ for a Horner plot, and from Fig. 5.7 $(\Delta t_{DA})_{esl} \simeq 0.0038$ for a Miller-Dyes-Hutchinson plot. Then, applying Eq. 13.3b,

$$\Delta t = \frac{(0.163)(14.7 \times 10^{-6})(1{,}742{,}400)}{(0.0002637)(0.11)(135)}\,(\Delta t_{DA})_{esl}$$
$$= 1{,}070\,(\Delta t_{DA})_{esl}.$$

The semilog straight line should end at about

$$\Delta t = (1{,}070)(0.013) = 14\ \text{hours}$$

for the Horner plot, and

$$\Delta t = (1{,}070)(0.0038) = 4.1\ \text{hours}$$

for the Miller-Dyes-Hutchinson graph. These times are probably conservative since the other wells will not be shut in, and thus, the shut-in well will not really be at the center of a closed 40-acre square. Nevertheless, the Horner plot should have a longer semilog straight line.

We estimate the slope of the semilog straight line from Eq. 13.4:

$$m = \frac{(162.6)\left[(132)(1.21) + (23)(1.00)\right]}{(0.11)(135)(63)}$$
$$= 31.8\ \text{psi/cycle}.$$

The relatively small m value indicates a slowly increasing pressure so we need a sensitive pressure gauge. We might consider stabilizing the well at a higher production rate before the buildup test to create a larger pressure response.

We may estimate the pressure level expected during the buildup test. A simple way to do that is to solve the skin-factor equation, Eq. 5.7, for $p_{1\text{hr}}$. We may then use $p_{1\text{hr}}$ and m to estimate the pressure at later times. Rearranging Eq. 5.7,

$$p_{1\text{hr}} = p_{wf}(\Delta t = 0) + m\left[\log\left(\frac{k}{\phi\mu c_t r_w^{\,2}}\right) - 3.2275 + 0.86859\,s\right]$$
$$= 2{,}450 + 31.8\left[\log\left(\frac{(0.11)(135)}{(0.163)(14.7 \times 10^{-6})(0.26)^2}\right) - 3.2275 + 0.86859\,s\right]$$
$$= 2{,}600 + 27.6\,s.$$

Then the pressure at any time on the semilog straight line can be estimated using Eq. 13.5:

$$p(\Delta t) \simeq 2{,}600 + 27.6\,s + 31.8 \log \Delta t.$$

If we expect $s = 2$ and a 24-hour test, $p \simeq 2{,}700$ psi. The pressure gauge we choose probably should be in the 3,300-psi range and still be capable of detecting a 30-psi change over a period of several hours.

The average pressure to be expected likewise can be estimated by the Dietz method, using $C_A = 30.88$ for the square drainage area. The time when the semilog straight line should reach $\bar{p}$ is given by Eq. 6.7a:

$$(\Delta t)_{\bar{p}} = \frac{(0.163)(14.7 \times 10^{-6})(1{,}742{,}400)}{(0.0002637)(0.11)(135)(30.88)}$$
$$= 34.5\ \text{hours}.$$

Using the equation above,

$$\bar{p} \simeq 2{,}600 + 27.6(2) + 31.8 \log(34.5)$$
$$\simeq 2{,}704\ \text{psi}.$$

Since the reservoir pressure is declining, we may have to

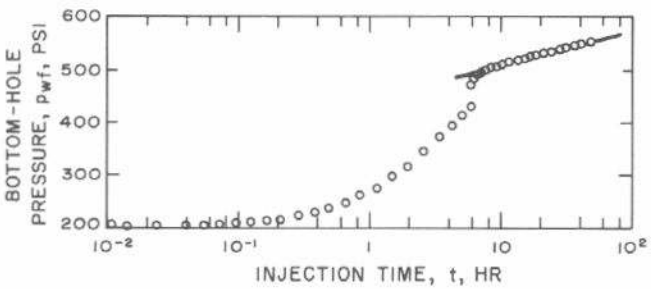

Fig. 13.1 Calculated injectivity pressure response for Example 13.2

consider that decline in the analysis, as indicated in Section 5.3. Nevertheless, the information estimated in this example indicates correct times; the pressure changes are in addition to the established trend at the well before testing. It would be worthwhile to try to measure that trend before doing the test, so it could be included in the analysis if necessary.

The pressure decline before shut-in may be estimated from Eq. 13.7:

$$m^* = \frac{dp}{dt}$$

$$= -\frac{(0.23395)\left[(132)(1.21) + (23)(1.0)\right]}{(0.163)(14.7 \times 10^{-6})(63)(1{,}742{,}400)}$$

$$= -0.16 \text{ psi/hr}.$$

Example 13.2 Injection-Well Test Design

An injection-well transient testing program was proposed for several input wells in a waterflooded reservoir before starting fluid injection for a tertiary recovery project. The reservoir was liquid-filled with water flowing at residual oil saturation. Reservoir pressure was low with the static liquid level standing about 600 ft below the surface. Because of the importance of the tests, and since changing wellbore storage could be expected as a result of the low liquid level, we decided to compute the expected pressure response by using a reservoir simulator.

We supplied estimated reservoir properties and computed the injectivity-test response shown in Fig. 13.1. As expected, the liquid level rose in the well during injection until it reached the surface about 5.9 hours after starting injection. The rapid increase in pressure in Fig. 13.1 is a result of the wellbore storage coefficient decreasing abruptly from a value corresponding to a rising liquid level to one for compression only. Note the similarity of the response in Fig. 13.1 to Figs. 11.5 and 11.6. We analyzed the apparent semilog straight line starting at about 10 hours to estimate a permeability about 15 percent lower than the input value and a skin factor that is *low* by 1.1. The discrepancy is due to choosing a semilog straight line with too steep a slope — apparently a result of the rapid wellbore storage decrease. The fact that the analysis of simulated data does not return the values supplied to the simulator indicates that the assumptions used in the analysis technique are not completely correct (assuming the simulator is working correctly). This says that if we wish to analyze data by standard techniques, we should seek a type of test for which conditions more closely approach the ideality of the analysis equations. Alternatively, we could use a more sophisticated analysis, perhaps one based on a reservoir simulator. Practically speaking, that is not often required.

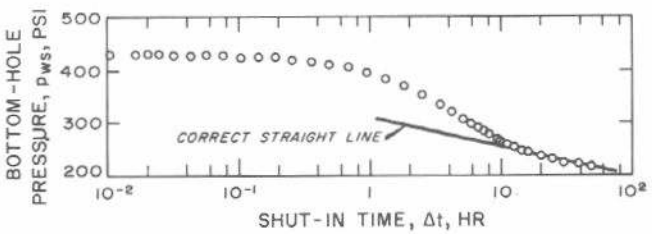

Fig. 13.2 Calculated falloff pressure response for Example 13.2.

Fig. 13.2 shows a simulated pressure falloff test following 48 hours of injection. The well goes on vacuum about 40 seconds after shut-in, so wellbore storage *increases* from compression to falling liquid level. To analyze data from a 24-hour falloff, it would be necessary to draw the straight line through the last five data points shown — a risky approach at best. We conclude the falloff test is essentially worthless. Although a computer program similar to the one used to generate the data could be used with regression analysis to analyze such falloff data, such an approach is not often practical. Even when that is done, the margin for error is significant because the analyst must make some assumptions about the wellbore storage characteristics (constant, step increase, gradual increase because of a gas cushion in the well, etc.). Thus, we prefer to find a type of test that is relatively insensitive to wellbore storage effects.

We also simulated a two-rate injection test, with the injection rate increasing by 73 percent after 48 hours. The second rate continues for 24 hours. Since the wellbore storage was from liquid compression only (wellhead pressure is positive), wellbore storage had little effect on the pressure response to the rate increase. Fig. 13.3 shows the data plotted as suggested by Eq. 4.6. The straight line can be analyzed to give k within 3 percent of the input value and a skin factor within 0.2 of the input value.

As a result of the design work shown in Figs. 13.1 through 13.3, the wells were tested with a two-rate injection followed by a falloff. The injection-pressure data were analyzed successfully; standard analysis was not possible for the falloff data; no attempt was made to use computer analysis.

13.4 Test Data and Operation Requirements

An important part of test planning and execution is complete data acquisition and safe and correct test operation. The important parts of test operation include good and complete rate stabilization (or rate control during tests requiring the well to be active), placement of the pressure instrument before the test begins, and careful documentation of what happens during the test, both at the test well and at nearby operating wells.

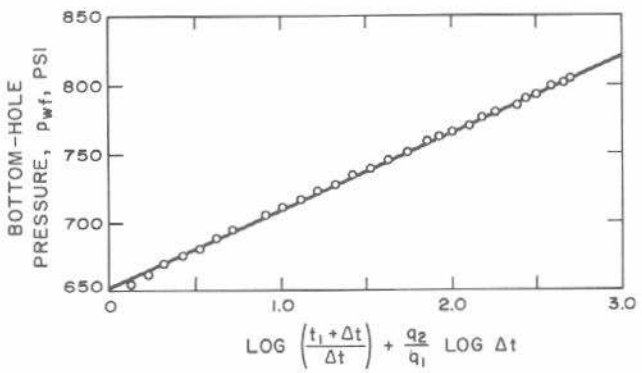

Fig. 13.3 Calculated two-rate test pressure behavior for Example 13.2.

The following general data check list is an aid to complete data acquisition. Depending on the testing situation and the information desired, it may require modification. When testing in wells or reservoirs that have been thoroughly tested before, much of the data may not be necessary based on past experience.

1. Well-Completion Data

Pipe in the Hole and Packers — Size and location of casing and tubing, location of any packers, and an indication of what pipe strings they separate should be recorded. A sketch of the well completion should accompany test data. Such information is important for running the gauge and determining the effects of wellbore storage. It also should assure that the gauge can be run to the depth where pressure is to be measured.

Type of Completion in the Producing Interval — Data should include information about whether the well is open hole, cased, perforated, uses a liner or a gravel pack, type of completion fluid, etc. If there is a dual completion, give details. Data should include location and number of perforations and indication of partial penetration, if applicable.

Stimulation — Has the well been stimulated by shooting, acidizing, fracturing, etc?

2. Pattern Data

Well Pattern — Data should include pattern size and shape, and information about location of other wells. Usually a map suffices.

Rate Information at Other Wells — When testing developed patterns, it may be important to know how the rates behave at other wells before and during the test. We must know of any major rate changes during the test since these may influence the test response considerably.

3. Rate Data

Stabilized Rate Before Testing — It is best to have spot checks on the rate for several days before testing so any problems can be isolated. Severe fluctuations may dictate postponing the test or changing the analysis technique. It is especially important to know when an active well might have been shut in before testing, if only for a few minutes.

Detailed Test-Rate Data — For producing, injecting, multiple-rate, and multiple-well tests, it is advantageous to have a detailed description of the rate behavior during testing. Ideally, one should use a recording flowmeter; if that is not possible, rate checks should be made frequently.

Fluid Type — It is important to know rates and properties of all fluids flowing at the well. It is advantageous to know the composite density and compressibility of the fluids for wellbore storage considerations and for correcting pressure measurements to some other datum. A separate pressure survey consisting of short stops at several depths in the wellbore will provide information relative to the density and distribution of fluids in the well.

4. Pressure Data

Bottom-Hole Measurements — Continuously recorded bottom-hole measurements are usually essential to good well test analysis. However, care in obtaining pressure data and additional data is also important, as stated below.

Trends Before Testing — We should know the pressure trend before testing since it may affect the analysis technique. Generally, such information is not important in undeveloped reservoirs or in fluid-injection projects with injection and production approximately balanced.

Short-Time Data — It is advisable to take pressure data at short intervals while wellbore storage is important. That allows isolation of the storage-affected part of the response data and aids in correct analysis. Design calculations give some indication of how rapidly such data are required. In the absence of other information, we recommend taking data as frequently as every 15 seconds for the first few minutes of the test. Data should be taken at least every 15 minutes until wellbore storage effects have essentially ended.

Pressure Just Before Testing — Record the pressure observed just before the test is started. Skin-factor calculations and log-log plots depend on this information.

Wellhead Pressures — In wells that have not been tested before and whose characteristic response is not well known, it is good practice to periodically record surface tubing *and* casing pressures. Such data are usually recorded manually at intervals of 1 to 4 hours from pressure gauges on the wellhead. It is sometimes particularly useful to have such data at short test times, so that unusual wellbore effects may be more thoroughly understood. Usually by comparing surface pressures with bottom-hole pressures, it is possible to estimate how much fluid is accumulating in or leaving the wellbore.

5. Other Data

Surface Piping — A diagram of wellhead and surface piping should accompany test data. That information often helps explain anomalous test behavior.

Chronology — A complete list of how things happen during the test is frequently the only key to unraveling unusual test response. Thus, the engineer should keep a log of times at which various events occur.

13.5 Pressure-Measurement Instruments

Accurate pressure data are an essential part of transient well testing. For best results, pressure should be measured near the sand-face. If that is impossible, useful data usually may be obtained by correcting wellhead-pressure or fluid-level measurements to bottom-hole conditions.[1]

Three basic types of bottom-hole pressure gauges are available:[2] self-contained wireline gauges; permanently installed surface-recording gauges; and retrievable surface-recording gauges.

Self-Contained Wireline Gauges

The self-contained wireline gauge, the gauge most often used in the petroleum industry, is lowered into a well on a solid wire (slick-line). The gauge has three essential components: (1) a pressure-sensing device, usually a Bourdon tube; (2) a pressure-time recorder; and (3) a clock. The clock is designed to run for a specific length of time; if data are

desired after that time, the gauge must be retrieved from the well, prepared for another period of recording, and rerun into the well.

Section 1 of Table 13.1 summarizes characteristics of several self-contained wireline gauges. The table also presents data for surface-recording gauges. Information in Table 13.1 is meant to be illustrative, not all-encompassing. Data shown are included because they are readily available and because the gauges are generally well known. Other gauges are available; we do not intend to imply that they are less useful than those in Table 13.1.

The Amerada RPG-3 is probably the most commonly used self-contained wireline gauge. It is typical of many such gauges. Fig. 13.4 schematically shows the important parts of the Amerada RPG-3 gauge. The clock, at the top of the instrument, is connected to a recording section that houses a metal chart covered with a black coating. The clock moves the chart vertically down across a stylus as time passes. The stylus is connected to a shaft that is twisted as the Bourdon tube coils and uncoils in response to pressure changes. Thus, pressure is recorded as a function of time by the stylus, which scratches a very fine line on the black coating of the metal chart. When the chart is removed from the instrument and is laid flat, the time scale is 5 in. long (for the RPG-3) and the pressure scale is 2 in. long. Because the size of the recording surface is fixed, most gauge manufacturers offer pressure-sensing elements (Bourdon tubes) in a variety of ranges; the lowest may be 0 to 500 or 1,000 psi; the highest ranges are 0 to the value given in Table 13.1. Similarly, a series of clocks is available.

In the Amerada RPG-3 gauge shown in Fig. 13.4, the pressure element is a helically wound Bourdon tube. The tube is anchored at the bottom and is free to rotate at the top. Fluid enters the lower end of the gauge and transmits pressure to the Bourdon tube, causing the tube to uncoil and rotate at the free end. The Bourdon tube is filled with oil by the manufacturer. The oil in the tube is generally protected from the fluid in the well by a bellows or filter arrangement.

Most self-contained gauges have provisions for recording bottom-hole temperature with a maximum recording thermometer, as indicated in Fig. 13.4. Temperature measurement is important, since the gauge calibration is somewhat temperature-dependent. Most gauges are temperature-compensated to about 175 to 200 °F; they must be specially calibrated at higher temperatures.

Self-contained (Amerada-type) gauges have a stated accuracy (ability to correctly indicate the pressure) of about ±0.25 percent of full scale. A 2,000-psi gauge with accuracy of ±0.25 percent can be considered to be correct within ±5 psi when properly calibrated and when operated at temperatures within the calibration range. The sensitivity of Bourdon-tube gauges to detect small pressure changes is much greater than the absolute accuracy of the gauge. For most gauges, the sensitivity is in the range of ±0.05 percent of the full-scale reading, or 1 psi for a 2,000-psi pressure element.

Fig. 13.5 shows the Leutert Precision Subsurface Pressure Recorder, which has a stated accuracy of ±0.025 percent of full scale and a precision of ±0.005 percent of full

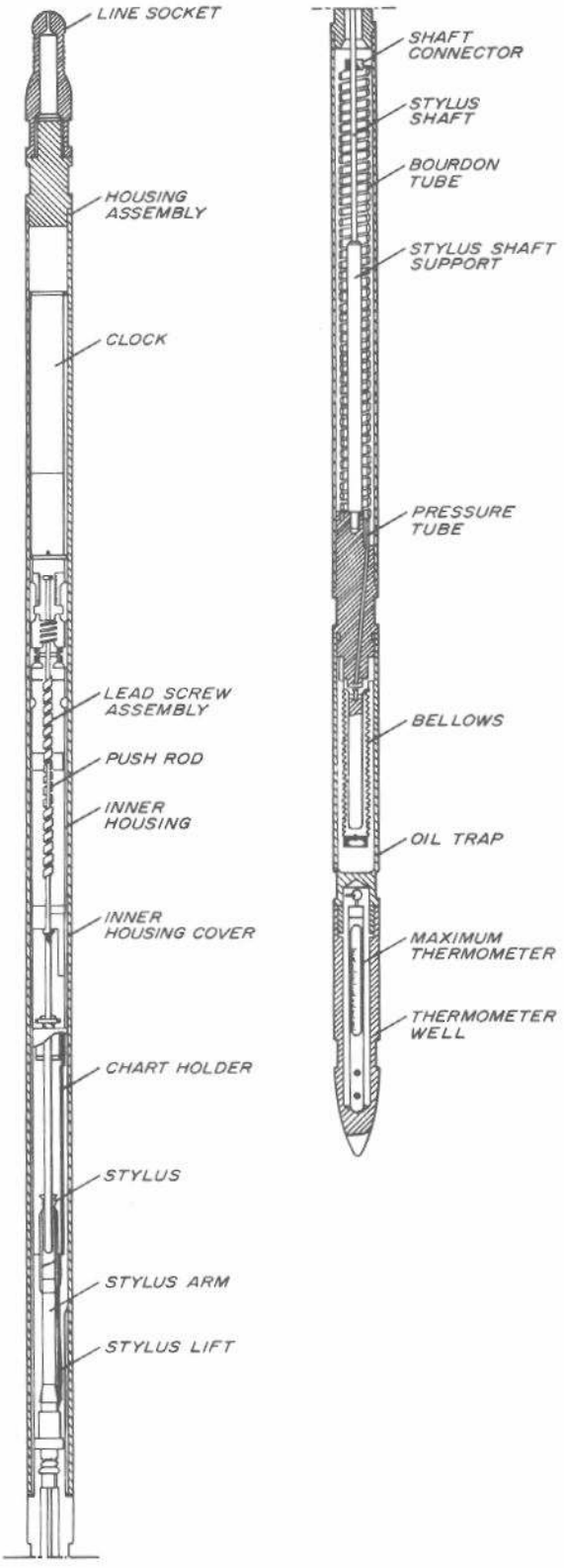

Fig. 13.4 Amerada RPG-3 gauge. Courtesy Geophysical Research Corp.

TABLE 13.1—DOWN-HOLE PRESSURE GAUGES.*

Section 1: Self-Contained Wireline Gauges

Gauge	Maximum Pressure[1] (psi)	Sensitivity, Percent of Full Scale	Accuracy, Percent of Full Scale	OD (in.)	Approximate Length[2] (in.)	Maximum Service Temperature[3] (°F)	Type Pressure Element[4]	Maximum Time Down Hole[5] (hours)	Approximate Chart Size, $p \times t$ (in.)
Amerada RPG-3	25,000	0.05	0.2	1.25	77	650	B	360	2 × 5
Amerada RPG-4	25,000	0.056	0.2	1	76	650	B	144	1.8 × 5
Amerada RPG-5	20,000	0.05	0.25	1.5	20	450	B	120	2 × 5
Kuster KPG	25,000	0.05	0.2	1.25	66	700	B	360	2 × 5
Kuster K-2	20,000	0.05	0.25	1	41	500	B	120	2 × 3
Kuster K-3	20,000	0.042	0.25	1.25	43	500	B	120	2.4 × 4
Kuster K-4	12,000	0.067	0.25	0.75	42	450	B	72	1.5 × 2.5
Leutert Precision Subsurface Pressure Recorder	6,400	0.005	0.025	1.25	139	300	P	360	9.8 × 3.1
Leutert Precision Subsurface Pressure Recorder	10,000	0.005	0.025	1.42	139	300	P	360	9.8 × 3.1
Sperry-Sun Precision Subsurface Gauge	16,000	0.005	0.05	1.5	108	300	B	672[6]	2.3 × 7.1

Section 2. Permanently Installed, Surface-Recording Gauges

Gauge	Maximum Pressure[1] (psi)	Sensitivity, Percent of Full Scale	Accuracy, Percent of Full Scale	OD (in.)	Approximate Length[2] (in.)	Maximum Service Temperature[3] (°F)	Type Pressure Element[4]	Type Signal[7]	Type Conductor[8]
Amerada EPG-512[9]	10,000	0.002	0.02	1.25	13	300	D	F	S
Amerada SPG-3	25,000	0.04	0.2	1.25	49	350	B	R	S
Flopetrol	10,000	0.001	0.06	1.42	29	257	S	F	S
Lynes Pressure Sentry MK-9PES	10,000	0.2	0.2	1.5	33	300	B	B	S
Maihak SG-2	5,700	0.1	1.0	3.54	11.54	176	D	F	S
Maihak SG-5	5,700	0.1	1.0	1.65	8.43	176	D	F	S
Sperry-Sun Permagauge	10,000	0.005	0.05	1.66	120 or 240	no max.	G	G	T
BJ Centrilift-PHD System[10]	3,500		3[11]	N/A[12]	N/A[12]		B	C	P

Section 3. Retrievable Surface-Recording Gauges

Gauge	Maximum Pressure[1] (psi)	Sensitivity, Percent of Full Scale	Accuracy, Percent of Full Scale	OD (in.)	Approximate Length[2] (in.)	Maximum Service Temperature[3] (°F)	Type Pressure Element[4]	Type Signal[7]	Type Conductor[8]
Amerada EPG-512[9]	10,000	0.002	0.02	1.25	13	300	D	F	S
Amerada SPG-3	25,000	0.04	0.2	1.25	49	350	B	R	S
Flopetrol[13]	10,000	0.001	0.06	1.42	29	257	S	F	S
Hewlett Packard HP-2811B	12,000	0.00009[14]	0.025[15]	1.44	39	302	Q	F	S
Kuster PSR	5,000	0.04	0.02	1.38	36	212	Q	F	S
Lynes Sentry MK-9PES	10,000	0.2	0.2	1.5	33	300	B	B	S
Maihak SG-3	5,700	0.1	1.0			176	D	F	S
Sperry-Sun Surface Recording	15,000	0.006	0.05	1.5	72	300	B	D	S

*Other gauges are available — no endorsement is implied by inclusion in this table. Data are from information supplied by the manufacturer and other sources believed to be reliable. Although we have been careful in assembling this table, neither the author nor SPE-AIME can guarantee accuracy of the data supplied. The reader should contact the manufacturer for specifics. Blank values could not be obtained by the author.

1. Normally, elements are available in several ranges, with the lowest being about 0 to 500 or 0 to 1,000 psi.
2. Length may vary depending on tool configuration; value is approximate normal length without weight sections.
3. Normally, temperature above which gauge cannot be used, not maximum temperature for normal calibration.
4. B — Bourdon tube.
   D — Diaphragm.
   G — Gas chamber with transducer at surface.
   P — Rotating piston.
   Q — Oscillating quartz crystal.
   S — Strain gauge.
5. Time depends on clock chosen. Clocks normally come in several ranges, starting as low as about 3 hours.
6. Clock is electronic without mechanical linkage to recorder.
7. B — Binary signal.
   C — Current.
   D — Digital.
   F — Frequency.
   G — Gas column to surface.
   R — Resistance.
8. P — Normal power cable for pump, no special conductor.
   S — Single-conductor armored cable, ground return.
   T — 3/32-in.-OD steel tubing.
9. Also measures temperature to an accuracy of 0.1 °F and a sensitivity of 0.01 °F.
10. Part of the BJ Centrilift submersible pump. Gauge is an integral part of the motor assembly.
11. Approximately 3 percent of reading.
12. Imbedded in pump motor assembly.
13. Flopetrol has under development a slick-line retrievable surface-recording gauge. The gauge is set in a side pocket mandrel; a conductor cable goes from the mandrel to the surface on the outside of the tubing.
14. Sensitivity is constant across the entire pressure range: 0.01 psi with nominal 1-second count time, 0.001 psi with nominal 10-second count time.
15. Accuracy, if temperature is known within 1° C: ±0.5 psi to 2,000 psi, ±0.025 percent of *reading* above 2,000 psi.

scale. Wellbore pressure causes a piston to operate against the tension of a helical spring. Piston extension, recorded on a metal chart by a stylus, is converted to pressure with calibration tables. The high accuracy of this gauge is obtained by rotating the measuring piston continuously to minimize frictional resistance in the instrument. Piston rotation is provided by a specially designed clock that simultaneously provides time displacement of the stylus on the chart.

The Sperry-Sun Well Survey Co. manufactures a high-precision wireline pressure gauge that is especially useful for long-time transient tests. Stated accuracy is ±0.05 percent of full scale and precision is ±0.005 percent of full scale. The gauge uses a Bourdon tube, but there is no physical connection between the Bourdon tube and the recording section, which is controlled by a battery-powered electronic programmer. Pressure recordings are made on a programmed time schedule rather than continuously. The programmer minimum is one recording every 15 seconds (giving a chart life of 5 hours) and the maximum is a recording every 32 minutes (for a chart life of 28 days).

Since pressure and time data are recorded as a finely scribed line on a metal chart in self-contained wireline gauges, a precision chart reader is needed to read the gauge charts. Chart readers should be capable of measurements at least five times as accurate as the accuracy of the pressure element. In most cases, that requires a reading accuracy of at least 0.001 in. in the pressure direction; slightly less accuracy is usually acceptable in the time direction. Although most manufacturers provide time scales for use with their chart scanners, our experience indicates that it is usually best to use two or more pressure events that occur at known times to determine a linear scale for the particular clock used.

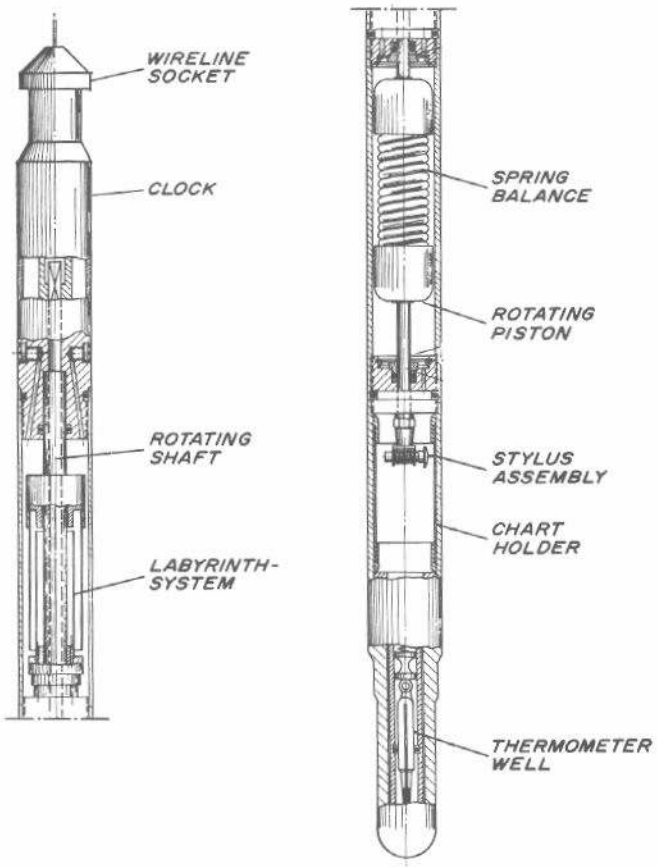

Fig. 13.5 Leutert Precision Subsurface Pressure Recorder. Courtesy Freidrich Leutert.

The factors influencing the accuracy of wireline gauges can be divided into two categories:[3-7]

1. Inherent errors owing to reproducibility of the gauge and to changes in the gauge characteristics with use.
2. Avoidable errors such as use of poor charts and stylus points, failure to reach thermal or mechanical equilibrium, neglect of temperature effects on the gauge, hysteresis effects, pressure shock during calibration, change in zero-pressure base line with temperature, etc. Ref. 3 lists several procedures that should help eliminate avoidable errors. It is important to check the calibration of the gauge frequently to verify that the calibration being used is still acceptably accurate. Generally, calibration checks should be made using a dead-weight tester. Most manufacturers will make calibration checks for a reasonable charge; all will recalibrate gauges when necessary. Nevertheless, the engineer should be aware of what constitutes good calibration. Ref. 3 presents a good explanation.

Permanently Installed Surface-Recording Gauges

Permanently installed surface-recording gauges are generally attached to the tubing string. Fig. 13.6 illustrates a common installation. These gauges are especially useful for performing transient tests on pumping wells. The instrument includes a means for measuring bottom-hole pressure and a way to transmit the measurements to the surface for recording as a function of time. Permanently installed surface-recording gauges may be used to provide continuous pressure data or occasional pressure data. Section 2 of Table 13.1 provides information about several permanently installed surface-recording gauges.

Most such gauges use a single-conductor armored cable to transmit the signal from the sensor to the recorder at the surface. Normally, the cable is strapped to the outside of the production tubing. Care must be exercised to prevent damage to the cable and the cable-to-instrument splice when the tubing is run. Formed steel protectors are normally used to protect the wire as it passes over tubing collars. To prevent damage to the cable resulting from tubing movement, a tubing anchor should be used for installations in rod-pumped wells. Hydraulic tubing anchors that can be set without turning the tubing are preferred.

One well known permanently installed surface-recording gauge is the Lynes Pressure Sentry[8] shown in Fig. 13.7. (This instrument is also available as a retrievable gauge.) The pressure element is a helically wound Bourdon tube similar in operation to that in an Amerada-type gauge. A code wheel attached to the shaft of the Bourdon tube rotates as pressure increases; the degree of rotation is an indication of the pressure applied. An electronic gating mechanism scans the code wheel and records either a 0 (the white portions of the code wheel in Fig. 13.7) or a 1 (the black

portions). The resulting surface readout is a series of 1's and 0's inscribed on a chart paper as illustrated in Fig. 13.8. Tables provided with the instrument are used to convert the binary output into a deflection number, which is then converted to pressure.*

The Maihak gauge listed in Table 13.1 uses a pressure sensor based on the displacement of a diaphragm. A frequency signal is measured by a tuned circuit in the receiver. The receiver frequency reading is converted to pressure using calibration tables. Kolb[9] reports that the Maihak gauge exhibits both temperature and elastic effects from 85 to 205 °F. He found that it is possible to obtain an accuracy of about 0.25 percent by calibrating the gauge under elastic equilibrium at operating temperatures. However, Kolb found that if this is not done errors of as much as 4 percent of full scale could be incurred.

Sperry-Sun offers a permanently installed surface-recording pressure instrument they call the Permagauge. Fig. 13.9 shows one possible installation of that gauge.

*Some newer models indicate pressure directly.

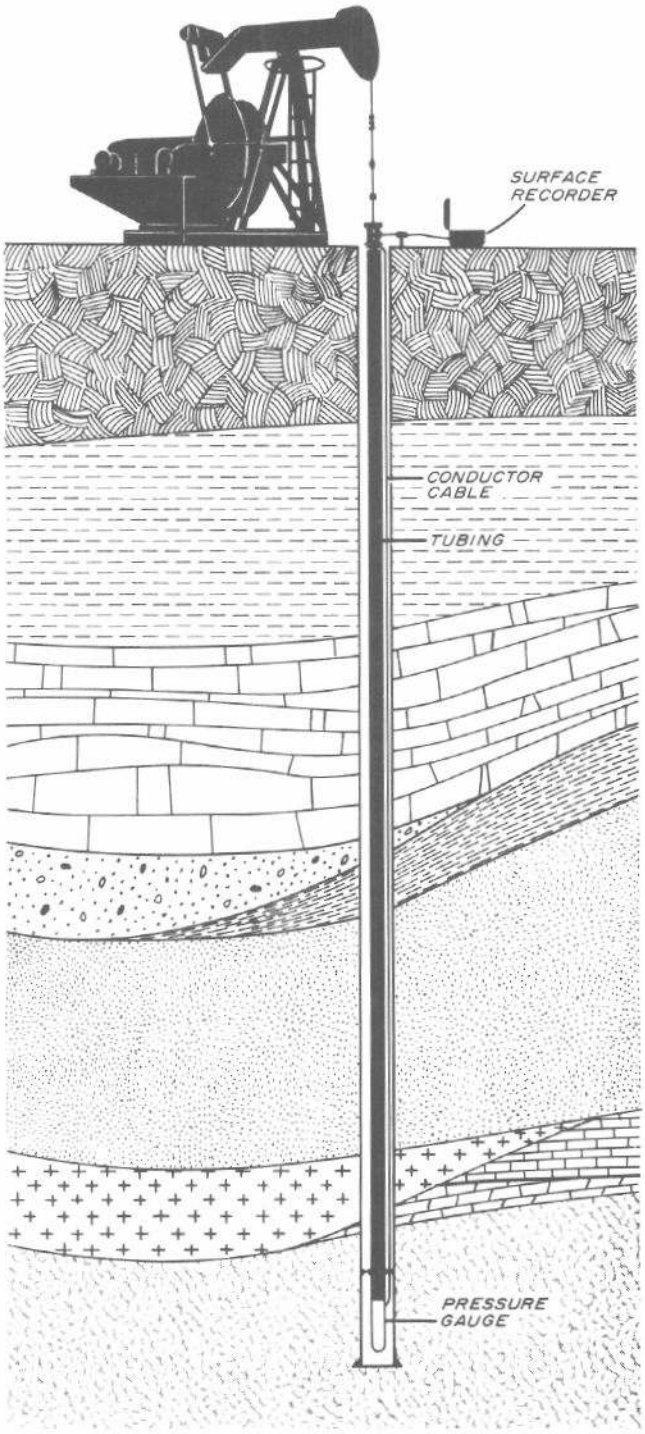

Fig. 13.6 Typical permanently installed surface-recording gauge installation. Courtesy Lynes, Inc.

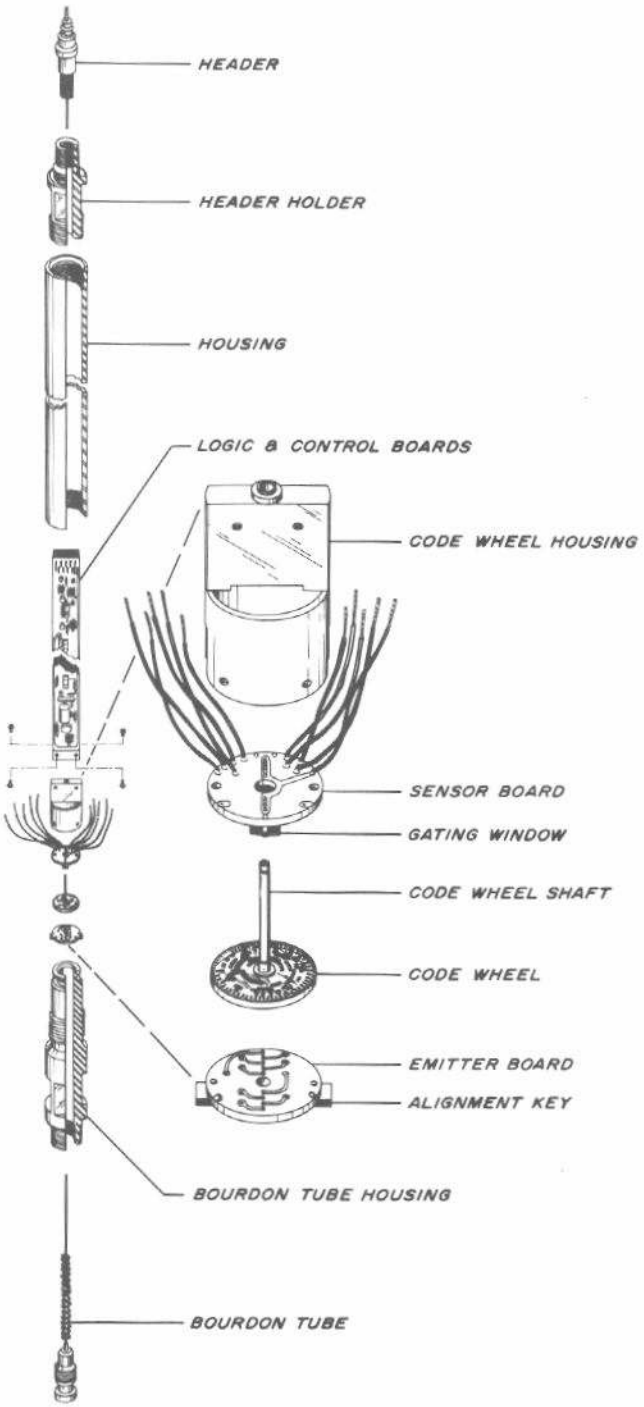

Fig. 13.7 Lynes Electronic Sentry System MK-9PES. Courtesy Lynes, Inc.

Concentric (with tubing) and suspension (like a sonde) expansion chambers are also available. The down-hole instrument is just an expansion chamber (pipe) connected to the surface by 3/32-in.-diameter stainless steel tubing. The expansion chamber and tube are charged with an inert gas and the pressure is measured at the surface by an accurate pressure transducer. Occasionally, it is necessary to purge the system with additional gas, but otherwise it requires no close supervision. The surface recorder provides pressure as a function of time. Sperry-Sun provides down-hole expansion chambers in 10- and 20-ft lengths; they come in saddle-mount installations as shown in Fig. 13.9 or concentric installations that completely surround the tubing. The surface pressure detection and recording equipment need be connected to the well only when pressure data are desired. The Sperry-Sun Permagauge system requires no down-hole power and has no apparent temperature, pressure, or life limitations. The 3/32-in.-OD stainless steel tubing is strapped to the exterior of the tubing just as is the single-conductor cable used for most permanently installed surface-recording gauges.

Permanently installed down-hole pressure gauges are especially valuable for observation wells in enhanced recovery tests. In the course of normal operation, many useful transient pressure effects are generated and can be routinely and inexpensively measured by such installations.

Retrievable Surface-Recording Gauges

Section 3 of Table 13.1 presents data on several retrievable surface-recording gauges. Many are similar in operation to the permanently installed surface-recording gauges, except that they are run on a single-conductor armored wireline. Most use Bourdon tubes for pressure measurement.

The Hewlett-Packard Corp. manufactures a gauge that uses a quartz crystal[10] as a pressure-sensing device. The quartz crystal changes vibrational frequency as the imposed pressure changes. That vibrational frequency is compared with the frequency of a reference crystal and then a frequency signal is transmitted to surface-monitoring equipment. Frequency output is converted to pressure at the appropriate temperature by use of calibration equations supplied by the manufacturer. The *accuracy* of the Hewlett-Packard gauge is stated to be ±0.5 psi or ±0.025 percent of the *reading* obtained, whichever is greater (for example, ±0.75 psi at 3,000 psi). The sensitivity is stated to be better

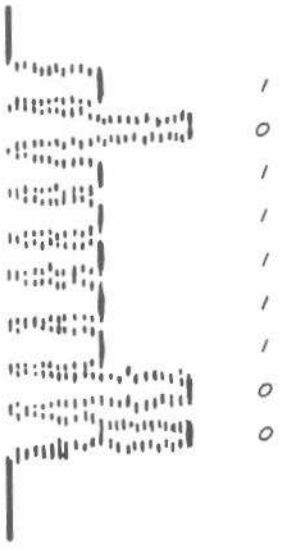

Fig. 13.8 Example of recording trace for Lynes Electronic Sentry MK-9PES. Courtesy Lynes, Inc.

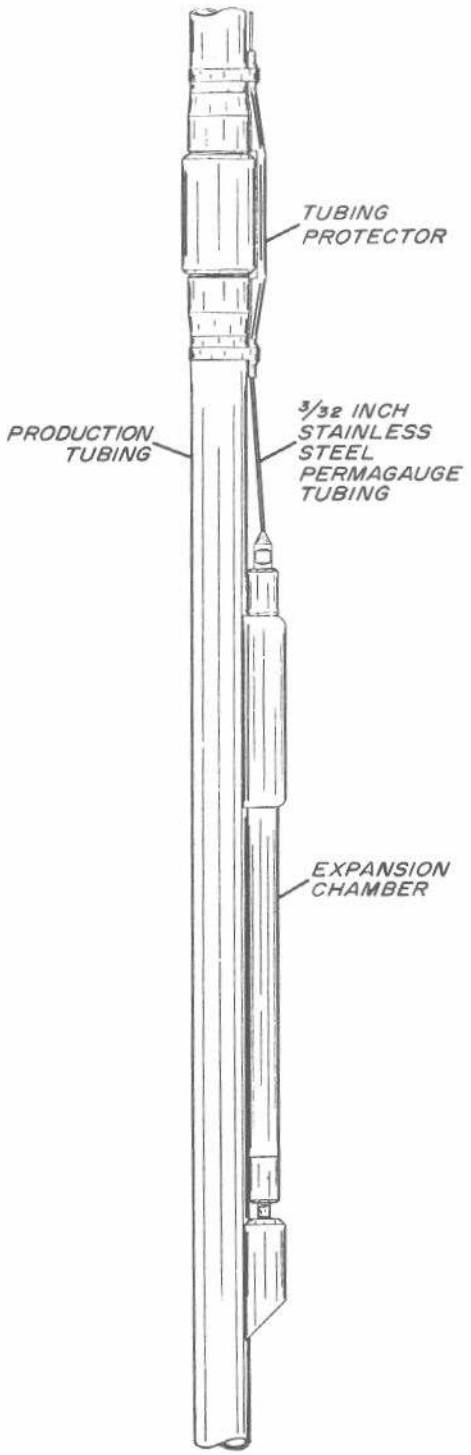

Fig. 13.9 Sperry-Sun Permagauge in saddle-mount configuration. Courtesy Sperry-Sun.

than ±0.01 psi at any pressure. Only one pressure range is offered. Although the gauge is temperature-compensated, it does have a definite response to temperature *changes* and cannot be used in changing temperature environments. About 30 minutes are required for temperature equalization of the Hewlett-Packard instrument.

Choice of Instrument

Gauge choice and operation must be considered during transient test design. We could devote dozens of pages to practical considerations. Instead, we point out only a few important items, leaving the practical aspects to be gained by experience. Many gauge manufacturers provide short instructive sessions in gauge maintenance and trouble-shooting for their customers.

It is advisable to choose the gauge pressure range so that the maximum observed pressure falls between 60 and 80 percent of the upper limit of the gauge. (However, Flopetrol and Hewlett-Packard state there is no need to limit the maximum pressure to the 80-percent value for their gauges.) If a gauge with too high a pressure range is chosen, the accuracy and sensitivity obtained may not be adequate.

All pressure gauges require periodic calibration checks and recalibration. When pressure is to be measured in high-temperature environments, it is usually necessary to specially calibrate the gauge at the temperature of interest. Bourdon-tube gauges demonstrate a hysteresis effect, so calibration must be done with a specific sequence of flexing and relaxing the Bourdon tube. The manufacturers' instructions should be followed.

When running a self-contained gauge, it is important to choose the clock so that most of the length of the chart is used during the test. It is also advisable to choose the clock so that the gauge need be run only once during the test, if that is possible. The times that the gauge is run into and out of the hole provide definite events on the pressure chart. It is recommended that those times be used to calibrate the time scale (by calculating hours per inch based on the distance between the events and the known elapsed time) to verify that the clock is running at a constant known rate and that it did not stop during the test. If there is doubt that a clock is running throughout a test, small pressure events may be put on the chart at known times simply by raising the gauge several feet and then lowering it back to its original position. The hours per inch calculated between each event should be the same.

During a test, a clock may stop for several reasons. It may be defective or damaged and not capable of running for its full term; or it may not have been wound completely. A tight recorder can stop an otherwise sound clock. Therefore, it is recommended that the recorder section of the gauge be checked before running the gauge to make sure that the stylus moves freely when the recorder is not connected to the clock or to the pressure element.

If the chart obtained from a gauge shows a stair-stepping pattern, a recorder malfunction is indicated. That pattern indicates that the pressure must change by a certain amount before the stylus moves. This difficulty must be corrected for good pressure results by freeing the recorder so it does not stick. Most manufacturers offer routine maintenance service for their gauges. In addition, many provide hints in the instruction manuals for detecting and correcting problems.

Operational problems with permanently installed gauges generally are not great. As mentioned previously, it is important to protect the cable so it is not damaged when the tubing is run in. That is usually adequately done by strapping the cable to the tubing, using protectors across the collars, and running the tubing without rotation. Readout method for permanent gauges varies depending on the application. In most situations, a portable readout device is adequate since only occasional pressures are required. However, if continuous pressure monitoring is desired, it may be necessary to provide readout devices at each wellhead, or to manifold the cables or tubing to a central location where one or more readout devices can be programmed to scan a series of wells and record the results. Most surface-recording pressure instruments require an electrical power supply (although some are battery powered). When a power supply is required, it should be determined that the voltage and frequency available fall within the range specified by the instrument manufacturer. Frequently, surface electronics are intolerant of extreme environments and must be kept in closed, heated (and possibly cooled) buildings. Such requirements should be investigated before acquiring instrumentation.

Retrievable surface-recording gauges generally are used for short-term applications. Therefore, readout is normally on a continuous basis while the gauge is in the hole. The comments above about power supply and environment apply. Normally, these gauges are used with a single-conductor armored cable.

13.6 Flow-Rate Measurement

Accurate production (or injection) rate measurement is as important as accurate pressure measurement for successful transient test analysis, since the flow rate is an integral part of all analysis equations.

Liquid flow rate is measured either by determining the time required to fill a calibrated container or by some type of flowmeter. Any suitable container can be used. For a low-rate well producing liquid with little or no gas, a rate measurement can be made by diverting the well stream into a barrel and measuring the time required to collect a given quantity of liquid. The water and oil rates are then determined from the amount of those two liquids collected during the test. The same kind of measurement can be made with a calibrated test tank.

Flowmeters are either direct or inferential. Direct flowmeters measure the total volume of fluid passing the meter. The stream is normally divided into segments of known volume and the volume segments are totaled and recorded on the meter dial. To measure flow rate with this type of meter, the time required for a given volume of fluid to pass through the meter is measured.

Inferential flowmeters measure instantaneous flow rate. Such instruments determine flow rate by measuring a related variable such as differential pressure, induced voltage, etc.

One example is a turbine flowmeter in which a precision turbine is rotated by liquid movement through the body of the meter. Rotational speed is proportional to the flow rate. As the turbine blade spins it creates measurable electrical impulses that can be converted to flow rate. Fig. 13.10 shows a turbine meter manufactured by the Halliburton Co.

All flowmeters require frequent calibration. Before using any meter on a transient test, it should be calibrated using a fluid similar to that to be measured during the test.

Gas flow-rate measurements are usually made with an orifice meter or a critical flow prover. (Orifice meters also may be used for high-rate liquid measurements.[11]) The orifice meter allows rate computation from the pressure drop occurring across an orifice placed concentrically in the flowline. Pressure taps on each side of the orifice plate allow the pressure difference across the orifice to be measured. Then, flow rate is estimated from

$$q = 0.024\, C_o \sqrt{h_w p}\ , \quad \ldots\ldots\ldots\ldots\ldots\ldots\ (13.8)$$

where

q = flow rate, Mcf/D
C_o = orifice flow constant = rate of flow in cu ft/hr at base conditions when $\sqrt{h_w p} = 1$
h_w = pressure differential, inches of water
p = static pressure upstream from the orifice, psia.

The orifice constant depends on orifice size, pressure tap location, gas gravity, and temperature. It is commonly expressed as*

$$C_o = (F_b)(F_{pb})(F_{tb})(F_g)(F_{tf})(F_{pv})(F_r)\ , \quad \ldots\ldots\ (13.9)$$

where

F_b = basic orifice flowmeter factor, cu ft/hr
F_{pb} = pressure base factor = $14.6955/p_b$
F_{tb} = temperature base factor = $T_b/520$
F_g = specific gravity factor = $\sqrt{1/\gamma}$
F_{tf} = flowing temperature factor = $\sqrt{520/T}$

*The nomenclature is taken from Ref. 11.

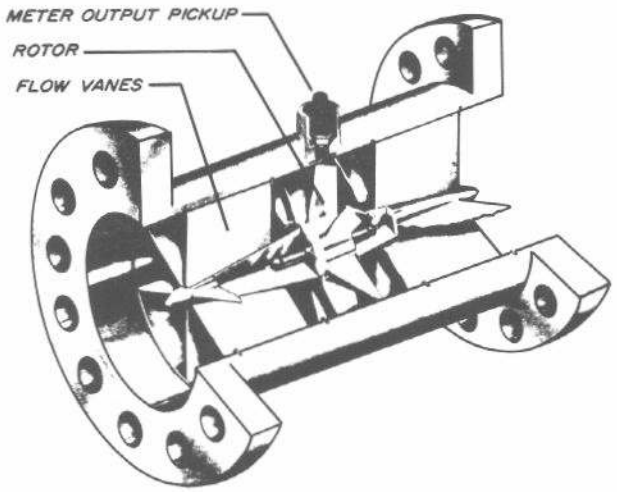

Fig. 13.10 Halliburton turbine flowmeter. Courtesy Halliburton Co.

F_{pv} = supercompressibility factor = $\sqrt{1/z}$
F_r = Reynolds number factor
T = temperature, °R.

Tables of orifice factors[11,12] are available for use in calculating C from Eq. 13.9. Precautions that should be observed in orifice-meter installation are summarized in Refs. 11 and 12.

Gas flow-rate measurement with a critical flow prover depends on gas flow through an orifice under critical conditions.[12] When gas is in critical flow, the velocity remains constant at a maximum value (sonic velocity) and the delivery rate depends only on gas density. Therefore, the flow rate is proportional to the pressure upstream of the orifice and does not change with variations in downstream pressure. A gas is normally in critical flow as long as the upstream pressure is about twice the downstream pressure.

Gas flow rate through an orifice under critical flow conditions is estimated from

$$q = \frac{0.024\, C_o p}{\sqrt{\gamma_g T}}\ , \quad \ldots\ldots\ldots\ldots\ldots\ (13.10)$$

where

q = flow rate, Mcf/D
C_o = orifice coefficient, cu ft/hr
p = upstream pressure, psia
T = upstream temperature, °R
γ_g = specific gravity of the gas.

Rawlins and Schellhardt[13] give C_o values for orifices in 2- and 4-in. pipe. They neglect deviations from the ideal gas law.

References

1. "Guide for Calculating Static Bottom-Hole Pressures Using Fluid-Level Recording Devices," ERCB Report 74-S, Energy Resources Conservation Board, Calgary, Alta., Canada (Nov. 1974).

2. Matthews, C. S. and Russell, D. G.: *Pressure Buildup and Flow Tests in Wells*, Monograph Series, Society of Petroleum Engineers of AIME, Dallas (1967) **1**, Chap. 11.

3. "Guide for the Planning, Conducting, and Reporting of Subsurface Pressure Tests," ERCB Report 74-T, Energy Resources Conservation Board, Calgary, Alta., Canada (Nov. 1974).

4. Brownscombe, E. R. and Conlon, D. R.: "Precision in Bottom-Hole Pressure Measurements," *Trans.*, AIME (1946) **165**, 159-174.

5. Laird, A. and Birks, J.: "Performance and Accuracy of Amerada Bottom-Hole Pressure Recorder With Special Reference to Use in Drill Stem Formation Tests and Repeatability of Reservoir Pressures Obtained Therein," *J. Inst. Pet.* (1951) **37**, 678-695.

6. Smith, R. V. and Dewees, E. J.: "Sources of Error in Subsurface-Pressure-Gage Calibration and Usage," *Oil and Gas J.* (Dec. 9, 1948) 85-98.

7. Brownscombe, E. R.: "A Field Calibration Technique for Bottom-Hole Pressure Measurement," *Pet. Eng.* (Aug. 1947) 84-88.

8. Nestlerode, W. A.: "Permanently Installed Bottom-Hole Pressure Gauge," Paper 875-16-L presented at the API Div. of Production meeting, Denver, April 11-13, 1962.

9. Kolb, R. H.: "Two Bottom-Hole Pressure Instruments Providing Automatic Surface Recording," *Trans.*, AIME (1960) **219,** 346-349.

10. Miller, G. B., Seeds, R. W. S., and Shira, H. W.: "A New, Surface-Recording, Down-Hole Pressure Gauge," paper SPE 4125 presented at the SPE-AIME 47th Annual Fall Meeting, San Antonio, Tex., Oct. 8-11, 1972.

11. *Engineering Data Book*, 9th ed., Gas Processors Suppliers Assn., Tulsa (1972) Sec. 1.

12. Katz, Donald L., Cornell, Donald, Kobayashi, Riki, Poettmann, Fred H., Vary, John A., Elenbaas, John R., and Weinaug, Charles F.: *Handbook of Natural Gas Engineering*, McGraw-Hill Book Co., Inc., New York (1959) Chap. 8, 761-763.

13. Rawlins, E. L. and Schellhardt, M. A.: *Back-Pressure Data on Natural-Gas Wells and Their Application to Production Practices*, Monograph 7, USBM (1936).